Genetic characterization of amino acid and N-acetylglucosamine utilization in *Aspergillus nidulans*

by

Heather Dawn Forster

B.A., University of Massachusetts Lowell, 1996
M.S., Emporia State University, 1998
M.S., Wichita State University, 2019

AN ABSTRACT OF A DISSERTATION

submitted in partial fulfillment of the requirements for the degree

DOCTOR OF PHILOSOPHY

Interdepartmental Genetics Graduate Program
Department of Plant Pathology
College of Agriculture

KANSAS STATE UNIVERSITY
Manhattan, Kansas

2025

Abstract

Nutrient acquisition is an essential and controlled process in all living organisms. In the model fungus *Aspergillus nidulans*, the transcription factor AreA regulates nitrogen utilization genes. The *areA102* pleiotropic altered function mutant shows increased growth on histidine as a nitrogen source, which is suppressed by the *suppressor of areA102* mutants *sarA* and *sarB*. The *sarA* gene (AN2350) encodes an L-amino acid oxidase (LAAO), but *sarB* has remained unidentified. Whole genome sequencing led to identification of AN8875 as a *sarB* candidate. By complementing the *sarB7* mutant phenotype on histidine with a wild-type AN8875 gene and phenocopying the *areA102 sarB7* mutant phenotype on histidine in an *areA102 AN8875*Δ mutant, we conclusively showed that *sarB* is AN8875.

sarB encodes a putative uridine diphosphate (UDP)-N-acetylglucosamine (UDP-GlcNAc) transporter that is conserved in fungi and animals. The SarB protein is likely localized to the ER or Golgi. Through generation of a *sarB*Δ *sarA*Δ double mutant, we confirmed that *sarB* and *sarA* are in the same genetic pathway. Using in-gel and spectrophotometric LAAO assays on cell-free protein extracts we demonstrated that SarA LAAO activity was greatly reduced in *areA102 sarB*Δ mutants compared to the *areA102* parent strain. SarA activity was increased and activity of a second putative LAAO, AN1808, was detected at a later timepoint.

Through treatment of growing mycelia with tunicamycin, we found evidence that SarA is N-glycosylated and that N-glycosylation is necessary for full SarA activity. However, deletion of genes involved in N-glycosylation (N-acetylglucosamine transferase, GNT) and O-GlcNAcylation (O-GlcNAc transferase, OGT) did not

phenocopy *sarB*Δ and *sarA*Δ mutants on histidine. Deletion of the GNT-encoding gene altered the electrophoretic mobility of SarA LAAO activity, suggesting a lack of GlcNAc decoration on N-glycans attached to SarA in the GNT mutant. Using RNA-seq analysis, we determined that *sarA* is upregulated on non-repressing nitrogen conditions and that *sarB* shows constitutive expression. Neither gene is regulated by the AreA co-repressor *nmrA*.

The Ndt80-like transcription factor XprG plays important roles in regulation of nutrient acquisition, including catabolism of GlcNAc. Extracellular GlcNAc is imported by the GlcNAc transporter NgtA (AN1427), phosphorylated by the hexokinase HxkC (AN4255) to GlcNAc-6-phosphate, deacetylated by DacA (AN1428) to glucosamine-6-phosphate, and deaminated by DamA (AN1418) to ammonium and fructose-6-phosphate, which can enter nitrogen and carbon metabolism, respectively. We confirmed the necessity of XprG in utilization of GlcNAc as a nitrogen source and identified a putative GlcNAc sensor and histone deacetylase, NgsA (AN1416).

We identified a second GlcNAc transporter in *A. nidulans*, NgtB (AN8127) that, when deleted, caused slightly reduced growth on GlcNAc as a nitrogen or carbon source. Simultaneous deletion of *ngtA* and *ngtB* was lethal. We showed that the GlcNAc utilization regulatory genes *xprG* and *ngsA* exhibit genetic interaction in GlcNAc catabolism and extracellular protease activity. RNA-seq experiments provided evidence that GlcNAc utilization is regulated by nitrogen metabolite repression and *nmrA*.

Overall, our work shows that GlcNAc has multiple roles in nutrient acquisition in *A. nidulans* and suggests that its recycling may be essential for hyphal growth.

Genetic characterization of amino acid and N-acetylglucosamine utilization in *Aspergillus nidulans*

by

Heather Dawn Forster

B.A., University of Massachusetts Lowell, 1996
M.S., Emporia State University, 1998
M.S., Wichita State University, 2019

A DISSERTATION

submitted in partial fulfillment of the requirements for the degree

DOCTOR OF PHILOSOPHY

Interdepartmental Genetics Graduate Program
Department of Plant Pathology
College of Agriculture

KANSAS STATE UNIVERSITY
Manhattan, Kansas

2025

Approved by:

Major Professor
Richard B. Todd

Copyright

Abstract

Nutrient acquisition is an essential and controlled process in all living organisms. In the model fungus *Aspergillus nidulans*, the transcription factor AreA regulates nitrogen utilization genes. The *areA102* pleiotropic altered function mutant shows increased growth on histidine as a nitrogen source, which is suppressed by the *suppressor of areA102* mutants *sarA* and *sarB*. The *sarA* gene (AN2350) encodes an L-amino acid oxidase (LAAO), but *sarB* has remained unidentified. Whole genome sequencing led to identification of AN8875 as a *sarB* candidate. By complementing the *sarB7* mutant phenotype on histidine with a wild-type AN8875 gene and phenocopying the *areA102 sarB7* mutant phenotype on histidine in an *areA102 AN8875*Δ mutant, we conclusively showed that *sarB* is AN8875.

sarB encodes a putative uridine diphosphate (UDP)-N-acetylglucosamine (UDP-GlcNAc) transporter that is conserved in fungi and animals. The SarB protein is likely localized to the ER or Golgi. Through generation of a *sarB*Δ *sarA*Δ double mutant, we confirmed that *sarB* and *sarA* are in the same genetic pathway. Using in-gel and spectrophotometric LAAO assays on cell-free protein extracts we demonstrated that SarA LAAO activity was greatly reduced in *areA102 sarB*Δ mutants compared to the *areA102* parent strain. SarA activity was increased and activity of a second putative LAAO, AN1808, was detected at a later timepoint.

Through treatment of growing mycelia with tunicamycin, we found evidence that SarA is N-glycosylated and that N-glycosylation is necessary for full SarA activity. However, deletion of genes involved in N-glycosylation (N-acetylglucosamine transferase, GNT) and O-GlcNAcylation (O-GlcNAc transferase, OGT) did not

phenocopy *sarB*Δ and *sarA*Δ mutants on histidine. Deletion of the GNT-encoding gene altered the electrophoretic mobility of SarA LAAO activity, suggesting a lack of GlcNAc decoration on N-glycans attached to SarA in the GNT mutant. Using RNA-seq analysis, we determined that *sarA* is upregulated on non-repressing nitrogen conditions and that *sarB* shows constitutive expression. Neither gene is regulated by the AreA co-repressor *nmrA*.

The Ndt80-like transcription factor XprG plays important roles in regulation of nutrient acquisition, including catabolism of GlcNAc. Extracellular GlcNAc is imported by the GlcNAc transporter NgtA (AN1427), phosphorylated by the hexokinase HxkC (AN4255) to GlcNAc-6-phosphate, deacetylated by DacA (AN1428) to glucosamine-6-phosphate, and deaminated by DamA (AN1418) to ammonium and fructose-6-phosphate, which can enter nitrogen and carbon metabolism, respectively. We confirmed the necessity of XprG in utilization of GlcNAc as a nitrogen source and identified a putative GlcNAc sensor and histone deacetylase, NgsA (AN1416).

We identified a second GlcNAc transporter in *A. nidulans*, NgtB (AN8127) that, when deleted, caused slightly reduced growth on GlcNAc as a nitrogen or carbon source. Simultaneous deletion of *ngtA* and *ngtB* was lethal. We showed that the GlcNAc utilization regulatory genes *xprG* and *ngsA* exhibit genetic interaction in GlcNAc catabolism and extracellular protease activity. RNA-seq experiments provided evidence that GlcNAc utilization is regulated by nitrogen metabolite repression and *nmrA*.

Overall, our work shows that GlcNAc has multiple roles in nutrient acquisition in *A. nidulans* and suggests that its recycling may be essential for hyphal growth.

Table of Contents

List of Figures

List of Tables

Acknowledgements

I'd like to thank my major professor, Dr. Richard B. Todd for all of his guidance and patience, and the opportunity to work on this project. Working with him has made me a better scientist and has heightened my intellectual curiosity. I will really miss him. Thank you also to my committee Dr. David Cook, Dr. Kathrin Schrick, and Dr. Tom Platt for all of their helpful advice.

My work was supported directly by the Kansas State University Genetics Doctoral Fellowship, the Johnson Cancer Research Center Dale Augustine Cancer Research Award, and a Kansas Academy of Science Graduate Research Award, as well as travel awards from the Genetics Society of America, the Johnson Cancer Research Center, and the Kansas State University Graduate Student Council.

Thank you to all of my friends and the Tatsumaki Yosakoi dance team for your support and friendship.

Dedication

This work is dedicated to my parents. I cannot express how much I love you.

Chapter 1 - Introduction and Objectives

1.1 Introduction

1.1.1 Nutrient acquisition

Nutrient acquisition is essential in all organisms, and mechanisms must exist to allow continued intake of nutrients during times of starvation. Many fungi have the ability to scavenge nitrogen from diverse sources. This allows pathogenic species to exploit resources available in their hosts and saprophytes to decompose a wide array of materials in the environment. Ammonium or glutamine are usually preferred nitrogen sources which can be assimilated easily. Other nitrogen sources require dedicated enzymatic pathways to enable their use. Nitrogen metabolism and the transcription factors that regulate nitrogen metabolism genes are implicated in virulence of human and plant pathogens, but many of these pathways are still poorly understood.

1.1.2 *Aspergillus nidulans* as a model fungus

The filamentous ascomycete fungus *Aspergillus nidulans* is a valuable model for study of the genetics of nutrient acquisition (Pontecorvo et al. 1953). This saprophyte is found throughout nature. While *A. nidulans* can infect persons with chronic granulomatous disease (Henriet et al. 2012), its primary value comes as a model for filamentous fungi, especially aspergilli. Many *Aspergillus* species, such as *Aspergillus oryzae, Aspergillus fumigatus*, *Aspergillus niger,* and *Aspergillus flavus*, have industrial, human health, and plant pathogenic relevance, but they are primarily asexual and thus difficult to manipulate genetically. *A. nidulans* is haploid but can survive as a stable diploid or heterokaryon, and is homothallic and capable of outcrossing (Todd et al. 2007a). It produces sexual ascospores inside of cleistothecia, which can be separated

from asexual spores and used for genetic analysis of progeny (Todd et al. 2007b) The *A. nidulans* draft genome sequence was published in 2005 (Galagan et al. 2005). It has recently been sequenced with telomere-to-telomere coverage and reannotated (provided by Adrian Tsang, Concordia University). *A. nidulans* has an approximately 30-Mbp genome spread across 8 chromosomes with few repetitive elements (Galagan et al. 2005). Many selectable markers are available for DNA-mediated transformation and molecular manipulations (*e.g.,* Upshall 1986; Oakley et al. 1987a, 1987b; Osmani et al. 1999).

A whole-genome knockout construct collection for *A. nidulans* is available at the Fungal Genetic Stock Center (McCluskey et al. 2010; De Souza et al. 2013). Constructs consist of the *Aspergillus fumigatus pyrG* (*AfpyrG*) gene selectable marker, flanked by sequences ~1 kbp upstream and downstream of the target genes. Transformation of the construct into a *nkuA*Δ non-homologous end-joining mutant recipient (Nayak et al. 2006) forces replacement of the target gene with the selectable marker via double homologous recombination. Transformation into a recipient with the *pyrG89* mutation allows selection of transformants for pyrimidine prototrophy (Oakley et al. 1987a). These resources make *A. nidulans* an excellent system for genetic manipulation.

1.1.3 Nitrogen metabolism in *A. nidulans*

Many fungi regulate nitrogen utilization through nitrogen metabolite repression (NMR; Arst and Cove 1973, reviewed in Todd 2016). This regulation ensures that the transporters and enzymes for nitrogen breakdown are produced only when needed. In *A. nidulans*, when the preferred nitrogen source ammonium or glutamine is present, the co-repressor NmrA is bound to the global GATA transcription factor AreA, which is

consequently unable to activate genes for utilization of other nitrogen sources, leading to their repression (Arst and Cove 1973; Kudla et al. 1990; Andrianopoulos et al. 1998). When preferred nitrogen sources are not available, NmrA is degraded and AreA is able to activate alternative nitrogen source utilization genes (Zhao et al. 2010; Li et al. 2021). This results in derepression of these genes and some degree of gene transcription. In many cases, the presence of an alternative nitrogen source can lead to induction of genes for degradation of that nitrogen source by binding of a pathway-specific transcription factor in the promoter(s) of the catabolic genes alongside AreA, leading to activation of high levels of gene transcription (Todd 2016).

1.1.4 Amino acids as nitrogen sources

Proteins in the environment can be broken down by extracellular proteases into amino acids, which can be further catabolized and used as sources of nitrogen by fungi (Cohen 1972). Some amino acids serve as substrates for amino acid-specific enzymes and degradation pathways. In *A. nidulans*, proline is catabolized in multiple steps by enzymes encoded by the *prn* utilization gene cluster (Sophianopoulou and Scazzocchio 1994), and the branched chain amino acids can be utilized by deamination via the Branched-chain amino acid Amino Transferase (BAT) enzymes (Steyer et al. 2021). In *A. fumigatus,* alanine can be broken down by alanine transaminase or alanine-glyoxylate aminotransferase (Kerkaert et al. 2022). However, some amino acids can also or alternatively be deaminated by L-amino acid oxidases (LAAOs) to α-keto acids. This process releases ammonium, which can enter nitrogen metabolism, and hydrogen peroxide (Davis et al. 2005).

1.1.5 N-acetylglucosamine and fungi

N-acetylglucosamine (GlcNAc) is a nitrogenous hexose sugar synthesized via the hexosamine pathway from glucose via fructose-6-phosphate. GlcNAc is ubiquitous throughout nature. Structurally, GlcNAc is a major component in the cell walls of fungi (in chitin) and of bacteria (in peptidoglycan), in the chitinous exoskeletons of insects, and in the mammalian extracellular matrix (Konopka 2012).

GlcNAc is often bound to the carrier molecule uridine diphosphate (UDP) to form the nucleotide sugar UDP-GlcNAc. In this form, it is a donor substrate for chitin biosynthesis and glycosylation. UDP-GlcNAc is transported to the fungal cell wall and synthesized into chitin by plasma membrane-bound chitin synthases (Latgé 2007). During cell wall remodeling or autolysis, chitinases split chitin into multimeric units and β-1,4-N-acetylglucosaminidases split multimeric units into individual GlcNAc molecules (Kim et al. 2002; Pusztahelyi et al. 2006; Yamazaki et al. 2008; Shin et al. 2009).

GlcNAc also plays vital roles in glycosylation, post-translational modifications that can affect proper protein structure and function (reviewed in He et al. 2024a). Synthesis of N-glycans begins in the membrane of the endoplasmic reticulum, facing the cytoplasm, where two covalently linked GlcNAc molecules form the base of the N-glycan (Anyaogu et al. 2021). After translocation of the growing glycan to the ER lumen, additional components are added to the mannose tree backbone of the glycan, including GlcNAc molecules in some fungi (Smith et al. 1975). This is catalyzed by N-glycosyltransferase(s) in the Golgi (Guillen et al. 1999). GlcNAc can also be a component of canonical O-glycans, though evidence is lacking that this occurs in fungi. In the process of O-GlcNAcylation, individual GlcNAc molecules are added to serine or

threonine residues of proteins in the cytoplasm, nucleus, or mitochondria via O-GlcNAc transferase (OGT); O-GlcNAc can be removed from proteins by the O-GlcNAcase enzyme (OGA) (Ma and Hart 2014).

1.2 Objectives

The objective of this research is to increase our understanding of amino acid and GlcNAc utilization in *A. nidulans*. In Chapter 3, we identify and characterize a UDP-GlcNAc transporter, SarB, with a role in amino acid utilization. In Chapter 4, we seek to understand how SarB impacts the L-amino acid oxidase (LAAO) SarA through investigating its role in LAAO activity and glycosylation. In Chapter 5, we characterize the genetic pathway by which extracellular GlcNAc is transported into the cell and used as a source of nitrogen and carbon. Through our investigation of *sarB*, we show that UDP-GlcNAc is required for efficient amino acid utilization by the SarA LAAO and that SarA is glycosylated with GlcNAc-decorated N-glycans. We identify the genes of the GlcNAc utilization pathway in *A. nidulans*, demonstrate that GlcNAc can serve as a sole nitrogen, carbon, or nitrogen and carbon source for growth, and provide evidence that import of extracellular GlcNAc is necessary for hyphal growth.

Chapter 2 - Experimental Procedures

2.1 Strains

2.1.1 *Aspergillus nidulans* strains

A. nidulans strains used in this research and developed in the lab of Michael J. Hynes at the University of Melbourne are listed in Table 2.1

Table 2.1 "Michael Hynes" *Aspergillus nidulans* strains.

Strain	Genotype
MH1	*biA1*
MH8	*biA1 areA102 niiA4*
MH10571	*yA1 pyroA4 su*(*adE20*) *adE20 areA102 sarA*Δ::*riboB+ riboB2*
MH10983	*pyrG89 pabaB22 riboB2*
MH11068	*pyrG89 pyroA4 nkuA*Δ::*Bar amdA7*

A. nidulans strains used in this research and developed in the lab of Margaret Katz at the University of New England are listed in Table 2.2

Table 2.2 "Margaret Katz" *Aspergillus nidulans* strains.

Strain	Genotype
MK85	*biA1 niiA4 xprG1*
MK160	*areA102 biA1 niiA4 sarB7*
MK205	*yA2 pabaA1 areA102 sarB7 xprG1*
MK414	*argB2 pabaA1 xprG*Δ::*argB+ yA2*
MK489	*argB2 hxkC*Δ::*argB niiA4*

A. nidulans strains used in this research and developed in the lab of Richard Todd by persons other than H. Forster are listed in Table 2.3

Table 2.3 "Richard Todd" *Aspergillus nidulans* strains constructed by others.

Strain	Genotype
RT626	*amdA7* AN1418Δ::*AfpyrG+ nkuA*Δ::*Bar pyrG89 pyroA4*
RT707	*amdA7* AN1416Δ::*AfpyrG+ nkuA*Δ::*Bar pyrG89 pyroA4*
RT708	*amdA7* AN1427Δ::*AfpyrG+ nkuA*Δ::*Bar pyrG89 pyroA4*
RT709	*amdA7* AN1428Δ::AfpyrG+ *nkuA*Δ::*Bar pyrG89 pyroA4*
RT763	*pyrG89 sarA*Δ::*riboB+ pyroA4 riboB2*

RT765	*areA102 pabaB22 pyrG89 pabaB22 riboB2 sarA*Δ::*riboB*+
RT774	AN1808Δ::*AfpyrG+ areA102 pabaB22 pyrG89 riboB2*
RT775	*pyrG89 areA102 pyroA4* AN1808Δ*::AfpyrG+ riboB2*
RT776	*pyrG89 areA102 pyroA4 sarA*Δ*::riboB+* AN1808Δ*::AfpyrG+ riboB2*

A. nidulans strains used in and developed during this research by H. Forster are listed in Table 2.4

Table 2.4 "Richard Todd" *Aspergillus nidulans* strains constructed by Forster.

Strain	Genotype
RT803	*pyrG89 pyroA4 nkuA*Δ*::Bar xprG1*
RT804	*pyrG89 pyroA4 nkuA*Δ*::Bar xprG1 niiA4*
RT811	*pyrG89 pyroA4 nkuA*Δ*::Bar xprG*Δ*::argB+*
RT812	*pyrG89 pyroA4 nkuA*Δ*::Bar xprG*Δ*::argB+ nkuA*Δ*::Bar*
RT813	*pyrG89 pyroA4 nkuA*Δ*::Bar xprG*Δ*::argB+ amdA7 nkuA*Δ*::Bar*
RT818	*pyrG89 pyroA4 nkuA*Δ*::Bar* AN1418Δ::*AfpyrG+* AN1418r
RT822	*pyrG*89 *pyroA4 nkuA*Δ*::Bar xprG*1 AN1416Δ::*AfpyrG+*
RT823	*pyrG*89 *pyroA4 nkuA*Δ*::Bar xprG*1 AN1416Δ::*AfpyrG+*
RT824	*pyrG*89 *pyroA4 nkuA*Δ*::Bar xprG*1 AN1416Δ::*AfpyrG+*
RT825	*pyrG*89 *pyroA4 nkuA*Δ*::Bar xprG*1 AN1416Δ::*AfpyrG+*
RT826	*pyrG*89 *pyroA4 nkuA*Δ*::Bar xprG*1 AN1416Δ::*AfpyrG+*
RT827	*pyrG*89 *pyroA4 nkuA*Δ*::Bar xprG*Δ AN1416Δ::*AfpyrG+*
RT828	*pyrG*89 *pyroA4 nkuA*Δ*::Bar xprG*Δ AN1416Δ::*AfpyrG+*
RT829	*pyrG*89 *pyroA4 nkuA*Δ*::Bar xprG*Δ AN1416Δ::*AfpyrG+*
RT830	*pyrG*89 *pyroA4 nkuA*Δ*::Bar xprG*Δ AN1416Δ::*AfpyrG+*
RT831	*pyrG*89 *pyroA4 nkuA*Δ*::Bar xprG*Δ AN1416Δ::*AfpyrG+*
RT832	*pyrG*89 *pyroA4 nkuA*Δ::*Bar* AN1428r#
RT833	*pyrG*89 *pyroA4 nkuA*Δ::*Bar* AN1428r#
RT834	*pyrG*89 *pyroA4 nkuA*Δ::*Bar* AN1428r#
RT835	*pyrG*89 *pyroA4 nkuA*Δ::*Bar* AN1428r#
RT836	*pyrG*89 *pyroA4 nkuA*Δ::*Bar* AN1428r#
RT843	*pyrG*89 *pyroA4 nkuA*Δ::*Bar* AN1427r#
RT844	*pyrG*89 *pyroA4 nkuA*Δ::*Bar* AN1427r#
RT845	*pyrG*89 *pyroA4 nkuA*Δ::*Bar* AN1427r#
RT851	*pyrG89 nmrA*Δ*::AfpyrG+ pyroA4 nkuA*Δ*::Bar amdA7*
RT852	*pyrG89 nmrA*Δ*::AfpyrG+ pyroA4 nkuA*Δ*::Bar amdA7*
RT853	*pyrG89 nmrA*Δ*::AfpyrG+ pyroA4 nkuA*Δ*::Bar amdA7*
RT854	*pyrG89 nmrA*Δ*::AfpyrG+ pyroA4 nkuA*Δ*::Bar amdA7*
RT855	*pyrG89 pyroA4* AN8875Δ::*AfpyrG+ amdA7 nkuA*Δ*::Bar*
RT856	*pyrG89 pyroA4* AN8875Δ::*AfpyrG+ amdA7 nkuA*Δ*::Bar*
RT857	*pyrG89 pyroA4* AN8875Δ::*AfpyrG+ amdA7 nkuA*Δ*::Bar*
RT858	*pyrG89 pyroA4* AN8875Δ::*AfpyrG+ amdA7 nkuA*Δ*::Bar*

RT859 *pyrG89 pyroA4* AN8875Δ::*AfpyrG+ amdA7 nkuA*Δ*::Bar*
RT865 *pyrG89 pyroA4 nkuA*Δ::*Bar*
RT890 *areA102 pyroA4* AN8875Δ::*AfpyrG+*
RT891 *biA1 areA102* AN8875Δ::*AfpyrG+ niiA4*
RT892 *areA102* AN8875Δ::*AfpyrG+*
RT893 *biA1 areA102* AN8875Δ::*AfpyrG+ niiA4*
RT927 *biA1 areA102 sarB7 niiA4* AN8875c*
RT928 *biA1 areA102 sarB7 niiA4* AN8875c*
RT929 *biA1 areA102 sarB7 niiA4* AN8875c*
RT930 *biA1 areA102 sarB7 niiA4* AN8875c*
RT931 *biA1 areA102 sarB7 niiA4* AN8875c*
RT943 *biA1 areA102 pyroA4* AN8875Δ::*AfpyrG+ niiA4*
RT944 *biA1 areA102 pyroA4* AN8875Δ::*AfpyrG+*
RT945 *areA102* AN8875Δ::*AfpyrG+ niiA4*
RT946 *biA1 areA102* AN8875Δ *niiA4 nkuA*Δ*::Bar*
RT947 *biA1 areA102 niiA4 sarB7* AN8875c*
RT948 *biA1 areA102 niiA4 sarB7* AN8875c*
RT949 *biA1 areA102 niiA4 sarB7* AN8875c*
RT950 *biA1 areA102 niiA4 sarB7* AN8875c*
RT951 *biA1 areA102 niiA4 sarB7* AN8875c*
RT952 *biA1 areA102 niiA4 sarB7* AN8875c*
RT953 *biA1 areA102 niiA4 sarB7* AN8875c*
RT954 *biA1 areA102 niiA4 sarB7* AN8875c*
RT955 *biA1 areA102 niiA4 sarB7* AN8875c*
RT957 *biA1 areA102 niiA4*
RT958 *areA102*
RT959 *pyrG*89 *pyroA4 nkuA*Δ::*Bar* AN1428r#
RT960 *biA1 areA102 niiA4*
RT961 *pyrG89 pyroA4 nkuA*Δ::*Bar* AN1418r#
RT962 *pyrG89 pyroA4 nkuA*Δ::*Bar* AN1418r#
RT963 *pyrG89 pyroA4 nkuA*Δ::*Bar* AN1418r#
RT964 *pyrG89 pyroA4 nkuA*Δ::*Bar* AN1418r#
RT965 *pyrG89 pyroA4 nkuA*Δ::*Bar* AN1418r#
RT971 *biA1 areA102* AN8875Δ::*AfpyrG niiA4* AN8875c*
RT972 *biA1 areA102* AN8875Δ::*AfpyrG niiA4* AN8875c*
RT973 *biA1 areA102* AN8875Δ::*AfpyrG niiA4* AN8875c*
RT974 *biA1 areA102* AN8875Δ::*AfpyrG niiA4* AN8875c*
RT975 *biA1 areA102* AN8875Δ::*AfpyrG niiA4* AN8875c*
RT981 *pyrG89 pyroA4 nkuA*Δ*::Bar* AN1416Δ::*AfpyrG+* AN1416c* *amdA7*
RT982 *pyrG89 pyroA4 nkuA*Δ*::Bar* AN1416Δ::*AfpyrG+* AN1416c* *amdA7*
RT983 *pyrG89 pyroA4 nkuA*Δ*::Bar* AN1416Δ::*AfpyrG+* AN1416c* *amdA7*
RT984 *pyrG89 pyroA4 nkuA*Δ*::Bar* AN1416Δ::*AfpyrG+* AN1416c* *amdA7*
RT985 *pyrG89 pyroA4 nkuA*Δ*::Bar* AN1416Δ::*AfpyrG+* AN1416c* *amdA7*
RT986 *pyrG89 pyroA4 nkuA*Δ*::Bar* AN1416Δ::*AfpyrG+* AN1416c* *amdA7*
RT987 *pyrG89 pyroA4 nkuA*Δ*::Bar* AN1416Δ::*AfpyrG+* AN1416c* *amdA7*

RT988 *pyrG89* AN8127Δ::*AfpyrG+ pyroA4 nkuAΔ::Bar*
RT989 *pyrG89* AN8127Δ::*AfpyrG+ pyroA4 nkuAΔ::Bar*
RT990 *pyrG89* AN8127Δ::*AfpyrG+ pyroA4 nkuAΔ::Bar*
RT991 *pyrG89* AN8127Δ::*AfpyrG+ pyroA4 nkuAΔ::Bar*
RT992 *pyrG89* AN8127Δ::*AfpyrG+ pyroA4 nkuAΔ::Bar*
RT993 *pyrG89* AN1427Δ::*AfpyrG+ riboB2*
RT994 *pyrG89 pabaB22* AN1427Δ::*AfpyrG+ riboB2*
RT995 *pyrG89 pabaB22* AN1427Δ::*AfpyrG+*
RT996 *pyrG89 pyroA4* AN1427Δ::*AfpyrG+*
RT997 *pyrG89 pabaB22 pyroA4* AN1427Δ::*AfpyrG+*
RT998 *pyrG89 pyroA4 nkuΔ::Bar* AN1428Δ::*AfpyrG+* AN1428c* *amdA7*
RT999 *pyrG89 pyroA4 nkuΔ::Bar* AN1428Δ::*AfpyrG+* AN1428c* *amdA7*
RT1000 *pyrG89 pyroA4 nkuΔ::Bar* AN1428Δ::*AfpyrG+* AN1428c* *amdA7*
RT1001 *pyrG89 pyroA4 nkuΔ::Bar* AN1428Δ::*AfpyrG+* AN1428c* *amdA7*
RT1002 *pyrG89 pyroA4 nkuΔ::Bar* AN1428Δ::*AfpyrG+* AN1428c* *amdA7*
RT1003 *pyrG89 pyroA4 nkuΔ::Bar* AN1427Δ::*AfpyrG+* AN1427c* *amdA7*
RT1004 *pyrG89 pyroA4 nkuΔ::Bar* AN1427Δ::*AfpyrG+* AN1427c* *amdA7*
RT1005 *pyrG89 pyroA4 nkuΔ::Bar* AN1427Δ::*AfpyrG+* AN1427c* *amdA7*
RT1006 *pyrG89 pyroA4 nkuΔ::Bar* AN1427Δ::*AfpyrG+* AN1427c* *amdA7*
RT1007 *pyrG89 pyroA4 nkuΔ::Bar* AN1427Δ::*AfpyrG+* AN1427c* *amdA7*
RT1008 *pyrG89 pyroA4 nkuΔ::Bar* AN1427Δ::*AfpyrG+* AN1427c* *amdA7*
RT1009 *pyrG89 pyroA4 nkuΔ::Bar* AN1418Δ::*AfpyrG+* AN1418c* *amdA7*
RT1010 *pyrG89 pyroA4 nkuΔ::Bar* AN1418Δ::*AfpyrG+* AN1418c* *amdA7*
RT1011 *pyrG89 pyroA4 nkuΔ::Bar* AN1418Δ::*AfpyrG+* AN1418c* *amdA7*
RT1012 *pyrG89 pyroA4 nkuΔ::Bar* AN1418Δ::*AfpyrG+* AN1418c* *amdA7*
RT1013 *pyrG89 pyroA4 nkuΔ::Bar* AN1418Δ::*AfpyrG+* AN1418c* *amdA7*
RT1014 *pyrG89 pyroA4 nkuΔ::Bar* AN1418Δ::*AfpyrG+* AN1418c* *amdA7*
RT1015 *pyrG89 pyroA4* AN8875Δ::*AfpyrG+ riboB2*
RT1016 *pyrG89 pyroA4* AN8875Δ::*AfpyrG+*
RT1017 *pyrG89* AN8875Δ::*AfpyrG+ riboB2*
RT1018 *pyrG89 pabaB22* AN8875Δ::*AfpyrG+*
RT1019 *pyrG89 pyroA4 nkuΔ::Bar* AN1427Δ::*AfpyrG-*
RT1020 *pyrG89 pabaB22 sarAΔ::riboB+* AN8875Δ::*AfpyrG+ riboB2*
RT1021 *pyrG89 pyroA4 sarAΔ::riboB+* AN8875Δ::*AfpyrG+ riboB2*
RT1022 *pyrG89 pabaB22 areA102 sarAΔ::riboB+* AN8875Δ::*AfpyrG+ riboB2*
RT1023 *pyrG89 pyroA4 areA102 sarAΔ::riboB+* AN8875Δ::*AfpyrG+ riboB2*
RT1024 *pyrG89 sarAΔ::riboB+* AN8875Δ::*AfpyrG+ riboB2*
RT1025 *pyrG89 areA102 sarAΔ::riboB+* AN8875Δ::*AfpyrG+ riboB2*
RT1035 *pabaB22 areA102* AN8875Δ::*AfpyrG+* AN1808Δ::*AfpyrG+*
RT1036 *pyrG89 pyroA4 nkuAΔ::Bar* AN11141Δ::*AfpyrG+*
RT1037 *pyrG89 pyroA4 nkuAΔ::Bar* AN0265Δ::*AfpyrG+*
RT1045 *areA102* AN11141Δ::*AfpyrG+niiA4*
RT1046 *areA102 pyroA4* AN11141Δ::*AfpyrG+*
RT1047 *areA102 pyroA4* AN0265Δ::*AfpyrG+*
RT1048 *areA102* AN0265Δ::*AfpyrG+niiA4*

RT1049	*biA1 areA102 xprG∆::argB+ niiA4*
RT1050	*biA1 areA102* AN1416∆*::pyrG+ niiA4*
RT1051	*biA1 areA102 xprG∆::argB+* AN1416∆*::pyrG+ niiA4*
RT1052	*areA102 pyroA4* AN1416∆*::AfpyrG+*
RT1053	*areA102* AN1416∆*::pyrG+ niiA4*
RT1055	*yA1 areA102 pyroA4 xprG∆::argB+* AN1416∆*::pyrG+*
RT1056	*yA2 areA102 xprG∆::argB+* AN1416∆*::pyrG+ niiA4*
RT1057	*areA102 xprG∆::argB+* AN1416∆*::pyrG+ niiA4*
RT1058	*areA102 xprG∆::argB+* AN1416∆*::pyrG+ pabaA1*
RT1059	*yA2 areA102 pabaA1 xprG∆::argB+*
RT1060	*yA2 areA102 xprG∆::argB+niiA4*
RT1064	*areA102* AN11141∆::*AfpyrG+* AN0265∆::*AfpyrG+ niiA4*

"r", repaired, denotes the wild type gene has replaced a gene knockout via homologous gene replacement.
* "c", complemented, denotes integration of a plasmid containing the indicated wild type gene by single crossover.

2.1.2 *Escherichia coli* strains

Plasmid construction and manipulation used the *Escherichia coli* strain NM522 [F' *proA*$^{+}$*B*$^{+}$ *lacI*^{q} ∆(*lacZ*)*M15/*∆(*lac-proAB*) *glnV thi*-1 ∆(*hsdS-mcrB*)5] (Gough and Murray 1983). Details of plasmid construction are provided in the applicable chapters.

2.2 Media and Growth Conditions

2.2.1 *Aspergillus nidulans* media and growth conditions

A. nidulans growth conditions and media were as described in Cove (1966). *Aspergillus* nitrogen-free minimal media (ANM) was pH adjusted to 6.5 and contained 1% (w/v) carbon source and 10 mM nitrogen source, unless otherwise stated, and supplemented for auxotrophic mutations. Genetic analysis was carried out using techniques described in Clutterbuck (1973) and Todd et al. (2007b).

2.2.2 *Escherichia coli* media and growth conditions

E. coli were grown on Luria broth (LB) agar supplemented with 50 μg/mL ampicillin to select for colonies containing an ampicillin resistance selectable marker.

For blue-white screening, 0.04 mM isopropyl-β-D-thiogalactopyranoside (IPTG) with 0.005% 5-bromo-4-chloro-3-indoyl-β-D-galactoside (X-gal) were used as needed (Sambrook and Russell 2001). Bacterial stocks were made by growing *E. coli* overnight in LB broth, and mixing the bacterial suspension with an equal volume of 30% glycerol, flash freezing, and storing at -80 °C.

2.3 Chemical Reagents and Solutions

DNA Lysis Buffer
50 mM Tris-HCl pH 7.2
50 mM EDTA
3% SDS
1% β-mercaptoethanol

RNA Extraction Buffer
7 M Urea
100 mM Tris-HCl pH 8.0
10 mM EDTA
1% Sodium dodecyl sulfate

LAAO In-Gel Assay HRP-OPD Substrate Solution
5 mM amino acid
1 mM O-phenylenediamine
0.5 U/mL Horseradish peroxidase
In Tris-HCl pH 8.0

LAAO In-Gel Assay Electrophoresis Buffer (10x)
250 mM Tris
2.5 M Glycine (pH 8.3)
1% Sodium dodecyl sulfate

LAAO In-gel Assay Sample Buffer (2x)
0.15 M Tris-HCl pH 6.8
20% Glycerol
4% Sodium dodecyl sulfate
0.2% Bromophenol blue

LAAO Spectrophotometric Assay HRP-OPD Substrate Solution
5 mM amino acid
2 mM O-phenylenediamine
0.81 U/mL Horseradish peroxidase
In Tris-HCl pH 8.0

2.4 Standard Molecular and Microbiology Techniques

2.4.1 DNA manipulation

Standard molecular techniques were generally performed as described in Sambrook and Russell (2001). *A. nidulans* genomic DNA was isolated according to Lee and Taylor (1990). PCR products and restriction enzyme digest products were isolated from agarose gels or PCR reaction tubes by the Wizard SV Gel and PCR Clean Up System (Promega) following the manufacturer's instructions. Restriction enzyme digests (Promega), dephosphorylation with Arctic shrimp alkaline phosphatase (Promega), and ligations using the T4 DNA ligase (Promega) were performed according to the manufacturer's instructions. Plasmid DNA was isolated using the Wizard Plus SV Miniprep DNA Purification Kit (Promega) according to the manufacturer's instructions. DNA was separated on 1% agarose gels by electrophoresis in 1x TAE buffer. DNA was quantified using the Nanodrop One spectrophotometer (Thermo Scientific).

2.4.2 RNA isolation

Total RNA was isolated by adding TRIzol Reagent (ThermoFisher), RNA extraction buffer, β-mercaptoethanol, and chloroform to ground mycelia (Steyer 2022). After centrifugation, the supernatant was retained and subjected to a phenol-chloroform-isoamyl alcohol extraction with chloroform purification. RNA was precipitated with 2 M ammonium acetate and 50% isopropanol and incubated overnight at -20 °C. A second precipitation was performed with DEPC water and 4 M lithium chloride and incubated overnight at -20 °C. RNA was resuspended in DEPC water and stored at -80 °C. RNA bands were visualized by electrophoresis in a 1.2% agarose gel containing 1.1%

formaldehyde in 1x MOPS buffer. RNA concentration was determined using a Nanodrop One spectrophotometer (Thermo Scientific).

2.4.3 Polymerase chain reaction

PCR was performed using 0.3 μL Ex-Taq (TaKaRa), GoTaq Flexi (Promega), or GoTaq G2 (Promega) DNA polymerase according to the manufacturer's instructions. Template DNA quantity was usually 1 ng for DNA isolated from plasmids and 100 ng for genomic DNA. All reactions followed recommended denaturing, annealing, and extension conditions (~1 minute per 1000 bp) for 35 cycles. Primers were either self-designed and purchased from IDT or provided by the Fungal Genetics Stock Center with the relevant *A. nidulans* knockout constructs.

2.4.4 Southern blot

Southern Blot was conducted as outlined in Sambrook and Russell (2001). DNA samples were separated by electrophoresis on 1% agarose gels and treated with 0.25 M HCl for depurination. DNA was transferred to Hybond XL positively charged membranes (Amersham) using capillary transfer with 0.4 M NaOH. DNA was crosslinked to the membranes using the autocrosslinking settings on a UV Stratalinker 1800 (Stratagene). Probe generation, hybridization (42 °C overnight), and detection were performed using the DIG (Digoxigenin) High Primer DNA Labeling and Detection Starter Kit II (Roche) following the manufacturer's instructions. Films exposed to blots were developed in an Economax X-ray film processor (Protec).

2.4.5 SDS-PAGE

Soluble cell-free protein extracts were prepared by grinding 0.2 g of frozen mycelium in 2 mL 0.1M Tris-HCl ph8.0 with acid-washed glass beads (≤ 106 μm)

(Sigma) for 30 s with a mortar and pestle, followed by centrifugation for 10 m at 20,800 x *g* at 4˚C twice to pellet and remove the insoluble fraction. Protein concentrations were determined by Nanodrop or Bradford determination (BioRad). Protein extract samples containing equal amounts of protein in 1x LAAO in-gel assay sample buffer (lacking dithiothreitol) were not heat-treated before loading into 7.5% SDS-PAGE gels with 5% stacking gels, made in-house. Gels were run on an Enduro Modular Vertical Gel System (Labnet) in Tris-glycine buffer. The Spectra Multicolor Broad Range Protein Ladder (Thermo Fisher) was used as a protein size marker.

2.5 *Aspergillus* Genetic Manipulation Protocols

2.5.1 *Aspergillus nidulans* growth testing and genetic analysis

A. nidulans growth testing was performed as described in Pontecorvo et al. (1953). When testing ammonium as a nitrogen source, 10 mM ammonium tartrate was used. When testing alternative carbon sources in which ammonium served as the nitrogen source, 10 mM ammonium chloride was used. Fungal crosses and manipulations followed Todd et al. (2007b). Heterokaryon rescue analysis followed Osmani et al. (2006).

2.5.2 *Aspergillus nidulans* transformation

A. nidulans transformations were performed as in Andrianopoulos and Hynes (1988) with modifications described in Downes et al. (2013).

2.6 Gene Expression Characterization Protocols

2.6.1 RNA sequencing

Three biological replicates of total RNA were isolated as described above in Section 2.4.2. Libraries for RNA-seq were prepared and sequenced at the Kansas State

University Integrated Genomics Facility (Manhattan, Kansas, USA). Illumina NGS libraries were prepared using the TruSeq Stranded mRNA kit and sequenced using NextSeq high output single-end 75 cycles with a NextSeq500 Sequencing System.

2.6.2 Reverse Transcription-Quantitative PCR

RNA samples were treated with qScript cDNA SuperMix (Quanta Biosciences) to generate cDNA. cDNA was added to iTAQ Universal SYBR Green Supermix (Bio-Rad) and analyzed on a My iQ thermocycler with the iQ5 v.21 program (Bio-Rad). Fold change was calculated using the $\Delta\Delta C_T$ method (Pfaffl 2001; Schmittgen and Livak 2008). The β-tubulin gene *benA* was used as a reference housekeeping gene (May et al. 1987). Primers (IDT) were designed to amplify cDNA by overlapping a splice junction within the target gene.

2.7 Bioinformatics and *in silico* analyses

2.7.1 Sequence identification and analysis

DNA and protein sequences were obtained from FungiDB (fungidb.org; Alvarez-Jarreta et al. 2024) or the NCBI database (ncbi.nlm.nih.gov). InterPro Registry (IPR) and Pfam protein domains were predicted by querying databases at InterPro (ebi.ac.uk/interpro/; Blum et al. 2025). Transmembrane domain number and locations were predicted by DeepTMHMM (Hallgren et al. 2022). AlphaFold 3 (Abramson et al. 2024) and i-TASSER (Zhang 2008; Roy et al. 2010; Yang et al. 2015) provided 3D protein structure models. To predict the subcellular localization of proteins we used Psort II (Nakai and Horton 1999), DeepLoc 2.1 (Ødum et al. 2024), and LocTree3 (Goldberg et al. 2014). ER-retention sequences were predicted by Psort II.

2.7.2 Phylogenetic analysis

Candidate orthologs were identified from predictions found in the OrthoMCL database (orthomcl.org; Li et al. 2003; Chen et al. 2006, 2007; Fischer et al. 2011), OrthoDB (orthodb.org; Tegenfeldt et al. 2025), and references in the literature. Candidates were further evaluated through sequence alignments and presence of key features. Pairwise sequence alignments were performed with EMBOSS Needle (EMBL-EBI) with default parameters. Multiple sequence alignments were performed with Clustal Omega on the EMBL-EBI server (Sievers et al. 2011, 2020; Sievers and Higgins 2018) or MAFFT 7 for phylogenetic tree generation with 100 bootstraps (mafft.cbrc.jp; Kuraku et al. 2013; Katoh et al. 2019). Alignments were visualized using Jalview 2.11.4.1 (jalview.org; Waterhouse et al. 2009). Trees were visualized using Interactive Tree of Life (iTOL) 4 (itol.embl.de; Letunic and Bork 2024).

2.7.3 RNA sequencing analysis

RNA-seq analysis was performed using the Galaxy Platform 25.0.2 (usegalaxy.org; The Galaxy Community 2024). FastQC (Babraham Institute) was used to determine sequence read quality and reads were aligned to the *A. nidulans* version 5 genome sequence (provided by Adrian Tsang, Concordia University) using HISAT2 (Kim et al. 2019) with default settings. Differential expression analysis was performed in the SeqMonk Mapped Sequence Data Analyser 1.48.1 (Babraham Institute) using DESeq2 with the Benjamini-Hochberg (BH) false discovery rate (FDR) adjusted *p*-value of 0.05 (Love et al. 2014).

Chapter 3 - Identification of the *sarB* gene

3.1 Abstract

In *Aspergillus nidulans*, the transcription factor AreA regulates nitrogen utilization genes. The *areA102* pleiotropic altered function mutant shows increased growth on histidine as a nitrogen source. The *suppressor of areA102* mutants *sarA* and *sarB* suppress this strong growth on histidine. The *sarA* gene (AN2350) is characterized and encodes an L-amino acid oxidase (LAAO), but *sarB* has remained unidentified. Whole genome sequencing led to identification of AN8875 as a *sarB* candidate. To investigate if *sarB* is AN8875, transformation of the wild-type AN8875 gene into the *areA102 sarB7* strain was performed. Introduction of the AN8875 gene led to restoration of the AreA102 phenotype, indicating that AN8875 complemented the *sarB7* mutant phenotype. The AN8875 gene was deleted by homologous gene replacement. In a wild-type background, the AN8875Δ mutant showed no growth phenotype on histidine. An *areA102* AN8875Δ mutant was constructed by crossing, and this mutant phenocopied the weak growth on histidine characteristic of the *areA102 sarB7* mutant, indicating that deletion of the AN8875 gene suppressed the AreA102 strong growth on histidine phenotype. Transformation of the wild-type AN8875 gene into the AN8875Δ *areA102* mutant complemented the AN8875Δ mutant phenotype and restored the *areA102* mutant strong growth on histidine phenotype. These experiments provide strong evidence that *sarB* is AN8875.

AN8875 (*sarB*) encodes a putative uridine diphosphate (UDP)-N-acetylglucosamine (UDP-GlcNAc) transporter. Growth of *sarB* mutants on media containing GlcNAc did not differ from wild type. Because GlcNAc is the building block of

chitin, we stained *sarB* mutant hyphae with calcofluor white and found a similar distribution of chitin, but lower levels of fluorescence compared with the wild-type strain.

sarB is conserved in the fungal and animal kingdoms. A single gene copy is found in *A. nidulans* and nearly all fungal species surveyed. Protein sequence analysis predicts that SarB contains 10 transmembrane domains and is likely localized to the endoplasmic reticulum (ER) or Golgi. We identified an insertion located between transmembrane domains 7 and 8 in most fungal SarB orthologs outside of ascomycete yeasts. While the presence of the insertion is conserved, its sequence is not.

3.2 Contribution Statement

Sara M. Hopkins and Dr. Joel T. Steyer of the Richard Todd lab performed complementation experiments with multiple *sarB* candidate genes prior to whole genome sequencing. Sara M. Hopkins and Dr. Cameron C. Hunter deleted several of these genes and assessed whether they suppressed the *areA102* mutant phenotype on histidine. Dr. Joel T. Steyer performed whole genome sequencing analysis of the *areA102* and *areA102 sarB7* mutants.

3.3 Introduction

Mutations in the *A. nidulans* transcription factor gene *areA* can have strong impacts on nitrogen metabolism. The *areA102* mutant is characterized by pleiotropic changes in utilization of various nitrogen sources, such as enhanced growth on acetamide, normally a poor source of nitrogen (Hynes 1972). Poor growth of the *areA102* mutant on uric acid, normally a good source of nitrogen, was also observed (Arst and Scazzocchio 1975). Growth of the *areA102* mutant on the amino acids histidine and lysine, which are poor sources of nitrogen, was enhanced (Hynes 1973).

The *areA102* strain MH8 was mutagenized and several mutants with weaker growth on histidine were isolated, suggesting that these mutants carried mutations which suppressed the AreA102 histidine growth phenotype (Polkinghorne and Hynes 1975). These mutants mapped to two different genes, named "*suppressor of areA102*", *sarA* and *sarB* (Polkinghorne and Hynes 1975). The *sarA* gene was cloned by complementation and shown to encode an L-amino acid oxidase (LAAO) involved in utilization of a range of amino acids (Davis et al. 2005) (see Chapter 4). However, *sarB* remained unidentified.

The molecular mechanism underlying the AreA102 phenotype has been identified. An L683V amino acid substitution at a highly conserved position within the DNA-binding domain changes the DNA binding preference from HGATAR (where H = A, C, or T and R = G or A) to TGATAR (Kudla et al. 1990; Ravagnani et al. 1997). This causes higher affinity for some nitrogen utilization gene promoters, and lower affinity for others, of the mutant AreA102 protein compared with wild type AreA, leading to pleiotropic effects on nitrogen utilization.

Our lab has attempted to identify the *sarB* gene. Mutations in *sarB* were mapped to chromosome VII (Polkinghorne and Hynes 1975). In a subsequent mapping cross between a *sarB7* mutant and an *xprG1* gain-of-function mutant, only three of 1149 progeny were found to be double mutants (Katz et al. 2000). This suggests that *sarB* and *xprG* are located within 0.26 cM of each other on chromosome VII. In *A. nidulans,* the average physical to map distance ratio has been reported as 8.1 kilobase pairs (kbp) per cM across the genome and as 7.9 kbp per cM on chromosome VII (Christians et al. 2011). Therefore, *sarB* could be expected to lie within several kbp of *xprG*. Katz et

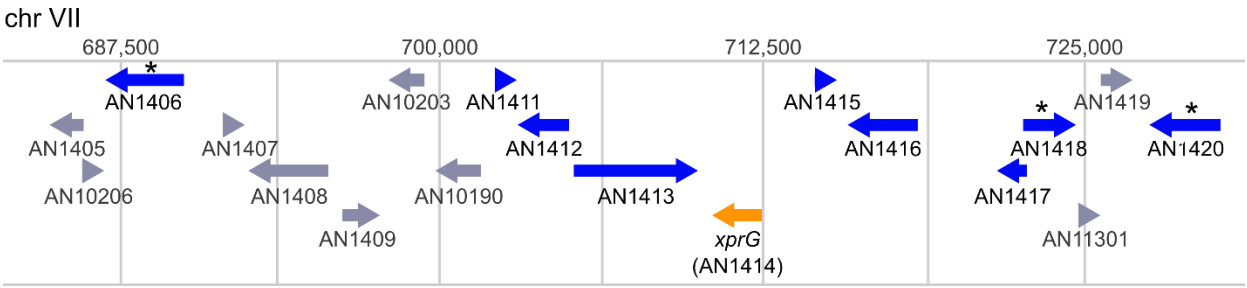

Figure 3.1 sarB *candidates were identified by chromosome walking from the* xprG *marker.*
xprG (in orange) and nine genes within 18 kbp upstream and 25 kbp downstream of *xprG* (in blue) on chromosome VII were transformed into MK160 (*areA102 sarB7*). Three genes, denoted with asterisks, and the predicted *sarA* paralog AN1808 (1250 kbp upstream of xprG) were also deleted and the mutants were crossed to MH8 (*areA102*) to observe the phenotype of the deletion in an *areA102* background.

al. (2006) considered whether the *sarB7* mutation might be allelic to *xprG.* However, a plasmid carrying the *xprG* gene failed to complement the *sarB7* phenotype upon introduction into an *areA102 sarB7* double mutant and sequence analysis of the *xprG* coding region in the *sarB7* mutant identified no mutations, indicating that *sarB7* is not an allele of the *xprG* gene (Katz et al. 2006). Other *sarB* candidate genes, identified by chromosome walking from *xprG* (which corresponds to AN1414 in the *A. nidulans* version 4 genome annotation), were assessed for the ability to complement the *sarB7* mutant histidine growth phenotype (Figure 3.1; S.M. Hopkins, J.T.Steyer and R.B. Todd, unpublished data). *xprG* and nine other candidate *sarB* genes (AN1406, AN1411, AN1412, AN1413, AN1415, AN1416, AN1417, AN1418, and AN1420) were each PCR-amplified and separately transformed into the *areA102 sarB7* double mutant MK160. All candidates failed to yield complementing transformants following direct selection for stronger growth on histidine (S.M. Hopkins, J.T. Steyer and R.B. Todd, unpublished data). Furthermore, four genes (AN1406, AN1418, and AN1420, which are near *xprG*, and a second LAAO-encoding gene, AN1808, which is also located on chromosome VII) were deleted, and the deletion mutants were crossed to the *areA102* mutant to produce double mutants. None showed suppression of the AreA102 histidine growth

phenotype in the progeny, indicating that the candidates were not *sarB* (S.M. Hopkins, C.C. Hunter and R.B. Todd, unpublished data). *xprG* (and therefore *sarB7*) are proximal to the chromosome VII centromere (Katz et al. 2006). Discrepancies between genetic and physical map distance have been reported near the centromeres of *A. nidulans* chromosomes III and IV due to reduced recombination near the centromere (Espeso et al. 2005). We therefore considered that the *sarB7* mutation may be a greater physical distance from *xprG* than the tight linkage suggests. This chapter describes an alternative approach using whole genome resequencing to identify the *sarB* gene. We provide robust evidence through complementation and construction of a deletion mutant by gene replacement that *sarB* corresponds to the gene AN8875. We reannotate AN8875 and characterize the *sarB* gene.

3.4 Materials and Methods

3.4.1 Whole genome sequencing

Whole genome sequencing of MH8 and MK160 genomic DNA and analysis were performed by Dr Joel T. Steyer and are described in Steyer (2022).

3.4.2 Strains

Strains used in Chapter 3 are found in Table 3.1.

Table 3.1 *A. nidulans* strains used in Chapter 3.

Strain	Genotype
MH1	*biA1*
MH8	*biA1 areA102 niiA4*
MH11068	*pyrG89 pyroA4 amdA7 nkuA*Δ*::Bar*
MK160	*biA1 areA102 sarB7 niiA4*
RT855	*pyrG89 pyroA4* AN8875Δ::*AfpyrG+ amdA7 nkuA*Δ*::Bar*
RT856	*pyrG89 pyroA4* AN8875Δ::*AfpyrG+ amdA7 nkuA*Δ*::Bar*
RT857	*pyrG89 pyroA4* AN8875Δ::*AfpyrG+ amdA7 nkuA*Δ*::Bar*
RT858	*pyrG89 pyroA4* AN8875Δ::*AfpyrG+ amdA7 nkuA*Δ*::Bar*
RT859	*pyrG89 pyroA4* AN8875Δ::*AfpyrG+ amdA7 nkuA*Δ*::Bar*

RT890	*areA102 pyroA4* AN8875Δ::*AfpyrG+*
RT891	*biA1 areA102* AN8875Δ::*AfpyrG+ niiA4*
RT892	*areA102* AN8875Δ::*AfpyrG+*
RT893	*biA1 areA102* AN8875Δ::*AfpyrG+ niiA4*
RT927	*biA1 areA102 sarB7 niiA4* AN8875c*
RT928	*biA1 areA102 sarB7 niiA4* AN8875c*
RT929	*biA1 areA102 sarB7 niiA4* AN8875c*
RT930	*biA1 areA102 sarB7 niiA4* AN8875c*
RT931	*biA1 areA102 sarB7 niiA4* AN8875c*
RT943	*biA1 areA102 pyroA4* AN8875Δ::*AfpyrG+ niiA4*
RT944	*biA1 areA102 pyroA4* AN8875Δ::*AfpyrG+*
RT945	*areA102* AN8875Δ::*AfpyrG+ niiA4*
RT946	*biA1 areA102* AN8875Δ *niiA4 nkuA*Δ*::Bar*
RT947	*biA1 areA102 niiA4 sarB7* AN8875c*
RT948	*biA1 areA102 niiA4 sarB7* AN8875c*
RT949	*biA1 areA102 niiA4 sarB7* AN8875c*
RT950	*biA1 areA102 niiA4 sarB7* AN8875c*
RT951	*biA1 areA102 niiA4 sarB7* AN8875c*
RT952	*biA1 areA102 niiA4 sarB7* AN8875c*
RT953	*biA1 areA102 niiA4 sarB7* AN8875c*
RT954	*biA1 areA102 niiA4 sarB7* AN8875c*
RT955	*biA1 areA102 niiA4 sarB7* AN8875c*
RT957	*biA1 areA102 niiA4*
RT958	*areA102*
RT960	*biA1 areA102 niiA4*
RT971	*biA1 areA102* AN8875Δ::*AfpyrG niiA4* AN8875c*
RT972	*biA1 areA102* AN8875Δ::*AfpyrG niiA4* AN8875c*
RT973	*biA1 areA102* AN8875Δ::*AfpyrG niiA4* AN8875c*
RT974	*biA1 areA102* AN8875Δ::*AfpyrG niiA4* AN8875c*
RT975	*biA1 areA102* AN8875Δ::*AfpyrG niiA4* AN8875c*

* “c” denotes integration of a plasmid containing the indicated gene.

3.4.3 PCR primers

Genomic PCR primers used in Chapter 3 are found in Table 3.2.

Table 3.2 Genomic PCR primers used in Chapter 3.

Target	Primer Name	Sequence (5’ → 3’)
AN8875	AN8875_outside_5’F	GGCCTACTCTTCTCTCTTCC
	AN8875_outside_3’R	GCACTCTATTGACACACCAC
	AN8875_inside_5’F	GGCCTACTCTTCTCTCTTCC
	AN8875_inside_3’R	GCACTCTATTGACACACCAC

ANID_08875.1_5'F	GTAACGCCAGGGTTTTCCCAGTCACGACGGGCCTACTCTTCTCTCTTCC
ANID_08875.1_3'R	GCGGATAACAATTTCACACAGGAAACAGCGCACTCTATTGACACACCAC

3.4.4 Plasmid construction

The pHF273 and pHF275 plasmids (Table 3.3) were constructed by cloning the AN8875 gene (-874 to +2475) PCR product amplified from wild type (MH8) and from the *areA102 sarB7* mutant (MK160), respectively, into the pGEM-T Easy vector (Promega).

Table 3.3 Plasmids used in Chapter 3.

Plasmid name	Insert	Backbone
pHF273	AN8875 wild type	pGEM-T Easy
pHF275	AN8875 *sarB7*	pGEM-T Easy

3.4.5 Complementation of the *sarB7* mutation

The wild-type AN8875 gene (-874 to +2475) from the wild-type strain (MH1) was PCR amplified from genomic DNA and transformed into the *areA102 sarB7* mutant (MK160) using the transformation protocol described in Downes et al. (2013). We separately transformed the wild-type AN8875 gene (-874 to +2475) PCR amplified from the *areA102* strain (MH8) and the pHF273 plasmid containing the AN8875 gene from MH8 into the *areA102 sarB7* mutant. As a negative controls, we transformed the mutant AN8875 gene (-874 to +2475) PCR-amplified from the *areA102 sarB7* mutant and the pHF275 plasmid containing the AN8875 mutant gene (see Section 3.4.4) into MK160. Transformants were directly selected for restoration of the AreA102 phenotype of strong growth on protoplast media containing 10 mM histidine as the sole nitrogen source.

Plasmid integration was confirmed through Southern blotting (see Section 2.4.4), using the linear AN8875 wild type gene amplified from pHF273 as a probe. Five transformants (RT947, RT948, RT950, RT951, RT952) were assessed using single restriction digests of genomic DNA with *Bst*XI, *Pst*I, and *Sal*I.

3.4.6 Strain construction

Construction of AN8875 deletion mutants

AN8875Δ mutants (RT855-RT859; Δ -18 to +1508) were constructed using the AN8875Δ::*AfpyrG* knockout construct made in the *A. nidulans* knockout project by De Souza et al. (2013) and obtained from the Fungal Genetics Stock Center, Manhattan, Kansas (McCluskey et al. 2010). Briefly, the construct consisted of the *Aspergilus fumigatus pyrG* (*AfpyrG*) gene selectable marker, flanked by sequences 850 bp upstream and 637 bp downstream of AN8875, which allowed for gene replacement by homologous recombination in a *nkuA*Δ non-homologous end-joining mutant recipient (Nayak et al. 2006). Transformation into a recipient with the *pyrG89* mutation allowed selection of transformants for pyrimidine prototrophy (Oakley et al. 1987a). Knockout construct integration was confirmed using PCR by observing presence of a band the size of the construct (1.7 kbp) in the transformants RT855-RT859. The expected band size of the wild-type gene seen in the wild-type control was 1.55 kbp.

Construction of the *areA102* AN8875Δ mutant

An AN8875Δ mutant (RT855) was crossed with an *areA102* strain (MH8) using protocols described in Todd et al. (2007b). Progeny with the *areA102* allele were identified by poor growth on uric acid. *areA102* progeny with the AN8875 deletion were detected by weak growth on histidine. Several progeny of each class were confirmed as

AN8875Δ or AN8875 wild type by PCR. To confirm the results of the first cross, a second cross was performed using an independent but identical AN8875Δ homologous gene-replacement transformant (RT856).

Complementation of the deletion mutant phenotype

The pHF273 plasmid was transformed into an *areA102* AN8875Δ strain recipient (RT891). Transformants were directly selected for increased growth on histidine (Figure 3.4A). Southern blotting was used to confirm plasmid integration for five transformants (RT971-RT975) using AN8875 PCR product amplified from pHF273 as a probe, following single restriction digests of genomic DNA by *BstX*I, *Pst*I, and *Sal*I.

3.4.7 Analysis of *sarB* gene expression

RNA was isolated from a wild-type strain (MH11068) and from a *nmrA*Δ mutant (RT851) and sequenced, and the data analyzed as described in Chapter 2. To assess the role of nitrogen source in regulation of *sarB*, gene expression under glutamine, alanine, and nitrogen starvation conditions were each independently compared to expression on ammonium within each strain. Additionally, expression under each condition was compared between the two strains.

3.4.8 Sequence analysis of SarB

SarB sequence analyses were performed using the 459-amino acid predicted protein sequence based on the version 5 AN8875 gene annotation. InterPro Registry (IPR) and Pfam protein domains were predicted by querying databases at InterPro (ebi.ac.uk/interpro/; Blum et al. 2025). SarB transmembrane domain number and locations were predicted by DeepTMHMM (Hallgren et al. 2022). AlphaFold 3 (Abramson et al. 2024) and i-TASSER (Zhang 2008; Roy et al. 2010; Yang et al. 2015)

provided 3D protein structure models. To predict the subcellular localization of SarB we used Psort II (Nakai and Horton 1999), DeepLoc 2.1 (Ødum et al. 2024), and LocTree3 (Goldberg et al. 2014). ER-retention sequences were predicted by Psort II.

3.4.9 Phylogenetic analysis of SarB

Candidate *sarB* orthologs were identified from predictions found in the OrthoMCL database (orthomcl.org; Li et al. 2003; Chen et al. 2006, 2007; Fischer et al. 2011) and OrthoDB (orthodb.org; Tegenfeldt et al. 2025), protein BLAST of the version 5 AN8875 sequence against the FungiDB (fungidb.org) and NCBI (ncbi.nlm.nih.gov) databases, and references in the literature. These candidates were evaluated through sequence alignments with the version 5 AN8875 protein sequence and presence of the PF08449 (UAA transporter family) protein domain.

Pairwise global sequence alignments and calculations of sequence identity and similarity were performed using EMBOSS Needle (ebi.ac.uk/jdispatcher/psa/emboss_needle). Sequence alignments for comparing sequences were performed using Clustal Omega (ebi.ac.uk/jdispatcher/msa/clustalo; Sievers et al. 2011, 2020; Sievers and Higgins 2018) and visualized using Jalview 2.11.4.1 (jalview.org; Waterhouse et al. 2009). Sequence alignments for generating phylogenetic trees were performed using the neighbor joining method MAFFT 7 (mafft.cbrc.jp/alignment/software; Kuraku et al. 2013; Katoh et al. 2019) with 100 bootstraps. Trees were visualized in the Interactive Tree of Life (iTOL) 4 (itol.embl.de; Letunic and Bork 2024).

3.4.10 Calcofluor white staining and microscopy

Wild-type (MH1) and *sarB*Δ (RT855) colonies were grown on complete media for 48 h at 37°C. Conidia from one colony were suspended in 500 µl Tween 80, vortexed, then 5 µl was inoculated to one well of a six-well plate containing supplemented glucose-ammonium minimal media and a cover slip, The plate was incubated for 24 h at 25°C. The cover slip, on which conidia had settled and germinated, was mounted over 5 µL of 1 mg/ml calcofluor white and 5 µL of mounting medium containing 10 mg/ml 1,4-diazabicyclo[2,2,2]octane (DABCO) dissolved in 100% glycerol on a sterile slide and observed under the microscope. Direct UV fluorescence microscopy was performed using an Olympus BX51 upright biological reflected fluorescence microscope equipped with Nomarski differential interference contrast (DIC), an EXFO X-Cite 120Q fluorescence illumination system, and a UPlanFLN Plan Semi Apochromat (field number FN26.5) Fluorite 100 oil objective (numerical aperture: 1.30). Calcofluor fluorescence was detected using a BrightLine DAPI (4, 6-diamidino-2-phenylindole) Hi Contrast filter set (excitation wavelength band pass, 387/11 nm; dichroic mirror, 409 nm; ZPIXEL). Images were captured using an Olympus DP72 12.8 Megapixel digital color camera and DP2-BSW digital camera software. Raw images are presented without adjustments to the tonal range.

3.5 Results

3.5.1 Identification of AN8875 as a *sarB* candidate

Whole genome sequencing of genomic DNA from the *areA102* parent (MH8) and the *areA102 sarB7* mutant (MK160) was performed, and sequence differences of the two strains compared with the *A. nidulans* version 5 reference genome sequence

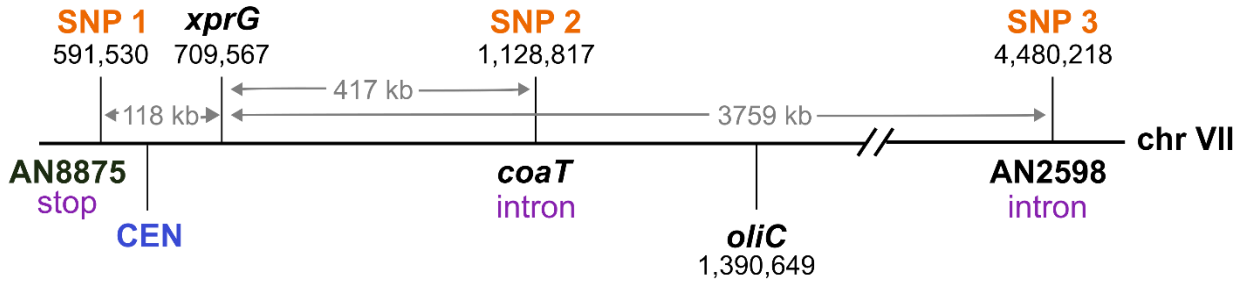

Figure 3.2 Whole genome sequencing identified three sarB7 *candidate SNPs*.
MH8 (*areA102*) and MK160 (*areA102 sarB7*) were whole genome sequenced and SNPs were compared to the wild-type reference sequence. Three SNPs (SNP1 (G to A), SNP2 (C to T), SNP3 (G to A)) on chromosome VII unique to MK160 are shown with their sequence coordinates from the left telomere. The centromere (CEN) is indicated. Both SNP2 and SNP3 were predicted to be in the introns of the genes in which they were located, whereas SNP1 was predicted to cause a nonsense truncation mutation in the reannotated AN8875 gene.

(provided pre-publication by Prof. Adrian Tsang, Concordia University) on chromosome VII were identified (J.T. Steyer and R.B. Todd, unpublished data). After removal of low-quality variants (quality score <30), three single nucleotide polymorphisms (SNPs) specific to MK160 remained as potential *sarB* candidate causative mutations (Figure 3.2). The SNPs were evaluated for both their proximity to *xprG* and the type of change they were predicted to produce in the genes in which they reside. The SNPs were located at positions 591530, 1128817, and 4480218, all exceeding the recombination-based map distance predicted from *xprG* (AN1414), at position 709567. Previous work showed that the gene *oliG*, located at position 1390649, is not linked to *xprG* (Katz et al. 2000). Because the SNP at 4480218 was far distal to this marker, it was unlikely to be *sarB*. The centromere is located between the SNP at 591530 and *xprG*. Because there is little recombination near centromeres, the physical distance between genes in such regions generally exceeds predicted map distances (Espeso et al. 2005) and thus the SNP at 591530 was a strong *sarB* candidate.

The SNPs at positions 1128817 (within the *coaT* gene, AN1547) and 4480218 (within AN2598) were predicted to be in introns and thus were unlikely to cause a

phenotype. The SNP at 591530 lies within the reannotated (see Section 3.5.2 below) uncharacterized gene AN8875 and introduces a stop codon at W148 via a G to A substitution at +604. Based on the SNP location and the predicted effect, AN8875 was the most likely *sarB* candidate.

3.5.2 Reannotation of the AN8875 gene

The *A. nidulans* genome sequence version 5 reannotation provided by A. Tsang (Concordia University) is improved based on stranded RNA-seq data (Steyer et al. 2021; D.J. Downes and R.B. Todd, unpublished data) and resulted in reannotation of the AN8875 gene structure (Figure 3.3A). When compared with the version 4 annotation, the second intron is lengthened from 34 bp to 53 bp, resulting in a shorter third exon, from 36 to 17 bp (Figure 3.3B-C). Additionally, the third intron is shortened from 326 to 55 bp and the fourth intron was eliminated, resulting in a longer final exon. The gene structure represented by the new annotation is conserved in aspergilli and is supported by existing RNA-seq data in multiple species, including *A. nidulans*. The version 4 annotation predicts a 345 amino acid-long protein, whereas the version 5 annotation predicts a protein length of 459 residues. These changes impact interpretation of the predicted effects of the *sarB7* mutation. Under the *A. nidulans* version 4 annotation, the mutation at position 591530 occurs in an intron within AN8875. However, in the version 5 reannotation it falls within the fourth exon and confers a nonsense mutation resulting in protein truncation at amino acid 148 in the predicted 459-residue protein. Our success in experimentally establishing AN8875 as *sarB*, described below, provides additional evidence that the AN8875 reannotation represents the correct gene structure.

A

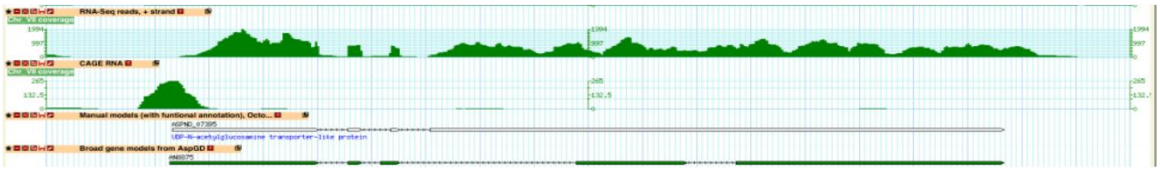

B

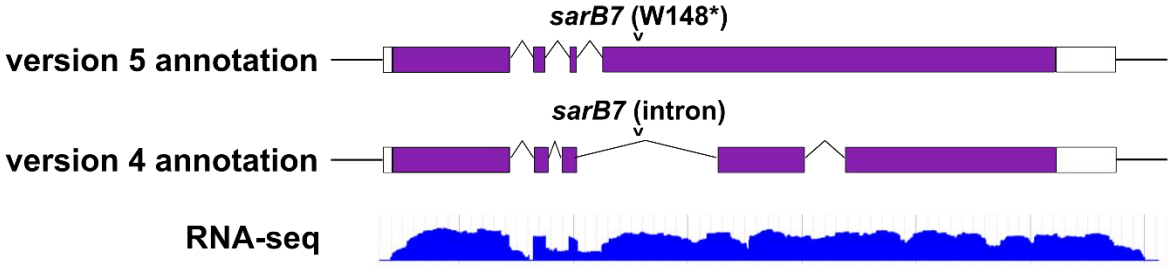

C

Feature	Version 5 AN8875 annotation	Version 4 AN8875 annotation
5' UTR	-22..0	-22..0
Exon 1	+1..+276	+1..+276
Intron 1	+277..+329	+277..+329
Exon 2	+330..+355	+330..+355
Intron 2	+356..+408	+356..+389
Exon 3	+409..+425	+390..+425
Intron 3	+426..+480	+$426..+751
Exon 4	+481..+1541	+752..+955
Intron 4	-	+956..+1045
Exon 5	-	+1046..+1541
3' UTR	+1542..+1683	+1542..+1683

Figure 3.3 Reannotation of AN8875.
(A) The reannotation genome browser for AN8875 shows combined RNA-seq data, CAGE-seq data of transcription start sites, and the version 5 reannotation and version 4 annotation gene models. (B) Gene models are shown for clarity against RNA-seq data for growth on the repressing nitrogen source glutamine (Steyer et al. 2022). (C) Coordinates for the version 4 and new AN8875 gene model features are shown.

3.5.3 Cloning of the *sarB* gene by complementation

To investigate if *sarB* is AN8875, we initially PCR-amplified the wild-type AN8875 gene from MH1 (*areA*+ *sarB*+), transformed it into the MK160 (*areA102 sarB7*) mutant, and directly selected transformants for enhanced growth on histidine (Figure 3.4A). Sixteen transformants were obtained and all exhibited the AreA102 phenotypes of strong growth on histidine and lysine as sole nitrogen sources (Figure 3.4B). We also

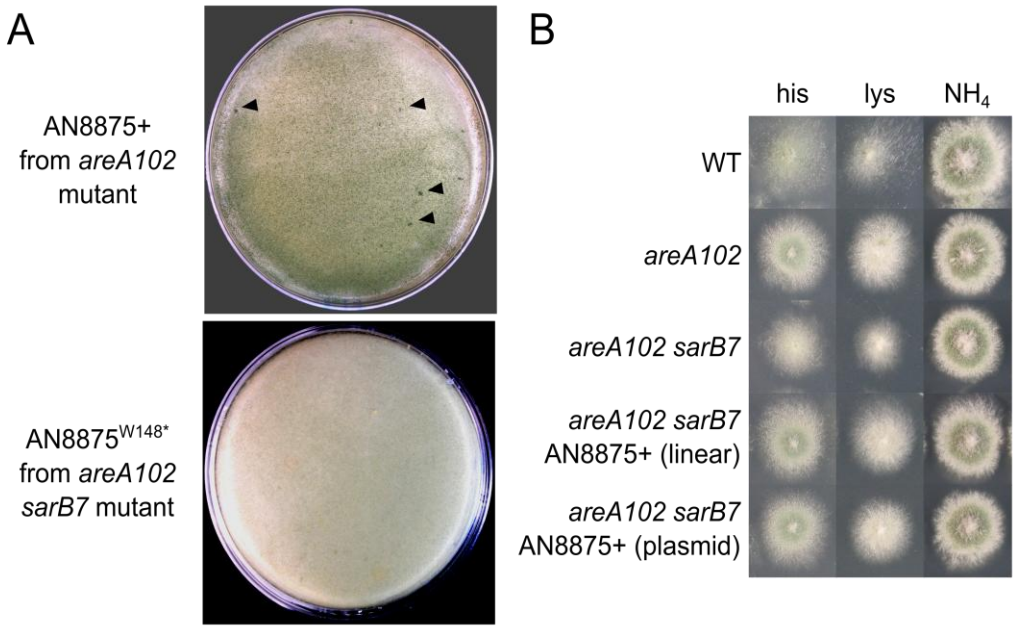

Figure 3.4 The wild-type AN8875 gene complemented the sarB7 *mutant phenotype*.
(A) PCR-amplified AN8875 from the *areA102* mutant (MH8; i.e. wild-type AN8875) or from the *areA102 sarB7* mutant (MK160) were transformed into MK160 and transformants were directly selected for growth on histidine as a sole nitrogen source after 72 h at 37ºC. Transformants were recovered only for the wild-type transforming DNA. (B) Complementing transformants with PCR-amplified wild-type AN8875 ("linear") DNA or pHF273 containing the wild-type AN8875 gene ("plasmid") integrated into the MK160 genome restored the AreA102 phenotypes of strong growth on histidine and on lysine as a sole nitrogen source. Strains of indicated genotypes were grown on supplemented 1% glucose-minimal media containing 10 mM nitrogen source for 48 h at 37ºC. Top to bottom: MH1, MH8, MK160, RT927, RT947.

transformed MK160 using the wild-type AN8875 gene PCR-amplified from MH8 (*areA102 sarB+*), the parent strain of MK160. Twenty transformants were obtained, all of which showed the AreA102 strong growth phenotypes on histidine and lysine media. As a control we transformed the PCR-amplified AN8875^{W148*} mutant gene from MK160. No transformants were recovered following selection on histidine media (Fig. 3.4A). We then cloned the wild-type AN8875 gene PCR-amplified from MH8 and the AN8875^{W148*} mutant gene from MK160 into pGEM-T Easy. The resultant plasmids, pHF273 (wild-type AN8875) and pHF275 (AN8875^{W148*}), were transformed into MK160 and transformants were directly selected for increased growth on histidine. Seven transformants were obtained with pHF273 and all exhibited the AreA102 phenotypes of strong growth on histidine or lysine as a sole nitrogen source (Fig. 3.4B). No

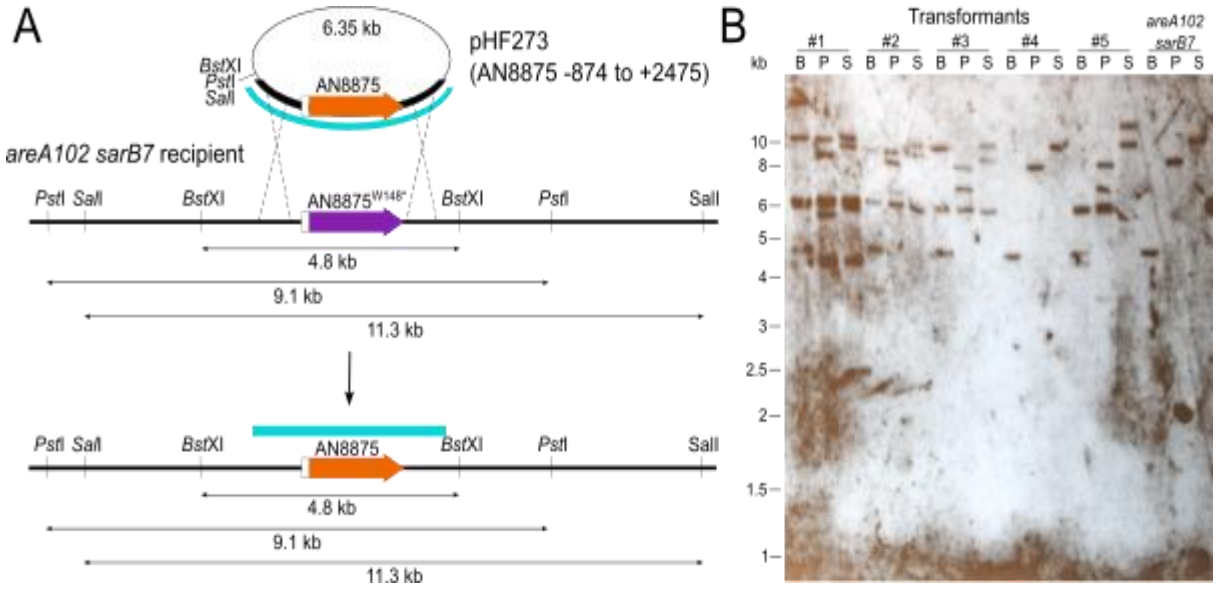

Figure 3.5 Southern analysis confirmed integration of wild-type AN8875 into the areA102 sarB7 *mutant genome*. The plasmid pHF273 containing the wild-type AN8875 gene was transformed into MK160 (*areA102 sarB7*). Single restriction digests of genomic DNA from five transformants were performed with *Bst*XI (B), *Pst*I (P), and *Sal*I (S). (A) Predicted band sizes for integration of the pHF237 insert, carrying AN8875, into MK160 by double homologous recombination. White boxes indicate UTRs, thick black lines indicate genomic DNA, and the cyan bars represent the probe. Note that integration may occur by homology or ectopically (not shown). (B) MK160 had only bands of the sizes predicted for a single copy of AN8875. Transformants 1, 2, 3, and 5 had multiple bands indicative of ectopic integrations of the plasmid, including the same bands as the recipient and bands the same size as the plasmid, indicating tandem repeat integrations. Transformant 4 had only the same bands as the recipient, indicating integration occurred by double homologous recombination.

transformants were obtained with the pHF275 plasmid containing the AN8875^{W148*} mutant gene. Together, these transformation experiments indicate that the wild-type AN8875 gene, but not the mutant AN8875^{W148*} gene, complemented the *sarB7* mutant phenotype.

To confirm integration of pHF273 into the genome, Southern blot analysis was performed. Genomic DNA from five complementing transformants was restriction digested separately with *Bst*XI, *Pst*I, and *Sal*I. The wild-type AN8875 gene PCR-amplified from pHF273 was used as a probe (Figure 3.5A). The recipient control

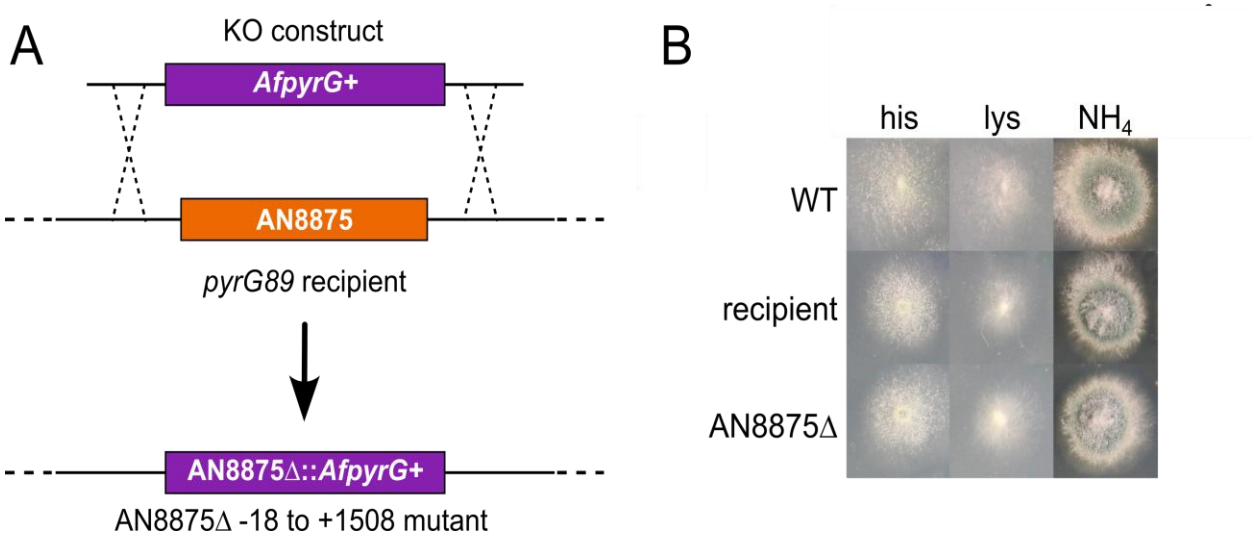

Figure 3.6 Deletion of AN8875 phenocopies the sarB7 mutant phenotype.
(A) Deletion mutants were constructed by transforming a knockout construct containing the *Aspergillus fumigatus pyrG* gene (*AfpyrG*+) into a *nkuA*Δ *A. nidulans* recipient and integration by homologous recombination. (B) The AN8875Δ mutant did not have a discernable growth phenotype on histidine or lysine as a sole nitrogen source. Strains of the indicated genotype were grown on supplemented 1% glucose-minimal media containing 10 mM nitrogen source and incubated for 48 h at 37ºC. Top to bottom: (B) MH1, MH11068, RT855; (C) MH1, MH8, MK160, RT891.

(MK160) showed only bands of the sizes predicted from the presence of the AN8875^{W148*} mutant gene, which does not differ from wild type (Figure 3.5B). Four transformants (Transformants 1, 2, 3, and 5) had the recipient bands and multiple additional bands indicating ectopic integrations of the plasmid, including a band corresponding to the size of the plasmid representing tandem repeat integrations. One transformant (Transformant 4) had only the same bands as the recipient, indicating that integration occurred by homologous gene replacement.

3.5.4 Deletion of AN8875 phenocopies the *sarB7* mutant phenotype

To determine the *sarB* complete loss-of-function phenotype, we deleted the AN8875 gene by transforming the AN8875Δ::*AfpyrG*+ knockout construct obtained from the FGSC into a *pyrG89* recipient strain MH11068 (*pyrG89 nkuA*Δ) (Figure 3.6A) and selecting for growth without pyrimidine supplementation. Five transformants were chosen for further analysis and were confirmed by PCR to have the correct gene

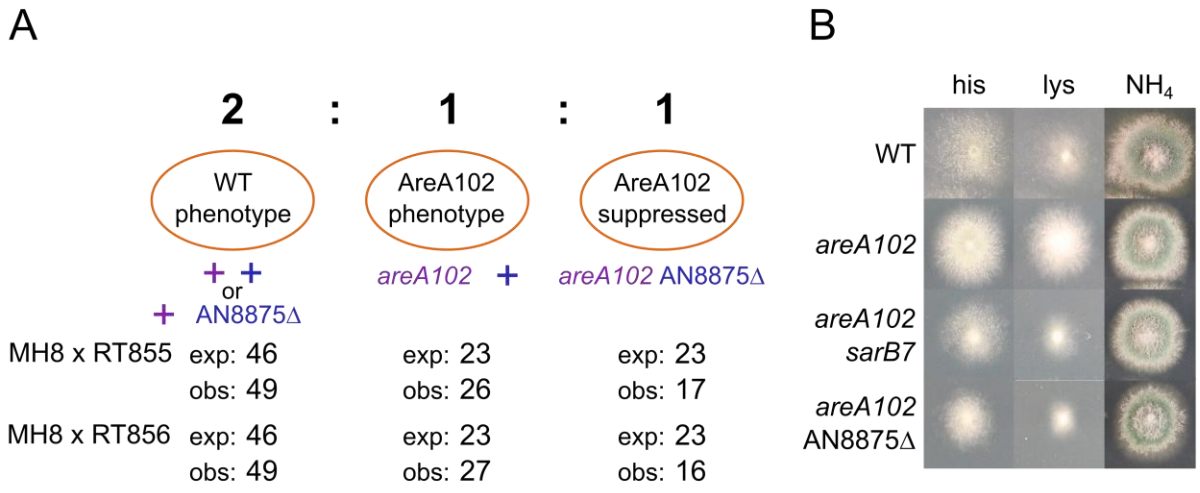

Figure 3.7 The areA102 *AN8875Δ mutant phenocopies the* areA102 sarB7 *mutant on histidine and lysine*. (A) An AN8875Δ mutant was crossed to the MH8 *areA102* mutant. As predicted by Mendelian genetics for haploid organisms, phenotypic classes conformed to the expected 2:1:1 ratio (MH8 x RT855: $\chi^2 = 2.2$; df = 2; $p = 0.34$; MH8 x RT856: $\chi^2 = 2.9$; df = 2; $p = 0.24$). Expected (exp.) and observed (obs.) data for two crosses are shown. (B) Like the *sarB7* mutation, the AN8875Δ mutation suppressed the AreA102 phenotype of strong growth on histidine or lysine as a sole nitrogen source. Strains of the indicated genotypes were grown on supplemented 1% glucose-minimal media containing 10 mM nitrogen source and incubated for 48 h at 37ºC. Top to bottom: MH1, MH8, MK160, RT891.

replacement of AN8875 (data not shown). These AN8875Δ mutants, similar to wild type, showed poor growth on histidine or lysine as sole nitrogen sources (Figure 3.6B).

To assess whether the AN8875Δ mutation suppressed the AreA102 strong growth on histidine phenotype, we crossed an AN8875Δ mutant (RT855) with MH8 (*areA102*). Based on Mendelian genetics for haploid organisms, we predicted half of the progeny to be *areA102,* and half of the *areA102* progeny to be AN8875+ and half AN8875Δ (Fig 3.7A). If *sarB* is AN8875, the AN8875Δ mutation should suppress the AreA102 phenotype. Out of 92 progeny resulting from the cross, 49 progeny had the AreA+ phenotype of strong growth on uric acid as a sole nitrogen source, while 43 showed weak growth on uric acid expected for the *areA102* progeny. Of the *areA102* progeny, 26 showed the Are102 strong growth phenotype on histidine as a sole nitrogen source, but 17 had weak growth, indicating suppression of the Are102 phenotype. This

observed phenotypic ratio (49 AreA+:26 AreA102:17 AreA102 suppressed) was not significantly different from the ratio expected if deletion of AN8875 suppresses the AreA102 phenotype of strong growth on histidine (46 AreA+:23 AreA102:23 Are102 suppressed; $\chi^2 = 2.152$ *df* = 2, *p* = 0.3409) (Figure 3.7B). Three progeny assessed as *areA102* AN8875Δ through growth tests were confirmed to contain AN8875Δ::*AfpyrG*+ using PCR (data not shown). Three progeny which growth tested as *areA102* AN8875+ were confirmed by PCR to carry the wild-type AN8875 gene. The cross to MH8 was replicated using a second AN8875Δ mutant (RT856). Of 92 progeny examined, 49 showed the AreA+ phenotype and 43 showed the AreA102 decreased growth phenotype on uric acid as a nitrogen source. Of the *areA102* progeny, 27 showed strong growth on histidine, while 16 showed weak growth, indicating suppression of the AreA102 growth phenotype. As with the first cross, the observed phenotypic ratio (49 AreA+:27 AreA102:16 AreA102 suppressed) was not significantly different from the ratio expected if deletion of AN8875 suppresses the AreA102 phenotype of strong growth on histidine ($\chi^2 = 2.870$, *df* = 2, *p* = 0.2382). These crosses showed that the AN8875Δ mutation suppresses the AreA102 histidine growth phenotype in a manner similar to the *sarB7* mutation.

To restore the wild-type phenotype in a AN8875Δ strain, we transformed the wild-type AN8875 plasmid pHF273 into an *areA102* AN8875Δ mutant (RT891) and directly selected transformants for increased growth on histidine. Forty-six transformants exhibited restoration of the wild type AreA102 phenotype of strong growth on histidine or lysine as a sole nitrogen source (Figure 3.8A). To confirm integration of pHF273, single restriction digests of genomic DNA from five transformants were performed using

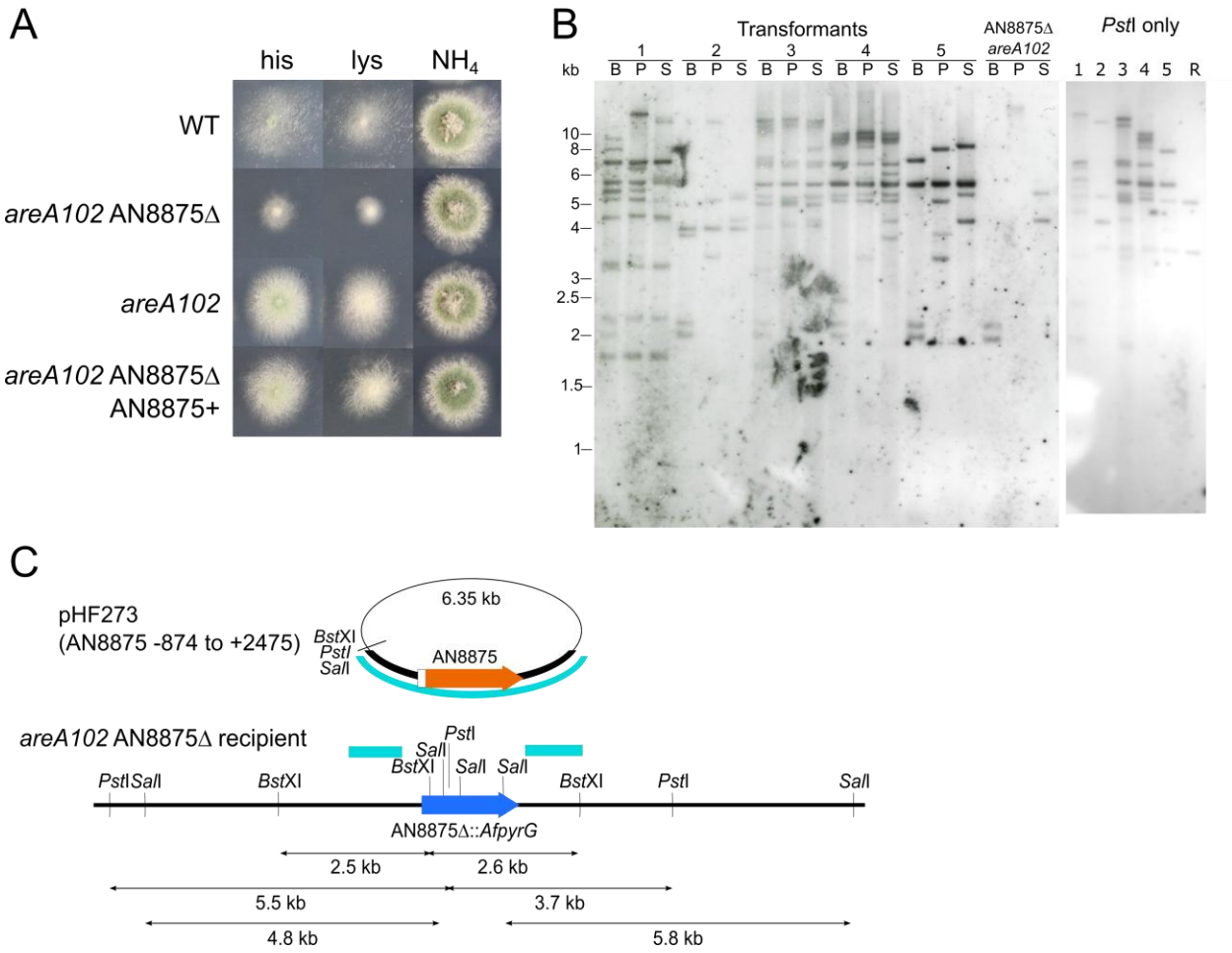

Figure 3.8 The wild-type AN8875 gene complemented the AN8875Δ deletion phenotype.
(A) The pHF273 plasmid containing the wild-type AN8875 gene was transformed into RT891 (*areA102* AN8875Δ), resulting in restoration of the AreA102 phenotype of strong growth on histidine and on lysine. Strains of the indicated genotypes were grown on supplemented 1% glucose-minimal media containing 10 mM of the indicated nitrogen source and incubated for 48 h at 37ºC. Top to bottom: MH1, RT891, MH8, RT971. (B) Single digests of genomic DNA from five transformants were performed with *Bst*XI (B), *Pst*I (P), and *Sal*I (S). Southern blotting using the wild-type AN8875 gene PCR-amplified from pHF273 as a probe showed the recipient contained only bands predicted for the AN8875Δ::AfpyrG gene replacement, depicted in (C). Transformants 2, 3, 4, and 5 showed multiple bands indicating that they contained ectopic integrations of the plasmid, with 3, 4, and 5 also containing a band the size of the plasmid, indicating tandem repeat integrations. Transformant 1 had a band pattern suggesting complex integration including a single homologous crossover on the 3' flank of the AN8875Δ::*AfpyrG* construct. Because the *Pst*I control DNA did not cut properly, a second the blot for the *PstI* single digests was performed. The recipient (R) had bands expected for the AN8875Δ::*AfpyrG* construct, and transformants had bands identical to those seen in the first blotting experiment. In (C), white boxes indicate UTRs, thick black lines indicate genomic DNA, and the cyan bars represent the probe.

*Bst*XI, *Pst*I, and *Sal*I. Southern blot analysis, using the AN8875 wild-type gene PCR-amplified from pHF273 as a probe, showed that the RT891 recipient had only bands predicted for the AN8875Δ::*AfpyrG* gene replacement (Figure 3.8B-C). Four transformants (Transformants 2, 3, 4, and 5) showed the recipient bands and multiple

additional bands, indicating that they contained ectopic integrations of the plasmid, with three of them (Transformants 3, 4, and 5) also containing a band the size of the plasmid, indicating tandem repeat integrations. Transformant 1 had a band pattern suggesting complex integration including a single homologous crossover on the 3' flank of the AN8875Δ::*AfpyrG* knockout. Because *Pst*I did not cut in the control, a second experiment was performed using a *Pst*I single digest only. The resulting blot showed that the control had the bands expected for the AN8875Δ::*AfpyrG* deletion, while all results for the transformants were the same as in the original blot.

At the conclusion of these experiments and analyses, we had three strong pieces of evidence that *sarB* is AN8875: 1) A nonsense truncation mutation found in the *sarB7* mutant lies within the coding region of the reannotated AN8875 gene; 2) AN8875 complements the *sarB7* mutant phenotype; and 3) The *areA102* AN8875Δ mutant phenocopies the *areA102 sarB7* mutant. Thus, we will refer to AN8875 as *sarB*.

3.5.5 *sarB* is constitutively expressed

To determine the *sarB* expression profile we examined publicly available RNA-seq datasets and RNA-seq datasets generated in the Todd lab at Kansas State University. In this study, *sarB* expression levels in a wild-type strain indicated constitutive expression across repressing (ammonium, glutamine) and de-repressing (alanine, nitrogen starvation) nitrogen regimes (Figure 3.9). Differences between the ammonium treatment and the other treatments were not statistically significant. Similar results were obtained for a deletion mutant of *nmrA*, a co-repressor of *areA* (data not shown). Differences between strains under each nitrogen condition were also not

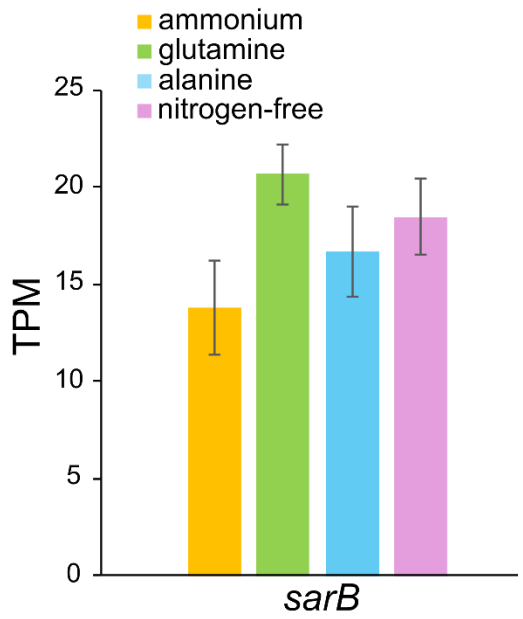

Figure 3.9 sarB *is constitutively expressed*.
Expression of *sarB* under four nitrogen conditions was examined using RNA-seq in a wild-type strain (MH11068), normalized to transcripts per million (TPM). Cultures were grown for 16 h at 37°C and 120 opm in glucose minimal medium with ammonium, glutamine, or alanine as a nitrogen source. The nitrogen-free treatment was grown with ammonium for 16 h and transferred to nitrogen-free media for 4 h. Expression under the glutamine, alanine, and nitrogen-free treatments did not differ significantly from the ammonium treatment.

statistically significant. These data are similar to those obtained by Steyer et al. (2021) for *sarB* expression in wild type (MH1) under ammonium, glutamine, and alanine nitrogen conditions. Overall, we found little evidence that *sarB* is regulated by nitrogen.

3.5.6 *sarB* encodes a putative transmembrane UDP-GlcNAc transporter

To assess the predicted function and localization of SarB, we used online tools to predict features of the reannotated 459-residue SarB protein. Interpro (ebi.ac.uk/interpro/; Blum et al. 2025) predicts UDP-GlcNAc transporter protein domains in multiple classification systems across the bulk of the protein length: IPR013657 (SLC35B1-4/HUT1; amino acids 74-449), PTHR10778 (solute carrier family 35 member B; 74-449), and PF08449 (UAA transporter family; 78-444).

DeepTMHMM (Hallgren et al. 2022) predicts SarB to be an alpha-type transmembrane protein with 10 transmembrane domains (Figure 3.10A-B) with the N- and C-termini on the inside of the organelle. This model also predicts an extended stretch of residues between transmembrane domains 7 and 8, outside the organelle.

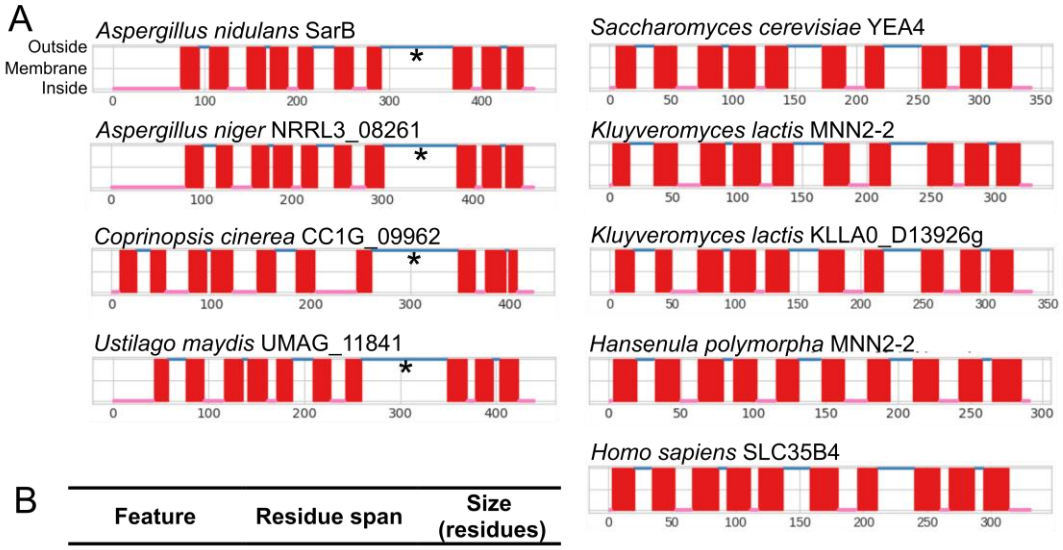

B

Feature	Residue span	Size (residues)
Inside	1-74	74
TM domain 1	75-95	21
Outside	96-106	11
TM domain 2	107-127	21
Inside	128-146	19
TM domain 3	147-167	21
Outside	168-171	4
TM domain 4	172-192	21
Inside	193-202	10
TM domain 5	203-219	17
Outside	220-241	22
TM domain 6	242-262	21
Inside	263-277	15
TM domain 7	278-293	16
Outside	294-370	77*
TM domain 8	371-391	21
Inside	392-401	10
TM domain 9	402-422	21
Outside	423-428	6
TM domain 10	429-446	18
Inside	447-459	13

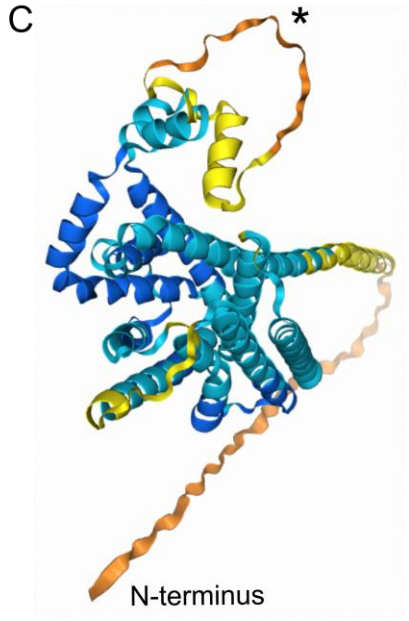

Figure 3.10 SarB and its orthologs have 10 transmembrane domains.
(A-B) DeepTMHMM predicted 10 transmembrane domains in SarB and all orthologs, with spacing that was roughly consistent between species. The insertion in diverse fungi relative to ascomycete yeasts and humans was observed to be on the inside of the organelle. (C) The AlphaFold3 prediction of the SarB structure predicted ten α-helices. The non-conserved region upstream of the annotated UDP-GlcNAc protein domain and the insertion observed in the protein sequence alignment (Figure 3.11) were low-confidence regions with no predicted structure. Asterisks in all three panels denote the insertion in filamentous fungi and non-ascomycete yeasts.
. Asterisks denote the insertion in non-ascomycete fungi.

AlphaFold 3 (Abramson et al. 2024) and i-TASSER (Zhang 2008; Roy et al. 2010; Yang et al. 2015) 3D models of SarB predict 10 alpha helices, with long stretches of low confidence at the N-terminal end and between helices 7 and 8 (Figure 3.10C). This

region corresponds to an insertion described below (see Section 3.5.7). To predict the subcellular localization of SarB we used Psort II (Nakai and Horton 1999), DeepLoc 2.1 (Ødum et al. 2024), and LocTree3 (Goldberg et al. 2014). Each tool predicted localization to the endoplasmic reticulum (ER), Golgi, or plasma membrane (Table 3.4). Psort II also predicted a KKXX-like ER retention sequence at the C-terminus (AQKK at residues 455-458). There is no evidence in other species of SarB orthologs with plasma membrane localization.

Table 3.4 SarB localization as predicted by online tools.

Compartment	PsortII	DeepLoc 2.1	LocTree3
Golgi	0	60.45%	83%
ER	55.6%	59.01%	0
Plasma membrane	44.4%	12.18%	0
Lysosome/vacuole	0	29.85%	0
Nucleus	0	21.31%	0
Mitochondria	0	12.05%	0
Cytoplasm	0	8.46%	0
Peroxisome	0	8.27%	0
Extracellular	0	5.33%	0
Plastid	0	4.23%	0

3.5.7 *sarB* is a conserved, single copy gene in most fungi

To determine whether *sarB* is a single copy gene or whether *sarB* paralogs occur, the *A. nidulans* genome was searched with the SarB protein sequence using BLASTp and tBLASTn. No candidate *sarB* paralog was found searches.

To examine conservation of SarB, protein sequence searches of the NCBI (https://www.ncbi.nlm.nih.gov) and FungiDB (fungidb.org) databases were conducted using the reannotated SarB protein sequence as a query. We found predicted orthologs of SarB across the fungal and animal kingdoms, but not in plants or prokaryotes. Most

fungal species have only one copy of a *sarB* ortholog. However, the *Kluyveromyces lactis* and *Coprinopsis cinerea* genomes contains two *sarB* orthologs. The SarB orthologs YEA4 in *Saccharomyces cerevisiae* and MNN2-2 in *Hansenula polymorpha,* have been characterized as involved in cell wall integrity whereas MNN2-2 in *K. lactis* and SLC35B4 in humans have roles in glycosylation (Smith et al. 1975; Douglas and Ballou 1982; Guillen et al. 1999; Roy et al. 2000; Sesma et al. 2009; Park et al. 2011). We aligned the predicted reannotated SarB protein sequence with orthologs from members of the fungal and animal kingdom (Table 3.5; Figure 3.11). Among these, SarB is 64.4-81.4% similar to its orthologs in other aspergilli, 50.0-61.4% similar to its orthologs in other filamentous ascomycetes, 47.1% similar to a basidiomycete ortholog, 33.5-42.5% similar to orthologs in ascomycete yeasts, and 38.9-40.6% similar to its counterparts in animals (Table 3.5). The ten transmembrane domains show strong sequence conservation in the aspergilli (Figure 3.11) and are predicted by DeepTMHMM modeling in each ortholog examined (Figure 3.9A). The C-terminal KKXX-type endoplasmic reticulum motif was observed in all species included in the multiple sequence alignment except for *K. lactis* KLLA0_D13926g (Figure 3.11). SarB contains an insertion from amino acid ~300 to ~363 relative to ascomycete yeasts and humans (Figure 3.10). This insertion is present in SarB orthologs in all fungi we examined outside of the ascomycete yeasts. Protein sequence alignment of the SarB orthologs for several *Aspergillus* species shows the insertion sequence is poorly conserved, even amongst closely-related species (Figure 3.11). Its location corresponds to the extended stretch of residues between transmembrane domains 7 and 8 in SarB

described in Section 3.5.6. This topology was not observed in humans or ascomycete yeasts but was present for all other fungi examined (Figures 3.9A and 3.11).

Table 3.5 Protein sequence alignments between reannotated AN8875 and selected orthologs.

Species	Gene	% identity / % similarity
Aspergillus mulundensis	DSM5745_09692	72.2 / 81.4
Aspergillus versicolor	ASPVEDRAFT_144129	68.4 / 79.4
Aspergillus sydowii	ASPSYDRAFT_522209	66.7 / 78.5
Aspergillus fumigatus	Afu8g02830	60.3 / 69.7
Aspergillus oryzae	AO090010000775 (reannotated) *	57.6 / 69.1
Aspergillus niger	NRRL3_08260	55.0 / 67.8
Aspergillus clavatus	putative *	51.9 / 64.4
Fusarium fujikuroi	FFUJ_01572	41.2 / 55.1
Magnaporthe oryzae	MGG_05631	40.5 / 53.9
Neurospora crassa	NCU02980	38.2 / 50.0
Ustilago maydis	UMAG_11841	31.0 / 47.1
Kluyveromyces lactis	KLLA0_D13926g	25.5 / 41.9
Kluyveromyces lactis	KLLA0_B03157g *(MNN2-2)*	26.6 / 41.7
Saccharomyces cerevisiae	YEL004W *(YEA4)*	27.7 / 41.4
Homo sapiens	SLC35B4 (isoform 1)	26.3 / 40.6
Drosophila melanogaster	Dmel_CG14511	24.9 / 39.0
Caenorhabditis elegans	*nstp-2*	25.3 / 38.9
Hansenula polymorpha	*MNN2-2*	20.0 / 33.5

* See Appendix A for information on the annotation of these genes.

We constructed a phylogenetic tree for SarB and its fungal orthologs using MAFFT v7 (mafft.cbrc.jp; Kuraku et al. 2013; Katoh et al. 2019) (Figure 3.12). Protein sequences clustered according to species evolutionary relationships. The two *K. lactis* homologs clustered together in the same clade indicating that these genes arose from a recent gene duplication. In contrast, the two *C. cinerea* homologs clustered in different Basidiomycete clades suggesting gene duplication early in the Basidiomycete lineage.

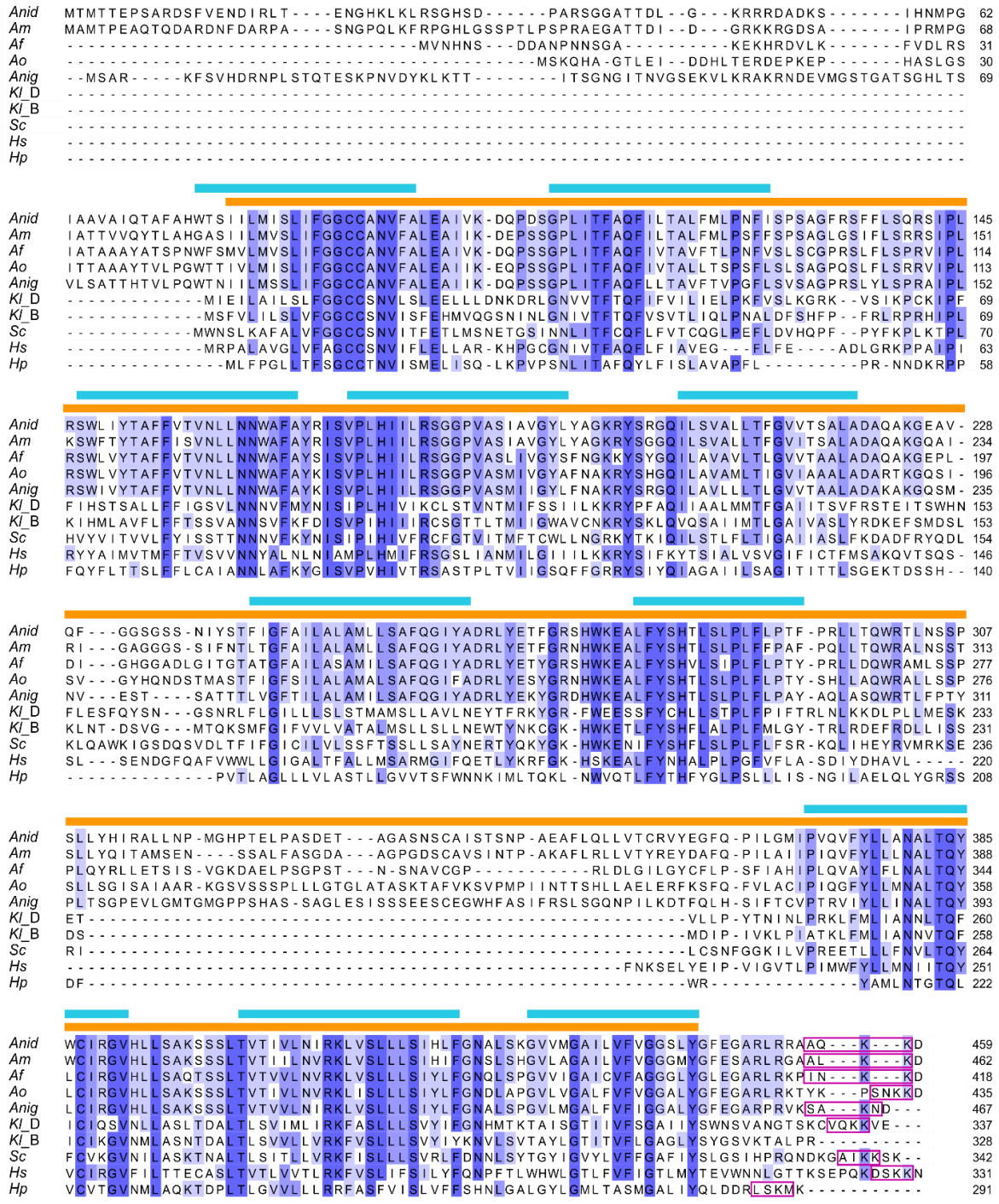

Figure 3.11 Alignment of SarB with its orthologs reveals conserved features.
Alignment shading is by percent identity. The orange bar denotes the protein domain PF08449, UAA transporter. Turquoise bars represent predicted transmembrane domains. Predicted C-terminal XXKK-type endoplasmic reticulum retention motifs are shown in purple boxes. Key: *Anid – Aspergillus nidulans* AN8875 (version 5 annotation); *Am – Aspergillus mulundensis* DSM5745_09692; *Af – Aspergillus fumigatus* Afu8g02830; *Ao – Aspergillus oryzae* AO090010000775 (reannotated); *Kl_D – Kluyveromyces lactis* KLLA0_D13926g; *Kl_B – K. lactis* KLLA0_B03157g (MNN2-2); *Sc = Saccharomyces cerevisiae* YEL004W (YEA4); *Hs – Homo sapiens* SLC35B4; *Hp – Hansenula polymorpha* MNN2-2. Alignment generated by Clustal Omega (ebi.ac.uk/jdispatcher/msa/clustalo) and visualized in Jalview 2.11.4.1).

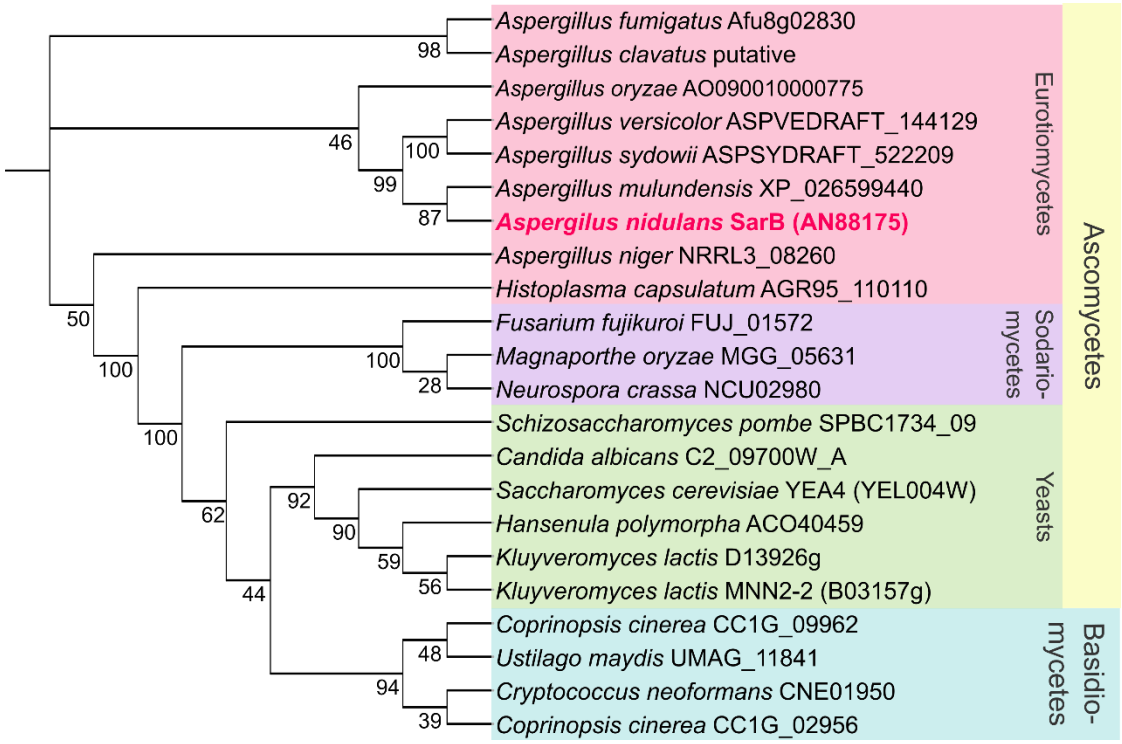

Figure 3.12 The relationships of SarB to its orthologs follows species evolutionary relationships. Phylogenetic tree developed using neighbor joining following multiple sequence alignment using MAFFT v7 and visualized with Interactive Tree of Life v7 (iTOL; itol.embl.de). The number at each node indicates bootstrap support from 100 bootstrap trials.

3.5.8 The *sarB*Δ mutant has reduced levels of cell wall chitin

In *S. cerevisiae,* the SarB ortholog YEA4 is involved in cell wall chitin biosynthesis (Roy et al. 2000; Sesma et al. 2009). To determine whether this function is conserved for SarB, we performed microscopic examination of a *sarB*Δ mutant (RT855) and a wild-type strain (MH1). Because GlcNAc is the building block of the chitin found in the fungal cell wall, we used calcofluor white staining to compare chitin distribution and content in 24-hour germlings of both strains. The distribution of chitin in the hyphal cell walls and septa was similar for both wild-type and *sarB*Δ mutant strains (Figure 3.13). However, the *sarB*Δ mutant exhibited lower levels of fluorescence, suggesting an overall lower chitin content than in wild type. This provides evidence that SarB is necessary for normal cell wall development.

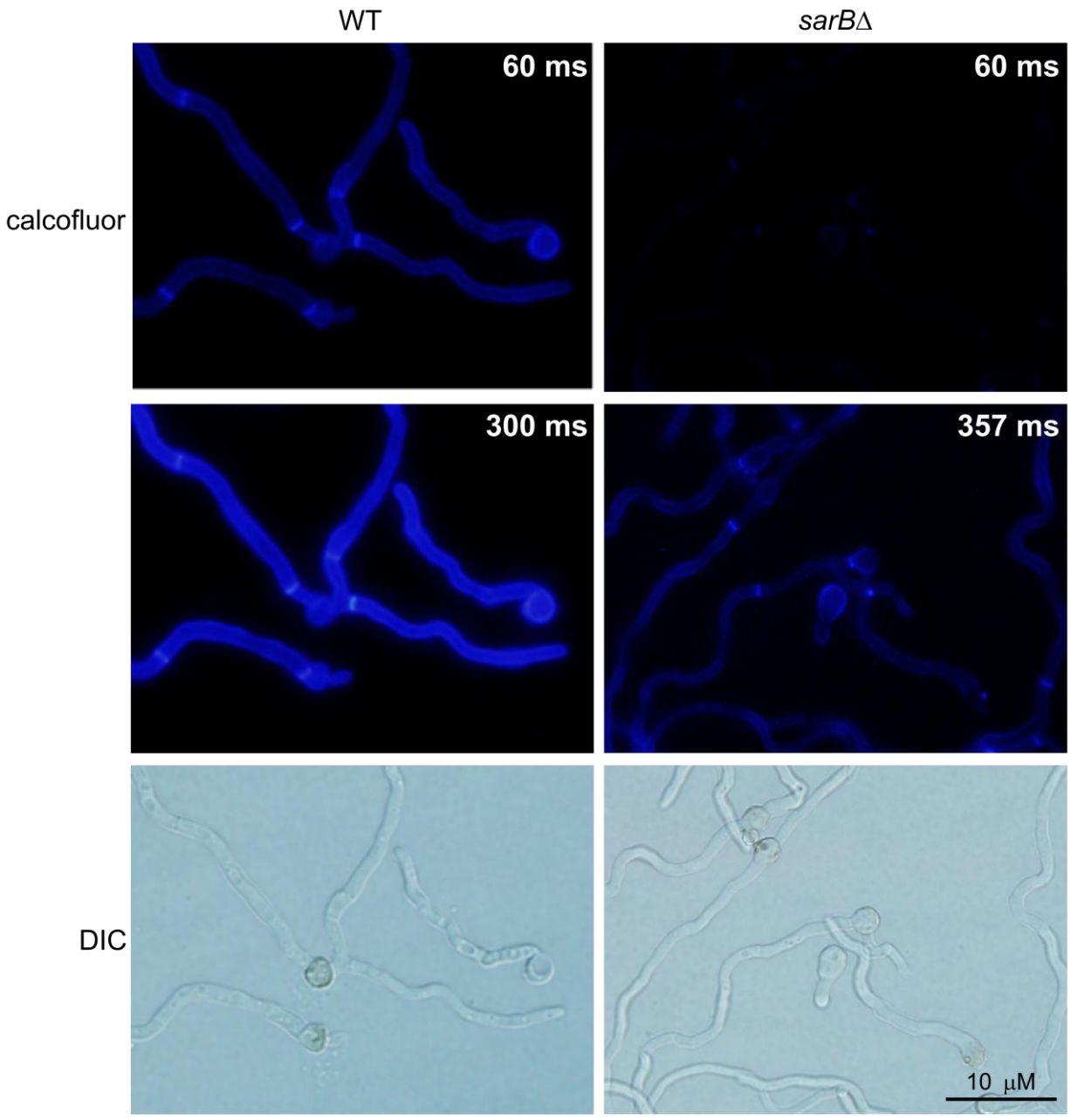

Figure 3.13 sarB *deletion confers decreased cell wall chitin content.*
Germlings from wild type (MH1) and a *sarB*Δ mutant (RT855) were stained with calcofluor white. The chitin distribution in cell walls and septa appeared similar in both strains. However, the intensity of brightness was lower in the *sarB*Δ strain at the same exposure (60 ms). Only at an increased exposure duration of 357 ms does the *sarB*Δ mutant show a brightness similar to wild type. DIC, Differential Interference Contrast.

3.5.9 The *sarB*Δ mutant has a wild-type growth phenotype on GlcNAc

GlcNAc can potentially serve as either a carbon source, or a nitrogen source, or as both a source of carbon and nitrogen (see Chapter 5). In *A. nidulans,* the utilization

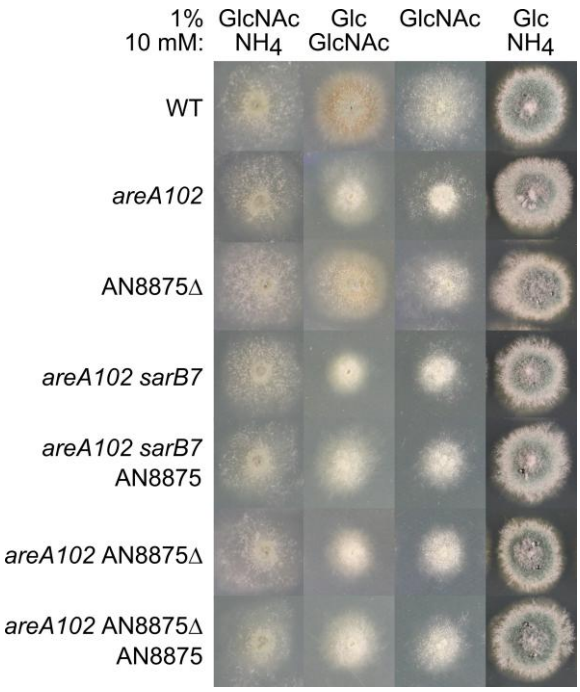

Figure 3.14 AN8875 mutations confer no detectable growth phenotype on GlcNAc.
The *areA102* mutation conferred decreased growth on media using GlcNAc as a sole nitrogen source but did not affect use of GlcNAc as a carbon source. AN8875 mutations or complemented strains did not affect growth on GlcNAc. Strains of the indicated genotypes were grown on supplemented minimal media with the indicated carbon and nitrogen sources for 48 h at 37ºC. Top to bottom: MH1, MH8, RT855, MK160, RT947, RT891, RT971. GlcNAc = N-acetylglucosamine; Glc = glucose; NH_4 = ammonium.

of compounds as either a carbon source or as a nitrogen source can be examined separately by addition of the preferred nitrogen source (ammonium or glutamine) or the preferred carbon source (glucose), respectively (Arst and Cove 1973).

Because *sarB* encodes a putative UDP-GlcNAc transporter, we assessed the growth of *sarB* mutants on GlcNAc as a substrate. The AN8875Δ mutant exhibited a growth morphology similar to wild type when GlcNAc served as a sole carbon source, a sole nitrogen source, a sole nitrogen and carbon source, or on the preferred carbon source glucose and preferred nitrogen source ammonium (Figure 3.14). All *areA102* strains showed a slightly inhibited or more compact growth morphology when GlcNAc served as a sole nitrogen source or as a sole carbon and nitrogen source. There were no obvious effects of *sarB* mutations on growth on any media tested.

3.6 Discussion

We have provided strong evidence that *sarB* is AN8875. Previous work established that *sarB* is on chromosome VII tightly linked to *xprG* (Polkinghorne and

Hynes 1975; Katz et al. 2000). Whole genome sequencing showed that AN8875 is the only gene on chromosome VII containing a SNP unique to the *sarB7* mutant in its coding region. The *sarB7* SNP is 117,423 bp from the *xprG1* mutation, i.e., 0.26cM equates to the physical distance 117,423 bp. This corresponds to a physical to genetic distance ratio of 451.627 kb per cM. Notably the chromosome VII centromere, positioned within the 60,426 bp interval between AN8871 and AN9418 in the version 5 genome sequence, lies between the *sarB7* SNP and the *xprG1* mutation. The presence of the centromere between *xprG* and AN8875 and their proximity to the centromere explains the physical location of *sarB* being further than predicted from *xprG* by recombinational mapping. Increased physical to map distance ratios have been reported previously proximal to the centromeres on chromosome III between *phenA2* and *halA2* (37.6 kb/cM) and on chromosome IV between *hisA10* and *gdhB1* (51.8 kb/cM) (Espeso et al. 2005). We successfully used the wild-type AN8875 gene to complement *sarB7* suppression of the AreA102 phenotype on histidine. We showed that, like the *sarB7* mutation, deletion of AN8875 suppresses the strong growth of the *areA102* mutant on histidine or lysine. Combined, these experiments demonstrate that *sarB* is AN8875.

The *sarB* gene encodes a putative UDP-GlcNAc transporter containing ten transmembrane domains. *sarB* orthologs are present in species throughout the fungal and animal kingdoms but are not found in plants or prokaryotes. The *S. cerevisiae sarB* ortholog, *YEA4*, encodes a UDP-GlcNAc transporter that supplies GlcNAc for inclusion into chitin, a major component of the fungal cell wall (Roy et al. 2000). The *sarB* ortholog *MNN2-2* has been studied in the yeast *H. polymorpha*. As with the Sc*yea4*Δ

mutant, the Hp*mnn2-2*Δ mutant exhibited decreased cell wall chitin content (Park et al. 2011). Hp*mnn2-2*Δ mutants showed sensitivity when treated with aminoglycoside antibiotics, which may be indicative of a change of cell wall permeability caused by defects in N-glycosylation of mannoproteins (Dean 1995). However, while Hp*mnn2-2*Δ mutants showed sensitivity to treatment with the N-glycosylation inhibitor tunicamycin, the N-glycosylation profiles of total cell wall mannoproteins did not differ from wild type (Park et al. 2011).

Unlike *S. cerevisiae* and *H. polymorpha,* the yeast *K. lactis* produces N-glycans with terminal GlcNAc moieties (Kim et al. 2003). Two mutants that produced N-glycans lacking GlcNAc on their side chains were identified in *K. lactis* (Smith et al. 1975). One mutant contained defects in the *sarB* ortholog *MNN2-2,* which codes for a UDP-GlcNAc transporter. The second mutant contained defects in *MNN2-1* (now called *GNT1*), which is adjacent to the *MNN2-2* gene and encodes a UDP-GlcNAc transferase which accepts UDP-GlcNAc from MNN2-2 (Douglas and Ballou 1982; Guillen et al. 1999). However, Kl*mnn2-2* mutants synthesized chitin at a similar rate to wild type (Douglas and Ballou 1982). Therefore, KlMNN2-2 is involved in N-glycosylation and whether it plays a role in cell wall synthesis is unclear. Unlike other SarB orthologs examined, KlMNN2-2 does not contain an ER retention sequence at the C-terminus. We identified in the *K. lactis* genome a *MNN2-2* paralog (KLLA0_D13926g) that encodes a protein 43.7% identical and 63.8% similar to MNN2-2. KLLA0_D13926g and contains the UDP-GlcNAc transporter domain seen in MNN2-2 plus an ER retention sequence at the C-terminus. The KLLA0_D13926g gene has not been studied, and it is unknown if it is expressed or if the protein it encodes is functional. It is unclear whether *MNN2-2* or KLLA0_D13926g

is the true *sarB* functional ortholog, as the proteins they encode show comparable degrees of identity and similarity to SarB.

In addition to fungal genes, AN8875 exhibits orthology with a UDP-GlcNAc transporter gene in humans, SLC35B4. This protein transports UDP-GlcNAc from the cytoplasm to the ER and/or Golgi (Ashikov et al. 2005) and acts in the post-translational modification of proteins by O-linked N-acetylglucosaminylation (O-GlcNAcylation; Park et al. 2021), further discussed in Chapter 4.

The discovery of *sarB* as a putative ER- or Golgi-localized UDP-GlcNAc transporter was surprising. Involvement of *sarB* orthologs, or of nucleotide sugar transporters in general, in amino acid deamination or nitrogen utilization has not been suggested in other species. In Chapter 4, we discuss the connection between *sarB* and *sarA* and the role of glycosylation in SarA activity.

Chapter 4 - The Relationship between *sarB* and *sarA*

4.1 Abstract

L-amino acid oxidases (LAAO) deaminate L-amino acids, liberating ammonium that can be used as a nitrogen source. In *Aspergillus nidulans, sarA* (AN2350) encodes an LAAO. We identified a second LAAO-encoding gene in the *A. nidulans* genome, AN1808, and the presence of multiple distinct LAAOs throughout the fungal kingdom. A *sarB*Δ *sarA*Δ double mutant produced a phenotype on histidine similar to the *sarB*Δ and *sarA*Δ single mutants, confirming that *sarB* and *sarA* are in the same genetic pathway. To test the effect of *sarB* mutation on SarA activity, we performed in-gel and spectrophotometric LAAO assays on cell-free extracts. Both assay methods showed that SarA activity was detected in the *areA102* parent strain after 4 hours of growth on histidine but was greatly reduced in the *areA102 sarA*Δ and *areA102 sarB*Δ mutants. No indication of AN1808 activity was found. At a later timepoint (72 hours), LAAO activity was elevated, and, in addition to SarA activity, an AN1808 activity that appeared to be SarA-dependent was detected, suggesting that AN1808 is active as a heterodimer with SarA under these conditions.

Treatment of growing mycelia with tunicamycin and treatment of cell-free extracts with PNGase F revealed evidence that SarA is N-glycosylated and that N-glycosylation is necessary for full SarA activity. However, deletion of genes involved in N-glycosylation (N-acetylglucosamine transferase, GNT) and O-GlcNAcylation (O-GlcNAc transferase, OGT) did not phenocopy the *sarB*Δ and *sarA*Δ mutants on histidine, and thus we found no genetic evidence either of these genes is part of the *sarB-sarA* genetic pathway. The putative *areA102* GNT deletion mutant, however, showed

increased electrophoretic mobility of SarA LAAO activity and exhibited slightly higher SarA LAAO activity than the *areA102* mutant suggesting that GlcNAc decorates SarA glycans. Furthermore, SarA activity in the *areA102* OGT deletion mutant was slightly lower than wild type, providing further evidence of the importance of glycosylation to SarA function. Through RNA-seq analysis of a wild-type strain, we determined that *sarA* is upregulated on non-repressing nitrogen conditions and that *sarB* shows constitutive expression. Neither gene is regulated by the *areA* co-repressor *nmrA*.

4.2 Contribution Statement

Sara M. Hopkins of the Richard Todd lab made the AN1808Δ deletion mutant and the *areA102 sarB7* AN1808Δ strain. Dr Richard B. Todd constructed *areA102* AN1808Δ and *areA102 sarA*Δ and *areA102 sarA*Δ AN1808Δ mutants. Preliminary analysis of the AN1808Δ mutant and its derivatives were carried out by Sara M. Hopkins and Richard B. Todd.

4.3 Introduction

SarA (AN2350) is an L-amino acid oxidase (LAAO), an enzyme that performs oxidative deamination of L-amino acids, releasing ammonium that can be directly utilized as a nitrogen source (Davis et al., 2005). SarA activity was detected in soluble cell-free extracts by detecting urocanoate production by histidine deamination using a histidase assay, before it was known that SarA was an LAAO (Polkinghorne and Hynes 1975). LAAOs are ubiquitous throughout taxa but are poorly characterized in fungi. The LAAO route is not the only means of amino acid breakdown, nor are all amino acids deaminated by all LAAOs (Polkinghorne and Hynes 1975; Davis et al. 2005). For example, branched-chain amino acids (BCAA) may be also broken down in *A. nidulans*

by BCAA amino transaminases (Steyer et al. 2021). The human LAAO, Interleukin 4 Induced 1 (IL4i1), is an N-glycosylated protein that is processed in acidic endosomes and, while primarily secreted, shows some intracellular activity (Mason et al. 2004; Boulland et al. 2007). It plays an important role in immunoregulation, tumor microenvironments, and proliferation of cancers (Grobben et al. 2023; Ye et al. 2023; Zeitler and Murray 2023; Zhang et al. 2023; Zhu et al. 2023). LAAOs are abundant proteins in snake venom, where generation of hydrogen peroxide by LAAOs contributes to the apoptotic activity of the venom (reviewed in Du and Clemetson 2002).

The identification of SarB as a putative UDP-GlcNAc transporter (see Chapter 3) was surprising, as it is unclear how the absence of such a protein in *sarB*Δ mutants would suppress the increased growth on histidine of the *areA102* mutant. Some SarB orthologs identified in other species play roles in glycosylation, in which trees of mannose sugars are decorated with other sugar residues. In *K. lactis*, the *sarB* ortholog, Golgi-bound MNN2-2, provides UDP-GlcNAc to the GlcNAc transferase (GNT) GNT1 (formerly MNN2-1), which adds GlcNAc to N-glycan trees (Smith et al. 1975; Douglas and Ballou 1982; Guillen et al. 1999). N-glycosylation can be necessary for protein activity, folding, stability, or solubility (reviewed in He et al. 2024).

In humans, the *sarB* ortholog SLC35B4 influences O-GlcNAcylation, a non-canonical form of protein glycosylation that covalently attaches a single GlcNAc sugar to the oxygen atom of the hydroxyl group of a serine or threonine residue (Torres and Hart 1984). O-GlcNAcylation acts on cytoplasmic, nuclear, and mitochondrial proteins; is mechanistically and functionally similar to phosphorylation; and may occur in response to nutrient and stress stimuli (reviewed in Hart 1997, 2019; Hart et al. 2011). While O-

GlcNAcylated proteins have been identified in *A. oryzae* (Machida and Jigami 1994), the O-GlcNAcylation process and the genes involved have not been studied in fungi. In animals, the enzyme O-GlcNAc transferase (OGT) adds GlcNAc and O-GlcNAcase (OGA) removes it in a dynamic cycling (Ma and Hart 2014). In humans, three OGT isoforms are found, each operating where their target proteins are localized (Hanover et al. 2002). In humans, defects in O-GlcNAcylation contribute to multiple cancers, neurodegeneration, and metabolic disorders such as diabetes (Ma and Hart 2013; Ferrer et al. 2016; Wani et al. 2017)

In this chapter, we sought to characterize the SarA LAAO and determine the relationship between *sarB* and *sarA*.

4.4 Materials and Methods

4.4.1 Strains used in this chapter

Strains used in Chapter 4 are listed in Table 4.1

Table 4.1 *Aspergillus nidulans* strains used.

Strain	Genotype
MH1	*biA1*
MH8	*biA1 areA102 niiA4*
MH10571	*yA1 adE20 su*(*adE20*) *pyroA4 areA102 sarA*Δ*::riboB+ riboB2*
MH10983	*pyrG89 pabaB22 riboB2*
MH11068	*pyrG89 pyroA4 nkuA*Δ*::Bar amdA7*
MK160	*biA1 areA102 sarB7 niiA4*
RT763	*pyrG89 sarA*Δ*::riboB+ pyroA4 riboB2*
RT765	*pyrG89 pabaB22 areA102 sarA*Δ*::riboB+ riboB2*
RT774	*pyrG89 pabaB22 areA102* AN1808Δ*::AfpyrG+ riboB2*
RT775	*pyrG89 areA102 pyroA4* AN1808Δ*::AfpyrG+ riboB2*
RT776	*pyrG89 areA102 pyroA4 sarA*Δ*::riboB+* AN1808Δ*::AfpyrG+ riboB2*
RT865	*pyrG89 pyroA4 nkuA*Δ*::Bar*
RT1015	*pyrG89 pyroA4* AN8875Δ*::AfpyrG+ riboB2*
RT1016	*pyrG89 pyroA4* AN8875Δ*::AfpyrG+*
RT1017	*pyrG89* AN8875Δ*::AfpyrG+ riboB2*
RT1018	*pyrG89 pabaB22* AN8875Δ*::AfpyrG+*
RT1020	*pyrG89 pabaB22 sarA*Δ*::riboB+* AN8875Δ*::AfpyrG+ riboB2*

RT1021	*pyrG89 pyroA4 sarA*Δ::*riboB*+ AN8875Δ::*AfpyrG*+ *riboB2*
RT1022	*pyrG89 pabaB22 areA102 sarA*Δ::*riboB*+ AN8875Δ::*AfpyrG*+ *riboB2*
RT1023	*pyrG89 pyroA4 areA102 sarA*Δ::*riboB*+ AN8875Δ::*AfpyrG*+ *riboB2*
RT1024	*pyrG89 sarA*Δ::*riboB*+ AN8875Δ::*AfpyrG*+ *riboB2*
RT1025	*pyrG89 areA102 sarA*Δ::*riboB*+ AN8875Δ::*AfpyrG*+ *riboB2*
RT1035	*pabaB22 areA102* AN8875Δ::*AfpyrG*+ AN1808Δ::*AfpyrG*+
RT1036	*pyrG89 pyroA4 nkuA*Δ*::Bar* AN11141Δ*::AfpyrG*+
RT1037	*pyrG89 pyroA4 nkuA*Δ*::Bar* AN0265Δ*::AfpyrG*+
RT1045	*areA102* AN11141Δ*::AfpyrG+niiA4*
RT1046	*areA102 pyroA4* AN11141Δ*::AfpyrG*+
RT1047	*areA102 pyroA4* AN0265Δ*::AfpyrG*+
RT1048	*areA102* AN0265Δ*::AfpyrG+niiA4*
RT1052	*areA102 pyroA4* AN1416Δ*::AfpyrG*+
RT1055	*yA1 areA102 pyroA4 xprG*Δ*::argB*+ AN1416Δ*::pyrG*+
RT1058	*areA102 xprG*Δ*::argB*+ AN1416Δ*::pyrG*+ *pabaA1*
RT1064	*areA102* AN11141Δ::*AfpyrG*+ AN0265Δ::*AfpyrG*+ *niiA4*

4.4.2 PCR primers

Genomic PCR and RT-qPCR primer sets used in Chapter 4 are shown in Tables 4.2 and 4.3, respectively.

Table 4.2 Genomic primers sets.

Target	Primer Name	Sequence (5'→ 3')
AN8875	AN8875_outside_5'F	GGCCTACTCTTCTCTCTTCC
	AN8875_outside_3'R	GCACTCTATTGACACACCAC
	AN8875_inside 5'F	CACGGAAGTAGTGTATGTG
	AN8875_inside 3'R	GGTAAGCCATCCTACTGAAG
	ANID_08875.1_5'F	GTAACGCCAGGGTTTTCCCAGTCACGACGGGCCTACTCTT CTCTCTTCC
	ANID_08875.1_3'R	GCGGATAACAATTTCACACAGGAAACAGCGCACTCTATTGA CACACCAC
AN11141	AN11141_outside_5'F	ATATGCTATGCTTCGACTCGG
	AN11141_outside_3'R	CCATCTACGGAAGATATGAGC
	AN11141_inside_5'F	CACGGAAGTAGTGTATGTG
	AN11141_inside_3'R	GGTAAGCCATCCTACTGAAG
	ANID_11141.1_5'F	GTAACGCCAGGGTTTTCCCAGTCACGACGCCACGGAAGTA GTGTATGTG
	ANID_11141.1_3'R	GCGGATAACAATTTCACACAGGAAACAGCGGTAAGCCATCC TACTGAAG
AN0265	AN0265_outside_5'F	CATCCAGCATTACTGCCAAG
	AN0265_outside_3'R	GATAATAGTTGGACGACCGC
	AN0265_inside_5'F	CTAGGACCGTGACTCTGAAT
	AN0265_inside_3'R	AGCAACAGAGCCTAAGAGAG

	ANID_00265.1_5'F	GTAACGCCAGGGTTTTCCCAGTCACGACGCTAGGACCGTG ACTCTGAAT
	ANID_00265.1_3'R	GCGGATAACAATTTCACACAGGAAACAGCAGCAACAGAGC CTAAGAGAG
AN1808	AN1808_5'F	GACATATAGACCAGGCGAGAC
	AN1808_3'R	GATTCTGAACGACTGGTCTG

Table 4.3 RT-qPCR primer sets.

Target	Primer name	Sequence (5'→ 3')
sarA	*sarA* qPCR 5'F	TTACGTGGGAATCGTACAGCG
sarA	*sarA* qPCR 3'R	CATTGACGGTTGTATATACCGG

4.4.3 Strain construction

Construction of the *sarB*Δ *sarA*Δ double mutant

A *pyrG89 sarB*Δ::*AfpyrG+ riboB2* mutant (RT1015) was crossed with a *pyrG89 areA102 sarA*Δ::*riboB+ riboB2* mutant (RT765) using protocols described in Todd et al. (2007b). Progeny with the *areA102* allele were identified by poor growth on uric acid. Progeny with the *sarB*Δ::*AfpyrG+* gene replacement were identified by pyrimidine prototrophy, and *sarA*Δ::*riboB+* gene replacement progeny were identified by riboflavin prototrophy. *areA+ sarB*Δ *sarA*Δ progeny (RT1020, RT1021, and RT1024) and *areA102 sarB*Δ *sarA*Δ progeny (RT1022, RT1023, and RT1025) were obtained.

Construction of the *sarB*Δ AN1808Δ double mutant

An *areA102* AN1808Δ mutant (RT774) was crossed to a *sarB*Δ mutant (RT855). Progeny with the *areA102* allele were identified by poor growth on uric acid and strong growth on sucrose-acetamide media. *areA102* progeny with the *sarB*Δ::*AfpyrG+* construct were identified by suppression of the AreA102 strong growth phenotype on histidine as a sole nitrogen source. Progeny with the *sarB*Δ::*AfpyrG+* gene, AN1808Δ::*AfpyrG+* gene, or both in an *areA+* background were identified by pyrimidine

prototrophy. To discriminate the gene deletions present in these progeny, several progeny were chosen for genomic DNA extraction, followed by PCR to confirm the presence of the knockout deletions. One *areA102 sarB*Δ AN1808Δ progeny (RT1035) was obtained.

Construction of glycosylation deletion mutants

An AN11141Δ mutant (RT1036; AN11141Δ -9 to +1304) and an AN0265Δ mutant (RT1037; AN0265Δ -10 to +5894) were constructed using knockout constructs made in the *A. nidulans* knockout project by De Souza et al. (2013) and obtained from the Fungal Genetics Stock Center, Manhattan, Kansas (McCluskey et al. 2010). Briefly, each construct consisted of the *Aspergillus fumigatus pyrG* (*AfpyrG*) gene selectable marker, flanked by ~1 kbp of sequences upstream and downstream of the gene of interest, which allowed for gene replacement by homologous recombination in a *nkuA*Δ non-homologous end-joining mutant recipient (Nayak et al. 2006). Transformation into a *pyrG89* mutant recipient allowed selection of transformants for pyrimidine prototrophy (Oakley et al. 1987a). Knockout construct integration by homology in each transformant was confirmed by the presence of a PCR band of the construct size (1.7 kb) and absence of a PCR band of the deleted gene size.

To construct AN11141Δ and AN0265Δ mutants in an *areA102* background, the AN11141Δ mutant (RT1036) and the AN0265Δ mutant (RT1037) were separately crossed to an *areA102* mutant (MH8) using protocols outlined in Todd et al. (2007b). Progeny with the *areA102* allele were identified by poor growth on uric acid and strong growth on sucrose-acetamide media, and progeny with the AN11141Δ::*AfpyrG*+ or AN0265Δ::*AfpyrG*+ construct were identified among pyrimidine prototrophic progeny

using PCR. *areA102* AN11141Δ mutants (RT1045 and RT1046) were PCR confirmed for the presence of the AN11141Δ::*AfpyrG+* band and absence of the wild-type gene bands. *areA102* AN0265Δ mutants (RT1047 and RT1048) were PCR confirmed for the presence of AN0265Δ::*AfpyrG+* and absence of the wild-type gene bands.

To create AN11141Δ AN0265Δ double mutants, the AN11141Δ mutant RT1036 was crossed to the *areA102* AN0265Δ mutant RT1047. *areA102* progeny were identified by poor growth on uric acid as a sole nitrogen source and strong growth on sucrose-acetamide media. Progeny potentially containing the AN11141Δ::*AfpyrG+* gene, AN0265Δ::*AfpyrG+* gene, or both were identified by pyrimidine prototrophy. AN11141Δ AN0265Δ double mutant progeny were PCR-confirmed for the presence of band sizes corresponding to both knockout genes and the absence of both wild-type gene bands. Two double mutants in an *areA+* background (RT1061 and RT1062) and two in an *areA102* background (RT1063 and RT1064) were obtained.

Construction of *xprG*Δ and AN1416Δ mutants in an *areA102* background

A crossing strategy was adopted to produce GlcNAc regulatory deletion mutants in an *areA102* background. Because *xprG* and AN1416 are tightly linked, three separate crosses were performed. MH8 was crossed to MK414 (*xprG*Δ) to produce the *areA102* *xprG*Δ mutants RT1049 and RT1058-RT1060. MH8 was crossed to RT707 (AN1416Δ) to produce the *areA102* AN1416Δ mutants RT1050 and RT1052-RT1053. MH8 was crossed to RT827 (*xprG*Δ AN1416Δ) to produce the *areA102 xprG*Δ AN1416Δ mutants RT1051 and RT1055-RT1057.

4.4.4 *In silico* analyses of LAAOs

InterPro Registry (IPR) and Pfam protein domains of SarA and AN1808 were predicted by querying databases at InterPro (ebi.ac.uk/interpro/; Blum et al. 2025) with each protein sequence. Protein transmembrane domain number and locations were predicted by DeepTMHMM (Hallgren et al. 2022). To predict the subcellular localization of LAAOs we used Psort II (Nakai and Horton 1999), DeepLoc 2.1 (Ødum et al. 2024), and LocTree3 (Goldberg et al. 2014). The presence of signal peptides was assessed by DeepTMHMM, Psort II, and SignalP 6.0.0.56 (https://biolib.com/DTU/SignalP-6:0.0.56/; Teufel et al. 2022). ER-retention sequences were predicted by Psort II.

Candidate *sarA* and AN1808 orthologs were identified from predictions found in the OrthoMCL database (orthomcl.org; Li et al. 2003; Chen et al. 2006, 2007; Fischer et al. 2011) and OrthoDB (orthodb.org; Tegenfeldt et al. 2025), protein BLAST of the two protein sequences against the FungiDB (fungidb.org) and NCBI (ncbi.nlm.nih.gov) databases, and references in the literature.

Pairwise global sequence alignments and calculations of sequence identity and similarity were performed using EMBOSS Needle (ebi.ac.uk/jdispatcher/psa/emboss_needle). Sequence alignments for comparing multiple sequences were performed using Clustal Omega (ebi.ac.uk/jdispatcher/msa/clustalo; Sievers et al. 2011, 2020; Sievers and Higgins 2018) and visualized using Jalview 2.11.4.1 (jalview.org; Waterhouse et al. 2009). Multiple sequence alignments for generating phylogenetic trees were performed using the neighbor joining method MAFFT 7 (mafft.cbrc.jp/alignment/software; Kuraku et al.

2013; Katoh et al. 2019) with 100 bootstraps. Trees were visualized in the Interactive Tree of Life (iTOL) 4 (itol.embl.de; Letunic and Bork 2024).

The SarA protein sequence was assessed for possible glycosylation sites. We used Deep O-GlcNAc (Zhang et al. 2024) to predict possible O-GlcNAc modification sites in SarA. NetNGlyc 1.0 (Gupta and Brunak 2002) was used to assess possible N-glycosylation sites.

4.4.5 LAAO activity assays

Colorimetric assays to assess LAAO activity were performed using cell-free protein extracts. This methodology detects release of hydrogen peroxide, a byproduct of the deamination reaction of LAAOs, using horseradish peroxidase (HRP)-catalyzed oxidation of the hydrogen peroxide-sensitive probe o-phenylenediamine (OPD) (Kishimoto and Takahashi 2001). When hydrogen peroxide is present, a golden-brown color is produced.

To assess intracellular activity, fungal cultures were grown for 16h at 37 °C and 120 opm in supplemented liquid 1% glucose-10mM ammonium liquid minimal media. Mycelia were harvested and washed in minimal media, then transferred to liquid 1% glucose-10 mM histidine minimal media for an additional 4h growth. Mycelia were harvested and cell-free soluble protein extracts made by grinding with a mortar and pestle for 30 s in 0.1 M Tris-HCl pH 8.0 buffer, followed by centrifugation to separate the soluble and insoluble fractions. This pH was chosen based on previous work with *A. nidulans* LAAOs by Polkinghorne and Hynes (1975, 1982). To evaluate possible extracellular SarA activity, we used the same protocol as described above. However,

when transferring to media containing histidine, only 2 mL of media was used, in an attempt to concentrate the enzyme and increase the likelihood of its detection.

To qualitatively visualize LAAO activity and assess potential differences in protein mobility between strains, in-gel assays were performed. Protein concentrations were determined by Nanodrop One Microvolume UV-Vis Spectrophotometer (Thermo Scientific) or Bradford determination (BioRad) to standardize loadings of equal amount of protein. SDS-PAGE (7.5%) gels were loaded with 30-90 µg of protein extract in 1x LAAO in-gel sample buffer lacking dithiothreitol and run for 4h in 1x Tris-glycine buffer. Following electrophoresis, gels were soaked for 10 minutes in 0.1 M Tris-HCl pH 8.0 buffer and transferred to LAAO in-gel assay HRP-OPD substrate solution (0.1 M Tris-HCl pH 8.0 with 5 mM histidine or ornithine, 0.5 U/mL HRP, and 1 mM OPD) for 16 h at room temperature to allow detection of LAAO activity as brown band(s) (Žun et al. 2017). In-gel assays were generally performed at least in duplicate.

To measure differences in LAAO activity between strains, a quantitative microplate-based spectrophotometric approach was used, as described in Kishimoto and Takahashi (2001). 20 µL of each soluble cell-free extract was treated with 180 µL of LAAO spectrophotometric assay HRP-OPD substrate solution (5 mM ornithine, 0.8 U/mL HRP, and 2 mM OPD) incubated for 1h at 37 ˚C, then treated with 2 M sulfuric acid (100 µL) to stop the reaction. Two technical replicates of samples were loaded across four wells into 96-well plates and absorbance was measured at the 492-nm wavelength. Following protein quantification via Bradford determination (BioRad), LAAO specific activity of each sample was calculated. Three biological replicates of each experiment were performed. Results were assessed for statistical significance using

analysis of variance (ANOVA) tests followed by Tukey's honest significance tests (HSD) in R Studio (2025.05.0, Posit Software; R version 4.5.0). A *p*-value of 0.05 was considered statistically significant. For thermolability experiments comparing two strains, the proportion of activity remaining following heat inactivation were assessed using ANOVA considering, proportion of activity remaining, replicate, strain, and the time-strain interaction. Line slopes were evaluated for the best-fit model followed by a likelihood ratio test. A *p*-value of 0.05 was considered statistically significant.

4.4.6 RT-qPCR of *sarA*

Three biological replicates of the *areA102* mutant (MH8) and the *areA102 sarB*Δ mutant (RT891) were grown for 16 h in liquid 1% glucose-10 mM ammonium minimal media, washed, and transferred to liquid 1% glucose-10 mM histidine media for an additional 4 h. RNA was isolated as outlined in Section 2.4.2. RT-qPCR was performed as described in Section 2.6.2. Data were analyzed using a two-way ANOVA using R Studio (2025.05.0, Posit Software; R version 4.5.0). A *p*-value of 0.05 was considered statistically significant.

4.4.7 Determination of glycosylation of SarA

We used the N-glycosylation inhibitor tunicamycin to assess the impact of preventing the formation of N-glycans in SarA. Cultures were grown for 16h at 37 °C and 120 opm in supplemented 1% glucose-10 mM ammonium liquid minimal media. Mycelia were harvested and washed in minimal media, then transferred to 1% glucose-10 mM histidine minimal media containing or lacking 20 µg /mL tunicamycin (Calbiochem) (Hill et al. 2006) for an additional 4h. LAAO activity in protein extracts

made from the mycelia were assessed using in-gel and microplate-based methods described in Section 4.4.5.

To evaluate the effect of possible de-glycosylation on SarA, we used PNGase F to cleave N-glycans from mature proteins. 40 µg of protein extract was treated with 4 µL of PNGase F (10 u/µL) (Promega) and incubated for 4h at 37 °C. LAAO activity was then assessed qualitatively and quantitatively, as described in Section 4.4.5.

To evaluate the effects of treatment with tunicamycin or PNGase F, treated versus untreated samples were compared within each strain using a two-way ANOVA considering strain, replicate, and treatment group, and analyzed separately. A *p*-value of 0.05 was considered statistically significant.

4.4.8 Analysis of gene expression

RNA was isolated from a wild-type strain (MH11068) and from a *nmrA*Δ mutant (RT851) and sequenced at the Integrated Genomics Facility (Kansas State University), and the data analyzed as described in Chapter 2. To assess the role of nitrogen source in regulation of *sarA,* AN1808, AN11141, and AN0265, gene expression under glutamine, alanine, and nitrogen starvation conditions were each independently compared to expression on ammonium within each strain. Additionally, expression under each condition was compared between the wild type and *nmrA*Δ strains. Statistical analyses were performed using DESeq2 as described in Section 2.7.3.

4.5 Results

4.5.1 The *A. nidulans* genome encodes two distinct LAAOs

To better understand the role of *sarB* in amino acid utilization, we sought to better characterize putative LAAOs in *A. nidulans*. Public databases predicted the

uncharacterized gene AN1808 as a paralog of *sarA*. To confirm this and identify any other possible paralogs, we performed BLASTp using the SarA sequence against annotated *A. nidulans* protein sequences. Aside from itself, the first hit was the protein encoded by the uncharacterized gene AN1808, which exhibited similarity along nearly the entire length of the protein. Pairwise sequence alignment using EMBOSS Needle (https://www.ebi.ac.uk/jdispatcher/psa/emboss_needle; Madeira et al. 2024) showed that SarA and the AN1808 protein share 37.7% identity and 54.4% similarity. We thus considered AN1808 a probable LAAO and *sarA* paralog. To check for possible unannotated *sarA* paralogs, we used tBLASTn to compare the SarA and AN1808 sequences to the *A. nidulans* genome. No additional regions with strong homology were found.

We characterized *sarA* and AN1808 through manual sequence inspection and use of online tools. *sarA* is predicted to have one intron and produce a protein of 685 amino acid residues in length with a predicted molecular weight of 74.9 kDa, while the AN1808 gene has no introns and encodes a protein of 698 amino acid residues in length and a predicted molecular weight of 79 kDa. Interpro predicted an LAAO-characteristic amine oxidoreductase domain (IPR002937/PF01593) from amino acids 179-657 in SarA and 187-673 in AN1808. Manual inspection revealed a dinucleotide binding motif at amino acids 171-200 in SarA and 179-208 in AN1808, and a GG-motif at 204-211 of SarA and 212-219 of AN1808, both conserved in LAAOs (Figure 4.1; Vallon 2000). DeepTMHMM predicted that SarA and AN1808 are globular proteins with cleavable signal peptides. SignalP 6.0.0.56 (https://biolib.com/DTU/SignalP-6:0.0.56/; Teufel et al. 2022) also predicted 22-residue signal peptides in both proteins,

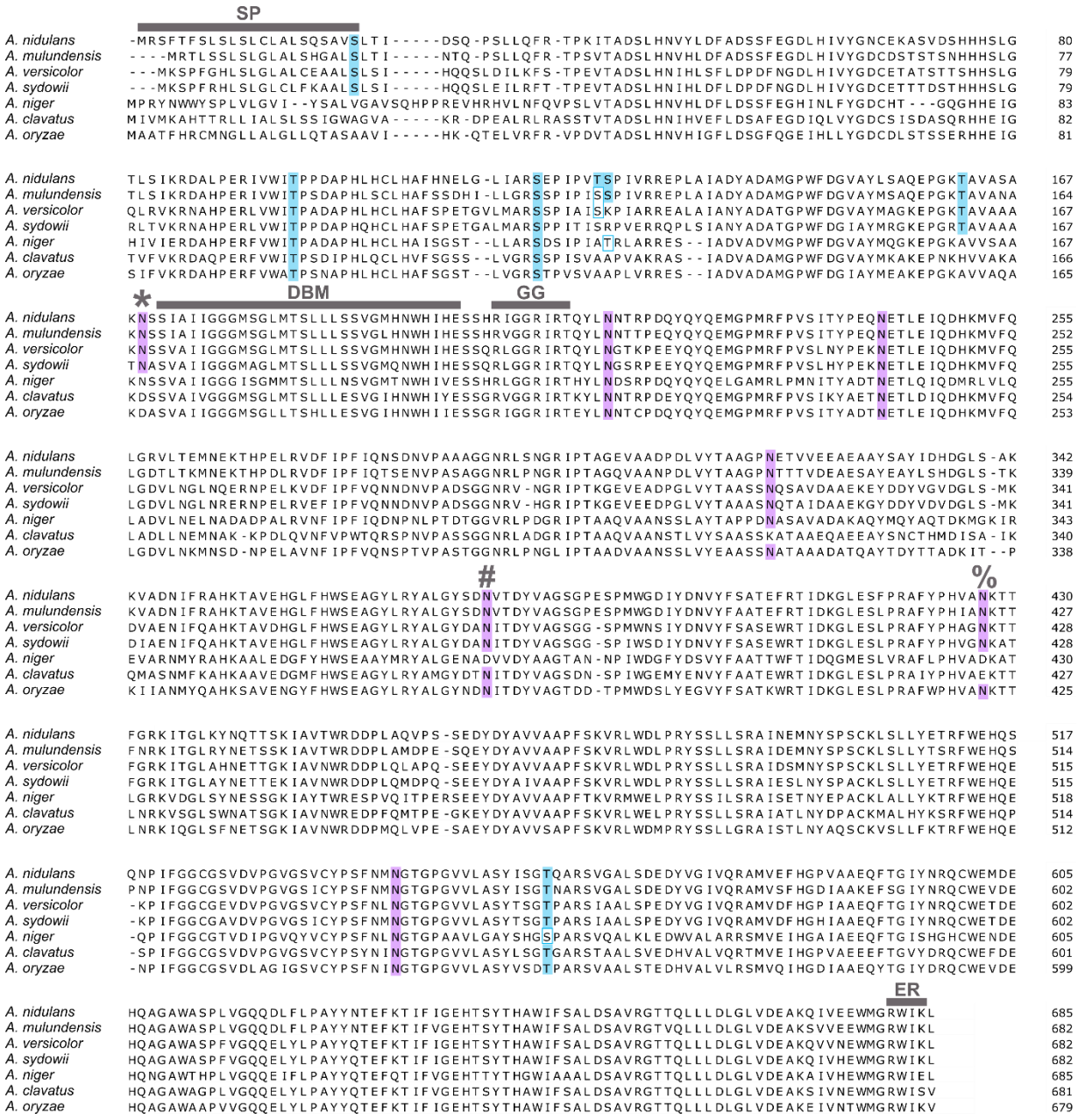

Figure 4.1 SarA contains conserved LAAO domains and shares some potential glycosylation sites with orthologs. A signal peptide (SP) at the N-terminus of SarA was predicted by SignalP 6.0.0.56. Manual inspection revealed a dinucleotide binding motif (DBM) and GG motif (GG), both conserved in LAAOs. An ER-retention sequence (ER) was predicted by Psort II. Multiple potential N-glycosylation (purple highlight) NetNGlyc 1.0. Of these, one was conserved with a confirmed N-glycosylation site in the basidiomycete fungus *H. cylindrosporum* LAAO4 (*), one with human IL4i1 (#), and one with zebrafish LAAO (%). Blue highlight shows potential O-GlcNAcylation sites predicted by Deep O-GlcNAc. Abbreviations: *A. nidulans* = *Aspergillus nidulans* SarA; *A. mulundensis* = *Aspergillus mulundensis* DSM5745_05734; *A. versicolor* = *Aspergillus versicolor* ASPVEDRAFT_25720; *A. sydowii* = *Aspergillus sydowii* ASPSYDRAFT_140934; *A. niger* = *Aspergillus niger* An08g10800; *A. clavatus* = *Aspergillus clavatus* ACLA_062240; *A. oryzae* = *Aspergillus oryzae* putative LAAO.

suggesting they are secreted. Psort II predicted ER retention sequences at the C-

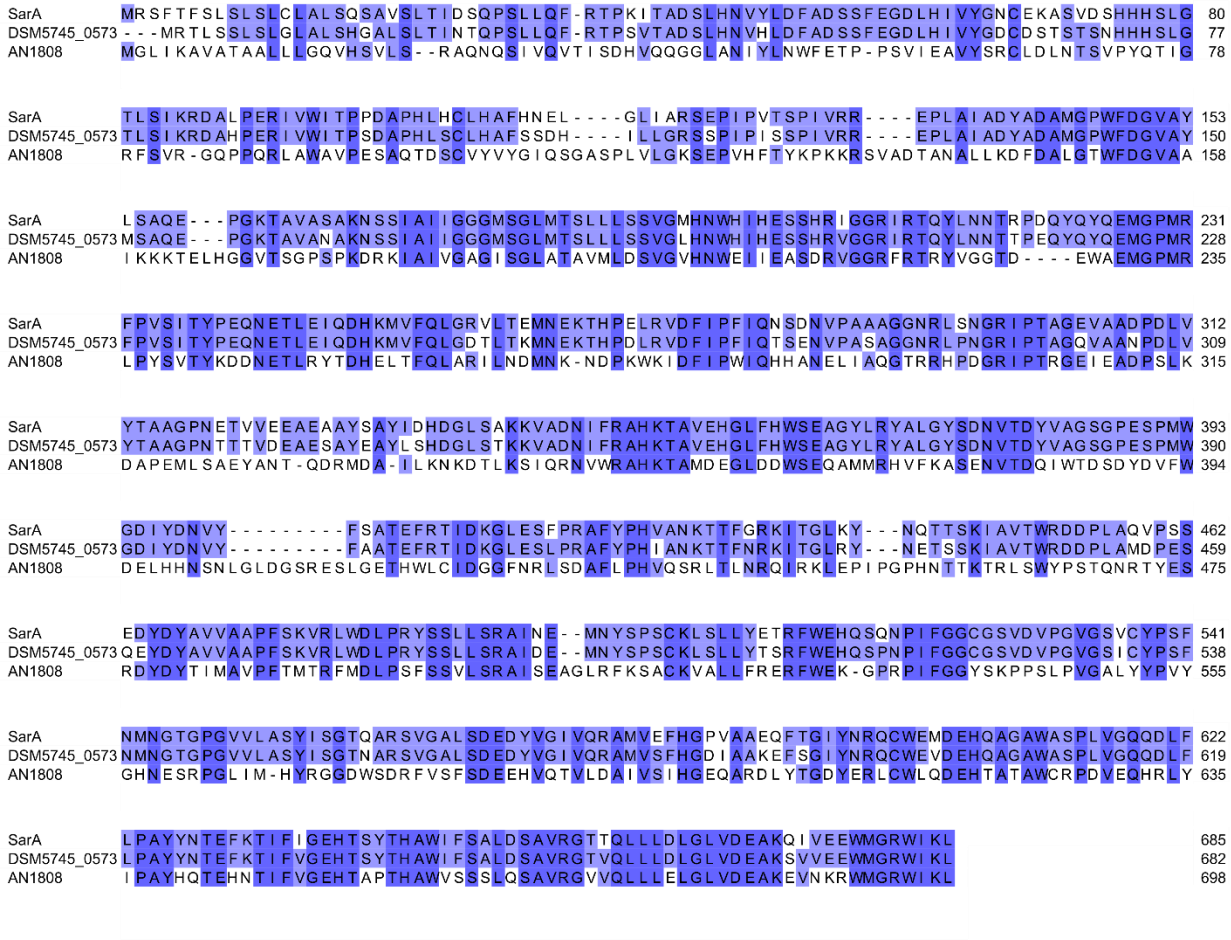

Figure 4.2 SarA has greater identity to orthologs in other species than to AN1808.
A sequence alignment between SarA, the SarA ortholog in *A. mulundensis* (DSM5745_05734), and AN1808 shows SarA is more identical to its ortholog than to AN1808. Alignment made with Custal Omega and visualized with Jalview 2.11.4.1.

terminus of each protein.

While LAAOs have not been found in ascomycete yeasts, LAAO production has been observed in many other fungi (Sikora and Marzluf 1982; Stasyk et al. 2010; Yang et al. 2011; Nuutinen et al. 2012; Isobe et al. 2014; Žun et al. 2017; Peng et al. 2021). However, the underlying LAAO genes are largely unstudied. We used the SarA and AN1808 sequences to search for orthologs among fungi. We found that SarA is more

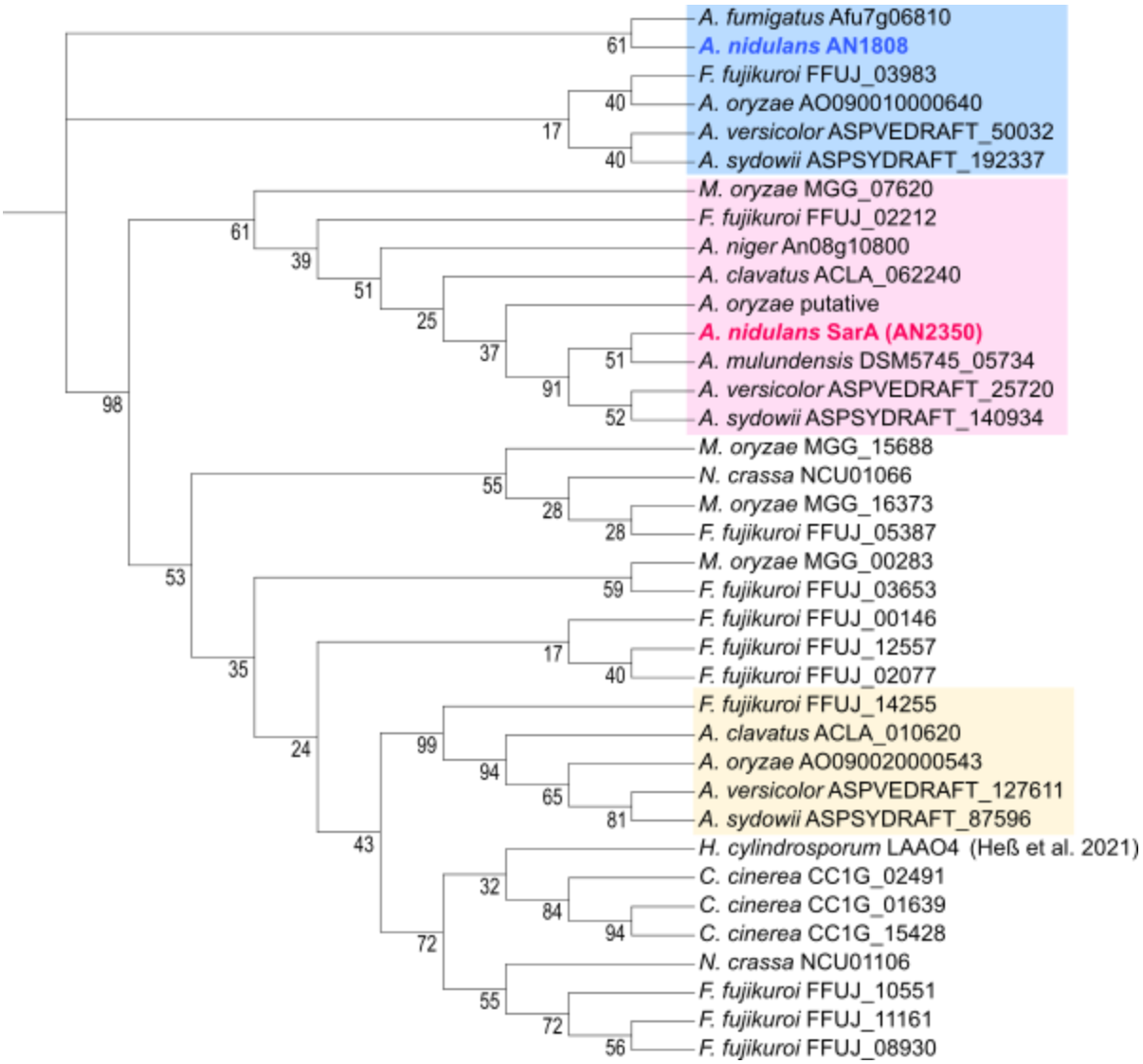

Figure 4.3 Multiple evolutionarily-distinct LAAOs are found in filamentous fungi.
SarA orthologs (pink), AN1808 orthologs (blue), and a third LAAO (yellow) are found in aspergilli. Tree developed using MAFFT v7 and visualized with Interactive Tree of Life v7 (iTOL; itol.embl.de).

similar to its orthologs than to AN1808, indicating they are different LAAOs (Figure 4.2). In aspergilli, we found at least three phylogenetically-distinct LAAOs (Figure 4.3)

In aspergilli, SarA-like LAAOs exhibit 60.7-87.2% identity and 75.5-93.9% to each other, while AN1808-like LAAOs have 59.3-80.8% identity and 66.2-89.0% similarity (Table 4.4). A third LAAO not present in *A. nidulans* was found in *Aspergilus oryzae, Aspergillus sydowii, Aspergillus versicolor, Aspergillus clavatus*, and other aspergilli. We confirmed the absence of this LAAO from *A. nidulans* by using the protein

sequence from its close relative *A. sydowii* for tBLASTn against both the version 4 *A. nidulans* genome and the version 5 unpublished telomere-to-telomere genomic sequence. Neither search yielded any likely candidate sequences. Phylogenetic analysis indicated the existence of other LAAOs in non-*Aspergillus* fungi, some of which cluster with Aspergillus LAAOs and some of which are evolutionarily distinct (Figure 4.3). LAAOs are found outside of the fungal kingdom. The human LAAO IL4i1 shares 17.7% identity and 26.8% similarity with SarA and 18.9% identity and 32.4% similarity with AN1808.

Table 4.4 . Comparison of SarA and AN1808 to other Aspergillus LAAOs.

Species	**Gene**	**% identity / % similarity to SarA**
A. mulundensis	DSM5745_05734	87.2 / 93.9
A. versicolor	ASPVEDRAFT_25720	77.9 / 87.0
A. sydowii	ASPSYDRAFT_140934	76.3 / 86.3
A. oryzae	(putative)	68.1 / 82.4
A. clavatus	ACLA_062240	66.9 / 80.0
A. niger	An08g10800	60.7 / 75.5
		% identity / % similarity to AN1808
A. versicolor	ASPVEDRAFT_50032	80.8 / 89.0
A. sydowii	ASPSYDRAFT_192337	79.8 / 88.7
A. fumigatus	Afu7g06810	79.8 / 88.0
A. oryzae	AO090010000640	59.3 / 66.2

4.5.2 *sarB* and *sarA* are in the same genetic pathway

Because mutations in *sarB* and *sarA* produce similar suppression of AreA102 growth phenotypes (Polkinghorne and Hynes 1975), we sought to determine if they did so through two different pathways of action or if they were in the same genetic pathway. Thus, we investigated the effect of deletion of both genes on the AreA102 phenotype of

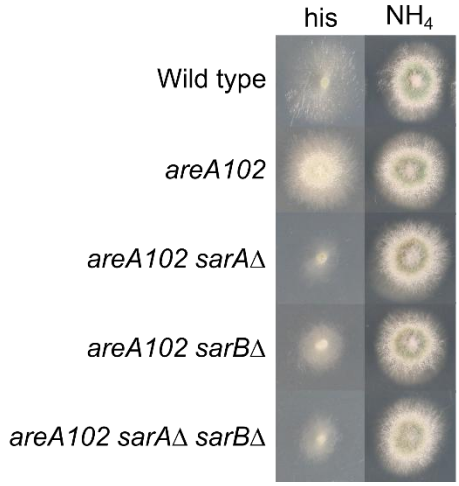

Figure 4.4 The sarBΔ *and* sarAΔ *mutations are not additive*. An *areA102 sarB*Δ *sarA*Δ mutant did not suppress the AreA102 strong growth on histidine to a greater degree than did an *areA102 sarA*Δ mutant or an *areA102 sarB*Δ mutant. Strains were grown on supplemented 1% glucose minimal media containing 10 mM nitrogen source and incubated for 48 h at 37 °C. Top to bottom: MH1, MH8, RT765, RT891, RT1022.

strong growth on histidine. We crossed a *sarB*Δ mutant (RT1015) with a *sarA*Δ *areA102* mutant (RT765) to produce *sarB*Δ *sarA*Δ mutants. *areA102* progeny were identified by weak growth on uric acid and strong growth on sucrose-acetamide media, and *sarB*Δ progeny, with the *sarB*Δ::*AfpyrG*+ selectable marker in a *pyrG89* background, were identified by pyrimidine prototrophy. *sarA*Δ progeny, with the *sarA*Δ::*riboB*+ selectable marker in a *riboB2* background, were identified by riboflavin prototrophy. Because we predict SarB is necessary for full SarA function, we hypothesized that no additive effect would be seen in the *sarB*Δ *sarA*Δ mutants. *sarB*Δ *sarA*Δ progeny in an *areA*+ background, like the single mutants, were phenotypically indistinguishable from wild type. *areA102 sarB*Δ *sarA*Δ progeny did not show a greater degree of suppression of the AreA102 strong growth phenotype on histidine compared to the single mutants (Figure 4.4). Because deleting both genes did not increase the severity of the phenotype, *sarB* and *sarA* are in the same genetic pathway.

4.5.3 SarA requires *sarB* for full function

To test the effects of *sarB* mutations on SarA function, we used LAAO assays to assess SarA activity. To ensure any LAAO activity measured in *sarB* mutants was due to SarA and not AN1808, we generated an *areA102 sarB*Δ AN1808Δ mutant by crossing a *sarB*Δ (AN8875Δ) mutant (RT855) to an *areA102* AN1808Δ mutant (RT774). Progeny exhibiting pyrimidine prototrophy were identified as having the AN8875Δ::*AfpyrG* and/or AN1808Δ::*AfpyrG* deletions. *areA102* progeny were identified by weak growth on uric acid as a sole nitrogen source and among these, *areA102* AN8875Δ progeny were identified by suppression of the *areA102* strong growth phenotype on histidine as a sole nitrogen source. To identify *areA102* AN8875Δ AN1808Δ mutants, several *areA102* AN8875Δ progeny were chosen for PCR confirmation. All were confirmed to have the AN8875Δ::*AfpyrG*+ gene replacement, with a subset also containing the AN1808Δ::*AfpyrG*+ gene replacement.

LAAO activity can be detected using in-gel or spectrophotometric assays (Kishimoto and Takahashi 2001; Žun et al. 2017). We adapted these assays to detect LAAO activity in *A. nidulans* protein extracts. We used in-gel LAAO assays to visually detect SarA activity. Mycelia were grown for 16 h with ammonium as a sole nitrogen source, harvested, washed, and transferred to growth media with histidine as a sole nitrogen source for 4 h to upregulate *sarA* expression. Cell-free extracts were made by grinding harvested mycelia with glass beads in 0.1 M Tris-HCl pH 8.0 buffer followed by centrifugation to separate the soluble cell-free extract from the pellet. Equal amounts of non-denatured proteins in each sample were separated by SDS-PAGE on a 7.5% resolving gel in 1x Tris-glycine buffer. The gel was incubated with a substrate solution

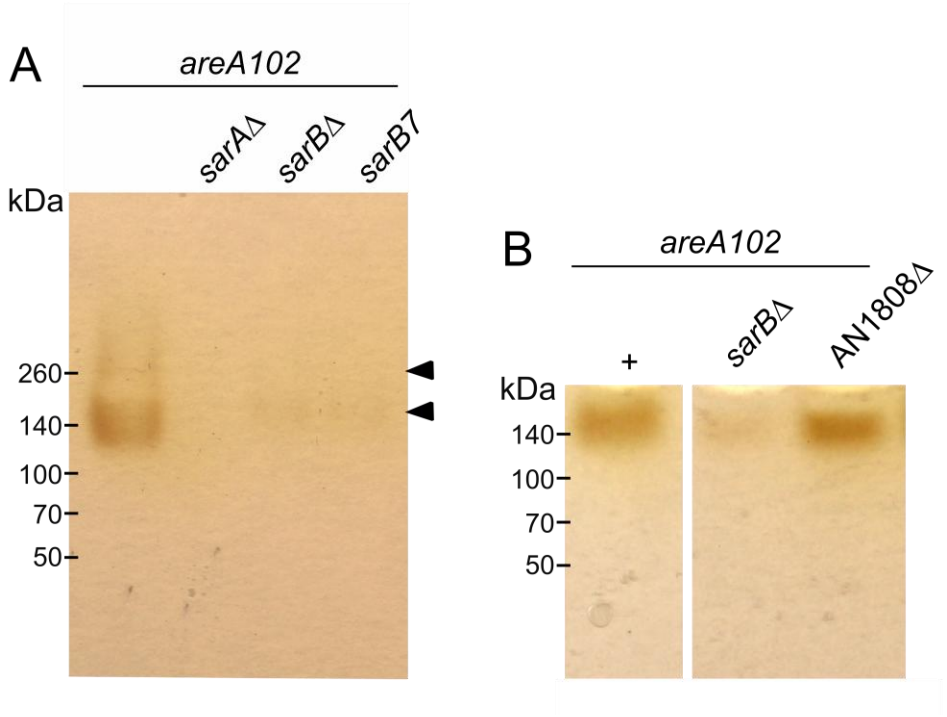

Figure 4.5 SarA activity is lower in sarB *mutants than wild type*.
(A) SarA activity is visible as a brown band with increased color intensity indicating higher activity. Bands for the *sarB* mutants are indicated by the black arrow. (B) Color intensity was similar for the *areA102* and *areA102* AN1808Δ mutants. Mycelia were grown in supplemented 1% glucose-10 mM ammonium minimal media for 16 h, washed, and transferred to supplemented 1% glucose-10 mM histidine for 4.h before harvesting. Soluble cell-free extracts in 0.1 M Tris-HCl pH 8.0 were separated on a 7.5% SDS-PAGE gel in 1x Tris-glycine buffer for 1.5 h. Protein concentrations were quantified using Nanodrop One to ensure equal loading of 30 μg of protein per well. Following electrophoresis the gel was soaked in a substrate solution of 5 mM histidine, 1 mM OPD, and 0.5 U HRP for 16 h at room temperature. Strains from left to right: MH8, RT765, RT891, MK160. A minimum of 2 biological replicates for each sample was performed.

consisting of either histidine or ornithine to provide a substrate for SarA, HRP, to interact with the hydrogen peroxide byproduct of the LAAO reaction, and OPD, to stain the HRP reaction products brown. If SarA activity was present, we expected to see a band at 75.9 kDa, the size predicted from the SarA 685-residue amino acid sequence. Because most LAAOs are active as dimers, and dimerization would likely not be disrupted in our samples, we also considered the possibility of a band at around twice that size. Because the predicted AN1808 and SarA proteins are similar in size, we expected AN1808 activity, if any, would produce bands at approximately the same locations as SarA.

After incubation overnight, a strong brown band was detected at ~150 kDa for the *areA102* mutant MH8, with a weak band at ~300 kDa (Figure 4.5A-B). These results strongly indicated activity of one or more LAAO proteins. As the protein samples were not denatured prior to electrophoresis due to the need to retain enzyme activity, the proteins may not run strictly according to size. However, the observed size is consistent with the LAAO activity in dimer form, with less abundant activity in a possible tetramer. No bands were visible for the *areA102 sarA*Δ mutant, indicating that the observed activities are SarA or *sarA*-dependent and AN1808 activity was not detected. Less intense LAAO activity bands of both sizes were seen for the *areA102 sarB*Δ and *areA102 sarB7* mutants, indicating that *sarB* is required for full SarA activity. No effect on LAAO activity was observed in the *areA102* AN1808Δ mutant, suggesting that the detected activity was independent of AN1808. These in-gel LAAO assay observations were reproducible in at least two biological replicates for each sample.

To quantify the effects of *sarB* mutations on SarA activity, we performed a quantitative LAAO assay by adding an amino acid-HRP-OPD substrate solution directly to soluble protein extracts from wild type and multiple mutant strains, and measured absorbance at 492 nm with a microplate reader. In cultures transferred to histidine for 4 h, LAAO activity was barely detectable in the (*areA*$^{+}$) wild-type strain (MH1) and in the *sarA*Δ and *sarB*Δ *sarA*Δ mutants (Figure 4.6A). The *areA102* mutant showed significantly higher LAAO specific activity (~11.5-fold) compared with wild type. This elevated specific activity was lost in the *areA102 sarA*Δ mutant, indicating that this increased LAAO specific activity observed in the *areA102* mutant was SarA-dependent and was likely SarA activity. The *areA102 sarB*Δ mutant exhibited ~30% of the specific

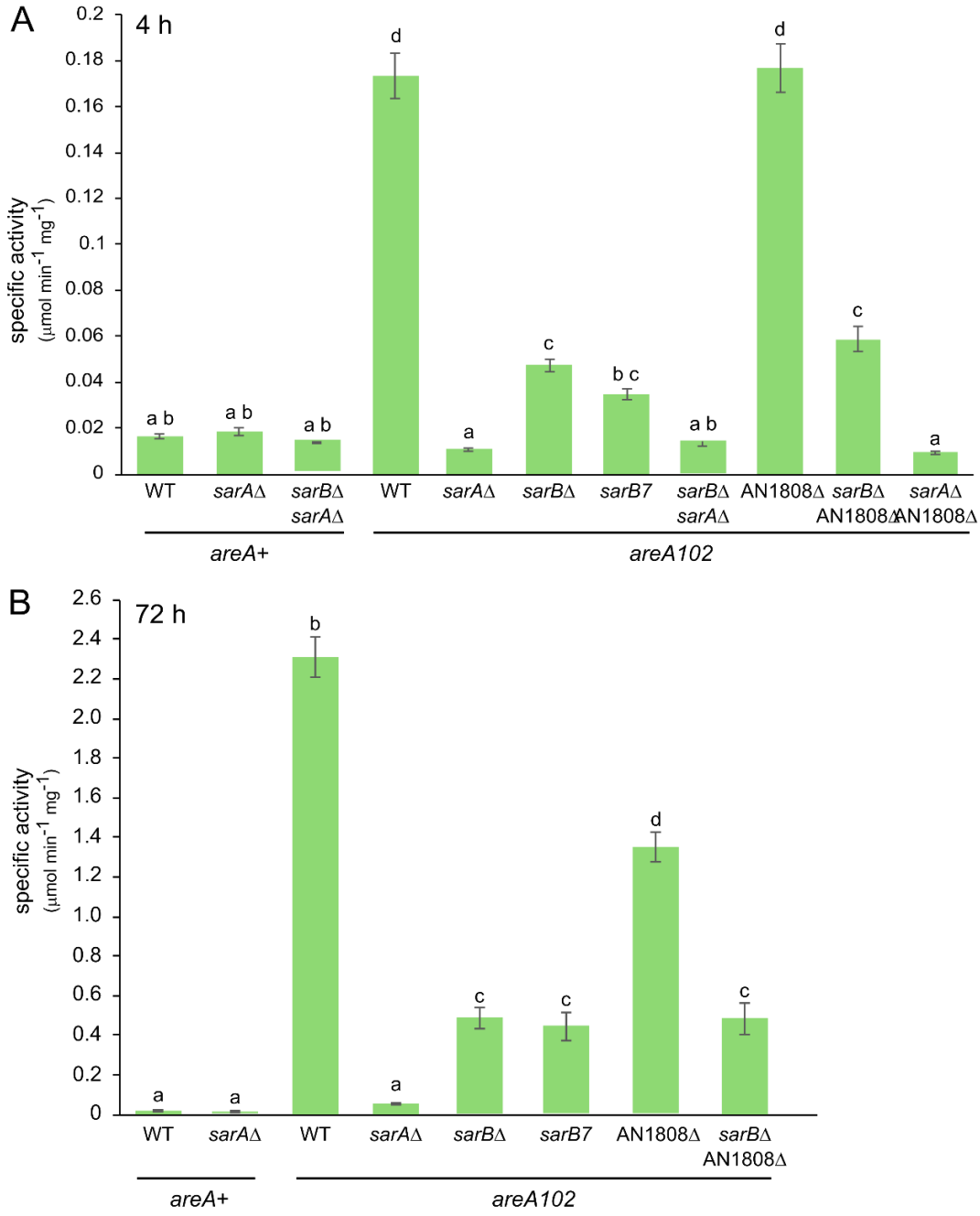

Figure 4.6 SarA specific activity varies between strains and timepoints.
(A) Mycelia were grown in supplemented 1% glucose-10 mM ammonium minimal media for 16 h, washed, and transferred to supplemented 1% glucose-10 mM histidine for 4.h before harvesting. Whole protein extracts in 0.1 M tris-HCl pH 8.0 were treated with a substrate solution of 5 mM ornithine, 2 mM OPD, and 0.8 U HRP for 1 h at 37 °C. Strains from left to right: MH1, RT763, RT1020, MH8, MH10571, RT891, MK160, RT1023, RT775, R1035, RT776. (B) Mycelia were grown in supplemented 1% glucose-10 mM ammonium minimal media for 16 h, washed, and transferred to supplemented 1% glucose-10 mM histidine for 72.h before harvesting. Whole protein extracts in 0.1 M Tris-HCl were treated with a substrate solution of 5 mM ornithine, 2 mM OPD, and 0.8 U HRP for 1 h at 37 °C. Strains from left to right: MH1, R763, MH8, MH10571, RT891, MK160, R775, RT1035. Two-way ANOVAs followed by Tukey's HSD tests were used to evaluate significant differences between strain activities within each timepoint. Letters indicate strains not significantly different from one another. *p*-values can be found in Appendix B. n=3 biological replicates with 2 technical replicates.

activity of the *areA102* mutant, supporting the visual evidence from the in-gel assay that *sarB* is necessary for full SarA activity. The *areA102 sarB*7 mutant (MK160) exhibited slightly lower specific activity than the *areA102 sarB*Δ mutant, but the difference was not statistically significant.

To ensure the activity detected was specifically from SarA, we included AN1808Δ mutants in our experiment. Activity in the *areA102* AN1808Δ mutant was similar to that observed in the *areA102* mutant (Figure 4.6A), indicating AN1808 activity played no detectable role in LAAO activity in the *areA102* mutant. Likewise, activity in an *areA102 sarB*Δ AN1808Δ mutant did not differ from the *areA102 sarB*Δ (AN1808+) mutant, indicating the LAAO activity detected in both strains was due only to SarA.

The mechanism by which SarA activity is detectable in an *areA102* background is likely due to the nature of the *areA102* mutation. The *sarA* gene contains seven potential AreA binding sites in its promoter, five of which are the TGATAR sequence to which AreA102 has increased affinity (Ravagnani et al. 1997; Davis et al. 2005). When *sarA* was expressed under a constitutive promoter in an *areA*+ background, it phenocopied the AreA102 strong growth on histidine phenotype (Davis et al. 2005). Thus, *sarA* is effectively upregulated in *areA102* mutants. However, AN1808 has only two potential AreA binding sites, CGATAG at -914 and AGATAA at -55. Both are sequences to which the AreA102 mutant protein has decreased affinity (Ravagnani et al. 1997). Thus, AN1808 may be downregulated in an *areA102* background. However, we did not detect LAAO activity in wild type, an *areA*+ *sarA*Δ mutant, or an *areA*+ *sarB*Δ *sarA*Δ mutant. Therefore, AN1808 does not contribute to LAAO activity in the wild type

or *areA102* mutant during growth on histidine 4 h after transfer. A full list of *p*-values associated with this experiment are found in Appendix B.

Because *sarA* was upregulated when grown in nitrogen-free conditions (see Section 4.5.8), we assessed SarA activity at a later timepoint when nutrients are depleted. Mycelia were grown for 16 h in supplemented 1% glucose-10 mM ammonium minimal media, washed, and transferred to supplemented 1% glucose-10 mM histidine for an additional 72 h of growth. Mycelia were harvested, cell-free soluble protein extracts were made, and LAAO specific activity was assessed using the quantitative assay. LAAO activity in wild type and the *sarA*Δ mutants remained low at levels similar to those observed at 4 h (Figure 4.6B). Therefore, even in older cultures, LAAO activity is still not experimentally detectable outside of an *areA102* background. LAAO activity was substantially higher in the *areA102* mutant at 72 h compared with 4 h. Similar to the observations at 4 h, LAAO activity was lost in the *areA102 sarA*Δ mutant indicating that the observed LAAO activity was SarA or SarA-dependent. LAAO activity was reduced to similar levels in the *areA102 sarB*Δ, *areA102 sarB*7, and *areA102 sarB*Δ AN1808Δ mutants, but these levels were higher than at 4 h. Additionally, the *areA102* AN1808Δ mutant also had higher SarA activity than at 4 h, but unlike at 4 h, at 72 h it was significantly lower than that seen in the *areA102* mutant MH8. This indicated that AN1808 activity accounted for around half of the LAAO activity seen in MH8 at this timepoint. The absence of AN1808 activity in *sarA*Δ mutants suggests that SarA must be present for AN1808 activity, perhaps involving a heterodimer. A full list of *p*-values associated with this experiment are found in Appendix B.

Because SarA has a predicted signal peptide at its N-terminus, we assessed SarA activity in the extracellular fraction of the growth cultures by growing mycelia for 16 h in our standard amount of supplemented 1% glucose-10 mM ammonium minimal media and then transferring to only 2 mL of media with histidine for 4 h, in an attempt to concentrate the enzyme and increase the likelihood of its detection. In-gel LAAO assays using 45 µg of proteins did not show any discernable secreted LAAO activity bands in the growth media for the *areA102* or *areA102 sarB*Δ mutants (data not shown).

4.5.4 *sarB* does not affect *sarA* at the transcriptional level

To determine the influence of *sarB* on transcription of SarA, we performed RT-qPCR to compare SarA expression in an *areA102* mutant versus an *areA102 sarB*Δ mutant (n = 3 biological replicates). We grew mycelia for 16 h in supplemented 1% glucose-10 mM ammonium minimal media before washing and transferring mycelia to 1% glucose-10 mM histidine media, then isolating RNA from both strains. Statistical analysis indicated there was no difference in *sarA* transcript abundance between the two strains ($F = 0.105$, $p = 0.78$). This indicates the effect of *sarB* on SarA activity is not due to regulation of transcription or mRNA stability and is post-transcriptional in nature.

4.5.5 SarA is N-glycosylated

sarB orthologs in *K. lactis* and humans both encode products that play roles in glycosylation of proteins. We thus considered one or more roles for SarB in glycosylation of SarA. To examine this possibility, we first sought to determine if SarA is glycosylated and if glycosylation is necessary for activity. Using online tools, we analyzed the SarA protein sequence for predicted glycosylation sites. We found no evidence in the literature that canonical O-glycans in fungi contain GlcNAc. Additionally,

we used BLASTp to compare the sequences of eleven human proteins involved in adding GlcNAc to O-glycans (GCNT1/2/3/4/7, MFNG, LFNG, RFNG, MGAT5B, POMGNT1/2; Schjoldager et al. 2020) against annotated proteins in *A. nidulans*. No likely orthologs of the human proteins were found. Therefore, we did not further consider canonical O-glycosylation and investigated the likelihood of only N-glycosylation and O-GlcNAcylation in *A. nidulans*. Although O-GlcNAcylation sites are difficult to predict and proteins with signal peptides are generally not O-GlcNAcylated, we used Deep O-GlcNAc (Zhang et al. 2024) to predict possible modification sites in SarA. Six potential O-GlcNAcylation sites were identified (Figure 4.1, blue), some of which are conserved in other aspergilli surveyed. We identified eight potential N-glycosylation sites in SarA (Figure 4.1, purple) using NetNGlyc 1.0 (Gupta and Brunak 2002). One, N168, aligned with the site identified in the basidiomycete fungus *Hebeloma cylindrosporum* as most crucial for LAAO4 function (Heß et al. 2021). N378 aligned with a confirmed N-glycosylation site in human IL4i1 (Chavan et al. 2002) and N427 aligned with a confirmed site in the zebrafish LAAO (Huang et al. 2021). No predicted N-glycosylation sites in *A. nidulans* SarA aligned with confirmed sites in LAAOs from snake venoms (Moustafa et al. 2006; Georgieva et al. 2011; Feliciano et al. 2017). Other predicted N-glycosylation sites in *A. nidulans* SarA were entirely or partially conserved in aspergilli (Figure 4.1).

Glycosylation can be required for mature protein activity, stability, solubility, or proper protein folding. To both test for the presence of N-glycosylation in SarA and assess the effects of preventing N-glycosylation establishment, growing mycelia were treated with tunicamycin, an antibiotic that inhibits the first step in N-glycan formation

(Elbein 1981). This approach allowed us to evaluate whether N-glycosylation plays any role in SarA activity, whether through influencing mature protein activity, stability, solubility, or folding. Mycelia from the *areA102* and *areA102 sarB*Δ mutants were each grown for 16 h in supplemented 1% glucose-10 mM ammonium minimal media, harvested, washed, and transferred to 1% glucose-10 mM histidine minimal media with or without tunicamycin for an additional 4 h. We expected that the majority of SarA protein would be produced during growth on histidine based on the low levels of SarA activity observed after transfer to ammonium and high levels of SarA activity after transfer to histidine in the *areA102* mutant (Polkinghorne and Hynes 1975). Our work in Section 4.5.3 established that only SarA LAAO activity is detected at this timepoint, without contribution from AN1808. After harvesting mycelia and preparation of protein extracts, we performed an in-gel LAAO assay to see if an increase in SarA mobility occurred that would indicate a lack of addition of N-glycans. The SarA activity band observed on the gel for the tunicamycin-treated *areA102* sample traveled further than the untreated sample band and was less intense in color, indicative of a smaller protein size and reduced activity (Figure 4.7A). The tunicamycin-treated band for the *areA102 sarB*Δ mutant was not visible, most likely due to loss of activity. We used the protein extracts to perform a quantitative LAAO assay. SarA activity in tunicamycin-treated samples from the *areA102* mutant was 74% of that in the untreated sample ($p < 0.000001$), and activity in the *areA102 sarB*Δ mutant was 62% of that in the untreated sample ($p < 0.00001$; Figure 4.7B). Therefore, the addition of tunicamycin to the growth media reduces SarA activity in the presence and absence of SarB. The in-gel and

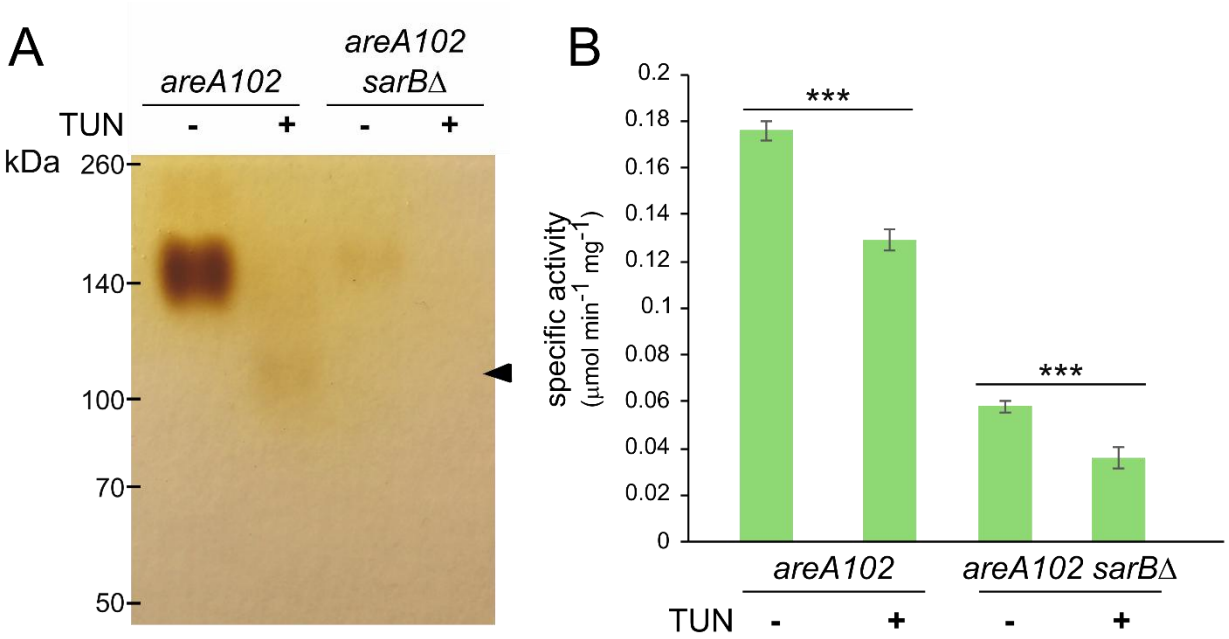

Figure 4.7 Treatment with the N-glycosylation inhibitor tunicamycin causes a change in mobility and a decrease in activity in SarA.
(A) In an in-gel LAAO assay, treatment with tunicamycin led to a mobility change of SarA and a less intense LAAO activity band compared to the untreated sample for the a*reA102* mutant. The tunicamycin-treated sample band was not discernable for the *areA102 sarB*Δ mutant. The protein extracts were separated by electrophoresis for 4 h on a 7.5% SDS-PAGE gel in 1x Tris-glycine buffer, then soaked in a substrate solution of 5 mM ornithine, 1 mM OPD, and 0.5 U HRP for 16 h at room temperature. Protein concentrations were quantified through Bradford assay to ensure equal loading of 90 μg of protein per well. n = 2 biological replicates with samples run in duplicate. (B) Tunicamycin-treated samples showed less LAAO enzyme activity than untreated samples in both the *areA102* and *areA102 sarB*Δ mutants in a quantitative LAAO assay. Protein extracts in 0.1 M Tris-HCl pH 8.0 were treated with a substrate solution of 5 mM ornithine, 2 mM OPD, and 0.8 U HRP for 1 h at 37 °C. For both assays, mycelia were grown in supplemented liquid 1% glucose-10 mM ammonium minimal media for 16 h, washed, and transferred to supplemented liquid 1% glucose-10 mM histidine minimal media lacking or containing 20 μg/mL tunicamycin for an additional 4 h before harvesting. Asterisks denote treated samples that were significantly different in activity from the corresponding untreated sample: *, $p < 0.05$, **, $p < 0.01$, *** $p < 0.001$. Two-way ANOVAs compared treated to untreated condition within each strain. n=3 biological replicates with 2 technical replicates.

quantitative assays together provide strong evidence that SarA is N-glycosylated and that N-glycosylation is necessary for full SarA activity.

To assess the effects of de-glycosylation of mature proteins, we used PNGase F to remove N-glycans from proteins in the *areA102* mutant and *areA102 sarB*Δ mutant. This enzyme breaks the linkage between the asparagine residue of the protein and the base of the N-glycan (Tarentino et al. 1989). Like the tunicamycin experiment, this protocol tests for the presence of N-glycans on SarA through observation of a mobility change in the in-gel assay. However, this approach additionally tests specifically for the

effect of N-glycosylation on mature protein activity, allowing a more granular examination of the SarA mechanism of activity. The manufacturer's instructions recommended incubation of proteins with PNGase F at 37 ˚C for 1-18 h and stated that the duration needed is target protein-dependent, particularly if the proteins are not denatured. Because we needed to measure LAAO enzyme activity after incubation and wanted to minimize loss of SarA activity during the incubation, we used an incubation time of only 4 h for both treated and untreated protein extracts in an attempt to balance the time needed for glycan removal and maintaining LAAO activity. In an in-gel LAAO assay, the gel showed bands of the same size in both the PNGase F-treated and untreated samples (Figure 4.8A). Treatment of the singly-N-glycosylated purified chicken ovalbumin protein with PNGase F under the same conditions as *A. nidulans* extracts confirmed partial de-glycosylation (Appendix C). For our experiments, we used whole cell-free extracts, and it is possible 4 h was insufficient to de-glycosylate SarA in the treated samples. If only a portion of SarA proteins in the sample were of a smaller size due to deglycosylation, they may have been of insufficient quantity to be visible on the gel, especially coupled with an overall decrease in activity in all samples from heating during the PNGase F treatment process. However, in the quantitative LAAO assay, the treated protein extracts of both strains showed a modest but statistically significant reduction in SarA activity compared with the untreated extracts, with SarA from the treated *areA102* mutant extract exhibiting 89% of that from the untreated ($p < 0.0001$), and the treated *areA102 sarB*Δ mutant extract having 72% as much activity as the untreated sample ($p = 0.0042$; Figure 4.8B). Despite the inconclusive results from

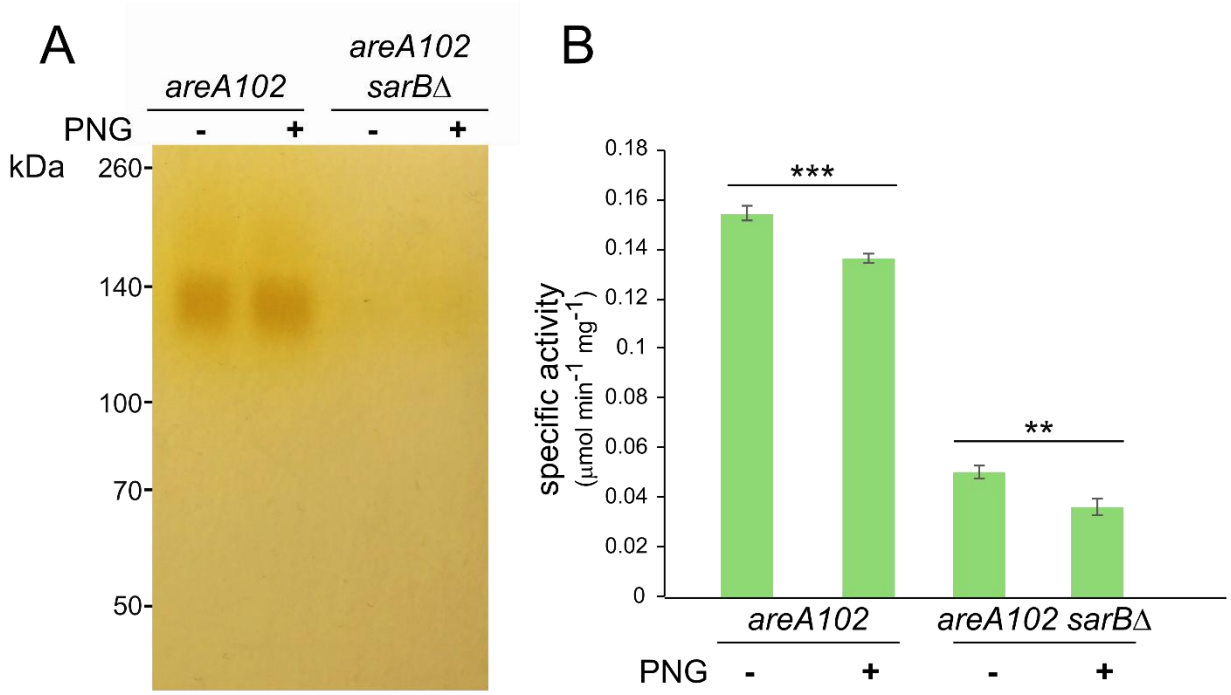

Figure 4.8 Treatment with the de-glycosylation agent PNGase F causes a slight reduction of SarA activity. (A) In an in-gel LAAO assay, treatment with PNGase F did not lead to visible change in mobility of SarA in the *areA102* mutant. The PNGase F-treated sample band was not discernable for the *areA102 sarB*Δ mutant. The protein extracts were separated by electrophoresis for 4 h on a 7.5% SDS-PAGE gel in 1x Tris-glycine buffer, then soaked in a substrate solution of 5 mM ornithine, 1 mM OPD, and 0.5 U HRP for 16 h at room temperature. Protein concentrations were quantified by Bradford assay to ensure PNGase F treatment of 40 μg of protein per sample. n = 2 biological replicates with samples run in duplicate. (B) PNGase-F-treated samples showed less protein activity than untreated samples in both the *areA102* and *areA102 sarB*Δ mutants in a quantitative LAAO assay. Protein extracts in 0.1 M Tris-HCl pH 8.0 were treated with a substrate solution of 5 mM ornithine, 2 mM OPD, and 0.8 U HRP for 1 h at 37 °C. For both assays, mycelia were grown in supplemented 1% glucose-10 mM ammonium minimal media for 16 h, washed, and transferred to supplemented 1% glucose-10 mM histidine minimal media for an additional 4 h before harvesting. Extracts were treated or not treated with PNGase F and incubated for 4 h at 37 °C before the assays. Asterisks denote treated samples that were significantly different in activity from the corresponding untreated sample: *, $p < 0.05$, **, $p < 0.01$, *** $p < 0.001$. Two-way ANOVAs compared treated to untreated condition within each strain. n=3 biological replicates with 2 technical replicates.

the in-gel assay, the microplate reader assay suggests that de-glycosylation of mature SarA protein negatively affects its activity level.

4.5.6 Glycosylation mutants do not phenocopy *sarB* mutants

After establishing that SarA is N-glycosylated, we sought to establish a connection between *sarB* and glycosylation of SarA. During the in-gel assay of *sarB* mutants described earlier (Section 4.5.3), no change in mobility was noted for the *areA102 sarB*Δ or *areA102 sarB7* mutants, suggesting that mutation of *sarB* does not

affect glycosylation of active SarA. However, in these mutant strains, SarA activity is reduced, not abolished. Given the role of *K. lactis* MNN2-2, we had no reason to believe that mutation of *sarB* would cause total loss of N-glycosylation of SarA, and thus it would be possible for the effects of *sarB* mutation on SarA protein size to be subtle and a mobility change difficult to detect. If SarB provides GlcNAc for N-glycosylation, its loss would eliminate terminal GlcNAc molecules on N-glycans and confer only a small change in mobility. Additionally, the in-gel LAAO assay does not produce tight activity bands, making discrimination of small changes in size difficult.

To better evaluate a possible role for *sarB* in glycosylation of SarA, we considered involvement N-GlcNAc transferase (GNT) required for N-glycosylation, and O-GlcNAc transferase (OGT) required for O-GlcNAcylation. Both use UDP-GlcNAc as a substrate and thus it is plausible that action of SarB, a putative UDP-GlcNAc transporter, affects their activities. Using the *K. lactis* GNT1 protein sequence, we queried a database of *A. nidulans* annotated proteins and found AN11141 as a possible ortholog. This gene has been reannotated in the version 5 reannotation of the *A. nidulans* genome, so we used the reannotated sequences going forward. Aligning *Kl*GNT1 and AN11141 showed they are 20.2% identical and 33.3% similar. AN11141 contains an IPR030518 (glucose N-acetyltransferase) domain and is annotated as a GNT. To search for an *A. nidulans* OGT, we used the full-length human OGT protein sequence (NCBI accession number NP_858058.1) to BLAST a database of annotated *A. nidulans* proteins. The best hit was for AN0265, which was 18.1% identical and 27.8% similar to human OGT.

We hypothesized that if either or both of AN11141 and AN0265 were in the *sarB-sarA* genetic pathway, mutants deficient in these genes should phenocopy the *sarB*Δ and *sarA*Δ mutant suppression of the AreA102 strong growth on histidine. To test this hypothesis, we constructed single deletion mutants for each gene. To construct an AN11141Δ mutant, the AN11141Δ::*AfpyrG* knockout construct obtained from the FGSC was transformed into a *pyrG89* recipient strain RT865 (*pyrG89 nkuA*Δ) (Figure 4.9A). To construct an AN0265Δ mutant, the AN0265Δ::*AfpyrG* knockout construct was transformed into RT865 (Figure 4.9B). Transformants were selected for pyrimidine prototrophy. Five transformants from each experiment were chosen for further analysis and were confirmed by PCR to have the correct gene replacement of AN11141 or AN0265 (data not shown).

Like *sarB* and *sarA* mutations in an *areA*+ background, neither the AN11141Δ mutant nor the AN0265Δ mutant showed a detectable growth phenotype on minimal media containing histidine as a sole nitrogen source (Figure 4.9C). To examine the mutant phenotypes in an *areA102* background, we crossed both strains to the *areA102* mutant strain MH8 to construct double mutants. *areA102* progeny were identified by weak growth on uric acid as a sole nitrogen source and strong growth on sucrose-acetamide media. In both crosses, no *areA102* progeny exhibited suppression of the AreA102 strong growth on histidine or lysine characteristic of *sarA*Δ or *sarB*Δ mutations. We used PCR to confirm that a subset of the *areA102* progeny in the AN11141Δ mutant cross were *areA102* AN11141Δ mutants and a subset of the progeny in the AN0265Δ mutant cross were *areA102* AN0265Δ mutants. Thus, deletion of neither gene phenocopied *sarA* or *sarB* mutants in an *areA102* background. If *sarB* affects SarA

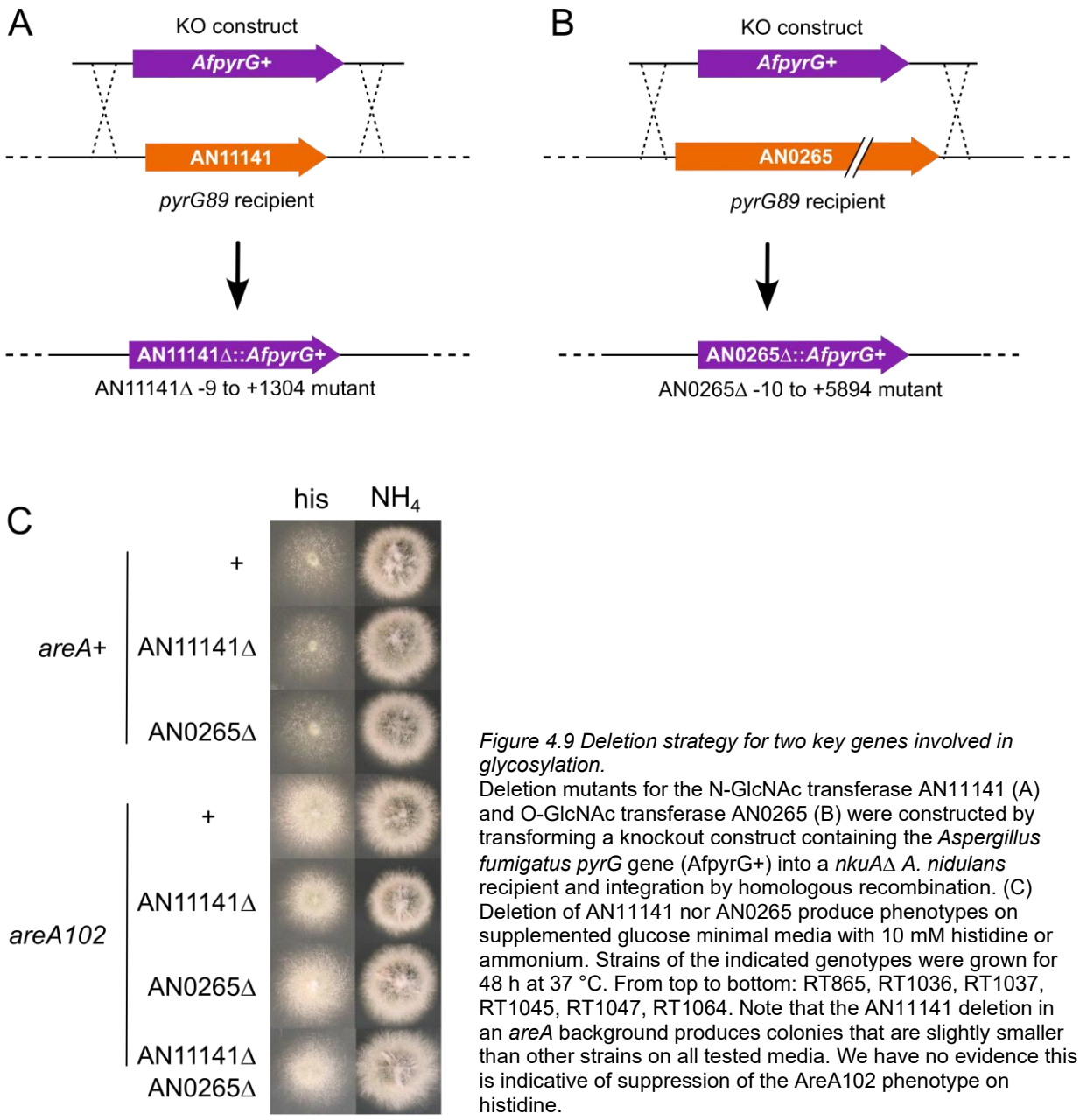

Figure 4.9 Deletion strategy for two key genes involved in glycosylation.
Deletion mutants for the N-GlcNAc transferase AN11141 (A) and O-GlcNAc transferase AN0265 (B) were constructed by transforming a knockout construct containing the *Aspergillus fumigatus pyrG* gene (AfpyrG+) into a *nkuAΔ A. nidulans* recipient and integration by homologous recombination. (C) Deletion of AN11141 nor AN0265 produce phenotypes on supplemented glucose minimal media with 10 mM histidine or ammonium. Strains of the indicated genotypes were grown for 48 h at 37 °C. From top to bottom: RT865, RT1036, RT1037, RT1045, RT1047, RT1064. Note that the AN11141 deletion in an *areA* background produces colonies that are slightly smaller than other strains on all tested media. We have no evidence this is indicative of suppression of the AreA102 phenotype on histidine.

activity via both the N-glycosylation and O-GlcNAcylation pathways, we considered that deletion of a single enzyme may mask the impact of *sarB* mutations. Therefore, we constructed AN11141Δ AN0265Δ double mutants by crossing an *areA102* AN11141Δ mutant to an AN0265Δ mutant. *areA102* progeny were identified as described above, but none exhibited suppression of AreA102 strong growth on histidine or lysine. To

ensure deletion of both genes was not synthetic lethal, we PCR confirmed double mutants in a proportion of the progeny. Therefore, neither AN11141 nor AN0265 appear to be part of the *sarB-sarA* genetic pathway.

To assess the effect of these gene deletions on SarA activity, we performed the LAAO assays using protein extracts from the *areA102* AN11141Δ and *areA102* AN0265Δ mutants. In the in-gel assay, neither mutant exhibited SarA LAAO activity obviously different than that of the *areA102* mutant (Figure 4.10A). However, subtle changes in activity would be difficult to detect through this method. For the *areA102* AN0265Δ mutant, no change in protein mobility was observed, but because OGTs add only single GlcNAc molecules to a threonine or serine residue, electrophoretic methods generally lack the sensitivity required to detect a loss of O-GlcNAcylation (Fu and Aalten 2020). However, the SarA activity band for the *areA102* AN11141Δ mutant migrated slightly further on the gel than for the *areA102* strain, indicative of a small change in mobility of at least a portion of SarA protein molecules. To ensure the observed change was reproducible, two biological replicates with two gels each were run. As a GNT, AN11141 is predicted to add GlcNAc molecules to N-glycan trees, and its absence would cause only a small reduction in N-glycan size and in overall protein size. The activity shift observed in the *areA102* AN11141Δ compared to the *areA102* samples suggests that, unlike *S. cerevisiae* and *H. polymorpha* (Kim et al. 2003)*, A. nidulans* is capable of producing N-glycans decorated with GlcNAc and that SarA is glycosylated with at least one GlcNAc-decorated glycan. However, the observed change in protein size exceeded what was observed for *sarB* mutants in the in-gel assay, making the relationship between *sarB* and AN11141 unclear.

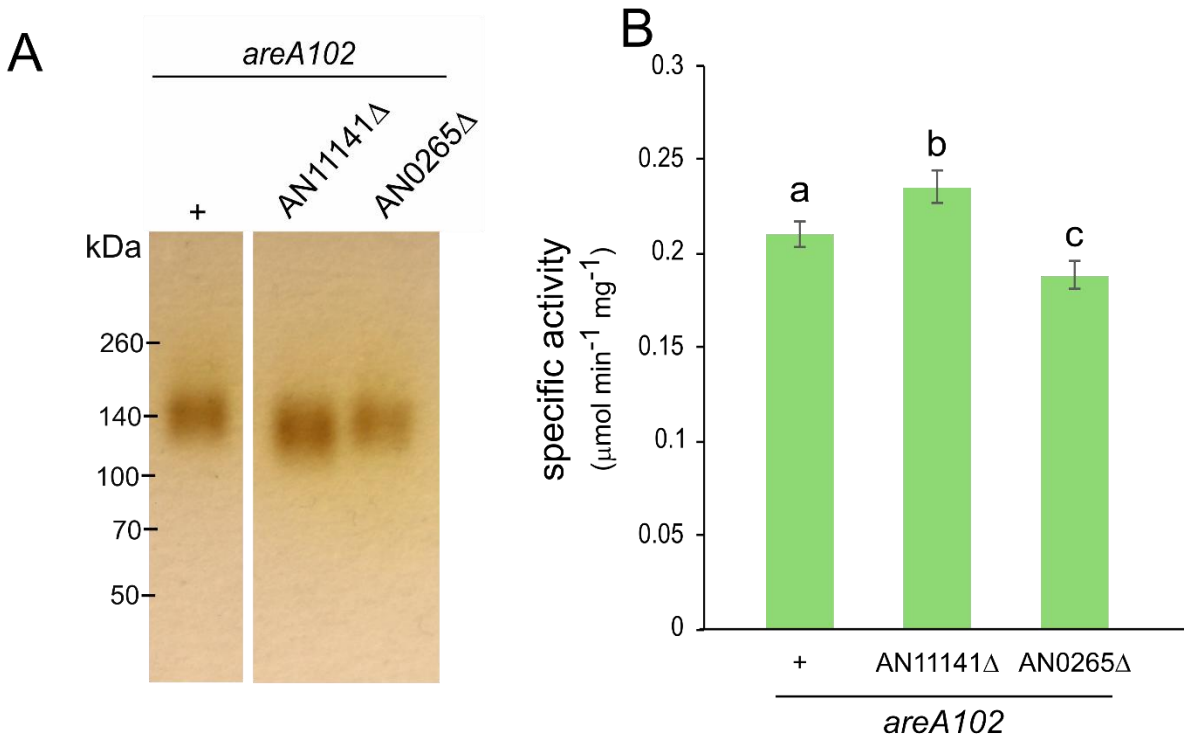

Figure 4.10 Mutation of glycosylation genes causes changes in SarA mobility and activity.
(A) In an in-gel LAAO assay, the *areA102* AN11141Δ mutant had slightly greater mobility of the SarA enzyme activity than the *areA102* mutant. Mobility of the SarA enzyme activity for the *areA102* AN0265Δ mutant did not change. The samples were separated by electrophoresis for 4 h on a 7.5% SDS-PAGE gel in 1x Tris-glycine buffer, then soaked in a substrate solution of 5 mM ornithine, 1 mM OPD, and 0.5 U HRP for 16 h at room temperature. Protein concentrations were quantified by Bradford assay to ensure equal loading of 90 μg of protein per well. n = 2 biological replicates with samples run in duplicate. (B) The *areA102* AN11141Δ mutant showed greater activity than the *areA102* mutant in the quantitative LAAO assay, while activity of the *areA102* AN0265Δ mutant was less than the *areA102* mutant. Protein extracts in 0.1 M Tris-HCl pH 8.0 were treated with a substrate solution of 5 mM ornithine, 2 mM OPD, and 0.8 U HRP for 1 h at 37 °C. For both assays, mycelia were grown in supplemented 1% glucose-10 mM ammonium minimal media for 16 h, washed, and transferred to supplemented 1% glucose-10 mM histidine minimal media for an additional 4 h before harvesting. Two-way ANOVAs followed by Tukey's HSD tests were used to evaluate significant differences between strain activities. Letters signify different statistical significance groups. $p < 0.00001$ for all comparisons. n=3 biological replicates with 2 technical replicates.

In quantitative microplate reader LAAO assays, the *are102* AN11141Δ mutant surprisingly showed 112% of the activity the *areA102* mutant, a difference that was statistically significant ($p < 0.0000001$; Figure 4.10B). The *areA102* AN0265Δ mutant showed a significant reduction in activity at 90% of the *areA102* mutant activity ($p < 0.00001$).

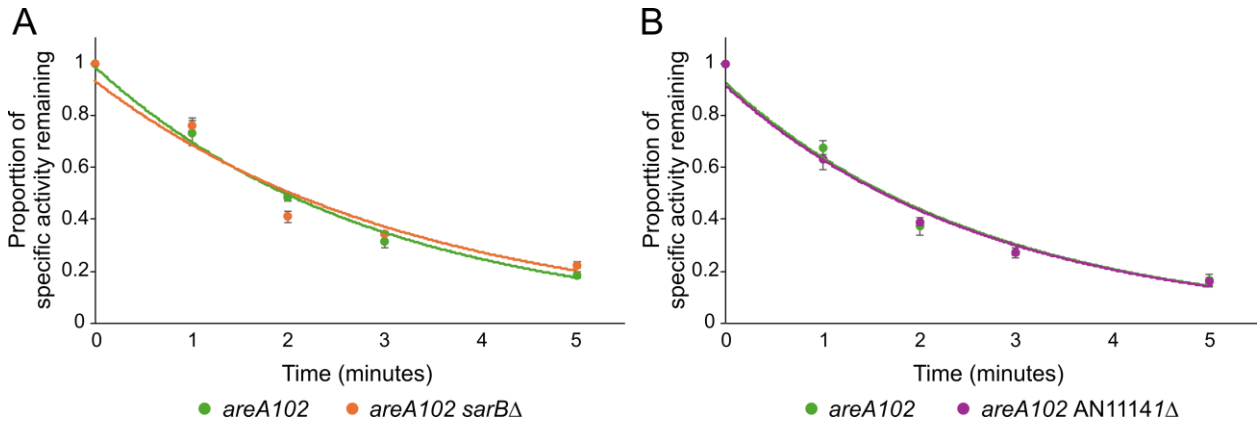

Figure 4.11 Deletion of sarB *or AN11141 does not change the thermolability of SarA in protein extracts.* Soluble cell-free extracts (20 μg) were heat-inactivated at 56˚C for 0, 1, 2, 3, or 5 minutes and subjected to a quantitative LAAO assay. (A) Loss of SarA specific activity in extracts, expressed as proportion of activity remaining, from the *areA102 sarB*Δ mutant and the *areA102* mutant did not differ (p = 0.6528) (B) Loss of SarA specific activity in extracts from the AN11141Δ mutant did not differ from that in extracts from the *areA102* mutant (p = 0.8862). For both assays, protein extracts in 0.1 M Tris-HCl pH 8.0 were treated with a solution of 5 mM ornithine, 2 mM OPD, and 0.8 U HRP for 1 h at 37 °C. Mycelia were grown in supplemented 1% glucose-10 mM ammonium minimal media for 16 h, washed, and transferred to supplemented 1% glucose-10 mM histidine minimal media for an additional 4 h before harvesting. Strains were compared using ANOVA considering time, replicate, strain, and the time-strain interaction. Line slopes were evaluated for the best-fit model followed by a likelihood ratio test. n = 3 biological replicates with 2 technical replicates for (A) and (B).

4.5.7 Deletion of *sarB* or AN11141 does not affect thermolability of SarA in protein extracts

To further attempt to discover the role of *sarB* on SarA activity, we hypothesized that *sarB* mutations may increase the thermolability of the SarA protein. To test this hypothesis, we heat-inactivated soluble protein extracts from the *areA102* mutant MH8 and the *areA102 sarB*Δ mutant RT891 for 0, 1, 2, 3, or 5 minutes at 56 °C, then performed the quantitative LAAO assay. Because previous experiments had shown the specific activity of the two strains to be very different, activity was assessed as the proportion of specific activity remaining at each timepoint. There was no difference in LAAO thermolability between the strains (p = 0.6528; Figure 4.11A), suggesting that the absence of SarB does not affect thermolability of SarA.

We additionally tested the effect of GlcNAc decoration of N-glycans on SarA thermolability in protein extracts by conducting a similar heat-inactivation experiment with protein extracts from the *areA102* AN11141Δ mutant. Again, there were no differences in proportion of specific activity remaining over time between the two strains (p = 0.8862; Figure 4.11B). We concluded that terminal GlcNAc molecules on N-glycans have no effect on thermolability of SarA.

4.5.8 *sarA* is upregulated in nitrogen-free conditions

To determine if *sarA*, *sarB*, AN1808, AN11141, and AN0265 are regulated by nitrogen, we used RNA-seq to assess the expression of these genes in a wild-type *areA* strain on ammonium, glutamine, and alanine as sole nitrogen sources and under 4-h nitrogen starvation. *sarA* had low expression under ammonium, glutamine, and alanine conditions but was upregulated under the nitrogen-free condition compared to ammonium (Figure 4.12). AN1808 had negligible expression under all tested conditions.

sarB, AN11141, and AN0265 were expressed constitutively and under all conditions, though there was a non-statistically-significant trend toward higher expression of the latter two under derepressing conditions. Constitutive expression of AN11141 and AN0265 suggests both N-glycosylation and O-GlcNAcylation may occur widely in *A. nidulans*. We also evaluated the role of the AreA co-repressor NmrA as a regulator of *sarB, sarA*, AN11141, and AN0265 by examining their expression in a *nmrA*Δ mutant. None of the genes were differentially expressed in the *nmrA*Δ mutant compared with wild type under any conditions (data not shown).

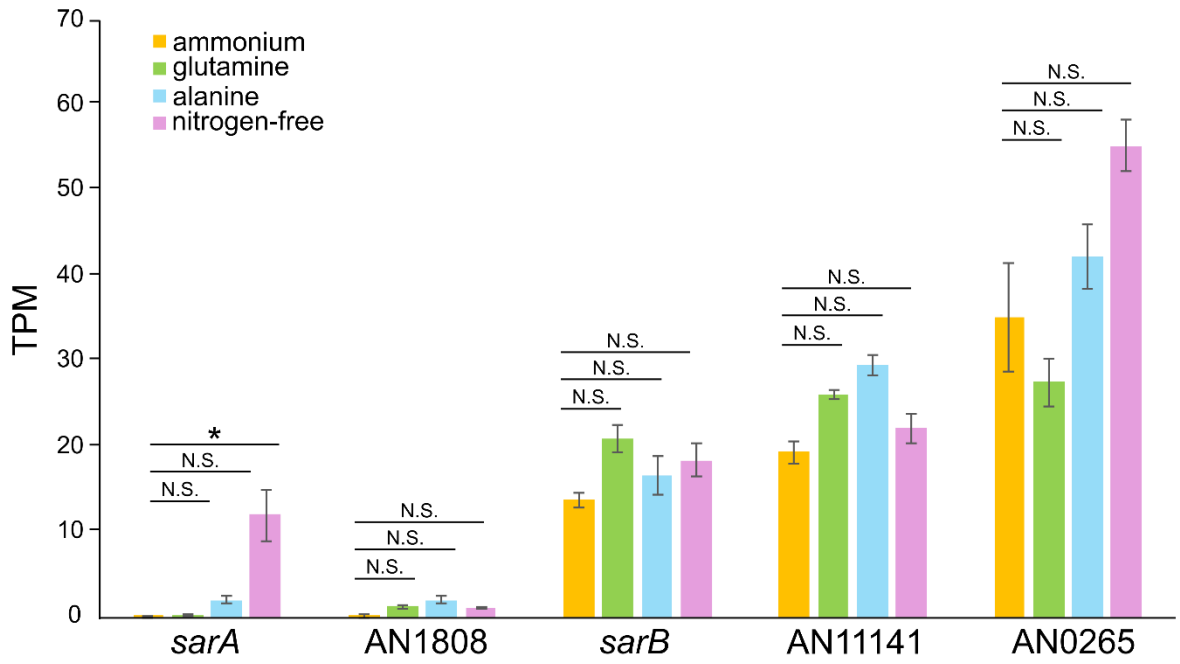

Figure 4.12 sarA *is upregulated under nitrogen starvation conditions*.
A wild-type strain was subjected to four nitrogen regimes and gene expression was assessed using RNA-seq. *sarA* was significantly upregulated under nitrogen-free conditions compared to growth on ammonium. The other genes shown showed no differential expression on glutamine, alanine, or nitrogen-free compared to ammonium. Mycelia were grown for 16 h in supplemented 1% glucose-10 mM nitrogen for 16 h at 37 °C before harvesting. For the nitrogen-free condition, mycelia were washed and transferred to media lacking nitrogen for 4 h at 37 °C before harvesting. Statistical analyses used DESeq2 in RStudio. *p*-values can be found in Appendix B. n=3 biological replicates.

4.5.9 Assessment of regulation of SarA activity by *xprG* and AN1416

The transcription factor *xprG* regulates multiple processes triggered by nutrient scarcity or starvation in *A. nidulans*, including GlcNAc utilization (see Chapter 5), autolysis, and extracellular protease and acid phosphatase production (Cohen 1973; MacRae et al. 1993; Katz et al. 2006, 2013, 2015). In *C. albicans,* an ortholog of the *A. nidulans* gene AN1416, Ngs1, encodes a protein that associates with the ortholog of XprG, Rep1, and helps lead to transcription of GlcNAc utilization genes (Su et al. 2016). Our work suggests that AN1416 also plays a role in extracellular protease production (see Chapter 5). Because SarA shows elevated expression under nitrogen-free

conditions and increased activity in 72-h cultures, we considered whether its expression could be regulated by *xprG*, AN1416, or both.

We examined the nucleotide sequence of the *sarA* promoter for potential XprG binding sites. Because the promotor region is not delineated for *sarA*, we searched within 1.5 kbp upstream of the start codon. At position -1208 we discovered a CGCAAAT sequence that matches a possible XprG binding site sequence based on that defined for the *S. cerevisiae* ortholog Ndt80 (Sopko and Stuart 2004). Though this sequence is from a yeast, there is evidence of high conservation in DNA-binding domains of Ndt80-family transcription factors across eukaryotes (Montano et al. 2002; Min et al. 2018; Liu et al. 2025) To evaluate the effect of deleting *xprG* and AN1416 on SarA activity, we crossed the *areA102* mutant MH8 with *xprG*Δ, AN1416Δ, and *xprG*Δ AN1416Δ strains to generate *areA102 xprG*Δ, *areA102* AN1416Δ, and *areA102 xprG*Δ AN1416Δ mutants*. areA102* progeny were identified by poor growth on uric acid as a sole nitrogen source and strong growth on sucrose-acetamide media. *xprG*Δ and AN1416Δ progeny were identified by poor growth on GlcNAc as a nitrogen source. AN1416Δ progeny exhibited enhanced clearing on media containing milk as a nitrogen source, whereas *xprG*Δ progeny were unable to clear milk. The presence of the AN1416 deletion was further confirmed in the *areA102 xprG*Δ AN1416Δ progeny through PCR (data not shown).

We used the microplate reader LAAO assay to quantify SarA activity in these mutants relative to the *areA102* strain. Mycelia were grown for 16 h in supplemented 1% glucose-10 mM ammonium minimal media, harvested, washed, and transferred to 1% glucose-10 mM histidine for 4 h. Soluble protein extracts were assessed for SarA

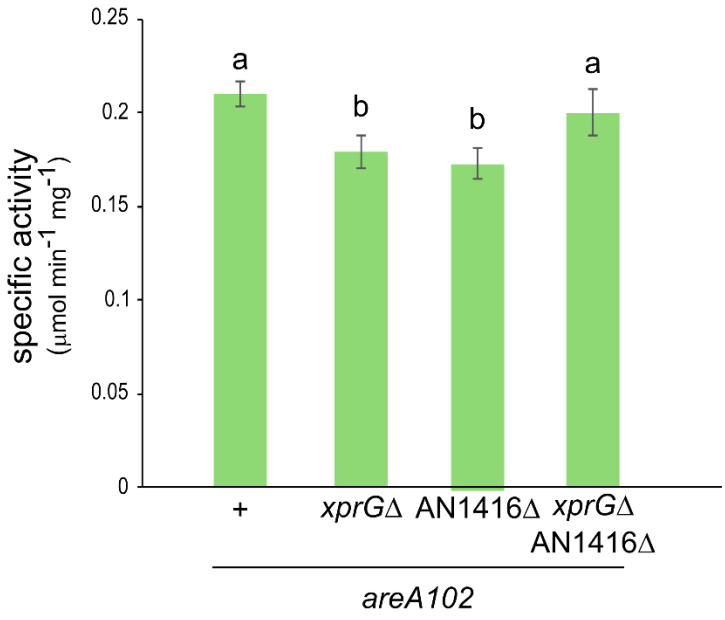

Figure 4.13 Deletion of xprG *or AN1416 slightly decreases SarA activity.* Both the *areA102 xprG*Δ and *areA102* AN1416Δ mutants exhibited lower SarA activity than the *areA102* mutant in a quantitative LAAO assay. There was no difference between the *areA102 xprG*Δ AN1416Δ double mutant and *areA102*. Soluble cell-free extracts in 0.1 M Tris-HCl pH 8.0 were treated with a substrate solution of 5 mM ornithine, 2 mM OPD, and 0.8 U HRP for 1 h at 37 °C. For both assays, mycelia were grown in supplemented 1% glucose-10 mM ammonium minimal media for 16 h, washed, and transferred to supplemented 1% glucose-10 mM histidine minimal media for an additional 4 h before harvesting. Letters signify different statistical significance groups. Two-way ANOVAs followed by Tukey's HSD tests were used to evaluate significant differences between strain activities. *p*-values are found in Appendix B. n=3 biological replicates with 2 technical replicates.

LAAO activity in a quantitative assay. The *areA102 xprG*Δ mutant had 85% of the activity of the *areA102* mutant MH8 (p = 0.0000005), and the *areA102* AN1416Δ mutant had 83% of the activity (p = 0.0000074; Figure 4.13). This decreased activity suggests *xprG* and/or AN1416 play only a minor role in regulation of *sarA* after 4 h growth on histidine. The *areA102 xprG*Δ AN1416Δ mutant did not differ in activity from *areA102*.

4.6 Discussion

We have shown that *sarB* and *sarA* act in the same genetic pathway, as the *sarB*Δ *sarA*Δ double mutant did not suppress the AreA102 strong growth on histidine phenotype to a greater extent than either single mutant. Additionally, we showed through quantitative and qualitative LAAO assays that SarA activity is significantly decreased in *sarB* mutants, indicating *sarB* is required for full SarA activity.

Based on the function of SarB orthologs as UDP-GlcNAc transporters affecting glycosylation, SarB may play a role in glycosylation in *A. nidulans*. We hypothesized

that SarB may provide UDP-GlcNAc to AN11141, a GNT, for use in N-glycosylation, a function seen in *K. lactis* MNN2-2. LAAOs in humans, snake venoms, and in limited studies of other fungi, are N-glycosylated (Geyer et al. 2001; Chavan et al. 2002; Yang et al. 2011; Abdelkafi-Koubaa et al. 2014; Heß et al. 2020). We found evidence that SarA is N-glycosylated through experimental disruption of N-glycans. Treatment of growing *A. nidulans* mycelia with tunicamycin, an antibiotic that prevents formation of N-glycans, led to evidence of smaller SarA proteins in protein extracts, providing strong evidence that SarA is N-glycosylated. Extracts from tunicamycin-treated mycelia exhibited decreased SarA activity. In the basidiomycete fungus *H. cylindroporum*, near abolition of activity in LAAO subjected to site-directed mutagenesis of all confirmed N-glycosylation sites was observed (Heß et al. 2021). Taking into account the possibility that tunicamycin did not prevent N-glycosylation of all available SarA proteins, our results are in line with these findings.

No obvious change in SarA mobility was observed after treatment of extracts with PNGase F, an enzyme that removes N-glycans. This differed from LAAOs in multiple fungal species and in venom of the snake *Cerastes cerastes*, all of which exhibited in-gel mobility changes following PNGase F treatment (Abdelkafi-Koubaa et al. 2014; Heß et al. 2021). However, these studies used purified LAAOs whereas we did not purify SarA from whole cell-free extracts. The presence of a signal peptide at the N-terminus and an ER retention sequence at the C-terminus of SarA made epitope-tagging for purification unlikely to be successful without disruption to localization or function. Therefore, because our extracts contained many species of N-glycosylated proteins, it is likely that the quantity of PNGase F used or incubation time of the reaction was

insufficient to fully de-glycosylate all of them and the proportion of de-glycosylated SarA was insufficient to produce a visible band on the gel. It is also possible that had more SarA been de-glycosylated, the observed loss of activity in the quantitative assay may have been greater. However, in contrast to our findings, no change in LAAO activity was seen in samples de-glycosylated by PNGase F in *H. cylindrosporum* or *C. cerastes* (Abdelkafi-Koubaa et al. 2014; Heß et al. 2020). N-glycosylation sites are not necessarily highly conserved, even among close relatives, and thus the impact of N-glycosylation on SarA could differ from its orthologs in other species (Chavan et al. 2002; Ullah 2020; Huang et al. 2021). Overlaying possible N-glycosylation sites predicted by NetNGlyc on a SarA structural model generated by AlphaFold3 could allow for exploration of possible impacts of N-glycosylation on SarA based on the proximity of N-glycans to structural features.

Deletion of the AN11141 gene, which encodes the putative *A. nidulans* GNT, caused a small change in mobility of SarA. This is the first indication that *A. nidulans* produces N-glycans with terminal GlcNAc molecules and provides additional evidence that SarA is N-glycosylated and decorated with GlcNAc moieties. SarA activity was, however, slightly higher in an AN11141Δ mutant compared with wild type. The reasons for this are unclear, as a defect in N-glycosylation of a protein would be expected to decrease its activity or have other negative effects on its function. However, deletion of a glycosylation gene can be expected to have pleiotropic effects, and this change in activity may be attributable to changes in N-glycosylation of another protein that exerts influence over SarA and not to the changes in N-glycosylation of SarA itself.

Because SarA has a signal peptide at its N-terminus, it is not predicted to be O-GlcNAcylated by OGT (AN0265). However, there is strong evidence for involvement of SarB orthologs in the O-GlcNAcylation pathway in animals. OGT is active in the cytoplasm, nucleus, or mitochondria, where it uses UDP-GlcNAc as a source of GlcNAc to attach to a serine or threonine residue in a target protein. SarB orthologs transport UDP-GlcNAc into the ER and/or Golgi, perhaps decreasing the amount available in the cytoplasm for use by OGT (Kang et al. 2025). In *A. nidulans,* deletion of the OGT AN0265 led to slightly reduced SarA activity. Deletion of *sarB* should cause an increase in O-GlcNAcylation system-wide due to accumulation of UDP-GlcNAc in the cytoplasm. However, *sarB* deletion causes a decrease in SarA activity. Therefore, perturbation of O-GlcNAcylation levels in either direction negatively impacts SarA function. However, in mammals, decrease in expression of the SarB ortholog SLC35B4 in RNAi knockdown experiments led to decreased O-GlcNAcylation of proteins in extracellular mitochondria in cerebrospinal fluid and of the oncogenic transcription factor c-Myc (Park et al. 2021; Jiang et al. 2022). Decreased expression of the human SarB ortholog led to greater O-GlcNAcylation of the transcription factor GATA4 (Kang et al. 2025). This highlights the pleiotropic nature by which SarB orthologs influence O-GlcNAcylation.

Despite finding that deletion of the GNT and OGT glycosylation enzymes impacted SarA activity, neither deletion mutant phenocopied the *sarB*Δ or *sarA*Δ suppression of AreA102 strong growth on histidine, nor did a double AN11141Δ AN0265Δ mutant. Because that phenotype is the defining feature of the *sarB-sarA* relationship, we were thus unable to establish that glycosylation genes are part of the *sarB-sarA* genetic pathway or that SarB plays a role in glycosylation in *A. nidulans*. Our

finding that SarA activity decays more slowly in a *sarB*Δ mutant than in a *sarB*+ strain provides additional evidence against a hypothesis that SarB directly contributes to N-glycosylation of SarA, as a loss of N-glycans would be more likely to decrease protein stability. An alternative possibility is that another enzyme may provide a redundant GNT or OGT activity. No paralogs for AN11141 or AN0265 are identified in the orthology analyses through OrthoMCL. However, we note that AN7983 encodes a predicted protein of 293 amino acid residues containing, like AN11141, an IPR030518 Glucose N-acetyl transferase 1 domain and, therefore, could potentially provide an activity redundant with that of AN11141.

The potential involvement of SLC35B4 in N-glycosylation in animals is poorly understood. Even its localization is unconfirmed, with studies differentially finding it in the ER, Golgi, or both (Ashikov et al. 2005; Maszczak-Seneczko et al. 2011; Bazan et al. 2018; Wex et al. 2018; Wang et al. 2025). Yet for N-glycosylation, its localization could be key to function. ER localization, such as observed in *S. cerevisiae* and *H. polymorpha*, would make it unlikely to provide substrate to GNT enzymes, which are located in the Golgi, whereas an apparent Golgi localization in *K. lactis* allows MNN2-2 to provide GlcNAc to GNT1. *In vitro* studies of SLC35B4 knockouts have failed to find changes in the composition of N-glycans produced (Bazan et al. 2018; Szulc et al. 2020). However, the contributions to N-glycosylation of the UDP-GlcNAc transporters SLC35A2 and SLC35A3, which have well-established Golgi localizations in humans, also remain difficult to ascertain (Szulc et al. 2020; Wiktor et al. 2021).

Given an inability to establish connections between *sarB* and AN11141 or AN0265, we considered other possible pathways in which SarB may be involved. Two

GlcNAc molecules comprise the base of all N-glycans. We thus considered that SarB may supply UDP-GlcNAc to the complex of enzymes involved in synthesis of this base. However, this phase of N-glycan synthesis occurs in the cytoplasm, where UDP-GlcNAc is formed, and thus no transmembrane transporter would be involved (He et al. 2024a).

We also considered that SarB may not be the only UDP-GlcNAc ER- or Golgi-localized transporter in *A. nidulans*, and that downstream proteins may receive UDP-GlcNAc from other sources when *sarB* is mutated. Humans have many nucleotide sugar transporters, some of which have specificity for multiple nucleotide sugars (Maszczak-Seneczko et al. 2022). *A. nidulans* appears to have orthologs of some of these transporters, though they differ significantly in sequence and in Pfam domains from SarB and do not appear to be paralogs. We could find no evidence that these proteins have been studied in fungi.

Through this work, we expanded the limited knowledge of LAAOs in fungi. Our phylogenetic analyses show evidence of expansion of the LAAO family in the fungal kingdom, with many species having multiple distinct LAAOs. This, coupled with our observation of AN1808 activity only in late-stage cultures, provides evidence that fungi have evolved the ability to efficiently exploit diverse amino acid resources under a variety of environmental conditions. Phytopathogenic fungi are known to use host amino acids as nutrient pools during pathogenesis (Struck 2015), and therefore a better understanding of LAAO diversity and function can help uncover key events during host infection.

We additionally provided evidence of a SarA-AN1808 heterodimer active in late cultures. Heterodimeric structures were observed during crystallization of *C. cerastes*

LAAOs and in LAAOs of the fish *Scomber japonicus* (Jung et al. 2000; El Hakim et al. 2015), however this is the first evidence for a heterodimeric LAAO in fungi. We also observed a weak band of LAAO activity at the size predicted for a SarA tetramer. Asymmetrical tetramer structures have been observed in snake LAAOs (Pawelek et al. 2000; Georgieva et al. 2011; Feliciano et al. 2017), but Feliciano et al. (2017) attributed the observations as artifacts caused by crystal packing during the structure crystallization process. We have provided evidence that SarA exhibits activity in tetrameric form, at least as a minor species.

sarA was shown to be regulated by nitrogen, as its expression increased under nitrogen starvation. The gene encoding the secreted protease PnmB, which may provide substrates for LAAOs in addition to its role in promoting derepression by cleavage of NmrA, is also highly upregulated during nitrogen starvation (Li et al. 2021). *sarB* expression did not differ across nitrogen treatments. There is evidence SLC35B4 is upregulated upon exposure to exogenous glucose (Wex et al. 2018) and may thus be regulated by carbon, a condition we did not explore.

Finally, we established *sarB* as an ortholog of the human gene SLC35B4, which is implicated in cancers, diabetes, and other diseases and plays important roles in glucose metabolism in humans. A survey of essential genes in *Caenorhabditis elegans* listed the *sarB* ortholog *nstp-2* as likely essential (Li-Leger et al. 2021), and even the most recent mammalian *in vivo* studies use RNAi-mediated knockdown to study SLC35B4 function in place of gene deletion (Wex et al. 2018; Liu et al. 2019; Park et al. 2021; Jiang et al. 2022; Wang et al. 2025). These studies suggest that deletion of SLC35B4 is lethal or near-lethal in animals, which complicates development of effective

research strategies into its function. However, because *sarB* is not essential in *A. nidulans*, this species can serve as a research model through which to provide insights into SLC35B4 function.

4.7 Future Directions

Through our work, we were unable to definitively find the connection between *sarB* and *sarA*. We conclude that SarB does not have a straightforward, direct effect on glycosylation of SarA. However, the SarB ortholog in *S. cerevisiae*, YEA4, has physical interactions documented with the proteins SEC61 and ERD1 (Miller et al. 2005; Cohen et al. 2023), orthologs of *A. nidulans* AN7721 and AN5682, respectively. SEC61 is part of a channel protein complex necessary for protein translocation into and export of misfolded proteins out of the ER (Plath et al. 2004; Tretter et al. 2013; Hosomi et al. 2020). ERD1 is necessary for retention of proteins in the ER lumen and recycling of GNTs between the late and early Golgi compartments (Pelham et al. 1988; Hardwick et al. 1990; Sardana et al. 2021). Further investigation of *sarB* in the context of either of these genes could lead to new insights about the *sarB*-*sarA* relationship.

The *sarB7* mutant produces a truncated SarB protein about one-third the length of the wild-type protein. In our quantitative LAAO assays, we observed slightly reduced LAAO activity in the *areA102 sarB7* mutant relative to the *areA102 sarB*Δ mutant and *areA102 sarB7* activity values clustered statistically with both the *areA102 sarB*Δ mutant and with several low-activity mutants. It is difficult to know if the observed sarBΔ versus *sarB7* difference is genuine or if it is biologically meaningful. If it is real, this would indicate the *sarB7* mutation acts in a dominant negative manner and suggests the presence of SarB in a protein complex. Further experiments to target the potential

difference between *sarB*Δ and *sarB7* could lead to a greater understanding of activity of SarB.

A greater understanding of glycosylation of SarA could lead to insights of ways in which it may be affected by SarB. It would be important to purify SarA either through epitope tagging or chromatography to further analyze the number and locations of its N-glycans and determine the importance of each with regard to SarA activity. Additionally, it would be beneficial to investigate the impacts of N-glycosylation on SarA folding and solubility. To assess the impact of N-glycosylation on growth of the *areA102* mutant media on solid media, the effects of treatment with tunicamycin on growth on histidine should be determined. If N-glycosylation of SarA is required for SarA LAAO activity, treatment with tunicamycin may be expected to suppress the AreA102 phenotype of increased growth on histidine. As mentioned in Section 4.6, AN7983 is a possible second GNT in *A. nidulans*. Generation of AN7983Δ and AN7983Δ AN11141Δ mutants could lead to a greater understanding of the impact of N-glycosylation on SarA activity and of growth of *sarA* mutants on histidine and perhaps uncover a role for either or both genes in the *sarB*-*sarA* genetic pathway.

We were unable to assess a possible role for O-GlcNAcylation in SarA. This could be done using a pulldown experiment using succinylated wheat germ agglutinin-coated beads, which bind specifically to GlcNAc moieties on glycans, would be used to purify all GlcNAc-containing glycosylated proteins in cell-free extracts from *areA102* strains. Detection of SarA activity in the purified fraction would add to evidence that SarA is glycosylated with N-glycans containing terminal GlcNAc molecules. Detection of SarA activity, following succinylated wheatgerm agglutinin pull-down purification, in

extracts from a GNT deletion mutant but not a GNT OGT double mutant would reveal the presence of O-GlcNAcylation modifications on SarA.

Though we could not establish that SarB provides UDP-GlcNAc to GNT for N-glycosylation, there are other possible pathways by which SarB might be involved in glycosylation and/or influence SarA LAAO activity. Further investigation will provide new insights into the functions of UDP-GlcNAc transporters

Chapter 5 - Characterization of the genes for N-acetylglucosamine transport and catabolism

5.1 Abstract

The *Aspergillus nidulans* Ndt80-like transcription factor XprG plays important roles in regulation of nutrient acquisition, including catabolism of N-acetylglucosamine (GlcNAc). We identified putative genes of the GlcNAc catabolic pathway in *A. nidulans*, primarily clustered on chromosome VII. Extracellular GlcNAc is imported by the GlcNAc transporter NgtA (AN1427), phosphorylated by the hexokinase HxkC (AN4255) to GlcNAc-6-phosphate, deacetylated by DacA (AN1428) to glucosamine-6-phosphate, and deaminated by DamA (AN1418) to ammonium and fructose-6-phosphate, which can enter nitrogen and carbon metabolism, respectively. As *hxkC* was previously deleted and characterized, we deleted the *ngtA*, *dacA* and *damA* genes using homologous recombination. Each deletion mutant showed impaired growth on media containing GlcNAc as a sole nitrogen, carbon, or nitrogen and carbon source. We also identified a putative GlcNAc sensor and histone deacetylase, NgsA (AN1416), expected to interact with XprG based on interactions of their orthologs in *Candida albicans*. Deletion of the *ngsA* gene confers inability to utilize GlcNAc. We used repair and complementation strategies to restore wild-type growth on GlcNAc in the *ngtA*Δ, *dacA*Δ, *damA*Δ, and *ngsA*Δ deletion mutants. We thus completed identification of the genes comprising the GlcNAc utilization pathway in *A. nidulans*.

We identified a second potential GlcNAc transporter in *A. nidulans*, NgtB (AN8127), located on chromosome II, outside of the GlcNAc catabolic gene cluster. We deleted the *ngtB* gene and the resulting mutant showed reduced growth on GlcNAc as a

nitrogen or carbon source. Therefore, NgtB is part of the GlcNAc utilization pathway. To determine if deletion of both transporter genes leads to abolition of growth on GlcNAc, we constructed a *ngtA*Δ *ngtB*Δ double mutant. Putative diploid and heterokaryotic transformants were obtained. A heterokaryon rescue test indicated that simultaneous deletion of both transporter genes is lethal and that transport of extracellular GlcNAc into the cell is necessary for hyphal growth.

We showed that the GlcNAc utilization regulatory genes *xprG* and *ngsA* exhibit genetic interaction in GlcNAc catabolism and extracellular protease activity. RNA-seq on a wild-type strain to examine the effect of different nitrogen conditions on gene expression. *xprG, ngtA, hxkC, dacA*, and *damA* all showed increased expression on non-repressing nitrogen sources (alanine and/or nitrogen-free) when compared to growth on the repressive nitrogen source ammonium. *ngsA* showed constitutive expression across all nitrogen sources and *ngtB* showed negligible expression under all conditions. We show evidence that GlcNAc utilization genes are regulated by nitrogen metabolite repression and the gene *nmrA*.

5.2 Contribution Statement

Sara M. Hopkins, Joel T. Steyer and Dr. Cameron C. Hunter of the Richard Todd Lab deleted several of the GlcNAc utilization genes and assessed their phenotypes on GlcNAc and glucosamine. The *hxkC*Δ mutant and *xprG* mutants were generous gifts of Prof. Margaret E. Katz, the University of New England, Australia.

5.3 Introduction

In fungi, members of the Ndt80-like transcription factor family play roles in fruiting body development, conidiation, secondary metabolite production, hyphal growth,

anastomosis, and are meiotic checkpoints, while in animals, as part of the p53-like protein family, they act as tumor suppressors (reviewed in Katz 2019). In *A. nidulans, xprG,* which encodes a member of the Ndt80-like transcription factor family, has been studied primarily in the context of nutrient acquisition, particularly its responses to nutrient limitation. It is a regulator of autolysis, a programmed cell death mechanism initiated during starvation, in which some cells are destroyed and their components harvested for nutrients (Katz et al. 2013, 2015). In response to nutrient starvation, *xprG* also regulates production of enzymes, such as extracellular proteases, necessary for utilization of extracellular proteins as nutrients (Katz et al. 2006). A gain-of-function mutation, *xprG1*, displays constitutive extracellular protease activity, while loss-of-function mutants *xprG2* and *xprG3* show decreased extracellular protease activity (Katz et al. 1996, 2000). *xprG* additionally regulates expression of acid phosphatases during phosphate starvation (MacRae et al. 1993; Katz et al. 2006).

Differential expression studies using microarrays showed that XprG regulates expression of genes predicted to be involved in catabolism of extracellular N-acetylglucosamine (GlcNAc) during carbon starvation (Katz et al. 2013). GlcNAc is the building block of chitin, a major component of the fungal cell wall, and can be an abundant nutrient source in the environment. It is released during autolysis occurring in *A. nidulans* and/or neighboring fungi and is found in the cell walls of bacteria, exoskeleton of insects, and extracellular matrix of mammalian cells (Konopka 2012).

Orthologs of *xprG* in other fungi are regulators of GlcNAc breakdown. This process is best studied is the mammalian fungal pathogen *Candida albicans*, where the XprG ortholog, CaRep1, recruits the GlcNAc sensor protein CaNgs1 to activate

expression of GlcNAc utilization genes (Su et al. 2016; Naseem et al. 2017; Min et al. 2020). The CaNgs1 protein has a glycoside hydrolase family 3 (GH3) domain capable of binding GlcNAc and thus acting as a GlcNAc sensor, and a GCN5-related N-acetyltransferase (GNAT) domain, which acetylates histones in the region of the promoter bound by the CaRep1-Ngs1 complex (Su et al. 2016). Extracellular GlcNAc is transported into the cell by the GlcNAc transporter CaNgt1 (Alvarez and Konopka 2007) and binds to CaNgs1. This triggers binding of CaRep1 to the promoters of GlcNAc catabolism genes, and coupled with histone acetylation by CaNgs1, leads to their transcription. GlcNAc catabolism occurs via CaHxk1 (CaNag5), a hexokinase, which phosphorylates GlcNAc, and is followed by deacetylation of GlcNAc-6-phosphate by CaDac1 (CaNag2; Kumar et al. 2000; Yamada-Okabe et al. 2001). Next, deamination of glucosamine-6-phosphate by CaNag1 produces fructose-6-phosphate, which enters the glycolytic pathway (Natarajan and Datta 1993). The genes encoding CaHxk1, CaDac1 and CaNag1 are clustered together in the *C. albicans* genome and are co-regulated at the transcriptional level (Kumar et al. 2000). *xprG* orthologs have also been shown to be necessary for GlcNAc catabolism in *Beauveria bassiana, Trichoderma reesei,* and *Magnaporthe oryzae* (Kappel et al. 2016; Bhatt et al. 2020; Qiu et al. 2022)

Study of the GlcNAc utilization genes in *C. albicans* has focused on its role in triggering a morphogenetic change leading to onset of pathogenesis (Simonetti et al. 1974; Lo et al. 1997; Konopka 2012). This control of morphogenesis also occurs in *Histoplasma capsulatum* and *Blastomyces dermatiditis* (Gilmore et al. 2013). GlcNAc utilization genes are essential for pathogenesis in *M. oryzae* where mutants lacking the *xprG* ortholog or GlcNAc utilization structural genes are unable to successfully colonize

host plants (Kumar et al. 2016). Mutants of the insect pathogen *B. bassiana* lacking orthologs of *xprG* or the GlcNAc sensor AN1416 are likewise unable to exhibit pathogenicity (Qiu et al. 2022; Zhang et al. 2024).

The role of GlcNAc as a nutrient source is poorly studied in fungi, especially as a source of nitrogen. In *Trichoderma reesei,* the genes for utilization of GlcNAc have been characterized in the context of it being a source of carbon (Kappel et al. 2016; Ullah et al. 2025) The *T. reesei* genes encoding the GlcNAc hexokinase (*hxk1*), the GlcNAc-6-phosphate deacetylase (*dac1*), and glucosamine-6-phosphate deaminase (*dam1*) form a GlcNAc utilization gene cluster that also includes the transcription factor gene *ron1* (the *xprG* ortholog) and the GlcNAc sensor gene (*nag3*), while the GlcNAc transporter gene (*ngt1*) is located separately (Kappel et al. 2016). GlcNAc utilization and regulatory genes are similarly clustered across fungal species (Bhatt et al. 2020; Ye et al. 2022), including in *A. nidulans*. In *A. nidulans,* the putative GlcNAc hexokinase *hxkC* (AN4255) gene, located on chromosome V outside the GlcNAc utilization gene cluster, was originally identified as an atypical regulatory hexokinsase (Bernardo et al. 2007). HxkC has since been shown to be involved in utilization of GlcNAc as a carbon source (Katz et al. 2016), but the remaining GlcNAc utilization pathway genes have not been characterized.

In this work, we identify and characterize the *A. nidulans* GlcNAc utilization pathway genes. We identify a second GlcNAc transporter gene and show that simultaneous deletion of both transporter genes confers a synthetic lethal phenotype. We also examine regulation of GlcNAc utilization by *xprG*, AN1416, and the *areA* co-repressor *nmrA*.

5.4 Materials and Methods

5.4.1 Strains

A. nidulans strains used in Chapter 5 are described in Table 5.1.

Table 5.1 *A. nidulans* strains used in Chapter 5.

Strain	Genotype
MH1	*biA1*
MH11068	*pyrG89 pyroA4 amdA7 nkuA*Δ*::Bar*
MH11132	*yA1 adE20 areA217 riboB2 su(adE20)*
MK85	*biA1 xprG1 niiA4*
MK205	*yA2 pabaA1 areA102 sarB7 xprG1*
MK414	*yA2 pabaA1 xprG*Δ*::argB+*
MK489	*hxkC*Δ*::argB+ argB2 niiA4*
RT626	*pyrG89 pyroA4 nkuA*Δ*::Bar* AN1418Δ*::AfpyrG+ amdA7*
RT707	*pyrG89 pyroA4 nkuA*Δ*::Bar* AN1416Δ*::AfpyrG+ amdA7*
RT708	*pyrG89 pyroA4 nkuA*Δ*::Bar* AN1427Δ*::AfpyrG+ amdA7*
RT709	*pyrG89 pyroA4 nkuA*Δ*::Bar* AN1428Δ*::AfpyrG+ amdA7*
RT803	*pyrG89 pyroA4 nkuA*Δ*::Bar xprG1*
RT804	*pyrG89 pyroA4 nkuA*Δ*::Bar xprG1 niiA4*
RT811	*pyrG89 pyroA4 nkuA*Δ*::Bar xprG*Δ*::argB+*
RT812	*pyrG89 pyroA4 nkuA*Δ*::Bar xprG*Δ*::argB+ nkuA*Δ*::Bar*
RT813	*pyrG89 pyroA4 nkuA*Δ*::Bar xprG*Δ*::argB+ amdA7 nkuA*Δ*::Bar*
RT818	*pyrG89 pyroA4 nkuA*Δ*::Bar* AN1418Δ*::AfpyrG+* AN1418r
RT822	*pyrG*89 *pyroA4 nkuA*Δ*::Bar xprG*1 AN1416Δ*::AfpyrG+*
RT823	*pyrG*89 *pyroA4 nkuA*Δ*::Bar xprG*1 AN1416Δ*::AfpyrG+*
RT824	*pyrG*89 *pyroA4 nkuA*Δ*::Bar xprG*1 AN1416Δ*::AfpyrG+*
RT825	*pyrG*89 *pyroA4 nkuA*Δ*::Bar xprG*1 AN1416Δ*::AfpyrG+*
RT826	*pyrG*89 *pyroA4 nkuA*Δ*::Bar xprG*1 AN1416Δ*::AfpyrG+*
RT827	*pyrG*89 *pyroA4 nkuA*Δ*::Bar xprG*Δ AN1416Δ*::AfpyrG+*
RT828	*pyrG*89 *pyroA4 nkuA*Δ*::Bar xprG*Δ AN1416Δ*::AfpyrG+*
RT829	*pyrG*89 *pyroA4 nkuA*Δ*::Bar xprG*Δ AN1416Δ*::AfpyrG+*
RT830	*pyrG*89 *pyroA4 nkuA*Δ*::Bar xprG*Δ AN1416Δ*::AfpyrG+*
RT831	*pyrG*89 *pyroA4 nkuA*Δ*::Bar xprG*Δ AN1416Δ*::AfpyrG+*
RT832	*pyrG*89 *pyroA4 nkuA*Δ*::Bar* AN1428r#
RT833	*pyrG*89 *pyroA4 nkuA*Δ*::Bar* AN1428r#
RT834	*pyrG*89 *pyroA4 nkuA*Δ*::Bar* AN1428r#
RT835	*pyrG*89 *pyroA4 nkuA*Δ*::Bar* AN1428r#
RT836	*pyrG*89 *pyroA4 nkuA*Δ*::Bar* AN1428r#
RT843	*pyrG*89 *pyroA4 nkuA*Δ*::Bar* AN1427r#
RT844	*pyrG*89 *pyroA4 nkuA*Δ*::Bar* AN1427r#
RT845	*pyrG*89 *pyroA4 nkuA*Δ*::Bar* AN1427r#
RT851	*pyrG89 nmrA*Δ*::AfpyrG+ pyroA4 nkuA*Δ*::Bar amdA7*

RT852	*pyrG89 nmrA∆::AfpyrG+ pyroA4 nkuA∆::Bar amdA7*
RT853	*pyrG89 nmrA∆::AfpyrG+ pyroA4 nkuA∆::Bar amdA7*
RT854	*pyrG89 nmrA∆::AfpyrG+ pyroA4 nkuA∆::Bar amdA7*
RT865	*pyrG89 pyroA4 nkuA∆::Bar*
RT959	*pyrG89 pyroA4 nkuA∆::Bar* AN1428r#
RT961	*pyrG89 pyroA4 nkuA∆::Bar* AN1418r#
RT962	*pyrG89 pyroA4 nkuA∆::Bar* AN1418r#
RT963	*pyrG89 pyroA4 nkuA∆::Bar* AN1418r#
RT964	*pyrG89 pyroA4 nkuA∆::Bar* AN1418r#
RT965	*pyrG89 pyroA4 nkuA∆::Bar* AN1418r#
RT981	*pyrG89 pyroA4 nkuA∆::Bar* AN1416∆::*AfpyrG+* AN1416c* *amdA7*
RT982	*pyrG89 pyroA4 nkuA∆::Bar* AN1416∆::*AfpyrG+* AN1416c* *amdA7*
RT983	*pyrG89 pyroA4 nkuA∆::Bar* AN1416∆::*AfpyrG+* AN1416c* *amdA7*
RT984	*pyrG89 pyroA4 nkuA∆::Bar* AN1416∆::*AfpyrG+* AN1416c* *amdA7*
RT985	*pyrG89 pyroA4 nkuA∆::Bar* AN1416∆::*AfpyrG+* AN1416c* *amdA7*
RT986	*pyrG89 pyroA4 nkuA∆::Bar* AN1416∆::*AfpyrG+* AN1416c* *amdA7*
RT987	*pyrG89 pyroA4 nkuA∆::Bar* AN1416∆::*AfpyrG+* AN1416c* *amdA7*
RT988	*pyrG89* AN8127∆::*AfpyrG+ pyroA4 nkuA∆::Bar*
RT989	*pyrG89* AN8127∆::*AfpyrG+ pyroA4 nkuA∆::Bar*
RT990	*pyrG89* AN8127∆::*AfpyrG+ pyroA4 nkuA∆::Bar*
RT991	*pyrG89* AN8127∆::*AfpyrG+ pyroA4 nkuA∆::Bar*
RT992	*pyrG89* AN8127∆::*AfpyrG+ pyroA4 nkuA∆::Bar*
RT993	*pyrG89* AN1427∆::*AfpyrG+ riboB2*
RT994	*pyrG89 pabaB22* AN1427∆::*AfpyrG+ riboB2*
RT995	*pyrG89 pabaB22* AN1427∆::*AfpyrG+*
RT996	*pyrG89 pyroA4* AN1427∆::*AfpyrG+*
RT997	*pyrG89 pabaB22 pyroA4* AN1427∆::*AfpyrG+*
RT998	*pyrG89 pyroA4 nku∆::Bar* AN1428∆::*AfpyrG+* AN1428c* *amdA7*
RT999	*pyrG89 pyroA4 nku∆::Bar* AN1428∆::*AfpyrG+* AN1428c* *amdA7*
RT1000	*pyrG89 pyroA4 nku∆::Bar* AN1428∆::*AfpyrG+* AN1428c* *amdA7*
RT1001	*pyrG89 pyroA4 nku∆::Bar* AN1428∆::*AfpyrG+* AN1428c* *amdA7*
RT1002	*pyrG89 pyroA4 nku∆::Bar* AN1428∆::*AfpyrG+* AN1428c* *amdA7*
RT1003	*pyrG89 pyroA4 nku∆::Bar* AN1427∆::*AfpyrG+* AN1427c* *amdA7*
RT1004	*pyrG89 pyroA4 nku∆::Bar* AN1427∆::*AfpyrG+* AN1427c* *amdA7*
RT1005	*pyrG89 pyroA4 nku∆::Bar* AN1427∆::*AfpyrG+* AN1427c* *amdA7*

RT1006	*pyrG89 pyroA4 nkuΔ::Bar* AN1427Δ::*AfpyrG+* AN1427c* *amdA7*
RT1007	*pyrG89 pyroA4 nkuΔ::Bar* AN1427Δ::*AfpyrG+* AN1427c* *amdA7*
RT1008	*pyrG89 pyroA4 nkuΔ::Bar* AN1427Δ::*AfpyrG+* AN1427c* *amdA7*
RT1009	*pyrG89 pyroA4 nkuΔ::Bar* AN1418Δ::*AfpyrG+* AN1418c* *amdA7*
RT1010	*pyrG89 pyroA4 nkuΔ::Bar* AN1418Δ::*AfpyrG+* AN1418c* *amdA7*
RT1011	*pyrG89 pyroA4 nkuΔ::Bar* AN1418Δ::*AfpyrG+* AN1418c* *amdA7*
RT1012	*pyrG89 pyroA4 nkuΔ::Bar* AN1418Δ::*AfpyrG+* AN1418c* *amdA7*
RT1013	*pyrG89 pyroA4 nkuΔ::Bar* AN1418Δ::*AfpyrG+* AN1418c* *amdA7*
RT1014	*pyrG89 pyroA4 nkuΔ::Bar* AN1418Δ::*AfpyrG+* AN1418c* *amdA7*
RT1019	*pyrG89 pyroA4 nkuΔ::Bar* AN1427Δ::*AfpyrG-*
RT1049	*biA1 areA102 xprGΔ::argB+ niiA4*
RT1050	*biA1 areA102* AN1416Δ::*pyrG+ niiA4*
RT1051	*biA1 areA102 xprGΔ::argB+* AN1416Δ::*pyrG+ niiA4*
RT1052	*areA102 pyroA4* AN1416Δ::*AfpyrG+*
RT1053	*areA102* AN1416Δ::*pyrG+ niiA4*
RT1055	*yA2 areA102 pyroA4 xprGΔ::argB+* AN1416Δ::*pyrG+*
RT1056	*yA2 areA102 xprGΔ::argB+* AN1416Δ::*pyrG+ niiA4*
RT1057	*areA102 xprGΔ::argB+* AN1416Δ::*pyrG+ niiA4*
RT1058	*areA102 xprGΔ::argB+* AN1416Δ::*pyrG+ pabaA1*
RT1059	*yA2 areA102 pabaA1 xprGΔ::argB+*
RT1060	*yA2 areA102 xprGΔ::argB+niiA4*

[#] "r", repaired, denotes the wild type gene has replaced a gene knockout via homologous gene replacement.
* "c", complemented, denotes integration of a plasmid containing the indicated wild type gene by single crossover.

5.4.2 PCR primers

Genomic PCR primers used in Chapter 5 are shown in Table 5.2.

Table 5.2 Genomic primers used in Chapter 5.

Target	Primer Name	Sequence (5'→ 3')
AN1416	AN1416_5'F	CCTCAAGCGACACTAGAAAC
	AN1416_3'R	AGACGGACTGTAGACGAATC
	AN1416_5'F	GACTATTCCTAAGCTACTCCTAC
	AN1416_3'R	CAAAGCATCACCCAATGACG
AN1418	5fAn1418	GATCCGCGTTAGCTG
	3fAn1418	GCACTAGCGGGGTTA
	AN1418_5'F	CTTTGGCGTTGACTGTATCAG

	AN1418_3'F	CTTACCGTGCTTCTTACAAG
AN1427	AN1427_5'F	AGTAGGTGTGGAGTGGAAGT
	AN1427_3'R	GAGGGACCCTACTACAGCTA
	AN1427_5'F_2	GGTACAGCACCATACAGACG
	AN1427_3'R_2	CGTACTTCTACCTGAGACTCTG
AN1428	AN1428_5'F	CACTCCACACCTACTGTC
	AN1428_3'R	CTATGACACTCCTGTCGATG
	AN1428_5'F_2	CACGGATTCTGGAACGATTG
	AN1428_3'R_2	GATTCCCTTCTGTCTCAACAC
AN8127	AN8127_5'F_outside	GAGCAGTACCGTATTCCCAT
	AN8127_3'R_outside	GAGTCAAGCTGATCTGACAG
	AN8127_5'F_inside	GCCCTAGTCATTATCTCCTG
	AN8127_3'R_inside	CTACAGAGCCCGTATTGAC
	ANID_08127.1_5'F	GTAACGCCAGGGTTTTCCCAGTCACGACGGCCCTAGTCATTATCTCCTG
	ANID_08127.1_3'R	GCGGATAACAATTTCACACAGGAAACAGCCTACAGAGCCCGTATTGAC
	AN8127_5'R	TGCGTGTAGGTTCGATAAAC
	AN8127_3'F	GGCGAAGAGAAGACAATGAG
AfpyrG	AfpyrG_5'R	ATCCACTTAACGTTACTGAAATC
	AfpyrG_3'F	CTCCTTCAATATCATCTTCTGTC

5.4.3 Plasmid construction

Plasmids containing wild-type GlcNAc utilization genes were constructed by cloning the PCR product of each gene of interest amplified from the deletion recipient strain (MH11068) individually into the pGEM-T Easy vector (Promega). The AN1418 gene fragment was excised from pGEM-T Easy using *Not*I restriction enzyme. AN1416, AN1427, and AN1428 were each excised using *Not*I and *Spe*I. Each resulting gene fragment was subcloned separately into the *wA*-targeting vector pCW6500 (Hunter et al. 2014). Plasmid names and insert specifications are shown in Table 5.3.

Table 5.3 Plasmids used in Chapter 5.

Plasmid name	Insert	Backbone
pHF280	AN1416 (-637 to +3719)	pGEM-T Easy
pHF281	AN1427 (-919 to +2814)	pGEM-T Easy
pHF279	AN1428 (-770 to +2165)	pGEM-T Easy
pHF278	AN1418 (-1211 to +2358)	pGEM-T Easy
pHF285	AN1416 (-637 to +3719)	pCW6500

pHF287	AN1427 (-919 to +2814)	pCW6500
pHF289	AN1428 (-770 to +2165)	pCW6500
pHF291	AN1418 (-1211 to +2358)	pCW6500

5.4.4 Strain construction

Construction of GlcNAc utilization gene deletion mutants

AN1416Δ (RT707; Δ -17 to +3004), AN1427Δ (RT708; Δ +9 to +1942), AN1428Δ (RT709; Δ -28 to +1288), AN1418Δ (RT626; Δ -113 to +1359), and AN8127Δ (RT988-RT992; Δ -22 to +1508) mutants were constructed using knockout constructs made in the *A. nidulans* knockout project by De Souza et al. (2013) and obtained from the Fungal Genetics Stock Center, Manhattan, Kansas (McCluskey et al. 2010). Briefly, each construct consisted of the *Aspergillus fumigatus pyrG* (*AfpyrG*) gene selectable marker, flanked by ~1 kbp of sequences upstream and downstream of the gene of interest, which allowed for gene replacement by homologous recombination in a *nkuA*Δ non-homologous end-joining mutant recipient (Nayak et al. 2006). Transformation into a recipient with the *pyrG89* mutation (MH11068 for AN1416Δ, AN1427Δ, AN1428Δ, and AN1418Δ; RT865 for AN8127Δ) allowed selection of transformants for pyrimidine prototrophy (Oakley et al. 1987a). Knockout construct integration was confirmed by the presence of a PCR band of the construct size (1.7 kb) and absence of a PCR band of the deleted gene size.

Repair of GlcNAc utilization gene deletion mutations

Wild-type AN1416 (-637 to +3719), AN1427 (-919 to +2814), AN1428 (-770 to +2165), and AN1418 (-1010 to +2451) genes were each PCR amplified from MH11068 genomic DNA and transformed into the corresponding deletion mutants (RT708, RT707, RT709, and RT626, respectively) using methods described in Downes et al. (2013).

Two selection methods were used for each transformation. Transformants were directly selected for restoration of the wild-type GlcNAc growth phenotype on protoplast media containing 10 mM GlcNAc as the sole nitrogen source. Additionally, transformants were selected on media containing 1 mg/mL 5-fluoroorotic acid (5-FOA), which is metabolized into a toxic product via the product of the *pyrG* gene. Because the recipient strains have the *pyrG89* mutation, growth on 5-FOA is only possible following gene replacement of the *AfpyrG* gene used as the selectable marker during construction of the deletion mutants.

Complementation of GlcNAc utilization deletion mutant phenotype

The pHF285 plasmid containing the wild-type AN1416 gene, the pHF287 plasmid containing the wild-type AN1427 gene, the pHF289 plasmid containing the wild-type AN1428 gene, and the pHF291 plasmid containing the wild-type AN1418 gene were each transformed into their corresponding deletion mutants (RT708, RT707, RT709, and RT626, respectively) containing the *pyroA4* mutation. Transformants were selected for pyridoxine prototrophy, conferred by the *AfpyroA* selectable marker in the pCW6500 plasmid.

Construction of an AN1427Δ AN8127Δ double mutant

Crossing and transformation strategies were both used during construction of an AN1427Δ AN8127Δ double mutant. Two AN1427Δ mutants (RT993 and RT995) were each separately crossed with an AN8127Δ (RT988) mutant using protocols described in Todd et al. (2007b).

To facilitate the transformation strategy, we recycled the *AfpyrG* selectable marker used to delete the AN1427 gene by selection of an *AfpyrG*- loss-of-function

mutant. A *pyrG89* AN1427Δ::*AfpyrG*- mutant (RT1019) was generated for use as a transformation recipient by growing a *pyrG89* AN1427Δ::*AfpyrG*+ mutant (RT996) on complete media with pyrimidine supplementation and containing 1.25 mg/mL 5-FOA, selecting for spontaneous mutations in the *AfpyrG* gene. The AN8127Δ::*AfpyrG*+ knockout construct described above was transformed into RT1019, and transformants were selected by pyrimidine prototrophy conferred by the *AfpyrG* gene. Transformants were initially picked by conidial transfer to complete media lacking pyrimidines, and simultaneously picked to 1% glucose-10 mM GlcNAc (i.e., GlcNAc as nitrogen source) and 1% GlcNAc-10 mM ammonium (i.e., GlcNAc as carbon source) minimal media.

Heterokaryon rescue experiments were performed by obtaining multiple conidia from each transformant on the primary selection plates with a flat toothpick and streaking them to pyrimidine-supplemented and unsupplemented complete media (Osmani et al. 2006).

Construction of *xprG*–AN1416Δ double mutants

To construct the *xprG*Δ AN1416Δ mutants (RT827-RT831), the AN1416Δ::*AfpyrG*+ knockout construct from the Fungal Genetics Stock Center was transformed into a *pyrG89 xprG*Δ::*argB*+ strain (RT811). Transformants were selected for pyrimidine prototrophy conferred by the *AfpyrG* selectable marker.

To construct the *xprG1* AN1416Δ mutants (RT822-RT826), the AN1416Δ::*AfpyrG*+ knockout construct was transformed into a *pyrG89 xprG1* strain (RT803). Transformants were selected for pyrimidine prototrophy conferred by the *AfpyrG* selectable marker.

5.5 Results

5.5.1 Genetic analysis of the GlcNAc utilization pathway

A. nidulans can utilize GlcNAc as a sole carbon or nitrogen source (Katz et al. 2016; S.M. Hopkins and R.B. Todd, unpublished data). Previous work in our lab identified putative *A. nidulans* genes encoding the GlcNAc utilization transporter and structural genes orthologous to those studied in *C. albicans* (Table 5.4; Figure 5.1A; R.B. Todd, unpublished data). The putative GlcNAc transporter that imports extracellular GlcNAc into the cell is encoded by AN1427 (Figure 5.1A). *hxkC* (AN4255) encodes a GlcNAc hexokinase that phosphorylates GlcNAc to produce GlcNAc-6-phosphate (Katz et al. 2016). This is followed by deacetylation by the GlcNAc-6-phosphate deacetylase enzyme encoded by AN1428, producing glucosamine-6-phosphate. Finally, AN1418 encodes a deaminase that acts on this product to release fructose-6-phosphate and ammonium used as carbon and nitrogen sources, respectively, for growth. In *A. nidulans,* the GlcNAc utilization gene cluster is on chromosome VII and is split into two parts due to a chromosomal inversion (Figure 5.1B; Kappel et al. 2016). AN1427 and AN1428 are adjacent in the genome on chromosome VII, approximately 25 kbp distal to AN1418, which lies adjacent to the GlcNAc transcription factor gene *xprG* (AN1414) and the GlcNAc sensor gene AN1416. *hxkC* is located on chromosome V and is not associated with the GlcNAc utilization gene cluster. Deletion mutants were constructed for AN1427, AN1428, and AN1418 (S.M. Hopkins, J.T. Steyer, C.C. Hunter, and R.B. Todd, unpublished data). Growth of these mutants, along with a previously-constructed *hxkC*Δ mutant (Bernardo et al. 2007), did not differ from wild type on glucose-ammonium minimal media (Figure 5.1C).

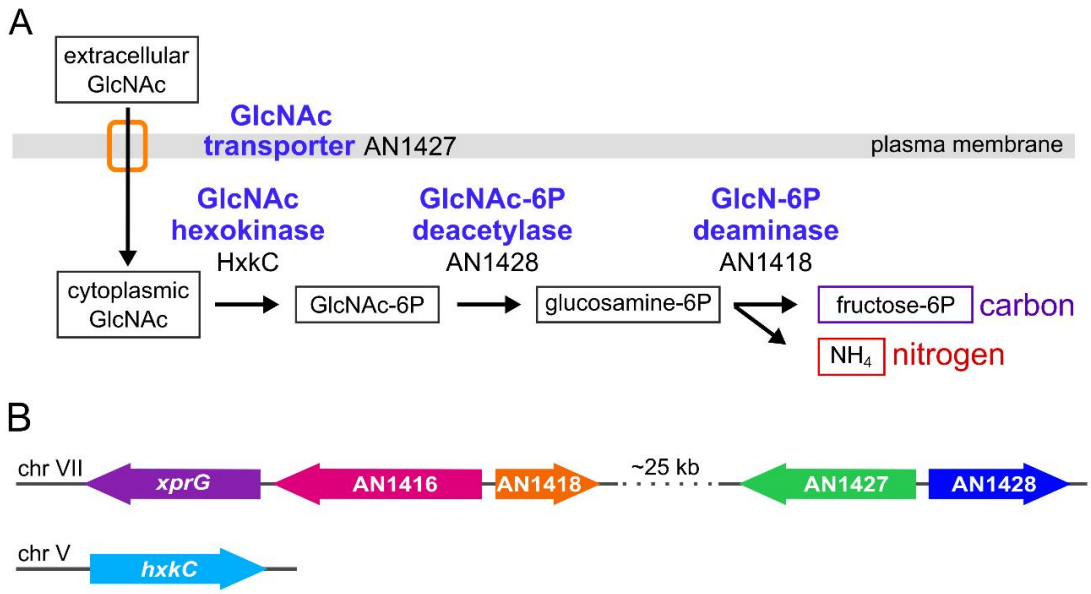

Figure 5.1 The proposed model for GlcNAc catabolism in A. nidulans *consists of one transporter gene and three catabolic genes.*
(A) GlcNAc enters the cell through a GlcNAc transporter (AN1427) and is catabolized by a GlcNAc hexokinase (HxkC), a GlcNAc-6-phosphate deacetylase (AN1428), and a glucosamine-6-phosphate deaminase (AN1418), to produce ammonium and fructose-6-phosphate, which can enter nitrogen and carbon metabolism, respectively.*(B)* GlcNAc utilization and regulatory genes are clustered on chromosome VII, except for *hxkC* on chromosome V. *(C)* Deletion of any of the four genes encoding the steps in the proposed GlcNAc utilization pathway results in reduced ability to catabolize GlcNAc indicated by reduced growth. Strains of the indicated genotypes were grown on supplemented minimal media containing the indicated compounds as carbon and/or nitrogen sources for 48 h at 37ºC. From top to bottom: MH11068, RT708, RT489, RT709, RT626.

However, all mutants exhibited weaker growth when provided with GlcNAc as a sole nitrogen, carbon, or nitrogen and carbon source. This establishes their roles in utilization of GlcNAc. We have named AN1427 *ngtA* (*N-acetylglucosamine transporter A*), AN1428 *dacA* (*deacetylase A*), and AN1418 *damA* (*deaminase A*). Genes regulating GlcNAc utilization will be discussed later in this chapter.

Table 5.4 GlcNAc utilization protein comparisons between *A. nidulans* and *C. albicans.*

A. nidulans	*C. albicans*	% identity / % similarity
NgtA (AN1427)	Ngt1	45.4 / 60.9
HxkC (AN4255)	Hxk1	23.9 / 41.9
DacA (AN1428)	Dac1	35.0 / 54.7
DamA (AN1418)	Nag1	35.0 / 46.9

To further establish the role of the putative GlcNAc pathway genes in GlcNAc utilization, we repaired and/or complemented the *ngtA*Δ, *dacA*Δ and *damA*Δ deletion mutants with the corresponding wild-type gene copies. The GlcNAc utilization mutant strains carry the *nkuA*Δ non-homologous end-joining (NHEJ) mutation, which facilitates integration by homologous double crossover at high frequency. Therefore, it should be possible to repair the deletion mutants by gene replacement with linear fragments containing the corresponding wild-type gene and flanking sequences (Figure 5.2A). These three deletion mutants were made with the *AfpyrG* gene as the selectable marker in a *pyrG89* auxotrophic mutant background. We attempted to repair gene deletions in the *ngtA*Δ, *dacA*Δ, and *damA*Δ mutants by transforming the corresponding wild-type genes PCR amplified from the strain used as the deletion recipient (MH11068: *pyrG89 pyroA4 nkuA*Δ) into their respective deletion mutants and directly selecting for wild-type growth on GlcNAc as a nitrogen source in the presence of pyrimidines. Although the background growth for each of the GlcNAc utilization mutant recipients was high in this novel selection, we were able to identify, with low efficiency, several transformants with very diffuse growth stronger than background. These putative transformants showed repair of the GlcNAc utilization phenotypes in growth tests (Figure 5.2B). However, due to the high background and diffuse growth of the transformants, the GlcNAc utilization genes are not suitable for use as selectable markers. We additionally used an

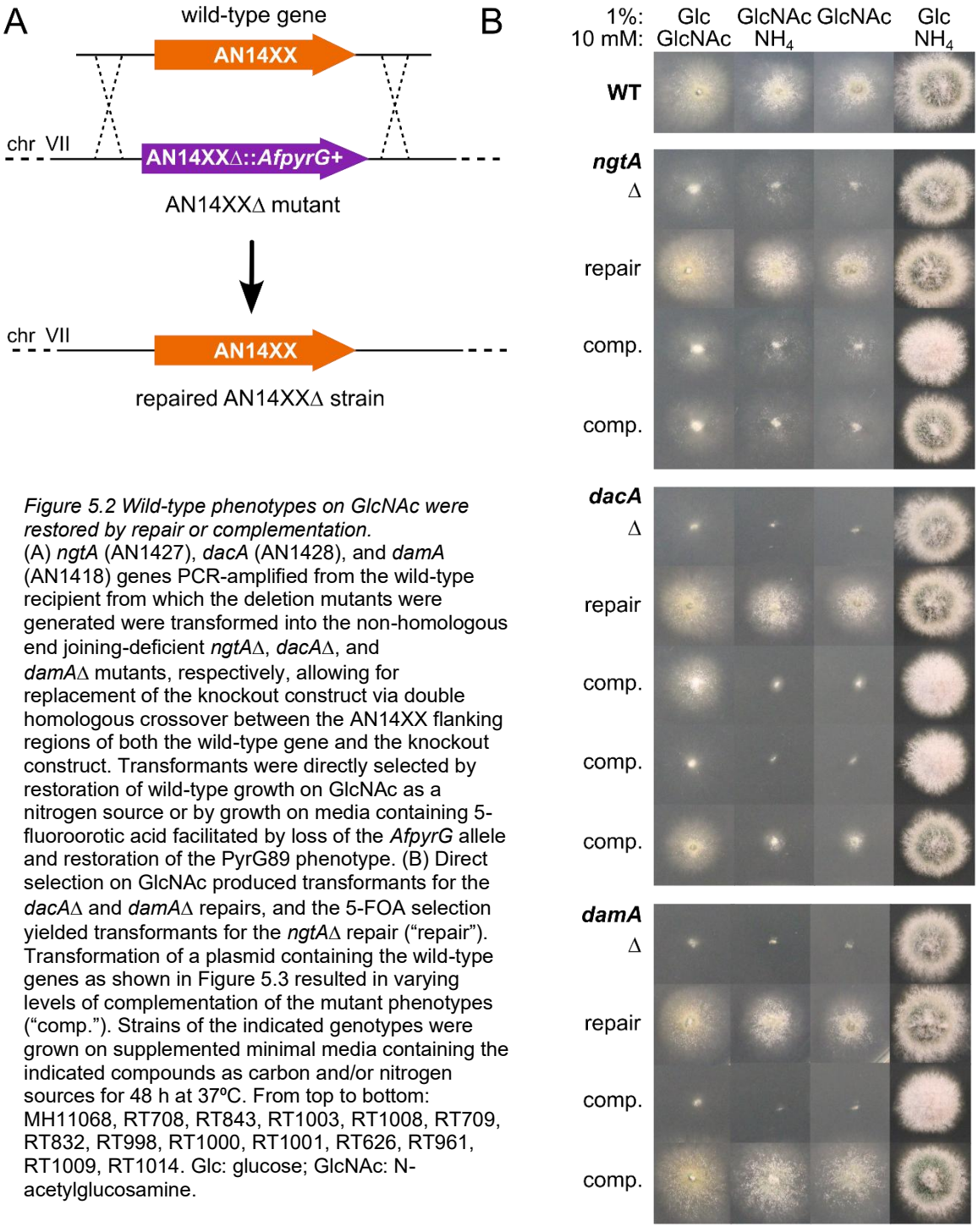

Figure 5.2 Wild-type phenotypes on GlcNAc were restored by repair or complementation.
(A) *ngtA* (AN1427), *dacA* (AN1428), and *damA* (AN1418) genes PCR-amplified from the wild-type recipient from which the deletion mutants were generated were transformed into the non-homologous end joining-deficient *ngtA*Δ, *dacA*Δ, and *damA*Δ mutants, respectively, allowing for replacement of the knockout construct via double homologous crossover between the AN14XX flanking regions of both the wild-type gene and the knockout construct. Transformants were directly selected by restoration of wild-type growth on GlcNAc as a nitrogen source or by growth on media containing 5-fluoroorotic acid facilitated by loss of the *AfpyrG* allele and restoration of the PyrG89 phenotype. (B) Direct selection on GlcNAc produced transformants for the *dacA*Δ and *damA*Δ repairs, and the 5-FOA selection yielded transformants for the *ngtA*Δ repair ("repair"). Transformation of a plasmid containing the wild-type genes as shown in Figure 5.3 resulted in varying levels of complementation of the mutant phenotypes ("comp."). Strains of the indicated genotypes were grown on supplemented minimal media containing the indicated compounds as carbon and/or nitrogen sources for 48 h at 37ºC. From top to bottom: MH11068, RT708, RT843, RT1003, RT1008, RT709, RT832, RT998, RT1000, RT1001, RT626, RT961, RT1009, RT1014. Glc: glucose; GlcNAc: N-acetylglucosamine.

alternative selective media containing 5-FOA to select for loss of the gene replacement *AfpyrG* selectable marker in each deletion mutant due to integration of the wild-type

gene by double crossover of the flanking sequences. Each transformation experiment produced zero to five transformants.

Using selection for growth on GlcNAc as a nitrogen source, transformations of the *dacA* wild-type gene into the *dacA*Δ mutant produced six total transformants (RT832-RT836; RT959) and transformations of the *damA* wild-type gene into the *damA*Δ mutant yielded a total of six transformants (RT818; RT961-RT965). Transformation of the *ngtA* wild-type gene into the *ngtA*Δ mutant yielded three transformants using 5-FOA selection (RT843-RT845). Each transformant was confirmed as genuine through pyrimidine auxotrophy conferred by loss of the *AfpyrG* gene, restoration of growth on GlcNAc (Figure 5.2B), and PCR product size confirming loss of the knockout construct (data not shown).

Because of the low rate of transformant recovery experienced using the repair methodology, we used an alternative strategy to restore wild-type function by complementation of the mutant phenotype. Each PCR-amplified wild-type gene was separately cloned into a pGEM-T Easy vector, then subcloned into pCW6500. This vector contains the *Aspergillus fumigatus pyroA* (*AfpyroA*) selectable marker, which complements the *pyroA4* mutation in each mutant, and allows for selection of pyridoxine prototrophs. The vector also contains an internal coding sequence fragment targeting the *wA* gene, disruption of which confers white conidia. Under this strategy, transformants of the circular plasmid with targeted integrations disrupting the *wA* gene by single homologous cross-over were white (Figure 5.3A) and those that integrated via single homologous crossover at the 5’ or 3’ flank of the GlcNAc utilization gene of

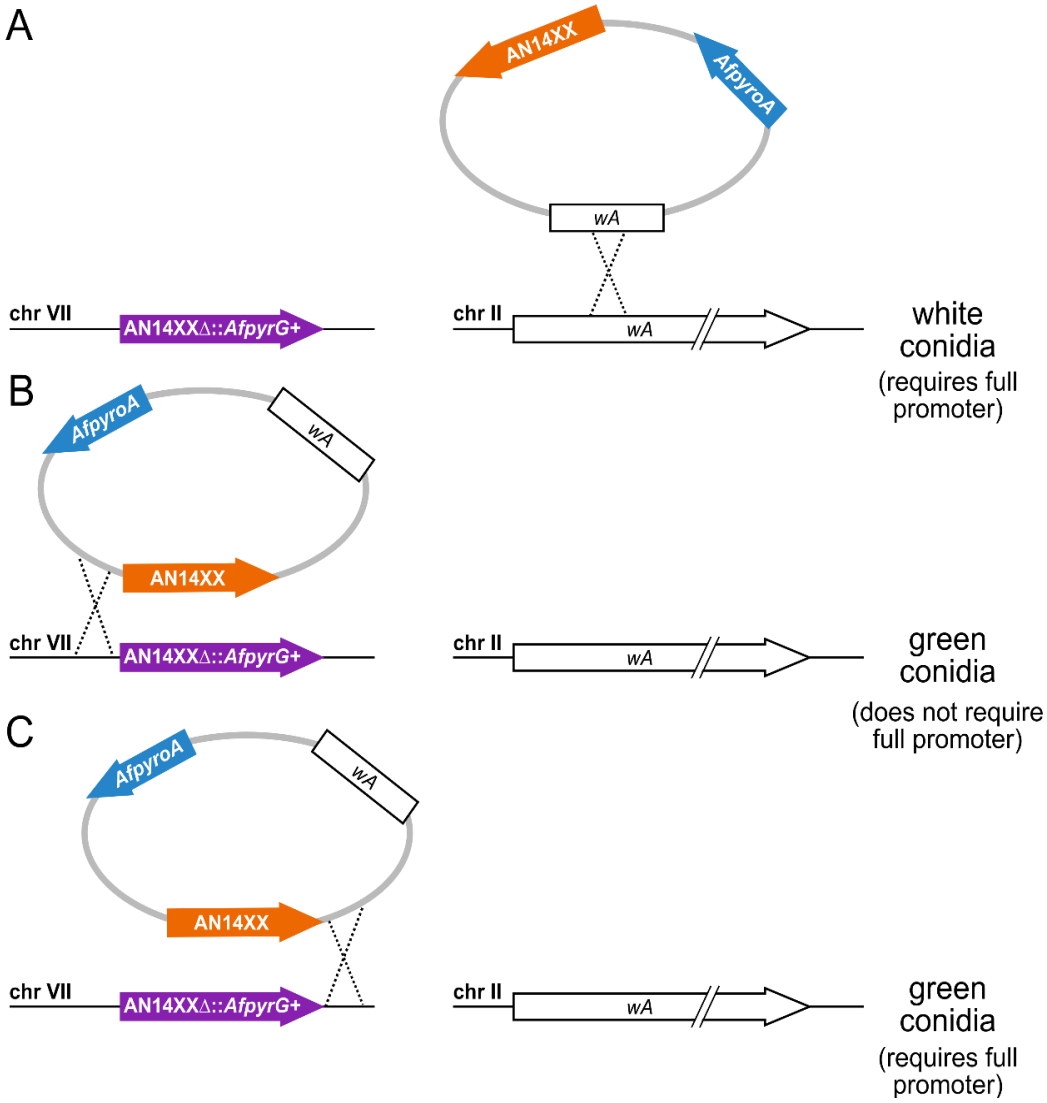

Figure 5.3 The pCW6500 plasmid targets the wA *gene.*
Wild-type GlcNAc utilization genes were cloned into pCW6500, which contains a fragment of the *wA* gene. (A) The construct may integrate via single crossover between the *wA* fragment in the construct and the *wA* gene on chromosome II to produce white conidia in transformants. (B) Integration may occur at the 5' end of the AN14XXΔ::*AfpyrG+* knockout construct via single crossover between the AN14XX 5' flanking region and the homologous sequence upstream of the knockout construct. If a portion of the AN14XX promoter is missing, it can be recapitulated by the recipient, allowing for full complementation of the mutant phenotype. (C) Integration may occur at the 3' end of the knockout construct via single crossover between the AN14XX 3' flanking region and the homologous sequence downstream of the knockout construct. In scenarios (A) and (C), all 5' elements necessary for gene expression must be intact for full complementation of the mutant phenotype to occur.

interest were green (Figure 5.3B-C). The overall observations are summarized in Table 5.5.

Transformation of the pHF287 plasmid containing the wild-type *ngtA* gene into the *ngtA*Δ strain produced abundant white and green transformants (RT1003-RT1008),

but none complemented the *ngtA* deletion phenotype when GlcNAc was either a nitrogen or carbon source (Figure 5.2B). This experiment was repeated and yielded the same results a second time.

Table 5.5. Summary of GlcNAc utilization mutant complementation experiments.

Gene	Transformant types	Complementation results
ngtA	• 19 white • 24 green	• No complementation
dacA	• 3 white • 8 green	• 2 whites transformant fully complemented on GlcNAc as a nitrogen source, partially complemented on GlcNAc as a carbon source • 1 white transformant partially complemented on GlcNAc as a nitrogen and as a carbon source • 4 green transformants fully complemented on GlcNAc as a nitrogen source, partially on GlcNAc as a carbon source
damA	• 9 white • 15 green	• No whites complemented • 1 green transformant fully complemented on GlcNAc as a nitrogen and as a carbon source

Transformation of the pHF289 plasmid containing the wild-type *dacA* gene into the *dacA*Δ strain yielded 10 transformants (Figure 5.2B). A subset of the green transformants fully complemented the *dacA* deletion on media containing GlcNAc as a nitrogen source and as a carbon source (RT1001-1002), indicating they integrated by single homologous crossover at the 5' end of the *dacA*Δ::*AfpyrG* gene, reconstructing the complete 5' regulatory region. Two white transformants fully complemented the deletion phenotype on GlcNAc as a nitrogen source but only partially on GlcNAc as a carbon source (RT998-999), consistent with the construct lacking the complete 5' regulatory sequences. One white transformant complemented the deletion partially on

GlcNAc as a nitrogen and as a carbon source (RT1000), which could be explained by integrations both at the *wA* gene and via the 5' flank of *dacA*.

Transformation of the pHF291 plasmid containing the wild-type *damA* gene into the *damA*Δ strain yielded numerous white transformants (RT1009-RT1013) but none complemented the deletion phenotype on GlcNAc either as a carbon or a nitrogen source (Figure 5.2B), indicating they lacked the full promoter sequence. One green transformant (RT1014) fully complemented the *damA* deletion on both media types, suggesting it integrated by single homologous crossover at the 5' end of the *damA*Δ::*AfpyrG* gene.

Because we did not observe full complementation of the deletion phenotypes in all transformants, we examined the promoter sequences of *ngtA*, *dacA*, and *damA*. Specifically, we looked for binding sites for XprG and for AreA, the general transcription factor for relief of nitrogen metabolite repression. These were assessed in relation to the probable 5' end of the transcript, as identified by available RNA-seq and CAGE-seq data, and the 5' forward primer used for generating the cloned fragment for each gene (Figure 5.4). Gene expression data suggested that the primary transcription start site in *ngtA* is ~0.35 kb upstream of the currently-annotated (version 4) 5' UTR. This places the potential XprG and AreA binding sites downstream of the *ngtA* (AN1427) 5' F primer (and therefore within the construct) within the 5' UTR, i.e., downstream of the transcription start site, and indicates that these DNA binding sites are not sufficient to drive expression of *ngtA*. Thus, there are likely no binding sites for either XprG or AreA in the promoter fragment of the construct transformed into the *ngtA*Δ mutant. The *dacA* and *damA* fragments transformed into their respective deletion mutants both possess

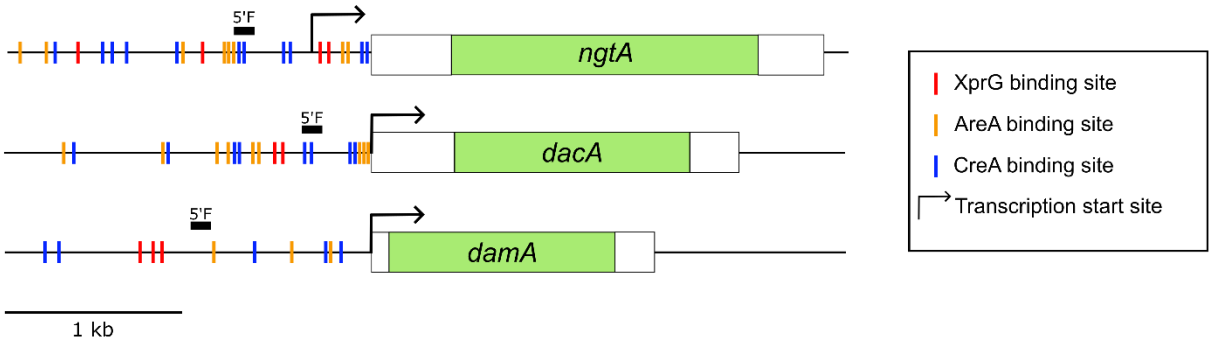

Figure 5.4 Gene fragments transformed into GlcNAc utilization deletion mutants lacked necessary upstream elements. The locations of consensus DNA binding sites for the transcription factors XprG (red bar), AreA (orange bar), and CreA (blue bar) were mapped in the 2-kb upstream region of *ngtA, dacA*, and *damA*. Also shown is the predicted transcription start site as indicated by CAGE-seq data (purple arrow) and the location of the 5' forward primer used to make the PCR product cloned into pCW6500 for complementation experiments. White boxes indicate annotated UTR regions.

potential AreA binding sites, however they, too, have no likely XprG binding sites present in the promoter fragments of either construct. For all three genes, putative XprG binding sites were observed further 5' than the promoter region included in the complementation constructs. These results highlight the necessity of XprG binding for full function of these genes.

5.5.2 AN8127 encodes a second GlcNAc transporter

The growth defect observed in the *ngtA*Δ GlcNAc transporter mutant using GlcNAc as a nitrogen, carbon, or nitrogen and carbon source was less severe than that seen in the *hxkC*Δ, *dacA*Δ, and *damA*Δ mutants (Figure 5.1C) or the *xprG*Δ and AN1416Δ GlcNAc utilization regulatory mutants (see Section 5.5.6 and Figure 5.10). This suggested that additional transporter(s) may be involved in transporting GlcNAc into the cell. Gilmore et al. (2013) showed experimental evidence for two GlcNAc transporter genes, *HcNGT1* and *HcNGT2*, in *Histoplasma capsulatum*. While *HcNGT1* was widely conserved in fungi, *HcNGT2* orthologs were absent in most fungal taxa, including *C. albicans* and other species in which GlcNAc catabolism has been

investigated. However, *HcNGT2* has a predicted ortholog in *A. nidulans*, AN8127 (Gilmore et al. 2013). We compared the AN8127 protein sequence with NgtA, HcNgt1 and HcNgt2 (Table 5.6). AN8127 shows 37.2% identity and 54.3% similarity to NgtA. Both proteins are more similar to their predicted orthologs in *H. capsulatum* than they are to each other, providing evidence that AN8127 represents a second putative GlcNAc transporter in *A. nidulans* that is evolutionarily distinct from NgtA.

Table 5.6 Percent sequence identity and similarity between GlcNAc transporters of *A. nidulans* and *H. capsulatum.*

	NgtA (AN1427)	AN8127	HcNgt1	HcNgt2
NgtA (AN1427)	100 / 100	37.2 / 54.3	58.6 / 71.1	33.4 / 49.4
AN8127		100 / 100	39.1 / 53.3	57.7 / 71.0
HcNgt1			100 / 100	34.1 / 48.4
HcNgt2				100 / 100

To better understand the relationship between *ngtA* and AN8127, we used online tools to document and predict features of the genes and the proteins they encode (Table 5.7). *ngtA* is located within the GlcNAc utilization gene cluster on chromosome VII, while AN8127 is outside of this gene cluster on chromosome II. Although *hxkC* is outside of this gene cluster in *A. nidulans*, in most species its orthologs are clustered with other GlcNAc utilization genes, providing evidence this is its ancestral location (Kappel et al. 2016). However, AN8127 orthologs are located outside of the GlcNAc utilization gene cluster in all species we examined.

Like NgtA, AN8127 belongs to the large Major Facilitator Superfamily of membrane-bound transporters (PF07690/IPR011701). Both proteins have 12 transmembrane domains arranged in two groups of 6, as is typical of this family (Figure

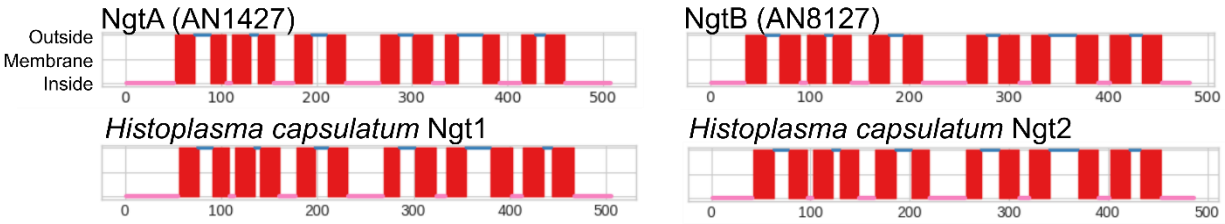

Figure 5.5 NgtA and AN8127 have the expected Major Facilitator Superfamily topology.
NgtA and AN8127 both contain 12 transmembrane domains characteristic of MFS proteins, arranged in two clusters of six. *H. capsulatum* orthologs Ngt1 and Ngt2, respectively, are shown for comparison. Predictions made by DeepTMHMM 1.0.

5.5). Over 250 genes in *A. nidulans* encode proteins with this domain and they are predicted to transport a diverse array of molecules. BLASTp analysis using the NgtA protein sequence indicated AN8127 as the top hit within *A. nidulans*, followed distantly by fewer than 20 additional MFS-encoding genes. Thus, merely having the MFS protein domain does not confer any great degree of sequence homology or indicate similarity of function. The high degree of similarity in sequence between NgtA and AN8127 suggests they may transport the same or similar cargo.

Table 5.7 Comparison of NgtA and AN8127.

	NgtA	**AN8127**
Genomic location	Chromosome VII, in the GlcNAc utilization gene cluster	Chromosome II
Gene structure	3 introns	1 intron
Protein length (residues)	508	482
Protein transmembrane domain predictions[+]	12	12
InterPro domains	MFS (PF07690)	MFS (PF07690)
Localization predictions[#]	Plasma membrane, ER, lysosome/vacuole	Plasma membrane, ER, lysosome/vacuole

[+] DeepTMHMM 1.0
[#] Psort II and DeepLoc 2.1

Localization predictions using Psort II and DeepLoc3 were not definitive for either protein, giving high localization likelihoods to the plasma membrane, ER, and lysosome/vacuole. Plasma membrane-bound proteins often pass through the ER endomembrane system during transport, and re-localization of transporters to and from their target membranes is a primary method of regulation (Bauer et al. 2015). Fluorescence-tagged CaNgt1 was observed primarily at the plasma membrane within seconds of exposure to GlcNAc (Alvarez and Konopka 2007; Hanumantha Rao et al. 2022). Degradation of CaNgt1 via an endosome-to-lysosome pathway has also been confirmed (Hanumantha Rao et al. 2022). These observations and the degree of sequence similarity between NgtA and AN8127, coupled with our direct evidence of their necessity for efficient utilization of extracellular GlcNAc presented below, provide strong evidence that both transporters are active in the plasma membrane but they may be located elsewhere transiently.

A phylogenetic tree was constructed for the NgtA and AN8127 proteins including representative sequences throughout the fungal kingdom (Figure 5.6A-B). Results showed distinct clades corresponding to the predicted NgtA and AN8127 orthologs.

To evaluate a possible role for AN8127 in utilization of extracellular GlcNAc, we deleted the AN8127 gene by transforming an AN8127Δ::*AfpyrG*+ knockout construct into the *pyrG89* recipient RT865 and selecting for pyrimidine prototrophy (Figure 5.7A). The resulting transformants did not differ from wild type when grown on glucose-ammonium minimal media but displayed reduced growth compared with wild type on media with GlcNAc as a sole nitrogen, carbon, or nitrogen and carbon source. However, growth of AN8127Δ mutants was leakier than that seen in *ngtA*Δ mutants (Figure 5.7B),

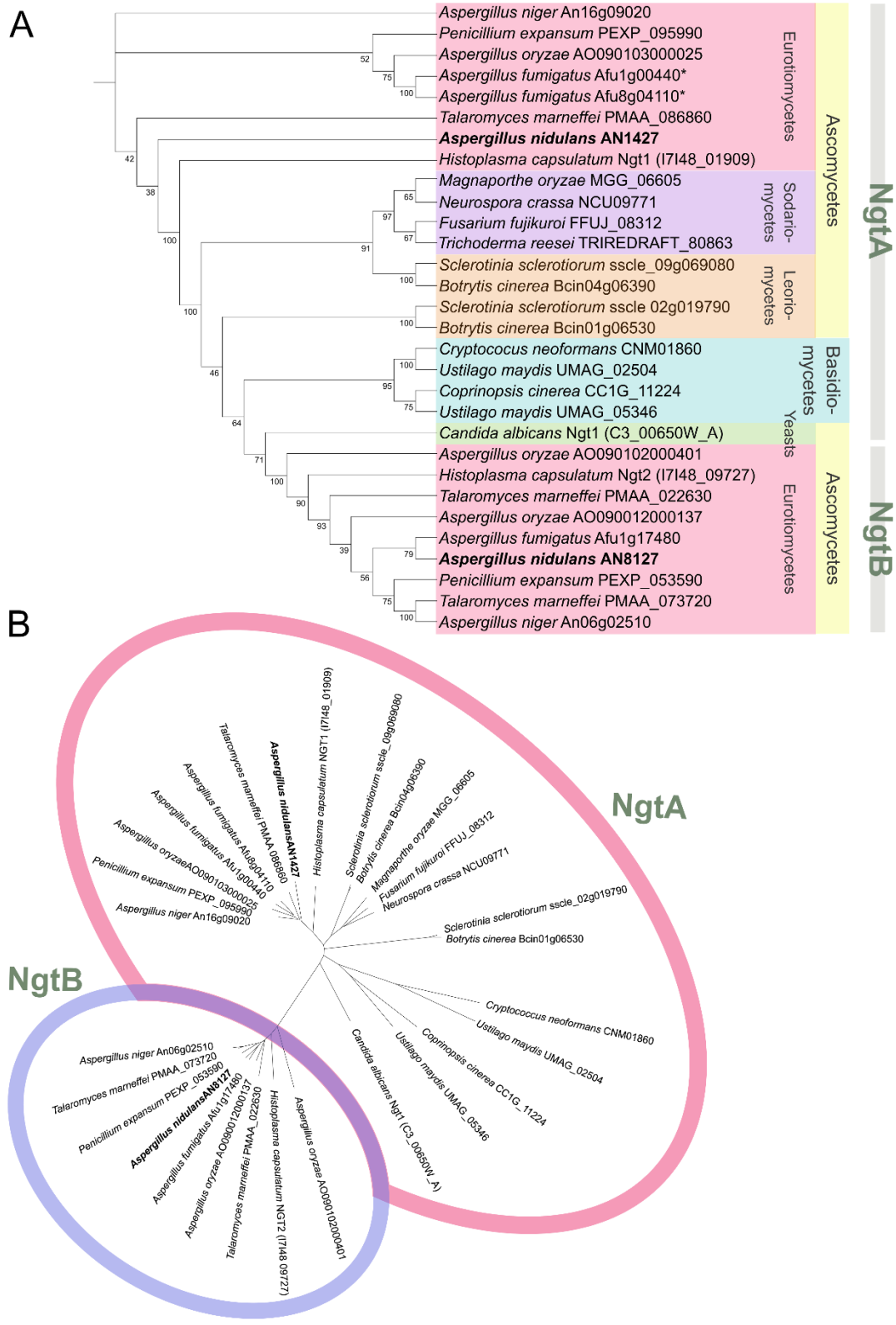

Figure 5.6 AN1427 and AN8127 form two distinct clades within the Eurotiomycetes.
Alignment of the protein sequences of fungal orthologs of *A. nidulans* AN1427 and AN8127 were used to construct rooted (A) and unrooted (B) trees. In the unrooted tree, two distinct clades are evident. Alignment by MAFFT and tree design by iTOL.

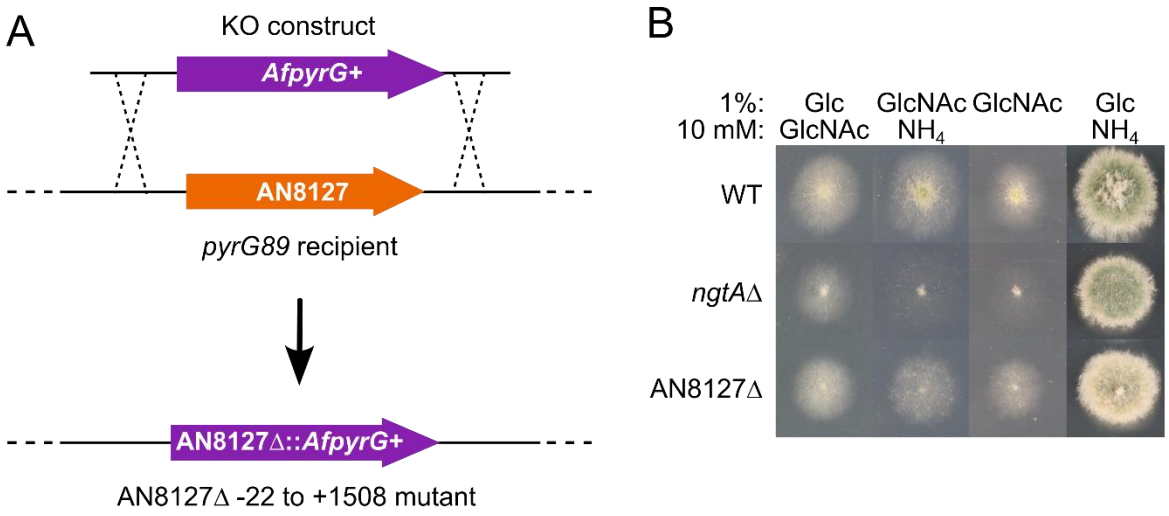

Figure 5.7 Deletion of AN8127 confers decreased growth on GlcNAc.
(A) Deletion mutants were constructed by gene replacement with a knockout construct containing the *Aspergillus fumigatus pyrG* gene (*AfpyrG*+) following transformation into a *nkuA*Δ *A. nidulans* recipient. (B) AN8127Δ mutants exhibited decreased growth on GlcNAc as a nitrogen source, carbon source, or nitrogen and carbon source. The decrease was not as pronounced as seen in *ngtA*Δ mutants. Strains of the indicated genotype were grown on supplemented minimal media containing 1% carbon source or carbon and nitrogen source and 10 mM nitrogen source and incubated for 48 h at 37ºC. Top to bottom: MH11068, RT708, RT988.

suggesting NgtA is the primary transporter and AN8127 plays a more minor role. Based on confirmation of its role in GlcNAc utilization, we named AN8127 *ngtB.*

5.5.3 Deletion of both GlcNAc transporter genes is lethal

Because deletion of *ngtA* and *ngtB* individually produced leakier phenotypes on GlcNAc than other GlcNAc pathway mutants, we hypothesized that the two genes may be partially redundant and that a double deletion mutant might exhibit a tight GlcNAc utilization phenotype. We first attempted to generate *ngtA*Δ *ngtB*Δ mutants by crossing a *ngtA*Δ mutant (RT993) with a *ngtB*Δ mutant (RT988). As per our normal protocol, we screened for hybrid cleistothecia by isolating four cleistothecia, bursting them to release ascospores, and spreading the individual ascospore suspensions on selective media on which only wild-type recombinant progeny lacking crossing marker auxotrophies could grow (Todd et al. 2007b). To verify the presence of viable progeny, we also spread

ascospore suspension on pyrimidine-supplemented complete media, on which all progeny could grow. Because no evidence of recombinant progeny was observed in our initial four cleistothecia, we screened an additional 12 cleistothecia. Again, there was no evidence any cleistothecia were hybrid. Additionally, a low number of progeny were observed for all ascospore suspensions on supplemented complete media. The cross was repeated and 12 additional cleistothecia were screened, without identifying any hybrid cleistothecia.

We attempted the cross again using a *ngtA*Δ mutant with different crossing markers (RT995). Of 16 cleistothecia examined, no hybrid cleistothecia were found. To further explore our observations, we selfed both parents. Visual inspection indicated the *ngtA*Δ mutant produced abundant cleistothecia of normal size, while the *ngtB*Δ mutant produced few cleistothecia of reduced size (data not shown). This indicated a fertility defect in the *ngtB*Δ mutant.

We devised a new strategy to construct the double mutant by transformation. First, we grew a *ngtA*Δ mutant (RT996) on media containing 5-FOA to select spontaneous mutations in the *AfpyrG* marker contained within the *ngtA*Δ allele, viz., *ngtA*Δ::*AfpyrG*. This, combined with the *pyrG89* mutation already present, rendered the mutant unable to grow on media without pyrimidine supplementation, thereby recycling the *AfpyrG* pyrimidine prototrophy selectable marker. This allowed us to transform the *ngtB*Δ::*AfpyrG*+ knockout construct used to make the *ngtB*Δ mutant (see Section 5.5.3) into the new *ngtA*Δ::*AfpyrG*- mutant and select for transformants by pyrimidine prototrophy (Figure 5.8).

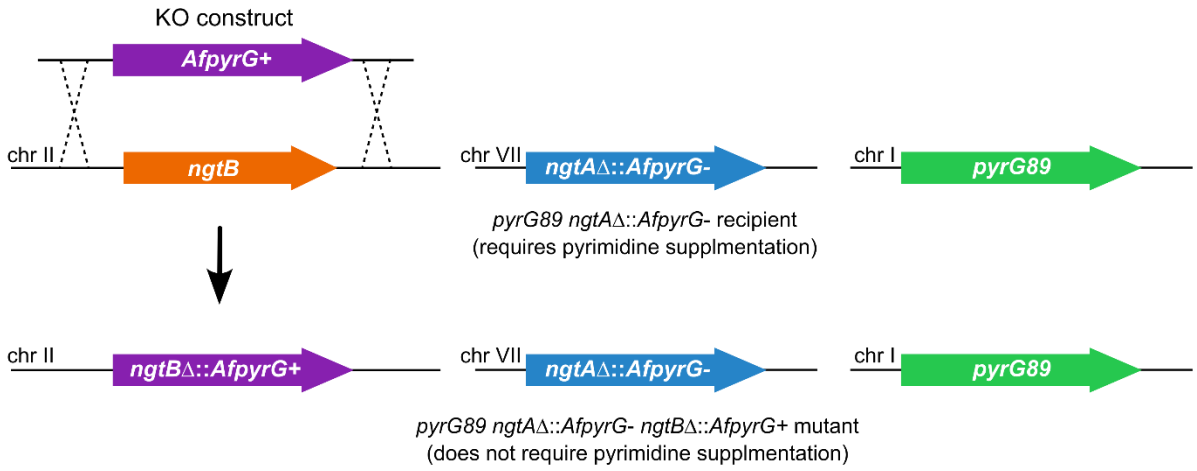

Figure 5.8 The ngtAΔ ngtBΔ *double mutant was created using a transformation strategy.* The *ngtB* knockout construct containing the *AfpyrG+* selectable marker was transformed into a *pyrG89 ngtAΔ::AfpyrG-* recipient exhibiting pyrimidine auxotrophy. The *AfpyrG+* marker complemented the PyrG- phenotype of the recipient, resulting in double mutants that were *pyrG89 ngtAΔ::AfpyrG- ngtBΔ::AfpyrG+* and exhibited pyrimidine prototrophy. Chr: chromosome.

We obtained transformants and, as per usual protocol, picked them by stabbing the colonies with a wire and transferring conidia to complete media lacking pyrimidines. To analyze the impacts of deletion of both transporters on growth using GlcNAc as a substrate, we also picked the same transformants to media containing GlcNAc as a nitrogen source or GlcNAc as a carbon source. Most of the transformants failed to grow on all three media types. However, four transformants grew normally on complete media and exhibited the NgtAΔ recipient phenotype on media containing GlcNAc as a nitrogen or carbon source. Taken alone, the NgtAΔ phenotype on GlcNAc could suggest that deletion of both transporters does not produce an additive effect on phenotype, but these four transformants could have arisen from gene conversion of the *AfpyrG* selectable maker or diploids arising from karyogamy of transformed and recipient nuclei (see below). The lack of growth on any of three types of media by most of the transformants that exhibited normal phenotypes on the transformation selection plates was surprising.

We considered whether the transformants that failed to grow might be heterokaryons in which a lethal *ngtB*Δ mutation might be rescued by complementation by the wild-type *ngtB* allele in an untransformed nucleus. In *A. nidulans*, streaking the uninucleate conidia for single colonies separates the two nuclear types from a heterokaryon. To investigate further, we performed a heterokaryon rescue test by streaking conidia from transformants on the primary transformation selection plates for single colonies on both selective media lacking pyrimidines and non-selective media supplemented with pyrimidines. On selective media conidia carrying the PyrG- recipient nuclei (of *pyrG89* and *AfpyrG*- genotype) will not germinate, whereas conidia carrying the transformed knockout nuclei will germinate but growth will arrest at the point the deleted gene is required (Figure 5.9A). On non-selective media, growth will be observed as the conidia carrying the PyrG- recipient nuclei will germinate and grow, even though the knockout conidia will arrest at the point the deleted gene is required. All transformants showed growth when streaked on non-selective media (Figure 5.9B). On selective media lacking pyrimidines, three transformants grew moderately well and one grew normally. All other transformants grew extremely poorly. We examined the poorly-growing transformants using the dissecting microscope and observed ungerminated conidia and germinated conidia with severely aborted growth (Figure 5.9C).

These observations suggest that simultaneous deletion of both *ngtA* and *ngtB* is lethal. In such an event, *A. nidulans* may form diploids and/or heterokaryons, that complement the lethal mutation(s) as a survival tactic. The transformation produced transformed nuclei which took in the knockout construct and replaced the wild-type *ngtB* gene. The resulting nuclei contained both the *ngtA*Δ::*AfpyrG*- and *ngtB*Δ::*AfpyrG*+

deletions and were phenotypically PyrG+ (Figure 5.9A). Additionally, untransformed recipient nuclei remained, which were *ngtA*Δ::*AfpyrG*-, *ngtB*+, *pyrG89*, and phenotypically PyrG-. When both types of nuclei were together in heterokaryotic mycelia, growth was possible because the wild-type *ngtB* gene complemented the *ngtB* deletion, but when separated via the uninucleate conidia, such as when stabbed or streaked for single colonies, each type of conidium exhibited different behavior. Conidia with untransformed nuclei exhibited the recipient (*ngtA*Δ) phenotype: normal growth on non-selective media, no germination on selective media, and the *ngtA*Δ level of growth reduction on media containing GlcNAc. Conidia with transformed nuclei grew only up to the point at which the deleted genes were necessary on all three media, however, this was masked on non-selective media by the abundant growth of the untransformed conidia. The heterokaryon rescue experiment also suggests at least one transformant formed a diploid which grew normally on both selective and non-selective media, because the *AfpyrG*-, *pyrG89* and *ngtB*Δ mutations were complemented in all transformed nuclei. Alternatively, transformants with this phenotype could have been recovered by gene conversion of *ngtA*Δ::*AfpyrG*- to *ngtA*Δ::*AfpyrG*+ from *AfpyrG* in the knockout construct (without gene replacement of *ngtB*).

We used PCR to confirm the presence of two genotypes in transformants. In a heterokayron, because both the wild-type *ngtB* and *ngtB*Δ::*AfpyrG*+ gene replacement are present, PCR should show bands of the sizes expected for each one. Transformant 4 retained its heterokaryotic growth patterns and was used for DNA extraction. After PCR amplification using primers for the *ngtA* gene, all transformants produced band sizes consistent with *ngtA*Δ knockout construct, as expected. Using primers for *ngtB*, we

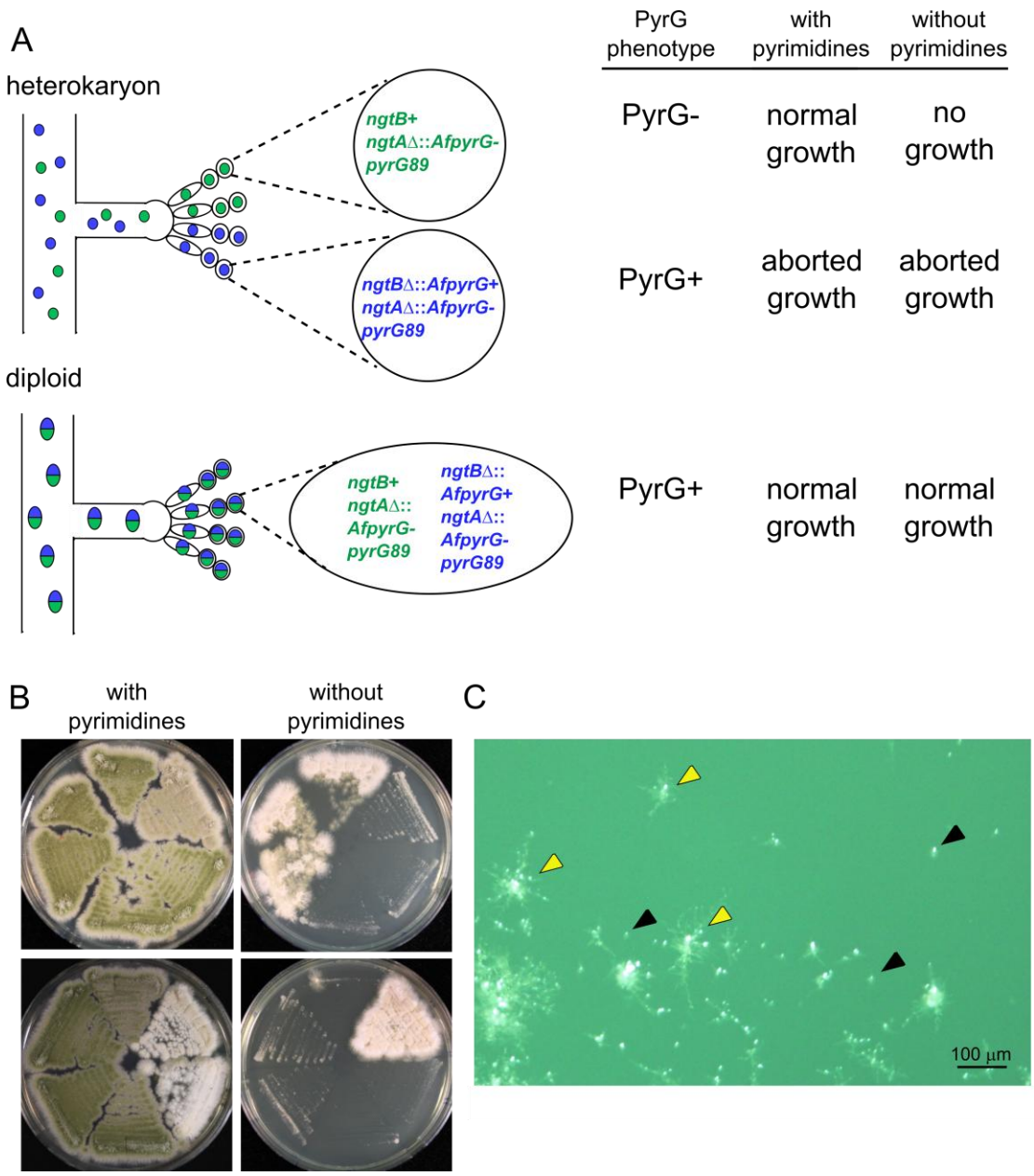

Figure 5.9 Deletion of both ngtA *and* ngtB *results in lethality.*
(A) In heterokaryon rescue experiments, uninucleate conidia from a putative heterokaryon are separated by streaking for single colonies. Growth after 48 h at 37 °C on complete media supplemented with pyrimidines (i.e., non-selective media) was observed for all 12 transformants shown as conidia carrying an untransformed nucleus can grow. On unsupplemented (selective) media, only one transformant grew normally, while three other transformants grew but appeared unstable or mixed, and most transformants grew extremely poorly. (B) Microscopic examination of poorly growing transformants after 48 h at 37 °C revealed ungerminated conidia (black arrows) and germinated conidia with aborted growth (yellow arrows). (C) In heterokaryotic mycelia, the presence of two types of nuclei allows complementation of the *ngtB*Δ mutation and relief of the *ngtA*Δ *ngtB*Δ phenotype. Uninucleate conidia have only one nucleus type. On supplemented media, the aborted growth of conidia with transformed nuclei is masked by normal growth of conidia with untransformed nuclei. On unsupplemented media, transformed nuclei show aborted growth but untransformed nuclei do not germinate due to the *AfpyrG-* and *pyrG89* mutations, thus revealing the heterokaryotic nature of the strain. Diploid transformants grow normally with or without pyrimidine supplementation because the *ngtB*Δ, *AfpyrG-*, and *pyrG89* mutations are complemented.

confirmed the presence of both the *ngtB* wild-type gene and the *ngtB*Δ::*AfpyrG*+ knockout construct. The presence of both *ngtB* alleles within a single transformant, coupled with the growth phenotype when the nuclei were separated by streaking for single colonies, is strong evidence Transformant 4 was a heterokaryon.

To ensure the original transformation and its results were genuine, we repeated the transformation of the *ngtB* knockout construct into the *ngtA*Δ *AfpyrG*- mutant. The results were similar, with several putative diploid transformants and several putative heterokaryons observed in a heterokaryon rescue experiment. This strengthens evidence that simultaneous deletion of both GlcNAc transporters is lethal (or near-lethal) in *A. nidulans*.

5.5.4 *xprG* and *ngsA* regulate GlcNAc utilization in *A. nidulans*

The XprG transcription factor was previously established as necessary for utilization of GlcNAc as a carbon source (Katz et al. 2016). We confirmed the growth phenotypes of the *xprG* deletion mutant on GlcNAc as a carbon source and also assessed growth on GlcNAc as a nitrogen source or carbon and nitrogen source (Figure 5.10A). The *xprG*Δ mutant showed partially reduced growth compared with wild type on GlcNAc as a nitrogen source and severely reduced growth compared with wild type when GlcNAc is either a sole carbon source or sole carbon and nitrogen source. The *xprG1* gain-of-function mutant grew better than the *xprG*Δ mutant but less robustly than wild type on GlcNAc as a nitrogen, carbon, or nitrogen and carbon source.

Based on the *C. albicans* model, XprG is hypothesized to physically associate with the putative GlcNAc sensor and histone acetylase AN1416. Previous work in our lab identified the AN1416 gene adjacent to *xprG* and constructed an AN1416Δ mutant.

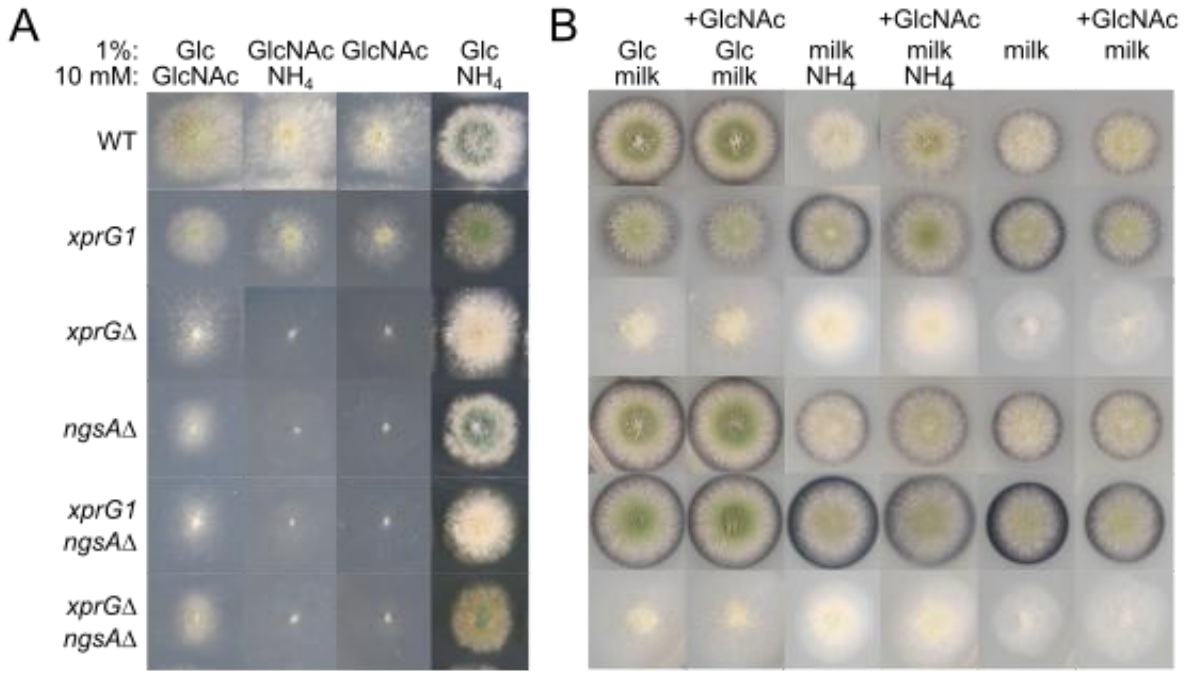

Figure 5.10 GlcNAc catabolism is regulated by xprG *and* ngsA*.*
(A) GlcNAc cannot be utilized efficiently without both *xprG* and *ngsA*. From top to bottom: MH11068, MK85, MK414, RT707, RT827, RT822. For 1% GlcNAc-10 mM ammonium medium, ammonium chloride was used. For 1% glucose-10 mM ammonium medium, ammonium tartrate was used. (B) *xprG* is necessary for milk clearing by extracellular proteases, but *ngsA* has a repressive effect on milk clearing. The *xprG1 ngsA+* mutant cleared milk slightly less in the presence of GlcNAc than without it. No differences were seen in any other strains. Strains of the indicated genotypes were grown on supplemented media containing the indicated compounds as carbon and/or nitrogen sources for 48 hours at 37º C. From top to bottom: MH11068, MK85, MK414, RT707, RT822, RT827. Glc: glucose; GlcNAc: N-acetylglucosamine.

Using growth testing, we showed that AN1416 is required for efficient utilization of GlcNAc as a sole nitrogen, carbon, or carbon and nitrogen source (Figure 5.10A), with the AN1416Δ mutant showing a similar reduction in growth to the *xprG*Δ mutant in each of the GlcNAc utilization growth tests. We gave AN1416 the name *ngsA (N-acetylglucosamine sensor A)*.

Evidence in *C. albicans* and *T. reesei* indicates their NgsA orthologs are descended from β-N-acetylglucosaminidase proteins of the glycoside hydrolase 3 (GH3) family, enzymes that cleave terminal N-GlcNAc molecules from GlcNAc chains (Su et al. 2016; Ullah et al. 2025). An example in *A. nidulans* is NagA, which breaks down GlcNAc chains released from the cell wall during autolysis (Kim et al. 2002). Four

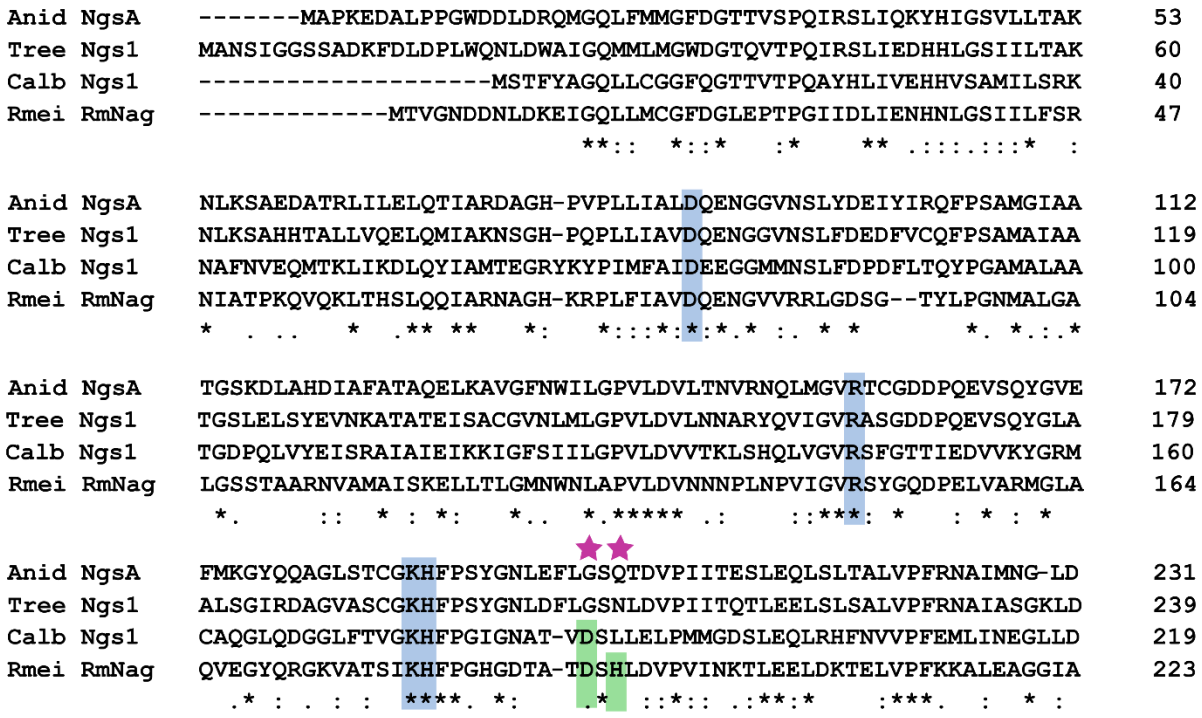

Figure 5.11 NgsA is a GlcNAc sensor.
Alignment of the NgsA protein sequence with its orthologs and other similar proteins shows conservation of four residues required for GlcNAc interaction (in blue). One or both of two key residues required for hydrolysis of terminal GlcNAc molecules from GlcNAc chains (in green) are not conserved in *Aspergillus nidulans (*Anid), *Trichoderma reesei* (Tree), and *Candida albicans* (Calb), indicated by purple stars. These key residues are intact in the basal fungus *Rhizomucor miehei* (Rmei).

essential residues are necessary for interaction with GlcNAc, and an additional two are needed for hydrolytic activity. However, in NgsA orthologs, mutation of one or both of those two key catalytic residues has eliminated their hydrolytic ability. Therefore, the proteins can bind but not hydrolyze GlcNAc, allowing them to act as GlcNAc sensors. Compare this with the basal fungus *Rhizomucor miehei* RmNag protein. Like NgsA orthologs, RmNag contains both a GH3 and an acetyltransferase domain, but both residues required for hydrolysis of GlcNAc are intact and its hydrolytic capability has been experimentally confirmed (Qin et al. 2015). Sequence alignment of NgsA with related proteins reveals that the four residues required for GlcNAc interaction are intact

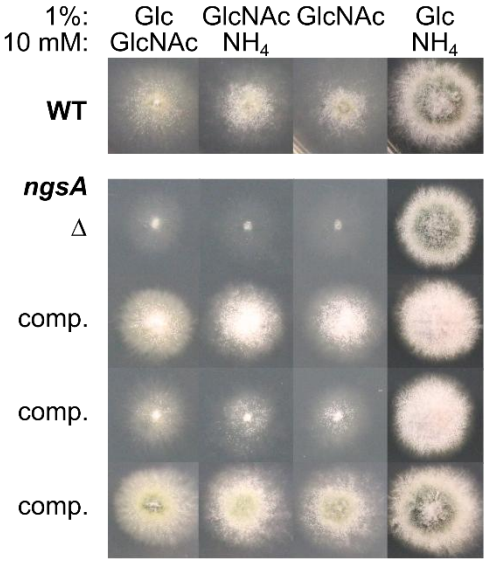

Figure 5.12 Full complementation of the ngsA∆ *mutant phenotype.*
Using the complementation strategy depicted in Figure 5.3, the *ngsA* wild-type gene was cloned into the pCW6500 plasmid and transformed into a *ngsA*∆ mutant, resulting in full complementation of the mutant phenotype and wild-type growth on GlcNAc as a nitrogen, carbon, or carbon and nitrogen source. Strains of the indicated genotypes were grown on supplemented minimal media containing the indicated compounds as carbon and/or nitrogen sources for 48 h at 37ºC. From top to bottom: MH11068, RT707, RT983, RT981, RT985.

but both residues necessary for hydrolysis of GlcNAc are mutated, providing additional evidence that it functions as a GlcNAc sensor in *A. nidulans* (Figure 5.11).

Multiple attempts to repair the *ngsA*∆ mutant phenotype using methodology outlined in Section 5.5.1 were unsuccessful, with no transformants obtained. To complement the *ngsA*∆ phenotype, we transformed the pHF285 plasmid containing the wild-type *ngsA* gene in a *wA* targeting vector with the *AfpyroA* selectable marker into the *ngsA*∆ mutant and selected for pyridoxine prototrophy. We obtained transformants with either green or white colored conidia that fully complemented the knockout phenotype by restoring wild-type growth on media containing GlcNAc as a nitrogen or as a carbon source (Figure 5.12; RT981-RT987; Table 5.5). Two white transformants complemented the mutant phenotype only partially, as indicated by growth that exceeded that of the deletion mutant but was poorer than wild type. PCR confirmation of five white transformants (two partially complementing and three fully complementing) indicated they contained both the *ngsA*∆::*AfpyrG*+ knockout construct and the *ngsA* wild-type gene, indicating successful integration of the pHF285 plasmid.

5.5.5 *xprG* and *ngsA* exhibit genetic interaction

We assessed *xprG-ngsA* genetic interactions by construction of two *xprG ngsA*Δ double mutants. As *xprG* (AN1414) and *ngsA* (AN1416) are tightly physically linked (~3.4 kbp apart), a crossing strategy was not used. An *xprG*Δ *ngsA*Δ double mutant was constructed by transforming a *ngsA* knockout cassette from the Fungal Genetics Stock Center into a *pyrG89 xprG*Δ strain (RT811). Transformants were selected for pyrimidine prototrophy. *xprG*Δ *ngsA*Δ mutants showed slightly reduced growth on glucose-ammonium medium, but like the *xprG*Δ mutant, showed less robust growth on GlcNAc as a nitrogen source and very reduced growth on GlcNAc as a carbon source or carbon and nitrogen source (Figure 5.10A). A *xprG1* AN1416Δ double mutant was constructed by transforming the *ngsA* knockout construct into a *pyrG89 xprG1* strain (RT803) and selecting for pyrimidine prototrophy. The resulting *xprG1 ngsA*Δ mutant also showed poor growth on GlcNAc as a nitrogen, carbon, and nitrogen and carbon source. This is similar to the *xprG*Δ mutant and the *ngsA*Δ mutant but in contrast to the stronger growth seen in the *xprG1 ngsA*+ strain, suggesting that the NgsA protein is necessary for XprG to function during growth on GlcNAc.

We also examined whether *ngsA* plays a role in extracellular protease regulation by *xprG*. To assess extracellular protease activity, we used growth tests with milk as a nitrogen or carbon source. In these tests, a zone of milk clearing, due to degradation of milk proteins, occurs around colonies that are producing extracellular proteases. Comparing the milk clearing zones around colonies of different genotypes provides qualitative evidence for extracellular protease activity of each genotype. On 1% glucose-1% milk media, i.e., milk as a nitrogen source, milk clearing was observed for

the wild type strain, and the *xprG1* gain-of-function mutant, and the levels of clearing appeared slightly increased in the *ngsA*Δ mutant and the *xprG1 ngsA*Δ double mutant, suggesting that NgsA may play a negative role in extracellular protease production (Figure 5.10B). However, milk clearing was not observed for the *xprG*Δ mutant or the *xprG*Δ *ngsA*Δ double mutant, consistent with activation of protease genes by XprG (Katz et al. 2006). Similar effects of each genotype were observed on 1% milk, i.e., milk as both a carbon and nitrogen source. On 1% milk-10 mM ammonium media, i.e., milk as a carbon source, the wild type strains produced little to moderate levels of milk clearing barely beyond the diameter of the colony, while *xprG1* and *xprG1 ngsA*Δ strains both showed enhanced milk clearing (Figure 5.10B). Surprisingly, the *ngsA*Δ mutant also produced enhanced milk clearing, indicating increased extracellular protease activity. The *xprG*Δ mutant, as expected, did not clear milk. Furthermore, the *xprG*Δ AN1416Δ double mutant did not clear milk, indicating *ngsA* cannot act independently of *xprG* in extracellular protease regulation. This observation indicates that NgsA acts to repress extracellular protease genes, in contrast to its role in activating GlcNAc utilization genes. To better understand the possible role of a GlcNAc sensor in extracellular protease regulation, we performed growth tests of the GlcNAc utilization regulatory gene knockout strains on media containing both milk and GlcNAc. No substantial change in phenotype was observed for any strains compared to milk alone, though the *xprG1* (*ngsA*+) mutant showed slightly reduced milk clearing. This suggests that, in contrast to its positive role in GlcNAc utilization, NgsA acts as a repressor of extracellular protease genes even when GlcNAc is present indicating that

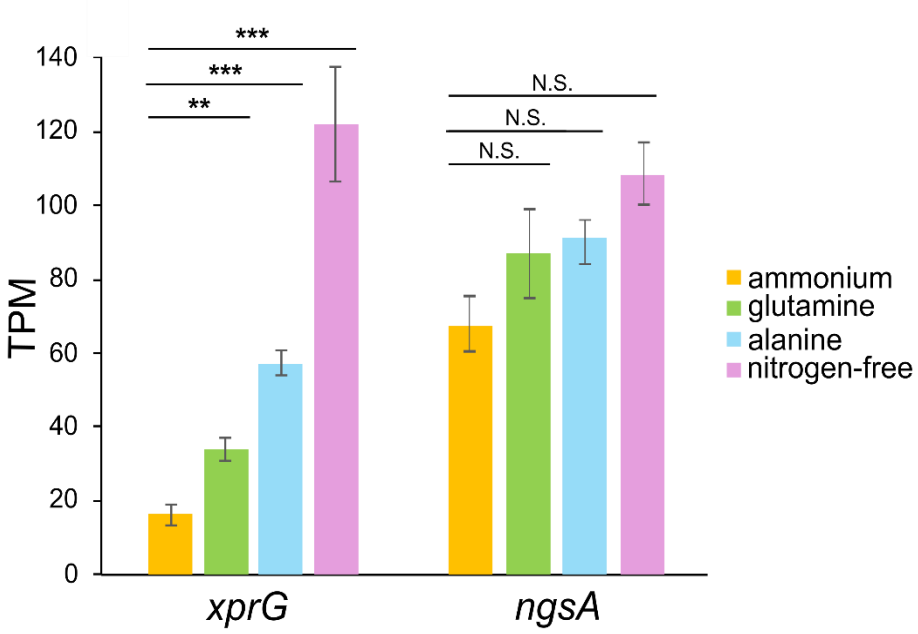

Figure 5.13 GlcNAc regulatory genes differ in their expression profiles.
xprG shows upregulation under glutamine and non-repressing conditions, while *ngsA* was constitutively expressed and did not differ between conditions. Expression levels are shown as normalized transcripts per million (TPM). Cultures were grown in supplemented liquid glucose-minimal medium with ammonium, glutamine, or alanine as the sole nitrogen source for 16 h at 37˚C. For the nitrogen-free condition, cultures were grown for 16 h in supplemented liquid glucose-ammonium minimal medium, washed, and transferred to nitrogen-free glucose-minimal media for 4 h before harvesting. Significance values of conditions are compared to ammonium: *, $p < 0.05$; **, $p < 0.01$; $p < 0.001$; N.S., not significant. Statistical analyses used DESeq2. n=3 biological replicates.

action as an activator or repressor is not simply due to the presence or absence of exogenous GlcNAc.

5.5.6 *xprG* and *ngsA* differ in their expression profiles

We analyzed RNA-seq data for GlcNAc regulatory genesin a wild-type (with respect to nitrogen regulation) strain (MH11068) under different nitrogen utilization conditions. *xprG* was upregulated in the glutamine, alanine, and nitrogen-free conditions relative to ammonium (Figure 5.13). *ngsA*, however, showed similar expression levels under all conditions, as may be expected if the NgsA protein functions as a GlcNAc sensor.

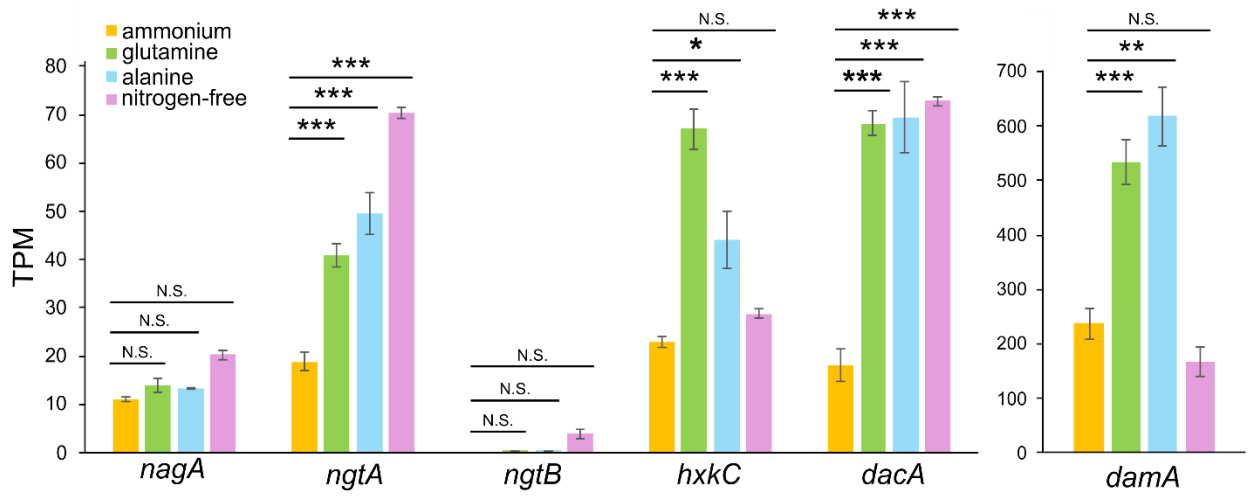

Figure 5.14 Most GlcNAc utilization genes are regulated by nitrogen.
The *ngtA* GlcNAc transporter and structural GlcNAc utilization genes were upregulated on glutamine and non-repressing conditions, relative to ammonium, except *nagA*. Transporter *ngtB* gene showed very low expression across all conditions. Expression is shown as normalized transcripts per million (TPM). Cultures were grown in supplemented liquid glucose-minimal medium with ammonium, glutamine, or alanine as the sole nitrogen source for 16 h at 37˚C. For the nitrogen-free condition, cultures were grown for 16 h in supplemented liquid glucose-ammonium minimal medium, washed, and transferred to nitrogen-free glucose-minimal media for 4 h before harvesting. Significance values of conditions are compared to ammonium: *, $p < 0.05$; **, $p < 0.01$; $p < 0.001$; N.S., not significant. Statistical analyses used DESeq2. *p*-values can be found in Appendix B. n=3 biological replicates.

5.5.7 GlcNAc utilization genes are regulated by nitrogen source

We examined expression of the GlcNAc utilization genes in RNA-seq data in the same strains and nitrogen conditions used for analysis of *xprG* and *ngsA* in Section 5.5.7. All GlcNAc utilization genes except *ngtB* were expressed under both repressing (ammonium and glutamine) and non-repressing (alanine and nitrogen-free) nitrogen regimes (Figure 5.14). Expression of *damA* under all conditions was considerably higher than the other GlcNAc utilization genes. *ngtA* and *dacA* were upregulated compared with ammonium on glutamine, alanine, and during nitrogen starvation. *hxkC* and *damA* were up-regulated compared with ammonium on glutamine and alanine, but interestingly, were not upregulated in the nitrogen-starvation condition. *nagA*, a gene involved in release of GlcNAc from chitin during autolysis (Reyes et al., 1989; Kim et al., 2002), was not differentially expressed in any condition relative to ammonium.

5.5.8 GlcNAc utilization is regulated by nitrogen metabolite repression

To assess whether the major regulator of nitrogen metabolism, AreA, which activates genes for utilization of alternative nitrogen sources to relieve nitrogen metabolite repression, regulates GlcNAc utilization, growth tests to compare wild type and *areA* mutants have been performed. *areA*Δ mutants grew very poorly compared with wild type on media with GlcNAc as a sole nitrogen or nitrogen and carbon source, but similar to wild type when GlcNAc was a sole carbon source (S.M. Hopkins and R.B. Todd, personal communication). Therefore, utilization of GlcNAc as a nitrogen source is regulated by the transcription factor AreA.

One mechanism that modulates AreA activity is repression in response to ammonium and glutamine by the transcription corepressor NmrA. Analysis of RNA-seq data in wild type compared with the *nmrA*Δ mutant reveals evidence of nitrogen metabolite repression by NmrA on glutamine, as modest but statistically significant derepression of *ngtA*, *hxkC,* and *dacA* was observed (Figure 5.15). Furthermore, strong, two-fold derepression of *damA*, which encodes the step that releases ammonium, was observed. Surprisingly, no evidence of derepression of the GlcNAc utilization genes in the *nmrA*Δ mutant was observed on ammonium. Furthermore, no effect of *nmrA* deletion on *xprG* or *ngsA* expression was observed on either glutamine or ammonium.

5.6 Discussion

GlcNAc was examined previously for its role in fungal pathogenicity and as source of carbon in *C. albicans, T. reesei, H. capsulatum, M. oryzae, B. bassiana, and C. deneoformans* (Simonetti et al. 1974; Gilmore et al. 2013; Kappel et al. 2016; Kumar et al. 2016; Vesely et al. 2017; Bhatt et al. 2020; Qiu et al. 2022, 2022; Ye et al. 2022;

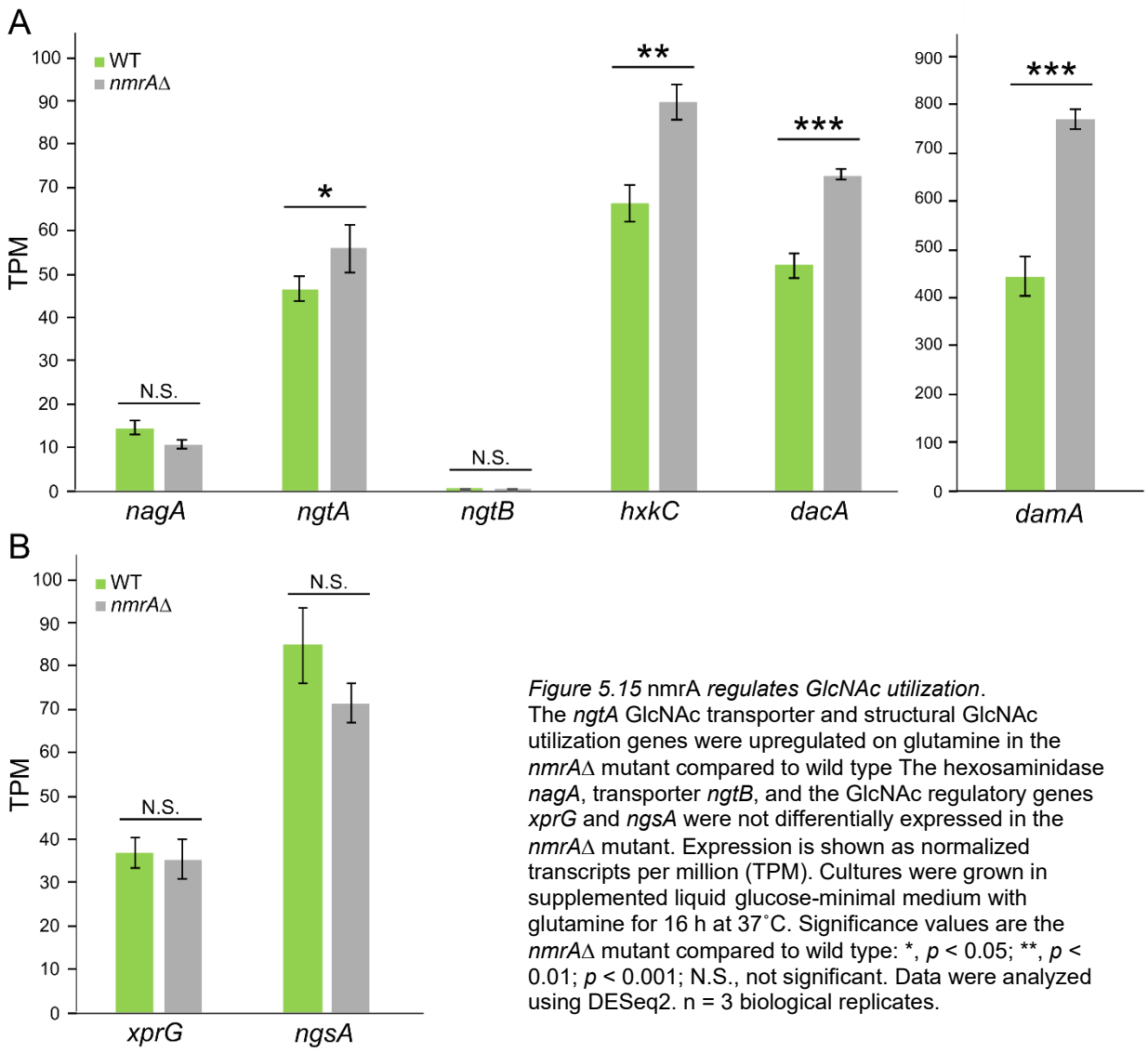

Figure 5.15 nmrA *regulates GlcNAc utilization*. The *ngtA* GlcNAc transporter and structural GlcNAc utilization genes were upregulated on glutamine in the *nmrA*Δ mutant compared to wild type The hexosaminidase *nagA*, transporter *ngtB*, and the GlcNAc regulatory genes *xprG* and *ngsA* were not differentially expressed in the *nmrA*Δ mutant. Expression is shown as normalized transcripts per million (TPM). Cultures were grown in supplemented liquid glucose-minimal medium with glutamine for 16 h at 37˚C. Significance values are the *nmrA*Δ mutant compared to wild type: *, $p < 0.05$; **, $p < 0.01$; $p < 0.001$; N.S., not significant. Data were analyzed using DESeq2. n = 3 biological replicates.

Yang et al. 2023; Zhang et al. 2024; Ullah et al. 2025). However, there has been no prior focus on its role as a source of nitrogen. Our work establishes that extracellular GlcNAc can be transported into the cell and catabolized for utilization in growth as a sole nitrogen source, a sole carbon source, or a sole nitrogen and carbon source. We demonstrated decreased growth on GlcNAc and impaired GlcNAc utilization in deletion mutants of the putative GlcNAc sensor *ngsA*, GlcNAc transporter *ngtA*, GlcNAc-6-phosphate deacetylase *dacA*, and glucosamine-6-phosphate deaminase *damA* (S.M.

Hopkins, C.C. Hunter, J.T. Steyer, and R.B. Todd, unpublished data). We also revealed phenotypes for GlcNAc utilization as a nitrogen source for the previously-characterized mutants of the transcription factor XprG and GlcNAc hexokinase *hxkC,* which were known to be affected in utilization of GlcNAc as a carbon source (Katz et al. 2016).

We complemented the decreased growth on GlcNAc as a nitrogen or carbon source in the *ngsA*Δ mutant, confirming the role of this gene in GlcNAc utilization. Additionally, we attempted to use the corresponding wild-type genes to complement the growth defects of the *ngtA*Δ, *dacA*Δ, and *damA*Δ mutants on GlcNAc as a carbon or nitrogen source. The construct we used for complementation of the *ngtA*Δ mutant phenotype failed to complement in the transformants generated, while *dacA* and *damA* transformants showed full, partial, or no complementation were obtained. Each construct contained the transcription start site, the full 5'UTR, coding sequence, and 3'UTR. However, our analysis of upstream elements of each native gene indicates that some of the predicted binding sites for the nitrogen metabolism regulatory transcription elements were not included in the constructs used in our complementation experiments. The absence of XprG DNA binding sites, along with the site of integration (targeted to *wA* or integration via single crossover in the 3' flanking sequence), likely account for the observed complementation failures in the structural genes. The complementing transformants obtained for the *damA*Δ and *dacA*Δ recipients indicate that the GlcNAc utilization phenotypes we observed are due to the deletion of these two genes. For the *dacA*Δ and *damA*Δ mutants, we obtained transformants with the corresponding linear gene using direct selection on GlcNAc as a nitrogen source, and for *ngtA*Δ we obtained transformants using 5-FOA selection. These transformants were indistinguishable from

the wild-type control when growth tested on GlcNAc as a nitrogen, carbon, or nitrogen or carbon source. Therefore, through deletion and complementation or repair experiments, we demonstrated that the three structural genes predicted to act in the GlcNAc utilization pathway showed GlcNAc utilization growth phenotypes and thus likely carry out their predicted role in GlcNAc utilization. Additionally, each gene is orthologous to one confirmed as involved in GlcNAc catabolism in *C. albicans* and *T. reesei* (Kumar et al. 2000; Yamada-Okabe et al. 2001; Kappel et al. 2016), the species in which the GlcNAc utilization pathway is best characterized. We therefore have completed identification of the genes comprising the GlcNAc utilization pathway in *A. nidulans*.

An unusual phenotype was observed for transformants during repair of deletion mutants with wild-type genes via homologous recombination on protoplast media selection plates containing with GlcNAc as the nitrogen source. Protoplast media contains a very high concentration of sucrose. Although a high level of background growth was observed for each of the GlcNAc utilization mutants, we were able to identify transformants with slightly stronger than background diffuse growth. We also noticed that growth of our wild-type strain MH1 (*biA1*) displayed diffuse growth when GlcNAc was a carbon or carbon and nitrogen source, spread out more than on other carbon sources. While neither of these observations of diffuse spreading growth are central to our research, they are noteworthy and raise questions regarding morphological changes in hyphal growth possibly triggered by the presence of GlcNAc under different conditions. Such morphological changes are essential for pathogenesis in species such as *C. albicans* (Simonetti et al. 1974; Lo et al. 1997).

We identified NgtB as a second putative GlcNAc transporter required for utilization of GlcNAc as a carbon source and/or as a nitrogen source. NgtB orthologs are predicted only within the Eurotiomycetes (Gilmore et al. 2013) and are thus absent in the majority of other taxa in which GlcNAc utilization has been studied. Deletion of *ngtB* produced a GlcNAc growth defect less severe than that seen in *ngtA*Δ deletion mutants. Expression of *ngtB* was nearly absent under conditions supplying either ammonium, alanine, or glutamine as a nitrogen source or during nitrogen starvation. Presently, we do not have expression data for growth on GlcNAc in *A. nidulans*. In *H. capsulatum,* the *ngtA* ortholog *HcNGT1,* but not the *ngtB* ortholog *HcNGT2,* was up-regulated on GlcNAc (Gilmore et al. 2013). These growth and expression data suggest that NgtB may have a primary function transporting GlcNAc under yet-undiscovered conditions and/or transporting an alternative sugar. Given the limited taxonomic distribution of the gene, this may represent a novel nutrient utilization function not seen in most fungi. Though most taxa do not have a *ngtB* ortholog, transporters of other hexose sugars can transport small amounts of GlcNAc into the cell in *S. cerevisiae* under high GlcNAc concentrations (Scarcelli et al. 2012). However, in *T. reesei* (which does not have a *ngtB* ortholog), Ullah et al. (2025) were unable to find a second transporter candidate that might contribute to GlcNAc transport.

To investigate if the functions of NgtA and NgtB were partially redundant, we attempted to construct a *ngtA*Δ *ngtB*Δ double mutant. Repeated attempts to use a crossing strategy between *ngtA*Δ and *ngtB*Δ mutants failed to produce hybrid cleistothecia. Observation of tiny cleistothecia during diagnostic *ngtB*Δ selfings suggests deletion of this gene causes defects in sexual reproduction. Upon switching to a

transformation strategy to generate a double mutant, only heterokaryon and putative diploid transformants were produced. Separation of uninucleate conidia from these transformants led to growth patterns that showed deletion of both genes confers a synthetic lethal phenotype.

If simultaneous deletion of the two GlcNAc transporters represents abolition of import of extracellular GlcNAc in *A. nidulans*, it is not obvious why this would impact growth on media containing preferred nitrogen and carbon sources, viz., ammonium and glucose, and suggests a vital role for extracellular GlcNAc even when GlcNAc is not a predominant nutrient. In *H. capsulatum*, HcNgt1 and HcNgt2 were not deleted, but instead separately subjected to RNA interference-mediated transcript depletion and thus the impact of deleting both transporters is unknown (Gilmore et al. 2013). However, in *C. albicans*, a diploid yeast, exposure to GlcNAc triggers a switch to hyphal growth and pathogenesis. In the absence of both copies of CaNgt1, hyphal growth and pathogenicity do not occur (Alvarez and Konopka 2007). HcNgt1 and HcNgt2 play a role in a switch to filamentous growth in *H. capsulatum* (Gilmore et al. 2013).

In addition to autolysis, cell wall remodeling during hyphal growth also generates extracellular GlcNAc (Figure 5.16; Konopka 2012). During hyphal extension and branching, the existing cell wall is broken down and reused to synthesize and deposit new chitin in at the extending hyphal tip. In *A. nidulans*, the chitinase ChiA is secreted during hyphal growth and GPI-anchored at the hyphal tip and secondary hyphal branch points to facilitate this breakdown (Yamazaki et al. 2008). UDP-GlcNAc is generated *de novo* through the hexosamine pathway (de Groot et al. 2009; Paneque et al. 2023). The anabolic hexosamine pathway acts in the opposite direction as the described catabolic

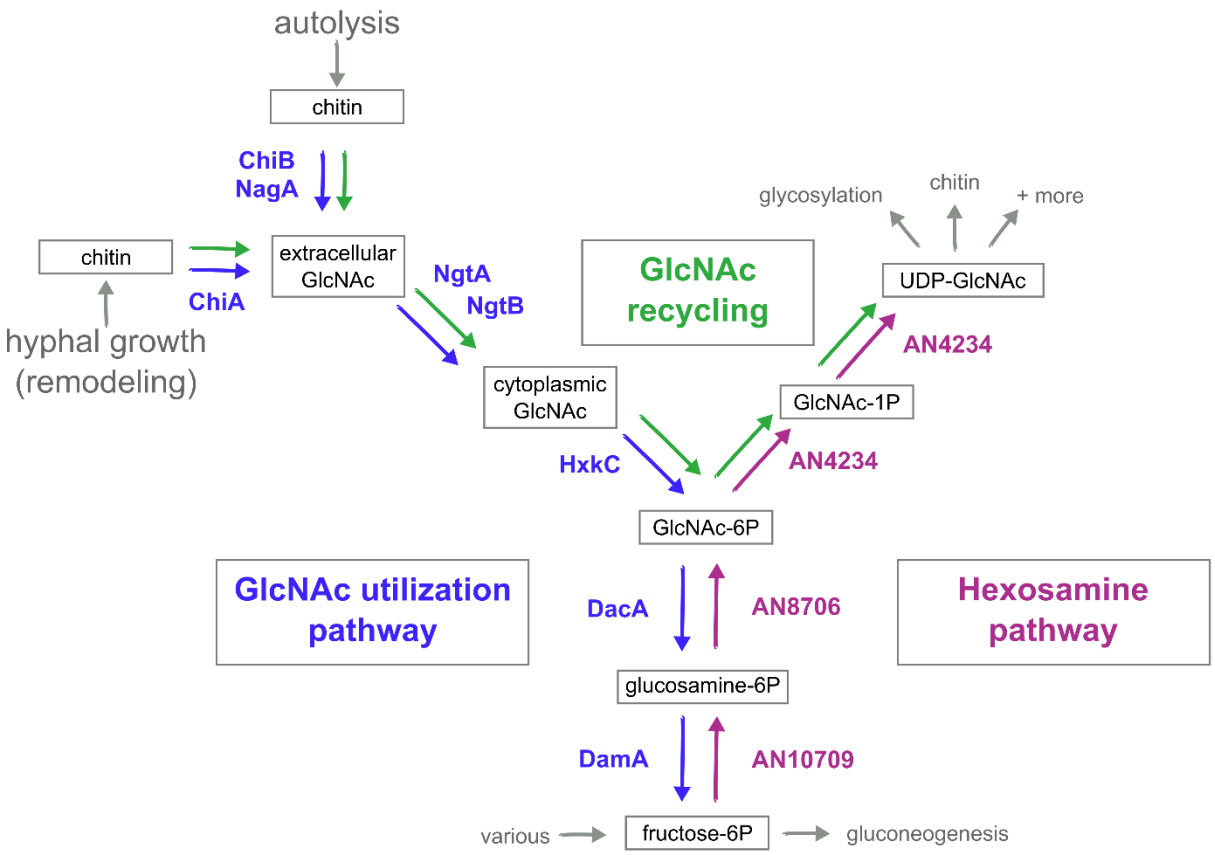

Figure 5.16 GlcNAc is involved in multiple metabolic pathways.
The catabolic GlcNAc utilization pathway provides energy by taking in extracellular GlcNAc and catabolizing it 1) to fructose-6-phosphate for direct use as carbon in gluconeogenesis and 2) to ammonium that enters nitrogen metabolism by NADP-glutamate dehydrogenase. The anabolic hexosamine pathway synthesizes GlcNAc de novo using a starting product of fructose-6-phosphate, for production of UDP-GlcNAc. Extracellular GlcNAc derived from autolysis or cell wall remodeling during hyphal growth can also be phosphorylated by HxkC and shunted into the latter part of the hexosamine pathway to recycle it into UDP-GlcNAc.

pathway, synthesizing GlcNAc-6-phosphate from fructose-6-phosphate using a different set of enzymes (Paneque et al. 2023). GlcNAc-6-phosphate is further metabolized to synthesize UDP-GlcNAc for use in processes such as glycosylation and chitin biosynthesis (Paneque et al. 2023). Additionally, extracellular GlcNAc transported into the cytoplasm can also be shunted into a recycling pathway and used for synthesis of new UDP-GlcNAc, which can then be used for glycosylation of proteins or for assembly into chitin (Kobae et al. 2015). Import and incorporation of extracellular GlcNAc into

chitin in the cell wall is confirmed in *Cryptococcus neoformans* (Camacho et al. 2017). Although fructose-6-phosphate can enter the hexosamine pathway through many routes, its ultimate origin is glucose. It is possible that uptake of glucose during early germination is insufficient to provide enough carbon for energy, carbon or nitrogen for chitin production, or both, due to the small surface area-to-volume ratio of the round conidium (or yeast cell, in other species). The energy and material demands inherent to transitioning to polar growth may require extracellular GlcNAc to serve as the building block for chitin.

Like in *ngtA*Δ and *ngtB*Δ mutants, the decrease in growth seen in *hxkC*Δ mutants on GlcNAc was less severe than that in other GlcNAc utilization mutants. This was also seen for the *T. reesei hxkC* ortholog mutant (Kappel et al. 2016). While hexokinases may have one primary substrate, hexokinases often have an affinity for multiple hexose sugars such as glucose, glucosamine, galactose, and GlcNAc, such as in the yeast *Yarrowia lipolytica* (Flores and Gancedo 2015). They can thus act in partially redundant manners. The *A. nidulans* genome contains multiple kinases of hexose sugars (Flipphi et al. 2003, 2009) and one or more of them could play a small role in GlcNAc phosphorylation during catabolism in the absence of *hxkC*. There is, however, no evidence that HxkD provides GlcNAc kinase activity, as the *hxkC*Δ *hxkD*Δ double mutant did not differ in growth on GlcNAc from the *hxkC*Δ mutant (Katz et al. 2016).

We showed that genetic interactions occur between XprG and NgsA. In *C. albicans*, both the XprG and NgsA orthologs were found to be associated with the promoters of the GlcNAc catabolic genes in a GlcNAc-independent manner (Su et al. 2016), indicating the presence of GlcNAc is required to trigger the NgsA histone

deacetylase activity necessary for transcription of the GlcNAc catabolic genes. This is consistent with our finding that the *xprG1* gain-of-function mutation showed poor growth on GlcNAc when *ngsA* was deleted but strong growth when *ngsA* was intact. In addition, the poor growth of the *xprG*Δ *ngsA*Δ double mutant on GlcNAc was not more severe than that of either single mutant, indicating that the presence of NgsA does not affect GlcNAc catabolism in the absence of XprG. These experiments underscore the necessity of the XprG-NgsA relationship in GlcNAc utilization.

Additionally, we showed a role for NgsA in regulation of extracellular proteases. XprG was previously shown to regulate extracellular proteases, and deletion of the *xprG* gene causes decreased extracellular protease activity (Katz et al. 2006). The *ngsA*Δ mutant, however, produced a cleared zone on milk, suggesting NgsA acts by repressing extracellular protease activity. This suggests that GlcNAc sensing may have a role beyond GlcNAc catabolism under poor nutrient conditions. Deletion of *xprG* and *ngsA* orthologs in *T. reesei* each had wide-ranging impacts on the transcriptome, far beyond GlcNAc utilization genes (Ullah et al. 2025). However, in our growth tests on media containing both milk and GlcNAc, there were no differences in milk clearing compared with milk alone other than a slight reduction in clearing in the *xprG1* gain-of-function mutant (Figure 5.10B), suggesting that the NgsA histone acetyltransferase has opposite gene regulation outcomes at GlcNAc utilization gene promoters and protease gene promoters. This indicates that GlcNAc does not convert NgsA to an activator, at least at protease gene promoters, and further suggests that promoter-specific differences occur in the molecular mechanisms of XprG-NgsA regulation at the promoters of GlcNAc utilization genes and those of protease genes.

Our work showed that GlcNAc utilization is subject to nitrogen metabolite repression and is regulated by *areA* and *nmrA*. In a wild-type strain, *xprG* and the GlcNAc structural genes (with the exception of *ngtB*) were upregulated under derepressive nitrogen conditions, while *ngsA* exhibited constitutive expression appropriate for a sensor. We saw additional upregulation under growth on glutamine in a *nmrA*Δ mutant. The N-acetylhexosaminidase *nagA* showed low expression under all conditions in our study, but research on older cultures indicates *nagA* is upregulated under conditions in which autolysis is predicted (Pusztahelyi et al. 2006). Release of GlcNAc from fungal cells walls is common under autolytic conditions and could serve as an important nutrient source. We might thus expect to see high expression of GlcNAc utilization genes in older cultures, as well. Work in *T. reesei* suggests that GlcNAc utilization genes are also regulated by carbon catabolite repression and the *creA* ortholog, with genes being downregulated in the presence of glucose (Ullah et al. 2025). Manual sequence inspections showed that *A. nidulans* GlcNAc utilization genes contain potential CreA binding sequences in their promoters. At 48 h, growth of *T. reesei* on GlcNAc as a carbon source exceeded that on glucose. Additionally, in *A. fumigatus*, growth on GlcNAc was much stronger than on glucose (He et al. 2024b). Yet in *A. nidulans*, GlcNAc produces weak growth whether serving as a nitrogen, carbon, or nitrogen and carbon source. Differences in lifestyle between the species may explain this. GlcNAc is a core component of many glucosaminoglycans (GAGs) in the mammalian extracellular matrix, and spores of the pathogen *A. fumigatus* germinate in mammalian tissues. Thus, the ability to grow robustly on GlcNAc would be an adaptation for successful host infection. *A. nidulan*s infects mammals only in very

limited circumstances. In *T. reesei* and *H. capsulatum*, GlcNAc is a strong inducer of GlcNAc utilization gene expression (Gilmore et al. 2013; Kappel et al. 2016; Ullah et al. 2025).

It appears that the handling of GlcNAc within the cell at any given time, as outlined in Figure 5.16, is dependent on environmental conditions, intracellular GlcNAc levels, and other factors. Work in the mycorrhizal species *Rhizophagus irregularis* has provided some insight into this. Expression of GlcNAc anabolic genes is upregulated in long-lived mycelia that absorb minerals from the soil, but GlcNAc catabolic genes are upregulated in ephemeral mycelia that absorb nutrients from host roots, as the mycelia collapse and the cell wall GlcNAc is resorbed and used for energy (Kobae et al. 2015).

5.7 Future Directions

Attempts to complement the GlcNAc mutant phenotypes with plasmids containing wild-type genes resulted in varying degrees of success. In *ngtA*Δ, *dacA*Δ, and *damA*Δ, transformants differed in their abilities to complement fully or partially, using GlcNAc as a nitrogen source or as a carbon source. While all three wild-type fragments used for transformation appear to have lacked XprG binding sites and there were multiple ways in which the gene fragments could integrate into the deletion mutants, the array of observed transformant phenotypes suggests there are additional factors influencing the outcome. Comparison of *ngtA, dacA*, and *damA* promoter sequences with those of *ngtB* and *hxkC* could reveal patterns not yet noticed. CreA, the regulator of carbon catabolite repression, adds additional complexity. Every transformant in the *ngsA*Δ complementation experiment fully complemented the mutant phenotype on GlcNAc as a nitrogen and as a carbon source. In fact, growth of the

transformants on GlcNAc appears to even slightly exceed that of wild type. While it is clear that XprG regulates GlcNAc utilization, little is known about the regulation of *ngsA,* as it shows constitutive expression across multiple nitrogen sources in *A. nidulans* and its ortholog is found at the promoters of GlcNAc utilization genes in a GlcNAc-independent manner in *C. albicans* (Su et al. 2016). Altogether, there is much yet to learn about regulation of GlcNAc utilization and its regulators and how it fits into the larger pictures of nitrogen and carbon metabolic regulation.

The finding that deletion of both GlcNAc transporters in *A. nidulans* is lethal was unexpected and suggests that import of extracellular GlcNAc is necessary for hyphal growth. Despite most fungal species having only one predicted GlcNAc transporter, it seems extremely likely that one or more additional transporters are active if the main transporter is deleted in these species. Understanding this better would shed light on the very basics of how filamentous fungi grow.

ngsA appears to have a vital role in GlcNAc utilization, and our work additionally showed its possible role in regulation of extracellular proteases. In the insect pathogenic fungus *B. bassiana*, deletion of the *ngsA* ortholog leads to decreases in chitin degradation proteins and Pr1 proteases necessary for breakdown of the insect cuticle (Zhang et al. 2024), and in *T. reesei* deletion of *NGS1* leads to differential expression of secondary metabolism and chitin degradation genes (Ullah et al. 2025). In *C. albicans*, the *ngsA* ortholog is required for utilization of sugars other than GlcNAc, such as maltose (Naseem et al. 2017). Thus, *ngsA* and its orthologs may play a regulatory role in diverse catabolic pathways related to nutrient acquisition. It would be valuable to

discover other XprG targets at which NgsA is found or if NgsA associates with proteins other than XprG.

Further research into the GlcNAc utilization pathway and its regulation could open up new understandings of nutrient acquisition during times of starvation and cycling of GlcNAc during growth.

Chapter 6 - Discussion and Future Directions

In Chapter 3, we identified the *A. nidulans sarB* gene and showed that it encodes a putative transmembrane UDP-GlcNAc transporter involved in amino acid utilization and cell wall and septal chitin deposition. The *sarB*Δ mutant was affected in histidine and lysine utilization. These two amino acids are catabolized via the LAAO SarA (Davis et al., 2005). In Chapter 4, we examined the relationship between SarB and SarA and confirmed that the *sarB*Δ and *sarA*Δ mutations do not have additive effects and therefore these genes are in the same genetic pathway. We showed that SarB is required for full SarA activity and explored whether the molecular mechanism may occur via a role for SarB in providing UDP-GlcNAc for glycosylation of SarA. While we provided evidence that SarA is N-glycosylated with a GlcNAc-decorated glycan, the molecular mechanism by which SarB is required for full SarA activity remains to be elucidated. Our inability to establish a clear link between SarB and N-glycosylation highlights difficulties encountered elucidating the roles for multiple UDP-GlcNAc transporters in humans. Knockdown of SLC35B4, the SarB ortholog, appeared to have no impact on N-glycans found in the Golgi (Bazan et al. 2018). Additional UDP-GlcNAc transporters, dissimilar in sequence to SLC35B4, are found in humans (e.g., Ishida et al. 2005; Zhao et al. 2023) and some appear to have orthologs in *A. nidulans*. Knockdown of one of these UDP-GlcNAc transporters, SLC35A3 (possible *A. nidulans* ortholog AN10676), led to a decrease in GlcNAc-branched tri-antennary and tetra-antennary N-glycans but produced no changes in other GlcNAc-decorated N-glycans (Song et al. 2022). In this study, SLC35A5 was found to physically associate with only the N-GlcNAc transferase GNT-IV, but not GNT-V, indicating that different transporters

may contribute to different placements of GlcNAc in N-glycans. Lastly, these researchers found that SLC35A3 was modified by OGT, meaning that O-GlcNAcylation, a process in which SLC35B4 is involved, regulates some types of N-glycosylation. This example alone underscores the complexity of interplay between UDP-GlcNAc transporters and glycosylation. It would be beneficial to see the effects of deletion of other UDP-GlcNAc transporters on amino acid utilization and SarA activity in *A. nidulans* and further investigate SarA in the context of O-GlcNAcylation.

To our knowledge, this study reflects the first deletion of the OGT gene in fungi. Despite seeing no obvious phenotypic effects on growth, we saw a slight reduction in SarA LAAO activity in the *areA102* OGT∆ mutant and our RNA-seq data indicate that OGT is expressed under multiple conditions in *A. nidulans*. O-GlcNAcylated proteins have been previously identified in *A. oryzae* (Machida and Jigami 1994).O-GlcNAc is established as a signal that helps regulate metabolism in animals (e.g., Ngoh and Jones 2008; Wex et al. 2018; Morino and Maegawa 2021), but connections between these observations and fungal processes have not been developed. As O-GlcNAc is an important metabolic signal in animals, further study of OGT function in fungi would be valuable. However, our preliminary investigations using publicly-available genome sequences indicate fungi differ from animals in a key aspect of O-GlcNAcylation: most fungi lack the gene encoding OGA, the enzyme that removes O-GlcNAc from proteins. Species that contain an OGA gene are scattered throughout the fungal kingdom. For example, close *A. nidulans* relatives *A. versicolor* and *A. sydowii* have clear OGA genes, but *A. nidulans* and most aspergilli do not. This suggests that O-GlcNAcylation may function differently in fungi, which would be a breakthrough in our understanding of

this process. Even understanding the evolution of the loss of the OGA gene in most fungi could be informative, given the sporadic appearance of the gene across fungal taxa. Further work on O-GlcNAc and O-GlcNAcylation in fungi could open up entirely new areas of knowledge.

Human orthologs of SarB and SarA are implicated in multiple diseases. Elevated levels of SLC35B4 are found in prostate, gastric, and liver tumors (Huang et al. 2018; Liu et al. 2019; Jiang et al. 2022), where it stabilizes the c-Myc protein, a positive regulator of cancer-promoting genes that is constitutively expressed in many cancers (Jiang et al. 2022). SLC35B4 is also a gluconeogenesis inhibitor and is implicated in diabetes and obesity (Yazbek et al. 2011; Wex et al. 2018), and recent evidence suggests a role in development of osteoarthritis (Kang et al. 2025). The human SarA ortholog, IL4i1, has important immunosuppressive roles in immune regulation and may help cancer cells evade the immune system (Romagnani 2016; Castellano and Molinier-Frenkel 2017; Zuo et al. 2023). IL4i1 additionally depletes essential amino acids, activating the aryl hydrocarbon receptor, which leads to tumor cell mobility, immunosuppression, and poor cancer outcomes (Sadik et al. 2020; Grobben et al. 2023; Zeitler and Murray 2023; Hirose et al. 2024). IL4i1 activity, transcripts, and/or protein levels are elevated in gliomas, ovarian, thyroid, and lung tumors and are associated with poor prognoses (Ye et al. 2023; Zhang et al. 2023; Zhu et al. 2023). IL4i1 may also compete for binding the spike protein of the SARS-Cov-2 virus (Gatineau et al. 2022). Fungal models can provide for valuable insights into the mechanisms by which the orthologs of both SarB and SarA promote disease progression.

GlcNAc plays multiple vital roles in all living things, yet this diversity of functions is sparsely studied in fungi. GlcNAc can serve as both a nitrogen and carbon source in *A. nidulans.* Our work in Chapter 5 characterized the genes involved in the GlcNAc catabolic pathway. We also showed the necessity of the GlcNAc sensor *ngsA* for GlcNAc utilization in *A. nidulans*, as also occurs in *C. albicans, T. reesei* and *B. bassiana* (Su et al. 2016; Zhang et al. 2024; Ullah et al. 2025). This finding provides evidence that its role is conserved in fungi. However, there are unanswered questions about both the evolution of this unique gene and its orthologs, and its possible wider role in responses to poor nutrient conditions. *ngsA* is clearly a result of gene fusion, with its N-terminus homologous to N-acetylhexosaminidases, which hydrolyze individual GlcNAc molecules from longer chains, and its C-terminus is homologous to histone acetyltransferases (Qin et al. 2015; Su et al. 2016). Additionally, its hydrolytic activity is prevented by mutations at key residues, resulting only in binding of GlcNAc. Our preliminary sequence analyses suggest that the loss of hydrolytic function occurred in the basal fungi, where some species have the key mutations and some do not. However, these taxa are not well delineated, so it is difficult to be more precise than that at this time. We had less success tracing the evolution of the gene fusion between N-acetylhexosaminidase and acetyltransferase genes, but it, too, appears to have occurred in fungi (Qin et al. 2015). Further research in this area could provide insights into gene evolution.

We showed evidence that NgsA, in addition to regulating GlcNAc utilization, plays a role in regulating extracellular protease activity. The structure of NgsA clearly shows it binds only GlcNAc and not another substrate associated with extracellular

proteases. This suggests GlcNAc may play a signaling role in nutrient starvation responses outside of GlcNAc catabolism in fungi. Because fungi exhibit less complexity overall than animals, elucidating GlcNAc signaling in fungi on a more granular level could allow for transfer of this information to animal systems and a more detailed understanding of metabolic diseases.

GlcNAc additionally serves as a trigger for virulence in fungi, as best studied in *C. albicans* (Min et al. 2020). For a mammalian pathogen, which is surrounded by GlcNAc in the extracellular matrix of its host, there is logic in using GlcNAc as a trigger. GlcNAc catabolism is also necessary for pathogenesis in *B. bassiana,* which as a pathogen of insects, encounters GlcNAc in the chitinous insect exoskeleton (Qiu et al. 2022; Zhang et al. 2024). It makes sense that this species would require the ability to break down chitin, but it is unclear if GlcNAc also acts in wider role as a signal for virulence. The necessity of GlcNAc catabolism for virulence in a plant pathogen like *M. oryzae* is puzzling (Kumar et al. 2016; Bhatt et al. 2020), as it is unlikely to encounter significant amounts of GlcNAc in its host plants. Future efforts toward a thorough understanding of GlcNAc signaling in fungal virulence could lead to identification of targets for fighting fungal infections. *ngsA* and its orthologs are necessary for GlcNAc catabolism and appear to have evolved in fungi. They may thus serve as possible targets for the development of therapeutics.

GlcNAc is important as an abundant sugar in the environment and is a component of vital signaling and structural features within the cell. A better understanding of the role of GlcNAc in nutrient acquisition, signaling, and fungal growth could lead to breakthroughs in treatment of fungal infections, metabolic diseases, and

cancers in humans, as well as general understandings of glycosylation and movement of nucleotide sugars like UDP-GlcNAc into the Golgi.

References

Abdelkafi-Koubaa Z, Jebali J, Othman H, Morjen M, Aissa I, Zouari-Kesentini R, Bazaa A, Ellefi AA, Majdoub H, Srairi-Abid N, Gargouri Y, El Ayeb M, Marrakchi N. 2014. A thermoactive L-amino acid oxidase from *Cerastes cerastes* snake venom: Purification, biochemical and molecular characterization. Toxicon 89:32–44.

Abramson J, Adler J, Dunger J, Evans R, Green T, Pritzel A, Ronneberger O, Willmore L, Ballard AJ, Bambrick J, Bodenstein SW, Evans DA, Hung C-C, O'Neill M, Reiman D, Tunyasuvunakool K, Wu Z, Žemgulytė A, Arvaniti E, Beattie C, Bertolli O, Bridgland A, Cherepanov A, Congreve M, Cowen-Rivers AI, Cowie A, Figurnov M, Fuchs FB, Gladman H, et al. 2024. Accurate structure prediction of biomolecular interactions with AlphaFold 3. Nature 630:493–500.

Alvarez FJ, Konopka JB. 2007. Identification of an N-acetylglucosamine transporter that mediates hyphal induction in *Candida albicans*. Molecular Biology of the Cell 18:965–975.

Alvarez-Jarreta J, Amos B, Aurrecoechea C, Bah S, Barba M, Barreto A, Basenko EY, Belnap R, Blevins A, Böhme U, Brestelli J, Brown S, Callan D, Campbell LI, Christophides GK, Crouch K, Davison HR, DeBarry JD, Demko R, Doherty R, Duan Y, Dundore W, Dyer S, Falke D, Fischer S, Gajria B, Galdi D, Giraldo-Calderón GI, Harb OS, et al. 2024. VEuPathDB: the eukaryotic pathogen, vector and host bioinformatics resource center in 2023. Nucleic Acids Research 52:D808–D816.

Andrianopoulos A, Hynes MJ. 1988. Cloning and analysis of the positively acting regulatory gene *amdR* from *Aspergillus nidulans*. Molecular and Cellular Biology 8:3532–3541.

Andrianopoulos A, Kourambas S, Sharp JA, Davis MA, Hynes MJ. 1998. Characterization of the *Aspergillus nidulans nmrA* gene involved in nitrogen metabolite repression. Journal of Bacteriology 180:1973–1977.

Anyaogu DC, Hansen AH, Hoof JB, Majewska NI, Contesini FJ, Paul JT, Nielsen KF, Hobley TJ, Yang S, Zhang H, Betenbaugh M, Mortensen UH. 2021. Glycoengineering of *Aspergillus nidulans* to produce precursors for humanized N-glycan structures. Metabolic Engineering 67:153–163.

Arst HN, Cove DJ. 1973. Nitrogen metabolite repression in *Aspergillus nidulans*. Molecular and General Genetics MGG 126:111–141.

Arst HN, Scazzocchio C. 1975. Initiator constitutive mutation with an "up-promoter" effect in *Aspergillus nidulans*. Nature 254:31–34.

Ashikov A, Routier F, Fuhlrott J, Helmus Y, Wild M, Gerardy-Schahn R, Bakker H. 2005. The human solute carrier gene SLC35B4 encodes a bifunctional nucleotide sugar

transporter with specificity for UDP-xylose and UDP-N-acetylglucosamine. Journal of Biological Chemistry 280:27230–27235.

Bauer NC, Doetsch PW, Corbett AH. 2015. Mechanisms regulating protein localization. Traffic 16:1039–1061.

Bazan B, Wiktor M, Maszczak-Seneczko D, Olczak T, Kaczmarek B, Olczak M. 2018. Lysine at position 329 within a C-terminal dilysine motif is crucial for the ER localization of human SLC35B4. PLOS ONE 13:e0207521.

Bernardo SM, H, Gray K, Todd RB, Cheetham BF, Katz ME. 2007. Characterization of regulatory non-catalytic hexokinases in *Aspergillus nidulans*. Molecular Genetics and Genomics 277:519–32.

Bhatt DN, Ansari S, Kumar A, Ghosh S, Narula A, Datta A. 2020. Magnaporthe oryzae MoNdt80 is a transcriptional regulator of GlcNAc catabolic pathway involved in pathogenesis. Microbiological Research 239:126550.

Blum M, Andreeva A, Florentino LC, Chuguransky SR, Grego T, Hobbs E, Pinto BL, Orr A, Paysan-Lafosse T, Ponamareva I, Salazar GA, Bordin N, Bork P, Bridge A, Colwell L, Gough J, Haft DH, Letunic I, Llinares-López F, Marchler-Bauer A, Meng-Papaxanthos L, Mi H, Natale DA, Orengo CA, Pandurangan AP, Piovesan D, Rivoire C, Sigrist CJA, Thanki N, et al. 2025. InterPro: the protein sequence classification resource in 2025. Nucleic Acids Research 53:D444–D456.

Boulland M-L, Marquet J, Molinier-Frenkel V, Möller P, Guiter C, Lasoudris F, Copie-Bergman C, Baia M, Gaulard P, Leroy K, Castellano F. 2007. Human IL4I1 is a secreted L-phenylalanine oxidase expressed by mature dendritic cells that inhibits T-lymphocyte proliferation. Blood 110:220–227.

Camacho E, Chrissian C, Cordero RJB, Liporagi-Lopes L, Stark RE, Casadevall A. 2017. N-acetylglucosamine affects *Cryptococcus neoformans* cell-wall composition and melanin architecture. Microbiology 163:1540–1556.

Castellano F, Molinier-Frenkel V. 2017. An overview of L-amino acid oxidase functions from bacteria to mammals: Focus on the immunoregulatory phenylalanine oxidase IL4I1. Molecules : A Journal of Synthetic Chemistry and Natural Product Chemistry 22:2151.

Chavan SS, Tian W, Hsueh K, Jawaheer D, Gregersen PK, Chu CC. 2002. Characterization of the human homolog of the IL-4 induced gene-1. Biochimica et Biophysica Acta (BBA) - Gene Structure and Expression 1576:70–80.

Chen F, Mackey AJ, Stoeckert CJ Jr, Roos DS. 2006. OrthoMCL-DB: querying a comprehensive multi-species collection of ortholog groups. Nucleic Acids Research 34:D363–D368.

Chen F, Mackey AJ, Vermunt JK, Roos DS. 2007. Assessing performance of orthology detection strategies applied to eukaryotic genomes. PLoS One 2:e383.

Christians JK, Cheema MS, Vergara IA, Watt CA, Pinto LJ, Chen N, Moore MM. 2011. Quantitative trait locus (QTL) mapping reveals a role for unstudied genes in *Aspergillus* virulence. PLOS ONE 6:e19325.

Clutterbuck AJ. 1973. Gene symbols in *Aspergillus nidulans*. Genetical Research 21:291–296.

Cohen BL. 1972. Ammonium repression of extracellular protease in *Aspergillus nidulans*. Journal of General Microbiology 71:293–299.

Cohen BL. 1973. Regulation of intracellular and extracellular neutral and alkaline proteases in *Aspergillus nidulans*. Journal of General Microbiology 79:311–320.

Cohen N, Aviram N, Schuldiner M. 2023. A systematic proximity ligation approach to studying protein-substrate specificity identifies the substrate spectrum of the Ssh1 translocon. The EMBO Journal 42:e113385.

Cove DJ. 1966. The induction and repression of nitrate reductase in the fungus *Aspergillus nidulans*. Biochimica et Biophysica Acta (BBA) - Enzymology and Biological Oxidation 113:51–56.

Davis MA, Askin MC, Hynes MJ. 2005. Amino acid catabolism by an *areA*-regulated gene encoding an L-amino acid oxidase with broad substrate specificity in *Aspergillus nidulans*. Applied and Environmental Microbiology 71:3551–3555.

De Souza CP, Hashmi SB, Osmani AH, Andrews P, Ringelberg CS, Dunlap JC, Osmani SA. 2013. Functional analysis of the *Aspergillus nidulans* kinome. PLOS ONE 8:e58008.

Dean N. 1995. Yeast glycosylation mutants are sensitive to aminoglycosides. Proceedings of the National Academy of Sciences of the USA 92:1287–1291.

Douglas RH, Ballou CE. 1982. Purification of an alpha-N-acetylglucosaminyltransferase from the yeast *Kluyveromyces lactis* and a study of mutants defective in this enzyme activity. Biochemistry 21:1561–1570.

Downes DJ, Davis MA, Kreutzberger SD, Taig BL, Todd RB. 2013. Regulation of the NADP-glutamate dehydrogenase gene gdhA in *Aspergillus nidulans* by the Zn(II)2Cys6 transcription factor LeuB. Microbiology (United Kingdom) 159:2467–2480.

Du X-Y, Clemetson KJ. 2002. Snake venom l-amino acid oxidases. Toxicon 40:659–665.

El Hakim AE, Salama WH, Hamed MB, Ali AA, Ibrahim NM. 2015. Heterodimeric L-amino acid oxidase enzymes from Egyptian *Cerastes cerastes* venom: Purification,

biochemical characterization and partial amino acid sequencing. Journal of Genetic Engineering & Biotechnology 13:165–176.

Elbein AD. 1981. The tunicamycins — useful tools for studies on glycoproteins. Trends in Biochemical Sciences 6:219–221.

Espeso EA, Cobeño L, Arst HN. 2005. Discrepancies between recombination frequencies and physical distances in *Aspergillus nidulans:* Implications for gene identification. Genetics 171:835–838.

Feliciano PR, Rustiguel JK, Soares ROS, Sampaio SV, Cristina Nonato M. 2017. Crystal structure and molecular dynamics studies of L-amino acid oxidase from *Bothrops atrox*. Toxicon 128:50–59.

Ferrer CM, Sodi VL, Reginato MJ. 2016. O-GlcNAcylation in cancer biology: Linking metabolism and signaling. Journal of Molecular Biology 428:3282–3294.

Fischer S, Brunk BP, Chen F, Gao X, Harb OS, Iodice JB, Shanmugam D, Roos DS, Stoeckert Jr. CJ. 2011. Using OrthoMCL to assign proteins to OrthoMCL-DB groups or to cluster proteomes into new ortholog groups. Current Protocols in Bioinformatics 35:6.12.1-6.12.19.

Flipphi M, Sun J, Robellet X, Karaffa L, Fekete E, Zeng A-P, Kubicek CP. 2009. Biodiversity and evolution of primary carbon metabolism in *Aspergillus nidulans* and other *Aspergillus* spp. Fungal Genetics and Biology 46:S19–S44.

Flipphi M, Vondervoort PJI van de, Ruijter GJG, Visser J, Arst HN, Felenbok B. 2003. Onset of carbon catabolite repression in *Aspergillus nidulans:* Parallel involvement of hexokinase and glucokinase in sugar signaling. Journal of Biological Chemistry 278:11849–11857.

Flores C-L, Gancedo C. 2015. The gene *YALI0E20207g* from *Yarrowia lipolytica* encodes an N-acetylglucosamine kinase implicated in the regulated expression of the genes from the N-acetylglucosamine assimilatory pathway. PLOS ONE 10:e0122135.

Fu C, Aalten DMF van. 2020. Native detection of protein O-GlcNAcylation by gel electrophoresis. Analyst 145:6826–6830.

Galagan JE, Calvo SE, Cuomo C, Ma L-J, Wortman JR, Batzoglou S, Lee S-I, Baştürkmen M, Spevak CC, Clutterbuck J, Kapitonov V, Jurka J, Scazzocchio C, Farman M, Butler J, Purcell S, Harris S, Braus GH, Draht O, Busch S, D'Enfert C, Bouchier C, Goldman GH, Bell-Pedersen D, Griffiths-Jones S, Doonan JH, Yu J, Vienken K, Pain A, et al. 2005. Sequencing of *Aspergillus nidulans* and comparative analysis with *A. fumigatus* and *A. oryzae*. Nature 438:1105–1115.

Gatineau J, Nidercorne C, Dupont A, Puiffe M-L, Cohen JL, Molinier-Frenkel V, Niedergang F, Castellano F. 2022. IL4I1 binds to TMPRSS13 and competes with SARS-CoV-2 spike. Frontiers in Immunology 13.

Georgieva D, Murakami M, Perband M, Arni R, Betzel C. 2011. The structure of a native L-amino acid oxidase, the major component of the *Vipera ammodytes ammodytesz* venomic, reveals dynamic active site and quaternary structure stabilization by divalent ions. Molecular BioSystems 7:379–384.

Geyer A, Fitzpatrick TB, Pawelek PD, Kitzing K, Vrielink A, Ghisla S, Macheroux P. 2001. Structure and characterization of the glycan moiety of L-amino-acid oxidase from the Malayan pit viper *Calloselasma rhodostoma*. European Journal of Biochemistry 268:4044–4053.

Gilmore SA, Naseem S, Konopka JB, Sil A. 2013. N-acetylglucosamine (GlcNAc) triggers a rapid, temperature-responsive morphogenetic program in thermally dimorphic fungi. PLoS Genetics 9:e1003799.

Goldberg T, Hecht M, Hamp T, Karl T, Yachdav G, Ahmed N, Altermann U, Angerer P, Ansorge S, Balasz K, Bernhofer M, Betz A, Cizmadija L, Do KT, Gerke J, Greil R, Joerdens V, Hastreiter M, Hembach K, Herzog M, Kalemanov M, Kluge M, Meier A, Nasir H, Neumaier U, Prade V, Reeb J, Sorokoumov A, Troshani I, et al. 2014. LocTree3 prediction of localization. Nucleic Acids Research 42:W350–W355.

Gough JA, Murray NE. 1983. Sequence diversity among related genes for recognition of specific targets in DNA molecules. Journal of Molecular Biology 166:1–19.

Grobben Y, Ouden JE den, Aguado C, Altena AM van, Kraneveld AD, Zaman GJR. 2023. Amino acid-metabolizing enzymes in advanced high-grade serous ovarian cancer patients: Value of ascites as biomarker source and role for IL4I1 and IDO1. Cancers 15:893.

Groot PWJ de, Brandt BW, Horiuchi H, Ram AFJ, Koster CG de, Klis FM. 2009. Comprehensive genomic analysis of cell wall genes in *Aspergillus nidulans*. Fungal Genetics and Biology 46:S72–S81.

Guillen E, Abeijon C, Hirschberg CB. 1999. The genes for the Golgi apparatus N-acetylglucosaminyltransferase and the UDP-N-acetylglucosamine transporter are contiguous in *Kluyveromyces lactis*. Journal of Biological Chemistry 274:6641–6646.

Hallgren J, Tsirigos K, Pedersen MD, Almagro Armenteros JJ, Marcatili P, Nielsen H, Krogh A, Winther O. 2022. DeepTMHMM predicts alpha and beta transmembrane proteins using deep neural network. bioRxiv 2022.04.08.487609; doi:https://doi.org/10.1101/2022.04.08.487609.

Hanover JA, Yu S, Lubas WB, Shin S-H, Ragano-Caracciola M, Kochran J, Love DC. 2002. Mitochondrial and nucleocytoplasmic isoforms of O-linked GlcNAc transferase encoded by a single mammalian gene. Archives of Biochemistry and Biophysics 409:287–297.

Hanumantha Rao K, Roy K, Paul S, Ghosh S. 2022. N-acetylglucosamine transporter, Ngt1, undergoes sugar-responsive endosomal trafficking in *Candida albicans*. Molecular Microbiology 117:429–449.

Hardwick KG, Lewis MJ, Semenza J, Dean N, Pelham HR. 1990. ERD1, a yeast gene required for the retention of luminal endoplasmic reticulum proteins, affects glycoprotein processing in the Golgi apparatus. The EMBO Journal 9:623–630.

He M, Zhou X, Wang X. 2024a. Glycosylation: mechanisms, biological functions and clinical implications. Signal Transduction and Targeted Therapy 9:194.

He R, Wei P, Odiba AS, Gao L, Usman S, Gong X, Wang B, Wang L, Jin C, Lu G, Fang W. 2024b. Amino sugars influence *Aspergillus fumigatus* cell wall polysaccharide biosynthesis, and biofilm formation through interfering galactosaminogalactan deacetylation. Carbohydrate Polymers 324:121511.

Henriet SSV, Verweij PE, Warris A. 2012. *Aspergillus nidulans* and chronic granulomatous disease: A unique host–pathogen interaction. The Journal of Infectious Diseases 206:1128–1137.

Heß MC, Bloess S, Risse JM, Friehs K, Fischer von Mollard G. 2020. Recombinant expression of an L-amino acid oxidase from the fungus *Hebeloma cylindrosporum* in *Pichia pastoris* including fermentation. MicrobiologyOpen 9:e1112.

Heß MC, Grollius M, Duhay V, Koopmeiners S, Bloess S, Fischer von Mollard G. 2021. Analysis of N-glycosylation in fungal L-amino acid oxidases expressed in the methylotrophic yeast *Pichia pastoris*. MicrobiologyOpen 10:e1224.

Hill TW, Loprete DM, Momany M, Ha Y, Harsch LM, Livesay JA, Mirchandani A, Murdock JJ, Vaughan MJ, Watt MB. 2006. Isolation of cell wall mutants in *Aspergillus nidulans* by screening for hypersensitivity to calcofluor white. Mycologia 98:399–409.

Hirose S, Mashima T, Yuan X, Yamashita M, Kitano S, Torii S, Migita T, Seimiya H. 2024. Interleukin-4 induced 1-mediated resistance to an immune checkpoint inhibitor through suppression of CD8+ T cell infiltration in melanoma. Cancer Science 00:1-13.

Hosomi A, Iida K, Cho T, Iida H, Kaneko M, Suzuki T. 2020. The ER-associated protease Ste24 prevents N-terminal signal peptide-independent translocation into the endoplasmic reticulum in *Saccharomyces cerevisiae*. Journal of Biological Chemistry 295:10406–10419.

Huang EY, Chang Y-J, Huang S-P, Lin VC, Yu C-C, Huang C-Y, Yin H-L, Chang T-Y, Lu T-L, Bao B-Y. 2018. A common regulatory variant in SLC35B4 influences the recurrence and survival of prostate cancer. Journal of Cellular and Molecular Medicine 22:3661–3670.

Huang Y, Han X, Peng H, Li A, Li R. 2021. Expression profile of the fish immune enzyme L-amino acid oxidase (LAAO) after *Streptococcus agalactiae* infection in zebrafish (*Danio rerio*). Developmental & Comparative Immunology 119:104040.

Hunter CC, Siebert KS, Downes DJ, Wong KH, Kreutzberger SD, Fraser JA, Clarke DF, Hynes MJ, Davis MA, Todd RB. 2014. Multiple nuclear localization signals mediate nuclear localization of the GATA transcription factor AreA. Eukaryotic Cell 13:527–538.

Hynes MJ. 1972. Mutants with altered glucose repression of amidase enzymes in *Aspergillus nidulans*. Journal of Bacteriology 111:717–722.

Hynes MJ. 1973. Pleiotropic mutants affecting the control of nitrogen metabolism in *Aspergillus nidulans*. Molecular Genes and Genetics 125:99–107.

Ishida N, Kuba T, Aoki K, Miyatake S, Kawakita M, Sanai Y. 2005. Identification and characterization of human Golgi nucleotide sugar transporter SLC35D2, a novel member of the SLC35 nucleotide sugar transporter family. Genomics 85:106–116.

Isobe K, Taira R, Hoshi Y, Matsuda S, Yamada M, Hibi M, Kishino S, Ogawa J. 2014. Characterization of a novel L-amino acid oxidase with protein oxidizing activity from *Penicillium steckii* AIU 027. Journal of Bioscience and Bioengineering 117:690–695.

Jiang T, Yang J, Yang H, Chen W, Ji K, Xu Y, Yu L. 2022. SLC35B4 stabilizes c-MYC protein by O-GlcNAcylation in HCC. Frontiers in Pharmacology 13:851089.

Jung S-K, Mai A, Iwamoto M, Arizono N, Fujimoto D, Sakamaki K, Yonehara S. 2000. Purification and cloning of an apoptosis-inducing protein derived from a fish infected with *Anisakis simplex,* a causative nematode of human anisakiasis. The Journal of Immunology 165:1491–1497.

Kang D, Lee J, Yook G, Jeong S, Shin J, Kim M-S, Kim Y-J, Jung H, Ahn J, Kim TW, Chang MJ, Chang CB, Kang S-B, Yang WH, Lee Y, Cho JW, Yi EC, Kang C, Kim J-H. 2025. Regulation of senescence-associated secretory phenotypes in osteoarthritis by cytosolic UDP-GlcNAc retention and O-GlcNAcylation. Nature Communications 16:1094.

Kappel L, Gaderer R, Flipphi M, Seidl-Seiboth V. 2016. The N-acetylglucosamine catabolic gene cluster in *Trichoderma reesei* is controlled by the Ndt80-like transcription factor RON1. Molecular Microbiology 99:640–657.

Katoh K, Rozewicki J, Yamada KD. 2019. MAFFT online service: multiple sequence alignment, interactive sequence choice and visualization. Briefings in Bioinformatics 20:1160–1166.

Katz ME. 2019. Nutrient sensing - the key to fungal p53-like transcription factors? Fungal Genetics and Biology 124:8–16.

Katz ME, Braunberger K, Yi G, Cooper S, Nonhebel HM, Gondro C. 2013. A p53-like transcription factor similar to Ndt80 controls the response to nutrient stress in the filamentous fungus, *Aspergillus nidulans*. F1000Research 2:72.

Katz ME, Braunberger KS, Kelly JM. 2016. Role of HxkC, a mitochondrial hexokinase-like protein, in fungal programmed cell death. Fungal Genetics and Biology 97:36–45.

Katz ME, Buckland R, Hunter CC, Todd RB. 2015. Distinct roles for the p53-like transcription factor XprG and autophagy genes in the response to starvation. Fungal Genetics and Biology 83:10–18.

Katz ME, Flynn PK, vanKuyk PA, Cheetham BF. 1996. Mutations affecting extracellular protease production in the filamentous fungus *Aspergillus nidulans*. Molecular and General Genetics 250:715–724.

Katz ME, Gray KA, Cheetham BF. 2006. The *Aspergillus nidulans xprG (phoG)* gene encodes a putative transcriptional activator involved in the response to nutrient limitation. Fungal Genetics and Biology 43:190–199.

Katz ME, Masoumi A, Burrows SR, Shirtliff CG, Cheetham BF. 2000. The *Aspergillus nidulans xprF* gene encodes a hexokinase-like protein involved in the regulation of extracellular proteases. Genetics 156:1559–1571.

Kerkaert JD, Le Mauff F, Wucher BR, Beattie SR, Vesely EM, Sheppard DC, Nadell CD, Cramer RA. 2022. An alanine aminotransferase Is required for biofilm-specific resistance of *Aspergillus fumigatus* to echinocandin treatment. mBio 13:e02933-21.

Kim D, Paggi JM, Park C, Bennett C, Salzberg SL. 2019. Graph-based genome alignment and genotyping with HISAT2 and HISAT-genotype. Nature Biotechnology 37:907–915.

Kim MW, Rhee SK, Kim J-Y, Shimma Y, Chiba Y, Jigami Y, Kang HA. 2003. Characterization of N-linked oligosaccharides assembled on secretory recombinant glucose oxidase and cell wall mannoproteins from the methylotrophic yeast *Hansenula polymorpha*. Glycobiology 14:243–251.

Kim S, Matsuo I, Ajisaka K, Nakajima H, Kitamoto K. 2002. Cloning and characterization of the *nagA* gene that encodes β-N-acetylglucosaminidase from *Aspergillus nidulans* and its expression in *Aspergillus oryzae*. Bioscience, Biotechnology, and Biochemistry 66:2168–2175.

Kishimoto M, Takahashi T. 2001. A spectrophotometric microplate assay for L-amino acid oxidase. Analytical Biochemistry 298:136–139.

Kobae Y, Kawachi M, Saito K, Kikuchi Y, Ezawa T, Maeshima M, Hata S, Fujiwara T. 2015. Up-regulation of genes involved in N-acetylglucosamine uptake and metabolism suggests a recycling mode of chitin in intraradical mycelium of arbuscular mycorrhizal fungi. Mycorrhiza 25:411–417.

Konopka JB. 2012. N-acetylglucosamine functions in cell signaling. Scientifica 2012:489208.

Kudla B, Caddick MX, Langdon T, Martinez-Rossi NM, Bennett CF, Sibley S, Davies RW, Arst HN. 1990. The regulatory gene *areA* mediating nitrogen metabolite repression in *Aspergillus nidulans*. Mutations affecting specificity of gene activation alter a loop residue of a putative zinc finger. The EMBO Journal 9:1355–1364.

Kumar A, Ghosh S, Bhatt DN, Narula A, Datta A. 2016. *Magnaporthe oryzae* aminosugar metabolism is essential for successful host colonization. Environmental Microbiology 18:1063–1077.

Kumar MJ, Jamaluddin MdS, Natarajan K, Kaur D, Datta A. 2000. The inducible N-acetylglucosamine catabolic pathway gene cluster in *Candida albicans:* Discrete N-acetylglucosamine-inducible factors interact at the promoter of NAG1. Proceedings of the National Academy of Sciences of the USA 97:14218–14223.

Kuraku S, Zmasek CM, Nishimura O, Katoh K. 2013. aLeaves facilitates on-demand exploration of metazoan gene family trees on MAFFT sequence alignment server with enhanced interactivity. Nucleic Acids Research 41:W22–W28.

Latgé J-P. 2007. The cell wall: a carbohydrate armour for the fungal cell. Molecular Microbiology 66:279–290.

Lee SB, Taylor JW. 1990. Isolation of DNA from Fungal Mycelia and Single Spores. In: PCR Protocols: A Guide to Methods and Applications. San Diego: Academic Press. p. 282–287.

Letunic I, Bork P. 2024. Interactive Tree of Life (iTOL) v6: recent updates to the phylogenetic tree display and annotation tool. Nucleic Acids Research 52:W78–W82.

Li A, Parsania C, Tan K, Todd RB, Wong KH. 2021. Co-option of an extracellular protease for transcriptional control of nutrient degradation in the fungus *Aspergillus nidulans*. Communications Biology 4:1–11.

Li L, Stoeckert CJ, Roos DS. 2003. OrthoMCL: Identification of ortholog groups for eukaryotic genomes. Genome Research 13:2178–2189.

Li-Leger E, Feichtinger R, Flibotte S, Holzkamp H, Schnabel R, Moerman DG. 2021. Identification of essential genes in *Caenorhabditis elegans* through whole-genome sequencing of legacy mutant collections. G3: Genes|Genomes|Genetics 11:jkab328.

Liu H, Zhang Q, Huang F, Shen S, Altaf M, Wang Y, Liu X, He Q. 2025. Transcription factor VIB-1 activates catalase-3 expression by promoting PIC assembly in *Neurospora crassa*. Nucleic Acids Research 53:gkaf174.

Liu J, Zhao X, Wang K, Zhang X, Yu Y, Lv Y, Zhang S, Zhang L, Guo Y, Li Y, Yang A, Zhang R, Li J. 2019. A novel YAP1/SLC35B4 regulatory axis contributes to proliferation and progression of gastric carcinoma. Cell Death & Disease 10:452.

Lo H-J, Köhler JR, DiDomenico B, Loebenberg D, Cacciapuoti A, Fink GR. 1997. Nonfilamentous *C. albicans* mutants are avirulent. Cell 90:939–949.

Love MI, Huber W, Anders S. 2014. Moderated estimation of fold change and dispersion for RNA-seq data with DESeq2. Genome Biology 15:550.

Ma J, Hart GW. 2013. Protein O-GlcNAcylation in diabetes and diabetic complications. Expert Review of Proteomics 10:365–380.

Ma J, Hart GW. 2014. O-GlcNAc profiling: from proteins to proteomes. Clinical Proteomics 11:1–16.

Machida M, Jigami Y. 1994. Glycosylated DNA-binding proteins from filamentous fungus, *Aspergillus oryzae:* Modification with N-acetylglucosamine monosaccharide through an O-glycosidic linkage. Bioscience, Biotechnology, and Biochemistry 58:344–348.

MacRae WD, Buxton FP, Sibley S, Garven S, Gwynne DI, Arst HN, Davies RW. 1993. Characterization of an *Aspergillus nidulans* genomic DNA fragment conferring phosphate-non-repressible acid-phosphatase activity. Gene 130:247–251.

Madeira F, Madhusoodanan N, Lee J, Eusebi A, Niewielska A, Tivey ARN, Lopez R, Butcher S. 2024. The EMBL-EBI Job Dispatcher sequence analysis tools framework in 2024. Nucleic Acids Research 52:W521–W525.

Mason JM, Naidu MD, Barcia M, Porti D, Chavan SS, Chu CC. 2004. IL-4-induced gene-1 is a leukocyte L-amino acid oxidase with an unusual acidic pH preference and lysosomal localization. The Journal of Immunology 173:4561–4567.

Maszczak-Seneczko D, Olczak T, Olczak M. 2011. Subcellular localization of UDP-GlcNAc, UDP-Gal and SLC35B4 transporters. Acta Biochimica Polonica 58.

Maszczak-Seneczko D, Wiktor M, Skurska E, Wiertelak W, Olczak M. 2022. Delivery of nucleotide sugars to the mammalian Golgi: A very well (un)explained story. International Journal of Molecular Sciences 23:8648.

May GS, Tsang ML, Smith H, Fidel S, Morris NR. 1987. *Aspergillus nidulans* beta-tubulin genes are unusually divergent. Gene 55:231–243.

McCluskey K, Wiest A, Plamann M. 2010. The Fungal Genetics Stock Center: a repository for 50 years of fungal genetics research. Journal of Biosciences 35:119–126.

Miller JP, Lo RS, Ben-Hur A, Desmarais C, Stagljar I, Noble WS, Fields S. 2005. Large-scale identification of yeast integral membrane protein interactions. Proceedings of the National Academy of Sciences of the USA 102:12123–12128.

Min K, Biermann A, Hogan DA, Konopka JB. 2018. Genetic analysis of NDT80 family transcription factors in *Candida albicans* using new CRISPR-Cas9 approaches. mSphere 3:e0054518.

Min K, Naseem S, Konopka JB. 2020. N-acetylglucosamine regulates morphogenesis and virulence pathways in fungi. Journal of Fungi 6:8.

Montano SP, Coté ML, Fingerman I, Pierce M, Vershon AK, Georgiadis MM. 2002. Crystal structure of the DNA-binding domain from Ndt80, a transcriptional activator required for meiosis in yeast. Proceedings of the National Academy of Sciences of the USA 99:14041–14046.

Morino K, Maegawa H. 2021. Role of O-linked N-acetylglucosamine in the homeostasis of metabolic organs, and its potential links with diabetes and its complications. Journal of Diabetes Investigation 12:130–136.

Moustafa IM, Foster S, Lyubimov AY, Vrielink A. 2006. Crystal structure of LAAO from *Calloselasma rhodostoma* with an L-phenylalanine substrate: Insights into structure and mechanism. Journal of Molecular Biology 364:991–1002.

Nakai K, Horton P. 1999. PSORT: a program for detecting sorting signals in proteins and predicting their subcellular localization. Trends in Biochemical Sciences 24:34–35.

Naseem S, Min K, Spitzer D, Gardin J, Konopka JB. 2017. Regulation of hyphal growth and N-acetylglucosamine catabolism by two transcription factors in *Candida albicans*. Genetics 206:299–314.

Natarajan K, Datta A. 1993. Molecular cloning and analysis of the NAG1 cDNA coding for glucosamine-6-phosphate deaminase from *Candida albicans*. Journal of Biological Chemistry 268:9206–9214.

Nayak T, Szewczyk E, Oakley CE, Osmani A, Ukil L, Murray SL, Hynes MJ, Osmani SA, Oakley BR. 2006. A versatile and efficient gene-targeting system for *Aspergillus nidulans*. Genetics 172:1557–1566.

Ngoh GA, Jones SP. 2008. New Insights into metabolic signaling and cell survival: The role of β-O-linkage of N-acetylglucosamine. The Journal of Pharmacology and Experimental Therapeutics 327:602–609.

Nuutinen JT, Marttinen E, Soliymani R, Hildén K, Timonen S. 2012. L-amino acid oxidase of the fungus *Hebeloma cylindrosporum* displays substrate preference towards glutamate. Microbiology 158:272–283.

Oakley BR, Rinehart JE, Mitchell BL, Oakley CE, Cannona C, Gray GL, May GS. 1987a. Cloning, mapping and molecular analysis of the *pyrG* (orotidine-5'-phosphate decarboxylase) gene of *Aspergillus nidulans*. Gene 61:385–399.

Oakley CE, Weil CF, Kretz PL, Oakley BR. 1987b. Cloning of the *riboB* locus of *Aspergillus nidulans*. Gene 53:293–298.

Ødum MT, Teufel F, Thumuluri V, Almagro Armenteros JJ, Johansen AR, Winther O, Nielsen H. 2024. DeepLoc 2.1: multi-label membrane protein type prediction using protein language models. Nucleic Acids Research 52:W215–W220.

Osmani AH, May GS, Osmani SA. 1999. The extremely conserved *pyroA* gene of *Aspergillus nidulans* is required for pyridoxine synthesis and is required indirectly for resistance to photosensitizers. Journal of Biological Chemistry 274:23565–23569.

Osmani AH, Oakley BR, Osmani SA. 2006. Identification and analysis of essential *Aspergillus nidulans* genes using the heterokaryon rescue technique. Nature Protocols 1:2517–2527.

Paneque A, Fortus H, Zheng J, Werlen G, Jacinto E. 2023. The hexosamine biosynthesis pathway: Regulation and function. Genes 14:933.

Park JH, Nakamura Y, Li W, Hamanaka G, Arai K, Lo EH, Hayakawa K. 2021. Effects of O-GlcNAcylation on functional mitochondrial transfer from astrocytes. Journal of Cerebral Blood Flow and Metabolism 41:1523–1535.

Park J-N, Choo J, Kang HA. 2011. Functional analysis of a *Hansenula polymorpha MNN2-2* homologue encoding a putative UDP-N-acetylglucosamine transporter localized in the endoplasmic reticulum. The Journal of Microbiology 49:1012–1017.

Pawelek PD, Cheah J, Coulombe R, Macheroux P, Ghisla S, Vrielink A. 2000. The structure of L-amino acid oxidase reveals the substrate trajectory into an enantiomerically conserved active site. The EMBO Journal 19:4204–4215.

Pelham HR, Hardwick KG, Lewis MJ. 1988. Sorting of soluble ER proteins in yeast. The EMBO Journal 7:1757–1762.

Peng K-C, Lin C-C, Liao C-F, Yu H-C, Lo C-T, Yang H-H, Lin K-C. 2021. Expression of L-amino acid oxidase of *Trichoderma harzianum* in tobacco confers resistance to *Sclerotinia sclerotiorum* and *Botrytis cinerea*. Plant Science 303:110772.

Pfaffl MW. 2001. A new mathematical model for relative quantification in real-time RT–PCR. Nucleic Acids Research 29:e45.

Plath K, Wilkinson BM, Stirling CJ, Rapoport TA. 2004. Interactions between Sec complex and Prepro-α-Factor during posttranslational protein transport into the endoplasmic reticulum. Molecular Biology of the Cell 15:1–10.

Polkinghorne M, Hynes MJ. 1975. Mutants affecting histidine utilization in *Aspergillus nidulans*. Genetics Research 25:119–135.

Polkinghorne MA, Hynes MJ. 1982. L-histidine utilization in *Aspergillus nidulans*. Journal of Bacteriology 149:1098–5530.

Pontecorvo G, Roper JA, Chemmons LM, Macdonald KD, Bufton AWJ. 1953. The Genetics of *Aspergillus nidulans*. In: M. Demerec, ed. Advances in Genetics. Academic Press. p. 141–238.

Pusztahelyi T, Molnár Z, Emri T, Klement É, Miskei M, Kerékgyártó J, Balla J, Pócsi I. 2006. Comparative studies of differential expression of chitinolytic enzymes encoded by *chiA, chiB, chiC* and *nagA* genes in *Aspergillus nidulans*. Folia Microbiologica 51:547–554.

Qin Z, Xiao Y, Yang X, Mesters JR, Yang S, Jiang Z. 2015. A unique GCN5-related glucosamine N-acetyltransferase region exist in the fungal multi-domain glycoside hydrolase family 3 β-N-acetylglucosaminidase. Scientific Reports 5:18292.

Qiu L, Song JZ, Li J, Zhang TS, Li Z, Hu SJ, Liu JH, Dong JC, Cheng W, Wang JJ. 2022. The transcription factor Ron1 is required for chitin metabolism, asexual development and pathogenicity in *Beauveria bassiana*, an entomopathogenic fungus. International Journal of Biological Macromolecules 206:875–885.

Ravagnani A, Gorfinkiel L, Langdon T, Diallinas G, Gorton D, Arst HNJ, Scazzocchio C. 1997. Subtle hydrophobic interactions between the seventh residue of the zinc finger loop and the first base of an HGATAR sequence determine promoter-specific recognition by the *Aspergillus nidulans* GATA factor AreA sites, is sufficient to ensure activation of transcription. The EMBO Journal 16:3974–3986.

Romagnani S. 2016. IL4I1: Key immunoregulator at a crossroads of divergent T-cell functions. European Journal of Immunology 46:2302–2305.

Roy A, Kucukural A, Zhang Y. 2010. I-TASSER: a unified platform for automated protein structure and function prediction. Nature Protocols 5:725–738.

Roy SK, Chiba Y, Takeuchi M, Jigami Y. 2000. Characterization of yeast Yea4p, a uridine diphosphate-N-acetylglucosamine transporter localized in the endoplasmic reticulum and required for chitin synthesis. Journal of Biological Chemistry 275:13580–13587.

Sadik A, Patterson LFS, Öztürk S, Mohapatra SR, Panitz V, Secker PF, Pfänder P, Loth S, Salem H, Prentzell MT, Berdel B, Iskar M, Faessler E, Reuter F, Kirst I, Kalter V, Foerster KI, Jäger E, Guevara CR, Sobeh M, Hielscher T, Poschet G, Reinhardt A, Hassel JC, Zapatka M, Hahn U, Deimling A von, Hopf C, Schlichting R, et al. 2020. IL4I1 Is a metabolic immune checkpoint that activates the AHR and promotes tumor progression. Cell 182:1252-1270.e34.

Sambrook J, Russell DW. 2001. Molecular Cloning: A Laboratory Manual. Cold Spring Harbor, N.Y. : Cold Spring Harbor Laboratory Press. 790 p.

Sardana R, Highland CM, Straight BE, Chavez CF, Fromme JC, Emr SD. 2021. Golgi membrane protein Erd1 Is essential for recycling a subset of Golgi glycosyltransferases. eLife 10:e70774.

Scarcelli JJ, Colussi PA, Fabre A-L, Boles E, Orlean P, Taron CH. 2012. Uptake of radiolabeled GlcNAc into *Saccharomyces cerevisiae* via native hexose transporters and its in vivo incorporation into GPI precursors in cells expressing heterologous GlcNAc kinase. FEMS Yeast Research 12:305–316.

Schjoldager KT, Narimatsu Y, Joshi HJ, Clausen H. 2020. Global view of human protein glycosylation pathways and functions. Nature Reviews Molecular Cell Biology 21:729–749.

Schmittgen TD, Livak KJ. 2008. Analyzing real-time PCR data by the comparative CT method. Nature Protocols 3:1101–1108.

Sesma JI, Esther CR, Kreda SM, Jones L, O'Neal W, Nishihara S, Nicholas RA, Lazarowski ER. 2009. Endoplasmic reticulum/golgi nucleotide sugar transporters contribute to the cellular release of UDP-sugar signaling molecules. Journal of Biological Chemistry 284:12572–12583.

Shin K-S, Kwon N-J, Kim YH, Park H-S, Kwon G-S, Yu J-H. 2009. Differential roles of the ChiB chitinase in autolysis and cell death of *Aspergillus nidulans*. Eukaryotic Cell 8:738–746.

Sievers F, Barton G, Higgins D. 2020. Multiple Sequence Alignment. In: A. Baxevanis, G. Bader, and D. Wishart, eds. Bioinformatics. Wiley. p. 227–250.

Sievers F, Higgins DG. 2018. Clustal Omega for making accurate alignments of many protein sequences. Protein Science 27:135–145.

Sievers F, Wilm A, Dineen D, Gibson TJ, Karplus K, Li W, Lopez R, McWilliam H, Remmert M, Söding J, Thompson JD, Higgins DG. 2011. Fast, scalable generation of high-quality protein multiple sequence alignments using Clustal Omega. Molecular Systems Biology 7:539.

Sikora L, Marzluf GA. 1982. Regulation of L-amino acid oxidase and of D-amino acid oxidase in *Neurospora crassa*. Molecular and General Genetics MGG 186:33–39.

Simonetti N, Strippoli V, Cassone A. 1974. Yeast-mycelial conversion induced by N-acetyl-D-glucosamine in *Candida albicans*. Nature 250:344–346.

Smith WL, Nakajima T, Ballou CT. 1975. Biosynthesis of yeast mannan. Isolation of *Kluyveromyces lactis* mannan mutants and a study of the incorporation of N-acetyl-D-

glucosamine into the polysaccharide side chains. Journal of Biological Chemistry 250:3426–3435.

Song W, Isaji T, Nakano M, Liang C, Fukuda T, Gu J. 2022. O-GlcNAcylation regulates β1,4-GlcNAc-branched N-glycan biosynthesis via the OGT/SLC35A3/GnT-IV axis. The FASEB Journal 36:e22149.

Sophianopoulou V, Scazzocchio C. 1994. The proline utilisation cluster of *Aspergillus nidulans*. The Genus Aspergillus FEMS Symposium 69:225–232.

Sopko R, Stuart DT. 2004. Purification and characterization of the DNA binding domain of *Saccharomyces cerevisiae* meiosis-specific transcription factor Ndt80. Protein Expression and Purification 33:134–144.

Stasyk T, Lutsik-Kordovsky M, Wernstedt C, Antonyuk V, Klyuchivska O, Souchelnytskyi S, Hellman U, Stoika R. 2010. A new highly toxic protein isolated from the death cap *Amanita phalloides* is an L-amino acid oxidase. The FEBS Journal 277:1260–1269.

Steyer JT. 2022. Characterization of the branched chain amino acid metabolic pathway and its regulators in *Aspergillus nidulans*. PhD Dissertation. Kansas State University.

Steyer JT, Downes DJ, Hunter CC, Migeon PA, Todd RB. 2021. Duplication and functional divergence of branched-chain amino acid biosynthesis genes in *Aspergillus nidulans*. mBio 12:10.1128/mbio.00768-21.

Struck C. 2015. Amino acid uptake in rust fungi. Frontiers in Plant Science 6:40.

Su C, Lu Y, Liu H. 2016. N-acetylglucosamine sensing by a GCN5-related N-acetyltransferase induces transcription via chromatin histone acetylation in fungi. Nature Communications 7:12916.

Szulc B, Sosicka P, Maszczak-Seneczko D, Skurska E, Shauchuk A, Olczak T, Freeze HH, Olczak M. 2020. Biosynthesis of GlcNAc-rich N- and O-glycans in the Golgi apparatus does not require the nucleotide sugar transporter SLC35A3. The Journal of Biological Chemistry 295:16445–16463.

Tarentino AL, Trimble RB, Plummer TH. 1989. Enzymatic approaches for studying the structure, synthesis, and processing of glycoproteins. In: A.M. Tartakoff, ed. Methods in Cell Biology. Academic Press. p. 111–139.

Tegenfeldt F, Kuznetsov D, Manni M, Berkeley M, Zdobnov EM, Kriventseva EV. 2025. OrthoDB and BUSCO update: annotation of orthologs with wider sampling of genomes. Nucleic Acids Research 53:D516–D522.

The Galaxy Community. 2024. The Galaxy platform for accessible, reproducible, and collaborative data analyses: 2024 update. Nucleic Acids Research 52:W83–W94.

Todd RB. 2016. Regulation of fungal nitrogen metabolism. In: D. Hoffmeister, ed. Biochemistry and Molecular Biology. Switzerland: Springer International Publishing. p. 281–303.

Todd RB, Davis MA, Hynes MJ. 2007a. Genetic manipulation of *Aspergillus nidulans:* heterokaryons and diploids for dominance, complementation and haploidization analyses. Nature Protocols 2:822–830.

Todd RB, Davis MA, Hynes MJ. 2007b. Genetic manipulation of *Aspergillus nidulans:* Meiotic progeny for genetic analysis and strain construction. Nature Protocols 2:811–821.

Tretter T, Pereira FP, Ulucan O, Helms V, Allan S, Kalies K-U, Römisch K. 2013. ERAD and protein import defects in a *sec61* mutant lacking ER-lumenal loop 7. BMC Cell Biology 14:56.

Ullah A. 2020. Structure–function studies and mechanism of action of snake venom L-amino acid oxidases. Frontiers in Pharmacology 11:110.

Ullah SF, Oreb M, Boles E, Srivastava V, Seidl-Seiboth V, Seiboth B, Kappel L. 2025. N-acetylglucosamine sensing in the filamentous soil fungus *Trichoderma reesei*. The FEBS Journal 292:3072–3090.

Upshall A. 1986. Genetic and molecular characterization of *argB*+ transformants of *Aspergillus nidulans*. Current Genetics 10:593–599.

Vallon O. 2000. New sequence motifs in flavoproteins: Evidence for common ancestry and tools to predict structure. Proteins: Structure, Function, and Bioinformatics 38:95–114.

Vesely EM, Williams RB, Konopka JB, Lorenz MC. 2017. N-acetylglucosamine metabolism promotes survival of *Candida albicans* in the phagosome. mSphere 2:e00357-17.

Wang G, Jiang L, Yan Y, Kong F, Li Q, Zhang J, Hou S, Wang B, Wang X, Kong H, Deng G, Shi J, Tian G, Zeng X, Chen H, Li C. 2025. Cellular SLC35B4 promotes internalization during influenza A virus entry. mBio 16:00194-25.

Wani WY, Chatham JC, Darley-Usmar V, McMahon LL, Zhang J. 2017. O-GlcNAcylation and neurodegeneration. Brain Research Bulletin 133:80–87.

Waterhouse AM, Procter JB, Martin DMA, Clamp M, Barton GJ. 2009. Jalview Version 2—a multiple sequence alignment editor and analysis workbench. Bioinformatics 25:1189–1191.

Wex B, Safi RM, Antonios G, Zgheib PZ, Awad DB, Kobeissy FH, Mahfouz RA, El-Sabban MM, Yazbek SN. 2018. SLC35B4, an inhibitor of gluconeogenesis, responds to glucose stimulation and downregulates Hsp60 among other proteins in HepG2 liver cell

lines. Molecules : A Journal of Synthetic Chemistry and Natural Product Chemistry 23:1350.

Wiktor M, Wiertelak W, Maszczak-Seneczko D, Balwierz PJ, Szulc B, Olczak M. 2021. Identification of novel potential interaction partners of UDP-galactose (SLC35A2), UDP-*N*-acetylglucosamine (SLC35A3) and an orphan (SLC35A4) nucleotide sugar transporters. Journal of Proteomics 249:104321.

Yamada-Okabe T, Sakamori Y, Mio T, Yamada-Okabe H. 2001. Identification and characterization of the genes for N-acetylglucosamine kinase and N-acetylglucosamine-phosphate deacetylase in the pathogenic fungus *Candida albicans*. European Journal of Biochemistry 268:2498–2505.

Yamazaki H, Tanaka A, Kaneko J, Ohta A, Horiuchi H. 2008. *Aspergillus nidulans* ChiA is a glycosylphosphatidylinositol (GPI)-anchored chitinase specifically localized at polarized growth sites. Fungal Genetics and Biology 45:963–972.

Yang C-A, Cheng C-H, Lo C-T, Liu S-Y, Lee J-W, Peng K-C. 2011. A novel L-amino acid oxidase from *Trichoderma harzianum* ETS 323 associated with antagonism of *Rhizoctonia solani*. Journal of Agricultural and Food Chemistry 59:4519–4526.

Yang D, Zhang M, Su C, Dong B, Lu Y. 2023. *Candida albicans* exploits N-acetylglucosamine as a gut signal to establish the balance between commensalism and pathogenesis. Nature Communications 14:3796.

Yang J, Yan R, Roy A, Xu D, Poisson J, Zhang Y. 2015. The I-TASSER Suite: protein structure and function prediction. Nature Methods 12:7–8.

Yazbek SN, Buchner DA, Geisinger JM, Burrage LC, Spiezio SH, Zentner GE, Hsieh C-W, Scacheri PC, Croniger CM, Nadeau JH. 2011. Deep congenic analysis identifies many strong, context-dependent QTLs, one of which, Slc35b4, regulates obesity and glucose homeostasis. Genome Research 21:1065–1073.

Ye F, Wang L, Li Y, Dong C, Zhou L, Xu J. 2023. IL4I1 in M2-like macrophage promotes glioma progression and is a promising target for immunotherapy. Frontiers in Immunology 14:1338244.

Ye L, Wang S, Zheng J, Chen L, Shen L, Kuang Y, Wang Y, Peng Y, Hu C, Wang L, Tian X, Liao G. 2022. Functional characterization of the GlcNAc catabolic pathway in *Cryptococcus deneoformans*. Applied and Environmental Microbiology 88:00437-22.

Zeitler L, Murray PJ. 2023. IL4i1 and IDO1: Oxidases that control a tryptophan metabolic nexus in cancer. Journal of Biological Chemistry 299:104827.

Zhang L-B, Yang Z-H, Yang W-W-J, Guan Y. 2024. A novel fungal sensor (*Ngs1*) of *N*-acetylglucosamine (GlcNAc) mediates the fungal response to GlcNAc in the interaction between entomopathogenic *Beauveria bassiana* and insect host. Journal of Invertebrate Pathology 207:108206.

Zhang S, Gao Y, Wang P, Wang S, Wang Y, Li M, Wang A, Zhao K, Zhang Z, Sun J, Guo D, Liang Z. 2023. Tryptophan metabolism enzymes are potential targets in ovarian clear cell carcinoma. Cancer Medicine 12:21996–22005.

Zhang Y. 2008. I-TASSER server for protein 3D structure prediction. BMC Bioinformatics 9:40.

Zhao N, Deng G, Yuan P-X, Zhang Y-F, Jiang L-Y, Zhao X, Song B-L. 2023. TMEM241 is a UDP-N-acetylglucosamine transporter required for M6P modification of NPC2 and cholesterol transport. Journal of Lipid Research 64.

Zhao X, Hume SL, Johnson C, Thompson P, Huang J, Gray J, Lamb HK, Hawkins AR. 2010. The transcription repressor NmrA is subject to proteolysis by three *Aspergillus nidulans* proteases. Protein Science 19:1405–1419.

Zhu L, Wang J, Hu J. 2023. High expression of IL4I1 is correlated with poor prognosis and immune infiltration in thyroid cancer. BMC Endocrine Disorders 23:148.

Žun G, Kos J, Sabotič J. 2017. Higher fungi are a rich source of L-amino acid oxidases. 3 Biotech 7:230.

Zuo M, Fang J, Huang P, Liu S, Hou P, Wang S, Liu Z, Feng C, Cao L, Li P, Shi Y, Shao C. 2023. IL4I1-catalyzed tryptophan metabolites mediate the anti-inflammatory function of cytokine-primed human muscle stem cells. Cell Death Discovery 9:269.

Appendix A - *Aspergillus sarB* ortholog annotations

A.1 *Aspergillus oryzae* RIB40 *sarB* ortholog reannotation

AO090010000775 was identified as a *sarB* ortholog in the *A. oryzae* RIB40 reference strain. The predicted gene structure differed markedly from that in other *Aspergillus* orthologs, including that of its closest relative, *A. flavus* AFLA_014279. After manual inspection of the gene sequence and its predicted protein, we reannotated the *A. oryzae* gene to follow the same gene structure as the orthologs in other aspergilli. Publicly-available RNA-seq data visualized in JBrowse at FungiDB (fungidb.org) support the reannotated gene structure. The start codon in *A. oryzae* (and *A. flavus*) is downstream of those in other aspergilli examined, but appears to be correct, as the next closest in-frame ATG sequence is far upstream of the annotated start codon. The predicted protein encoded by this reannotated gene is 435 amino acids in size and contains the same predicted UDP-GlcNAc transporter domain as SarB (Figure A.1).

```
MSKQHAGTLEIDDHLTERDEPKEPHASLGSITTAAAYTVLPGWTTIVLMISLIFGGC
CANVFALEAIIKEQPSSGPLITFAQFIVTALLTSPSFLSLSAGPQSLFLSRRVIPLR
SWLVYTAFFVTVNLLNNWAFAYKISVPLHIILRSGGPVASMIVGYAFNAKRYSHGQI
LAVAMLTIGVIAAALADARTKGQSISVGYHQNDSTMASTFIGFSILALAMALSAFQG
IFADRLYESYGRNHWKEALFYSHTLSLPLFLPTYSHLLAQWRALLSSPSLLSGISAI
AARKGSVSSSPLLLGTGLATASKTAFVKSVPMPIINTTSHLLAELERFKSFQFVLAC
IPIQGFYLLMNALTQYLCIRGVHLLSAKSSSLTVTIVLNVRKLISLLLSIYLFGNDL
APGVLVGALFVFVGGALYGFEGARLRKTYKPSNKKD
```

Figure A.1 Predicted protein sequence of the putative SarB ortholog in *A. oryzae.*

A.2 *Aspergillus clavatus* putative *sarB* ortholog

After noting that the *A. clavatus* NRRL 1 reference strain contained no annotated *sarB* ortholog, we used the reannotated *A. nidulans* SarB protein sequence to search the *A. clavatus* genome for a possible unannotated ortholog. A sequence located at 123176..124694 translated to a sequence with high similarity to SarB. NRDB protein

sequence data visualized at FungiDB show multiple protein alignments at this region, between ACLA_042880 and ACLA_042890. After manually inspecting the sequence, we annotated it using the same predicted gene structure as for the orthologs in other aspergilli. There are no publicly-available RNA-seq data with which to compare this reannotation, however NRDB protein alignment data supports our predicted gene structure. The resulting protein is 453 amino acids in length and contains the same predicted UDP-GlcNAc transporter domain as SarB (Figure A.2). Predicted gene structure details for *A. oryzae* and *A. clavatus* are shown in Table A.1.

```
MRAIRSFMSMSGIKHYWSNQEGIRPRLMTEKMINRSGNGKVKDSSIDSPKLVDQEGY
KKTLYSSLETIADALVHANPASCISMVLMISLIFGGCCANVFALEAIIKQQPSSGPL
ITFAQFLVTALLTLPSFLSPSSGAYSLFLTPRVIPLRSWVIYTAFFVTVNLLNNWAF
AYRISVPLHIILRSGGPVASLIIGYFFNQKRYSHGQIVAVAMLTFGVFTAALTDART
KEKSLEMGPIKESSDLVTTATGFLILALAMILSAFQGIYADRLYETYGRNHWKEALF
YSHILSLPLFLPTYPQLLDQWRAMRSSPSLVCPALGSNTISENKGITGLMSSLSSAI
GSVTLSPLAVINTVPYFISQIPTQAAFLLLNALTQYLCIRGVHLLSAQTSSLTVTVI
LNVRKLVSLLLSIYIFGNDLAPGVLIGAVCVFSGGGLYALESTRLRQHGSSKRD
```

Figure A.2 Predicted protein sequence of the putative SarB ortholog in *A. clavatus.*

Table A.1. Gene structures of the reannotated *A. oryzae* and putative *A. clavatus* *sarB* orthologs.

Feature	***A. oryzae* RIB40 AO090010000775**	***A. oryzae* reannotation**	***A. clavatus* putative *sarB* ortholog**
Exon 1	+1..+188 (188)	+1..+180 (180)	+1..+270 (270)
Intron 1	+189..+367 (179)	+181..+233 (53)	+271..344 (53)
Exon 2	+368..+1490 (1123)	+234..+259 (26)	+345..+370 (26)
Intron 2	-	+260..+315 (56)	+371..+427 (57)
Exon 3	-	+316..+332 (17)	+428..+444 (17)
Intron 3	-	+333..+405 (73)	+445..+512 (68)
Exon 41	-	+406..+1490 (1085)	+513..+1540 (1028)

Appendix B - Details of statistical analysis results

B.1 Quantitative LAAO assay strain comparisons

Quantitative LAAO assays are described in Chapter 4. Differences in specific activities between strains were analyzed by analysis of variance (ANOVA) followed by Tukey's Honestly Significant Difference (HSD) post-hoc test. For tests of the effect of sarB on SarA activity, significant differences were found between strains at 4 h (F = 179.214, df = 10, $p < 2 \times 10^{-16}$) and at 72 h (F = 187.320, df = 7, $p < 2 \times 10^{-16}$). For tests of the effects of xprG and AN1416 on SarA activity, significant differences were found between strains (F -= 14.32, df = 3, $p < 0.00001$). Results of Tukey's HSD comparisons are presented in Table B.1 and Table B.2.

Table B.1 Effect of *sarB* mutations on SarA activity – 4 h.

Strain comparison	Tukey's HSD *p*-value
MH1-MH10571	0.9983087
MH1-MH8	0.0000000
MH1-MK160	0.2045985
MH1-RT1020	0.9999951
MH1-RT1023	0.9999993
MH1-RT1035	0.0000002
MH1-RT763	0.9999999
MH1-RT775	0.0000000
MH1-RT776	0.9901841
MH1-RT891	0.0004560
MH10571-MH8	0.0000000
MH10571-MK160	0.0190311
MH10571-RT1020	0.9999982
MH10571-RT1023	0.9999862
MH10571-RT1035	0.0000000
MH10571-RT763	0.9826465
MH10571-RT775	0.0000000
MH10571-RT776	0.0000000
MH10571-RT891	0.0000105
MH8-MK160	0.0000000
MH8-RT1020	0.0000000
MH8-RT1023	0.0000000

MH8-RT1035	0.0000000
MH8-RT763	0.0000000
MH8-RT775	0.9999926
MH8-RT776	0.0000000
MH8-RT891	0.0000000
MK160-RT1020	0.0656465
MK160-RT1023	0.0823472
MK160-RT1035	0.0169216
MK160-RT763	0.3659219
MK160-RT775	0.0000000
MK160-RT776	0.0094098
MK160-RT891	0.7025691
RT1020-RT1023	1.0000000
RT1020-RT1035	0.0000000
RT1020-RT763	0.9995024
RT1020-RT775	0.0000000
RT1020-RT776	0.9999105
RT1020-RT891	0.0000662
RT1023-RT1035	0.0000000
RT1023-RT763	0.9998246
RT1023-RT775	0.0000000
RT1023-RT776	0.9997215
RT1023-RT891	0.0000950
RT1035-RT763	0.0000009
RT1035-RT775	0.0000000
RT1035-RT776	0.0000000
RT1035-RT891	0.8222352
RT763-RT775	0.0000000
RT763-RT776	0.9451465
RT763-RT891	0.0014791
RT775-RT776	0.0000000
RT775-RT891	0.0000000
RT776-RT891	0.0000039

Table B.2 Effect of *sarB* mutations on SarA activity – 72 h.

Strain comparison	Tukey's HSD *p*-value
MH1-MH10571	0.9998758
MH1-MH8	0.0000000
MH1-MK160	0.0000547
MH1-RT1035	0.0000056
MH1-RT763	1.0000000
MH1-RT775	0.0000000
MH1-RT891	0.0000043
MH10571-MH8	0.0000000
MH10571-MK160	0.0002882
MH10571-RT1035	0.0000325
MH10571-RT763	0.9996013
MH10571-RT775	0.0000000
MH10571-RT891	0.0000250
MH8-MK160	0.0000000
MH8-RT1035	0.0000000
MH8-RT763	0.0000000
MH8-RT775	0.0000000
MH8-RT891	0.0000000
MK160-RT1035	0.9992785
MK160-RT763	0.0000395
MK160-RT775	0.0000000
MK160-RT891	0.9985270
RT1035-RT763	0.0000040
RT1035-RT775	0.0000000
RT1035-RT891	1.0000000
RT763-RT775	0.0000000
RT763-RT891	0.0000030
RT775-RT891	0.0000000

Table B.3 Effect of *xprG* and AN1416 on SarA activity.

Strain comparison	Tukey's HSD *p*-value
MH8-RT1052	0.0000000
MH8-RT1055	0.3864399
MH8-RT1058	0.0000938
RT1055-RT1058	0.0011983
RT1058-RT1052	0.8597539
RT1058-RT1055	0.0113876

B.2 RNA-seq analysis by DESeq2

RNA-seq experiments are described in Chapters 4 and 5. For each gene of interest, DESeq2 was used to assess differences in gene expression between the glutamine, alanine, and nitrogen-free conditions and ammonium in the wild-type strain. Details of statistical analyses methods are found in Section 2.8.3. Adjusted *p*-values (FDR) are shown in Table B.3.

Table B.4 Comparisons between nitrogen conditions in wild type.

Gene	Glutamine vs NH_4	Alanine vs NH_4	Nitrogen-free vs NH_4
sarB	N.S.	N.S.	N.S.
sarA	N.S.	0.00017	0.0000000000035
AN11141	N.S.	N.S.	N.S.
AN0265	N.S.	N.S.	N.S.
xprG	0.0098	0.000000000017	6.6×10^{-19}
ngsA	N.S.	N.S.	N.S.
nagA	N.S.	N.S.	N.S.
ngtA	0.000095	0.0000013	0.000000018
ngtB	N.S.	N.S.	N.S.
hxkC	0.00000000016	0.016	N.S.
dacA	0.000000012	0.00000015	0.00000017
damA	0.00085	0.000024	N.S.

N.S. = not significant at $p = 0.05$

For each gene of interest, DESeq2 was used to assess differences in gene expression between the ammonium, glutamine, alanine, and nitrogen-free conditions in wild type and the *nmrA*Δ mutant. Significant differences between strains were found only in the glutamine treatment. Details of statistical analyses methods are found in Section 2.8.3. Adjusted *p*-values (FDR) are shown in Table B.4.

Table B.5 Comparisons between the glutamine condition in wild type and *nmrA*Δ.

Gene	Wild type vs *nmrA*Δ
sarB	N.S.
sarA	N.S.
AN11141	N.S.
AN0265	N.S.
xprG	N.S.
ngsA	N.S.
nagA	N.S.
ngtA	0.028
ngtB	N.S.
hxkC	0.0035
dacA	0.00020
damA	0.0000051
N.S. = not significant at $p = 0.05$	

Appendix C - Deglycosylation of ovalbumin with PNGase F

Ovalbumin was treated with PNGase F as described in Section 4.4.6, run on an SDS-PAGE gel, and stained with Coomassie Blue. Because we handled this protein in an identical manner to our *A. nidulans* soluble cell-free extracts, we did not treat the ovalbumin with additional heat or chemicals prior to running the gel.

The PNGase F-treated sample showed a change in mobility in protein migration. Two bands on the gel at ~60 kDa represent glycosylated (top band) and deglycosylated (bottom band) ovalbumin after treatment with PNGase F (Figure 1). The presence of both bands in the treated sample indicates the sample was partially deglycosylated.

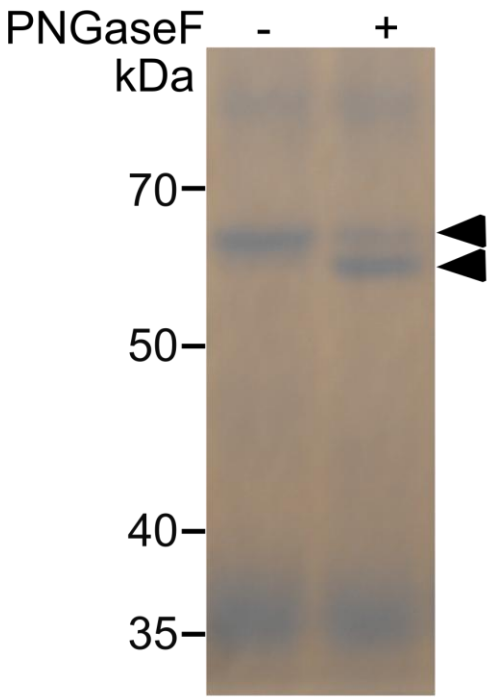

Figure C.1 Deglycosylation of ovalbumin with PNGase F.